Prifysgol Caerdydd
Yr Ysgol Meddygaeth
Sefydliad Ymchwil Systemau Imiwnedd

Cardiff University
School of Medicine
Systems Immunity Research Institute

Structural and biophysical characterisation of T-cell receptor cross-reactivity in health and disease

A thesis submitted to Cardiff University for the candidature of Doctor of Philosophy

June 2021

Aaron Wall

Acknowledgements

The work I present in this thesis was only made possible by the professional and personal support given by the following people.

Firstly, I want to thank **Professor Andrew Sewell** for giving me the opportunity to work with his laboratory, as well as providing the guidance I needed to progress as a researcher. I especially want to thank him for his patience during the thesis write up period and for helping me improve my written skill. I also want to thank my co-supervisor **Dr David Cole** for his structural biology and biochemistry guidance. The structural pictures I present in this theses would not have been possible without his help.

In regards to my lab work I want to thank the following: **Anna Fuller** for teaching me to be a functioning member of the lab and for guiding me through my PhD, **Dr Garry Dolton** for guiding me through my brief stint in tissue culture and for helping me understand where my work fits in the grand scheme of immunology, **Dr Pierre Rizkallah** for teaching me about crystallography and structure determination, **Dr Barbra Szomolay** for her webtool, and **Dr Thomas Whalley** for showing me how to use Modeller. I also want to thank every member of the Sewell group past and present for kindly accepting my awful social skills, and for making the last few years the pleasure it has been.

I want to thank the **Wellcome Trust** and **Life Sciences Research Network Wales** for funding my PhD. I also want to thank **Professor Awen Gallimore**, **Professor Ian Humphreys** and **Dr Richard Stanton** for reading my yearly appraisal reports, for providing a crucial outsider perspective on my work, and for the 'nagging' (Ian's words).

I want to thank all of my friends and family for their emotional support outside of the lab. Specifically, I would like to thank my wonderful partner **Dr Jade Hopkins** for tolerating me when I got stressed and moody, and for just tolerating me in general. Lastly and perhaps most importantly, I want to thank my cats, **Kevin** and **Liam**, for allowing me to stroke their soft, fluffy faces, and for all the 'gifts' they have brought me while I've been writing.

Thank you all again for everything!

Publications

Greenshields-Watson, A., Attaf, M., Maclachlan, B. J., Sewell, A. K., Godkin, A. J., Cole, D. K., Whalley, T., & **Wall, A**., *et al.* (2020). $CD4^+$ T Cells Recognize Conserved Influenza A Epitopes through Shared Patterns of V-Gene Usage and Complementary Biochemical Features. *Cell Reports*, *32*(2), 107885. https://doi.org/10.1016/j.celrep.2020.107885

Whalley, T., Dolton, G., Brown, P. E., **Wall, A**., Wooldridge, L., Berg, H. Van Den, Fuller, A., Hopkins, J. R., Crowther, M. D., Szomolay, B., & Sewell, A. K. (2020). GPU-Accelerated Discovery of Pathogen-Derived Molecular Mimics of a T-Cell Insulin Epitope. *11*(February), 1–18. https://doi.org/10.3389/fimmu.2020.00296

Galloway, S. A. E., Dolton, G., Attaf, M., **Wall, A**., Fuller, A., Rius Rafael, C., Bianchi, V., Theaker, S., Lloyd, A., Caillaud, M. E., Svane, I. M., Donia, M., Cole, D. K., Szomolay, B., Rizkallah, P., & Sewell, A. K. (2019). Peptide super-agonist enhances T-cell responses to melanoma. *Frontiers in Immunology*, *10*(MAR), 1–18. https://doi.org/10.3389/fimmu.2019.00319

Dolton, G., Zervoudi, E., Rius Rafael, C., **Wall, A**., Thomas, H. L., Fuller, A., Yeo, L., Legut, M., Wheeler, S., Attaf, M., Chudakov, D. M., Choy, E., Peakman, M., & Sewell, A. K. (2018). Optimized peptide-MHC multimer protocols for detection and isolation of autoimmune T-cells. *Frontiers in Immunology*, *9*(JUN), 1–18. https://doi.org/10.3389/fimmu.2018.01378

Fuller, A., **Wall, A**., Crowther, M., Lloyd, A., Zhurov, A., Sewell, A., Cole, D., & Beck, K. (2017). Thermal Stability of Heterotrimeric pMHC Proteins as Determined by Circular Dichroism Spectroscopy. *Bio-Protocol*, *7*(13). https://doi.org/10.21769/bioprotoc.2366

Cole, D. K., van den Berg, H. A., Lloyd, A., Crowther, M. D., Beck, K., Ekeruche-Makinde, J., Miles, J. J., Bulek, A. M., Dolton, G., Schauenburg, A. J., **Wall, A**., Fuller, A., Clement, M., Laugel, B., Rizkallah, P. J., Wooldridge, L., & Sewell, A. K. (2016). Structural mechanism underpinning cross-reactivity of a CD8+ T-cell clone that recognises a peptide derived from human telomerase reverse transcriptase. *Journal of Biological Chemistry*, *292*, 802–813. https://doi.org/10.1074/jbc.M116.741603

Summary

Background – T-cells are a crucial component of the adaptive immune system, responsible for host immunity to numerous pathogens. T-cells recognise pathogenic peptides presented on target cells via the T-cell receptor. To facilitate comprehensive immune coverage, T-cell receptors can 'cross-react' with multiple pathogenic peptides. However, T-cell cross-reactivity has also been implicated in autoimmune disease, where recognition of a pathogenic epitope can trigger autoimmune recognition. While the biochemical mechanism governing T-cell cross-reactivity has been previously investigated, many of these studies involve non-clinically relevant T-cells. To understand the physiological consequences of T-cell cross-reactivity and its biochemical mechanisms, clinically relevant T-cells needed to be studied.

Results – I have studied several T-cells which have been implicated in disease. The first, the MEL8 T-cell, had previously been shown to cross-react with multiple tumour-associated antigens, resulting in a more potent T-cell response against tumour cells. I presented structural evidence that the MEL8 T-cell receptor recognises these different peptide residues via conserved hotspot residues present on its target peptides. I also showed that this hotspot recognition was present in another cancer-specific T-cell, MEL5, which can recognise the same tumour-associated antigens as MEL8. These findings demonstrate a new mechanism by which T-cells could respond to tumour cells, thus highlighting a clinical benefit to T-cell cross-reactivity. To address the potential drawbacks of T-cell cross-reactivity I also studied several T-cells clones (4C6, InsB4, and Clone 29) which have been implicated in type 1 diabetes. Using a combinatorial library screen, I identified multiple pathogenic epitopes that were recognised by 4C6 and InsB4 which may act as a pathogenic trigger. Structural data showed these T-cells also utilise hotspot recognition to achieve cross-reactivity between peptides, implicating hotspot cross-reactivity in the progression of type 1 diabetes. Combinatorial peptide library data for the Clone 29 T-cell suggested a different mechanism of cross-reactivity may be involved, indicating multiple mechanisms of cross-reactivity may facilitate the triggering of type 1 diabetes.

Conclusion – Using clinically relevant T-cells I have demonstrated the role that cross-reactivity plays in both cancer immunity and autoimmunity, while showing the importance of hotspot binding in these contexts. By adding to the existing literature, these examples may inform therapeutic design for the treatment or prevention of disease.

Abbreviations

ACT	Adoptive cell therapy
APC	Antigen presenting cell
APL	Altered peptide ligand
BCG	Bacillus Calmette–Guérin
BST2	Bone Marrow Stromal antigen 2
CAR	Chimeric antigen receptor
CAR-T	chimeric antigen receptor transduced
CD	Cluster of differentiation
CDR	Complementarity determining region
CPL	Combinatorial peptide library
Cryo-EM	Cryo-electron microscopy
cTEC	Cortical thymic epithelial cell
CTLA4	Cytotoxic T-lymphocyte-associated protein 4
DAG	Diacylglycerol
DENV	Dengue virus
DMSO	Dimethyl-sulfoxide
DN	Double negative
DP	Double positive
DTT	Dithiothreitol
EBI	European Bioinformatics Institute
EBNA3	EBV nuclear antigen 3
EBV	Epstein-Barr virus
ECDC	European Center for Disease Control
EDTA	Ethylenediaminetetraacetic acid
ELISA	Enzyme-linked immunosorbent assay
EMDB	Electron microscopy data bank
ER	Endoplasmic reticulum
ERAP	Endoplasmic reticulum aminopeptidase
FACS	Fluorescence-activated cell sorting
FADD	Fas-associated death domain
FasL	Fas ligand
FDA	US food and drug association
FPLC	Fast Protein Liquid Chromatography
GAD65	Glutamic acid decarboxylase
GvHD	Graft-vs-host disease
hCMV	Human cytomegalovirus
HEPES	M 4-(2-hydroxyethyl)-1-piperazine ethane sulfonic acid
HEV	Human enterovirus
HIC	Hydrophobicity interaction column
HIV	Human immunodeficiency virus
HLA	Human leukocyte antigen
HSV	Herpes simplex virus
HTA	Human Tissue Act

IFN-γ	Interferon-γ
Ig	Immunoglobulin
IGRP	Islet-specific glucose-6-phosphatase catalytic subunit-related protein
Ii	Invariant chain
IL13Rα2	Interleukin-13 receptor alpha 2
IMGT	Immunogenetics Information System
IMP2	Insulin-like growth factor 2 mRNA binding protein 2
InsB	Insulin B-chain
IP3	Inositol phosphate-3
IPTG	Isopropyl β-D-1-thiogalactopyranoside
IRAE	Immune related adverse effect
ITAM	Immunoreceptor tyrosine kinase associated motifs
LB	Luria broth
LCL	Lymphoblastoid cell line
MACS	Magnetic activated cell sorting
MBP	Myelin basic protein
MHC	Major Histocompatibility Complex
MIIC	MHC-II compartment
MOPS	3-(N-morpholino) propanesulfonic acid
MS	Multiple sclerosis
mTEC	Medullary thymic epithelial cell
NA	Neuraminidase
NK	Natural killer
NOD	Non-obese diabetic
nPOD	Pancreatic Organ donors with Diabetes
PBMC	Peripheral blood mononuclear cells
PD-1	Programmed cell death protein 1
PDB	Protein data bank
PD-L1	PD ligand 1
PHA	Phytohemagglutinin
PI(4,5)P2	Phospholipid phosphatidylinositol 4,5 bisphosphate
PLC-γ1	Phospholipase-C-γ1
pMHC	peptide:major histocompatibility complex
PPI	Preproinsulin
RAG	Recombination activation gene
RBC	Red blood cell
RSS	Recombination signal sequence
RU	Response units
scVf	Single-chain variable fragment
SDS-PAGE	sodium dodecyl sulphate–polyacrylamide gel electrophoresis
SEC	Size exclusion chromatography
SP	Single positive
SPR	Surface Plasmon Resonance
T1D	Type-1-Diabetes
TAA	Tumour-associated antigen
TAP	Transporter associated with antigen processing

TAPI-0	TNF-α processing inhibitor-0
TCR	T-cell receptor
Tfb	Transformation buffer
TGF-β	Tumour growth factor-β
Th	T-helper
TIL	Tumour infiltrating lymphocyte
TNF	Tumour necrosis factor
TOPSORT	T-cell receptor-optimised peptide skewing of the T-cell repertoire
Tpn	Tapasin
T-reg	T-regulatory
TRIS	Tris(hydroxymethyl)aminomethane
TRuC	T-cell receptor fusion construct
VZV	Varicella-zoster virus
ZIKV	Zika virus
β2M	β_2 microglobulin

All units of measurement in this thesis follow the International System of Units, unless otherwise specified. Amino acids are referred to by their standard single- or three-letter code.

Table of Contents

List of Figures

List of Tables

1. Introduction

1.1. T-cell immunology

The immune system allows organisms to protect themselves from pathogens. In jawed vertebrates, components of the immune system are generally classified as being part of 'innate' immunity or 'adaptive' immunity. The innate immune system consists of broad responses to pathogens and is considered the first line of defence against infection. The innate immune system includes molecular components such as proinflammatory cytokines and the complement system, as well as cellular components such as phagocytes and natural killer cells (Romo et al., 2016). The adaptive immune system carries out a more specific response which adapts over time. Adaptive immunity is comprised of pathogen-specific lymphocytes that can retain immunologic memory. Within the adaptive immune system there are two types of lymphocyte, B-cells and T-cells.

1.1.1. Generation of T-cells

Both B-cells and T-cells are produced in the bone marrow as progenitor cells and their fate depends on their expression of Notch1. Notch1$^-$ cells will remain in the bone marrow and mature into B-cells (Pui et al., 1999). B-cells provide humoral adaptive immunity; recognising cognate antigens via immunoglobulins (Igs) (Eibel et al., 2014). Notch1$^+$ cells will migrate to the thymus and mature into T-cells. During thymic maturation, T-cells acquire the ability to provide cellular adaptive immunity via expression of the cell surface T-cell receptor (TCR). TCRs are heterodimers comprised of two polypeptide chains linked by a disulphide bond. There are four TCR chains (α, β, γ, and δ) and T-cells are classified based on which chains they express. The four TCR chains have a propensity to form two heterodimers – αβ and γδ. The most well studied class of T-cell is the αβ T-cell, which expresses an αβ TCR. αβ T-cells conventionally recognise and respond to small pathogen-derived peptide fragments, presented to the T-cell on surface-expressed major histocompatibility complex (MHC) molecules, this is known as 'MHC restriction' (Zinkernagel et al., 1974a; Zinkernagel et al., 1974b). In addition to their αβ TCR, αβ T-cells express one of two characteristic surface markers, known as the T-cell co-receptors, cluster of differentiation (CD)4 or CD8. γδ T-cells are less well-studied and are thought to eschew typical MHC restriction in favour of unconventional antigen recognition (Fahl et al., 2014). This thesis will focus on the activity of αβ T-cells (referred to as T-cells henceforth).

1.1.1.1. Generation of the T-cell receptor

Each class of T-cell begins life as an immature Notch1^{+} thymocyte that lacks expression of the TCR. These early thymocytes are known as double negative (DN) thymocytes as they exhibit the CD4^{-}CD8^{-} phenotype. The process of TCR generation begins in DN thymocytes, via TCR gene recombination (Hozumi et al., 1976) (**Figure 1.1**). The genes which encode the α and β TCR chains are made up of different gene regions known as the variable (V), diversity (D, only present for the β chain), joining (J) and constant (C) regions (Bassing et al., 2002). Within these gene regions are several different segments. During T-cell development, recombination occurs to produce an open reading frame containing a single segment from each gene region, which will result in expression of a single, complete TCR chain.

Recombination is conducted via the recombination activating gene (RAG)-1 and RAG-2 enzymes (Oettinger et al., 1992). RAG-1 and RAG-2 recognise recombination signal sequences (RSS) that are present at either side of each gene exon. An RSS consists of a conserved heptamer and nonamer nucleotide sequence, separated by either a 12 (12RSS) or 23 (23RSS) nucleotide spacer (Early et al., 1980). RAG-1 and RAG-2 introduce single-strand nicks in the RSS, exposing the 3'-OH group of the DNA strand (Morrow et al., 1993). The exposed 3'-OH group covalently links to the anti-parallel phosphodiester bond present on the same DNA strand, which becomes accessible due to the single-strand nick, forming a hairpin loop known as a blunt end. A blunt end can be formed in either the 12RSS or the 23RSS (Roth et al., 1993). TCR gene exons are then recombined together via non-homologous end joining of these blunt ends (Ramsden et al., 1995). To ensure the correct order and orientation of recombined exons, ligation follows the '12/23 rule', where a 12RSS blunt end can only recombine with a 23RSS blunt end and vice versa (Bassing et al., 2000). The diversity generated by this recombination event is bolstered by the addition of non-template nucleotides to the exon joining regions, catalysed by an enzyme called terminal deoxynucleotidyl transferase (Desiderio et al., 1984).

In developing DN thymocytes, the TCRβ chain is expressed first. TCRβ variable gene recombination occurs in a strict order; D to J, V to DJ, and finally VDJ to C. The completed TCRβ chain pairs with a pre-TCRα chain, an Ig-like single chain glycoprotein (Boehmer et al., 1997). This pre-TCR-α/β complex associates with a CD3ζ chain (Oers et al., 1995). If T-cell signalling via the CD3ζ chain is successful, pre-TCR-α expression is then inhibited. The TCRα chain is then expressed, resulting in αβ DN thymocytes (Negishi et al., 1995; Germain, 2002;

Hernandez et al., 2010). Most T-cells only express a single TCRβ chain due to allelic exclusion, where only one allele is expressed, which serves to reduce incidences of auto-reactivity (Pernis et al., 1965). However, it has been suggested that a degree of allelic inclusion, where multiple TCR chains can be expressed on a single T-cell, can result in increased immune coverage (Brady et al., 2010). Following the successful folding of a TCRα chain, αβ DN thymocytes begin to express both CD8 and CD4 co-receptors, becoming double positive (DP) thymocytes (Egerton et al., 1990).

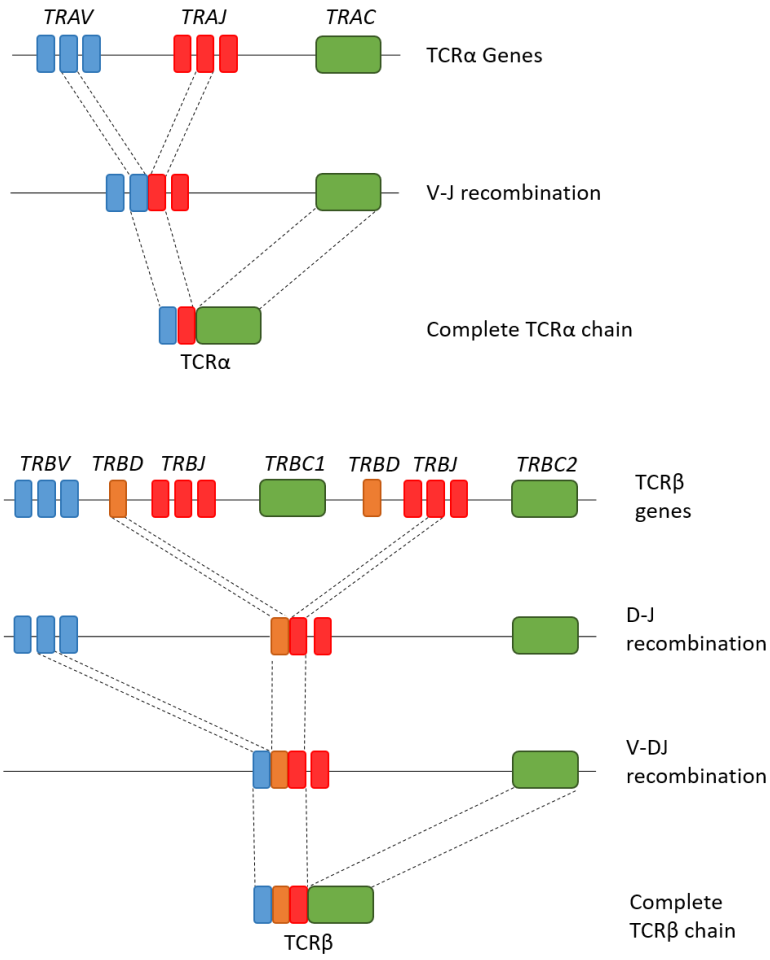

Figure 1.1. V(D)J recombination.
A schematic demonstrating gene recombination of the TCRα and TCRβ chains.

1.1.1.2. Thymic selection

For DP thymocytes to commit to either the $CD8^+$ or $CD4^+$ lineage, they must first undergo positive selection in the thymic cortex (**Figure 1.2**), where they interact with peptide:MHC (pMHC) molecules expressed on cortical thymic epithelial cells (cTECs) (Richie et al., 1998). The peptides presented by the MHCs expressed on cTECs are unique to cTECs due to the presence of cathspin L peptidase and thymus-specific serine proteases, which generate

thymus-specific peptide ligands (Nakagawa et al., 1998; Bowlus et al., 1999). The cTEC immunoproteasome is also unique, further facilitating the generation of cTEC-specific peptide ligands (Murata et al., 2007). The nature of the DP cell/cTEC pMHC interaction determines the lineage that a T-cell will commit to. Successful interaction with a class II pMHC (pMHC-II)-expressing cTEC results in DP thymocytes losing expression of CD8, whereas a successful interaction with a class I pMHC (pMHC-I)-expressing cTEC results in DP thymocytes losing expression of CD4. If a DP T-cell cannot maintain a persistent T-cell activation signal, it suffers death from neglect (Watanabe et al., 2000). Once a DP T-cell has committed to a lineage, one of the co-receptors is lost and they are then termed single positive (SP) thymocytes.

After positive selection, SP thymocytes migrate to the thymic medulla to undergo negative selection (**Figure 1.2**) (Kurobe et al., 2006). Medullary thymic epithelial cells (mTECs) express many self-antigens under the regulation of the autoimmune regulator transcription factor (Anderson et al., 2002). SP thymocytes cells that interact with these self-antigens too strongly are subsequently deleted to prevent autoreactive T-cells from entering the periphery. T-cells that pass negative selection migrate to the periphery as naïve T-cells expressing their TCR and a single co-receptor.

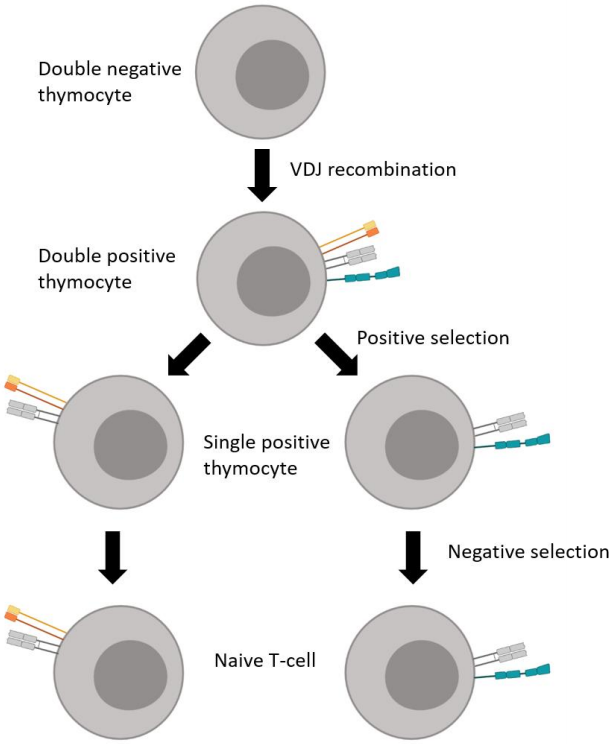

Figure 1.2. T-cell development.
A schematic showing the progression of a $CD8^+$ and a $CD4^+$ T-cell.

1.1.2. T-cell function

Interaction of the TCR and co-receptor with a target pMHC presented on a professional APC, in conjunction with secondary signalling mediated by CD28, results in the activation of naïve T-cells. Once activated, these T-cells undergo rapid proliferation and become effector T-cells. Once the pathogen is cleared, a large proportion of these effector T-cells are deleted. Some persist and differentiate into antigen-specific memory T-cells, allowing for faster responses to recurring pathogen infections (Bonilla et al., 2010). While both $CD8^+$ and $CD4^+$ T-cells share this process, the effector functions differ drastically depending on the co-receptors expressed.

1.1.2.1. $CD8^+$ T-cells

$CD8^+$ T-cells are responsible for direct killing of pathogen-infected cells. $CD8^+$ T-cells recognise intracellular pathogen-derived antigens presented on pMHC-I complexes (Elliott et al., 1990). These pMHC-I complexes are presented on almost all nucleated cells, including pathogenically-infected cells and professional antigen presenting cells (APCs) such as B-cells or dendritic cells (Reimann et al., 1997).

$CD8^+$ T-cells can induce apoptosis in target cells in response to activation by target pMHCs. $CD8^+$ T-cells can directly induce apoptosis via their surface-expressed Fas ligand (FasL), which is upregulated on activated T-cells. FasL is recognised by Fas, which is constitutively expressed on the surface of potential target cells (Arends et al., 1995). This interaction recruits the Fas-associated death domain (FADD) protein, which in turn activates the caspase cascade in the target cell (Carrington et al., 2006). $CD8^+$ T-cells can also trigger the caspase cascade through secretion of tumour necrosis factor (TNF) which binds TNF receptor 1, recruiting FADD (Schneider-brachert et al., 2004).

$CD8^+$ T-cells can also induce apoptosis indirectly via exocytosis of cytosolic granules containing cytotoxic proteins such as perforin and granzyme B. Perforin creates pores in the target cell membrane to allow cytotoxins such as granzyme B to enter the cell (Young et al., 1986). Granzyme B is a serine protease found in $CD8^+$ T-cells and NK cells that induces cellular apoptosis via multiple mechanisms such as inducing DNA fragmentation, activating caspases, and promoting mitochondrial permeability (Heusel et al., 1994; Adrain et al., 2005; Alimonti et al., 2001). Additionally, granzyme B has also been shown to have a proinflammatory function, contributing to viral suppression and immune regulation (Afonina et al., 2010).

1.1.2.2. CD4⁺ T-cells

$CD4^+$ T-cells carry out a variety of mechanisms designed to assist other components of the immune system. $CD4^+$ T-cells recognise extracellular pathogen-derived peptides presented by MHC-II molecules. These pMHC-II molecules are expressed on 'professional' APCs such as dendritic cells and B-cells. $CD4^+$ T-cells can differentiate into several different linages, each with their own function and cytokine repertoire (Geginat et al., 2013).

$CD4^+$ T-cell linages are generalised into several groups of varying function, including helper cells and regulatory cells. The primary $CD4^+$ helper T-cell linages are T-helper (Th)1, Th2 and Th17. Th1 cells are generated by IL-12 stimulation of undifferentiated $CD4^+$ T-cells and produce Interferon-γ (IFN-γ) under the influence of the transcription factor T-Bet. IFN-γ enhances inflammatory responses and the recruitment of macrophages (Szabo et al., 2000). Th2 cells are generated through IL-4 stimulation of undifferentiated $CD4^+$ T-cells and produce IL-4, IL-5, IL-10 and IL-13, under the influence of GATA3. These cytokines promote the humoral immune response by inducing IgE antibody production (Zheng et al., 1997). Th17 cells are generated by tumour growth factor-β (TGF-β) and IL-6 stimulation of undifferentiated $CD4^+$ cells, Th17 cells produce IL-17 under the influence of RORγt, allowing them to recruit neutrophils. Th17 cells also express the chemokine receptor CCR6, allowing them to migrate to inflamed tissues. Th17 cells are primarily recruited in response to fungal infections (Acosta-Rodriguez et al., 2007).

Further Th cell subsets include: Th1/17, Th22 and Th9. These are less well characterised than Th1, Th2, and Th17 cells. Th1/17 cells exhibit IFN-γ and IL-17 production and have been observed at the site of autoimmune disease (Cosmi et al., 2011). Th9 cells express IL-9 and exhibit anti-tumour properties (Purwar et al., 2012). Th22 cells are characterised by expression of IL-22, which helps regulate inflammation and a lack of IL-17 expression (Sara et al., 2009).

$CD4^+$ T-cells involved in regulating the immune response are also divided into subsets, including Tr1 cells and T-regulatory (Treg) cells. Tr1 cells regulate T-cell function through expression of IL-10, which suppresses T-cell activity (Uhlig et al., 2006). Treg cells are characterised by a $CD4^+/CD25^+$ phenotype and expression of FOXP3 (Fontenot et al., 2003). FOXP3 promotes cytotoxic T-lymphocyte-associated protein 4 (CTLA-4) expression, which

inhibits the maturation of APCs, thus indirectly suppressing effector T-cell activity. FOXP3 also inhibits IL-2 expression which reduces the abundance of IL-2 in the environment and restricts T-cell activity. Tregs can release cytotoxic proteins, such as perforin and granzymes, to destroy effector T-cells (Sakaguchi et al., 2010).

1.1.3. T-cell signalling cascade

Upon TCR recognition of a pMHC complex, the T-cell signalling cascade is triggered. There are several proposed models by which the signalling cascade is initiated. One model is called the 'conformational shift' model and involves conformational shifts in CD3 proteins, a series of protein dimers which are non-covalently linked to the TCR. There are two CD3 heterodimers, consisting of CD3γε and CD3δε, and a CD3γγ homodimer (Weiss et al., 1984). Conformational shifts in the CD3 proteins expose immunoreceptor tyrosine kinase associated motifs (ITAMs) on the cytoplasmic tails of the CD3ζ proteins, which are subsequently phosphorylated by Src family protein tyrosine kinases, such as Lck and Fyn (Mkaddem et al., 2017). Another model of T-cell activation is the 'kinetic segregation' model. This model proposes that, while the TCR is unbound, non-specific phosphorylation of the ITAMs is inhibited by CD45 and CD148. When the TCR successfully binds a pMHC, CD45 and CD148 are displaced as the extracellular domains of these phosphatases are too large to enter T-cell/target contact zones, allowing subsequent phosphorylation of the ITAMs by Src family protein tyrosine kinases (Choudhuri et al., 2005; Choudri et al., 2009; Van der Merwe, 2006). Evidence for both conformational shift and kinetic segregation models of TCR triggering suggests they may not be mutually exclusive.

The phosphorylation of the ITAM results in recruitment of another protein tyrosine kinase, ZAP-70. ZAP-70 activity results in activation of phospholipase-C-γ1 (PLC-γ1) (Sommers et al., 2005, Beach et al., 2007). The activation of PLC-γ1 results in hydrolysis of phospholipid phosphatidylinositol 4,5 bisphosphate ($PI(4,5)P_2$) into diacylglycerol (DAG) and inositol phosphate-3 (IP_3), both of which activate further signalling pathways. DAG principally activates two signalling pathways; the MAP kinase and PKCθ pathways. (Genot et al., 2000; Vallabhapurapu et al., 2009). IP_3 is responsible for activating the Ca^{2+} signalling pathway, which results in increased intracellular Ca^{2+} levels. (Savignac et al., 2007). Collectively, these signalling pathways result in the activation of various transcription factors, which allow expression of genes essential for T-cell function.

It is important to note that other proteins present on the T-cell surface can affect the T-cell signalling cascades. As mentioned in **Section 1.1.2**, CD28 is an example of a co-stimulatory receptor. CD28 binds CD80 and CD86 expressed on APCs and has been shown to enhance T-cell proliferation and the production of cytokines (Acuto et al., 2003). Conversely, the T-cell surface receptors programmed cell death protein 1 (PD-1) and CTLA-4, bound by PD ligand 1 (PD-L1) and CD80/CD86 on APCs respectively, are examples of co-inhibitory receptors which regulate T-cell activity (Nishimura et al., 2001; Waterhouse et al., 1995).

1.2. The TCR:pMHC interaction

1.2.1. T-cell receptor structure

The TCR is clearly of paramount importance to T-cell function. Our understanding of how engagement of the TCR by its pMHC ligand brings about T-cell activation has been greatly enhanced by TCR-pMHC atomic resolution co-structures (**Figure 1.3**). The earliest structure of a human TCR in the Protein Data Bank (PDB) was published in 1996 by Garboczi *et al.* This structure showed that the TCR is a cell surface heterodimeric protein, comprising α and β chains, which both possess a constant and a variable region (Garboczi et al., 1996). The constant region is proximal to the cell membrane and is largely conserved among different TCRs. The constant regions of both TCRα and TCRβ chains consist of an intracellular cytoplasmic tail, a transmembrane domain, a extracellular globular domain, and a connecting peptide which links the transmembrane domain to the extracellular domain (Bäckström et al., 1996). The extracellular component of the constant domain and the peptide that connects it to the transmembrane domain are primarily responsible for interactions between the TCR and the CD3 proteins (Dong et al., 2019).

The variable region of the TCR is distal to the cell surface and differs between different TCRs. At the most distal point of the variable region are beta turns collectively known as the complementarity determining region (CDR) loops. Each chain has three CDR loops; CDR1, CDR2 and CDR3. The CDR1 and CDR2 loops are encoded by the TCR V gene region and are thus germline encoded (Rudolph et al., 2002). The CDR3 loops by contrast are encoded by regions that span V, D and J genes, including the junctions created by recombination and are thus only partially germline encoded. Due to the insertion and deletion of random nucleotides at the recombination sites, the CDR3 loops exhibit greater variability than CDR1 and CDR2 (Hughes et al., 2003). These CDR loops are highly flexible and are largely responsible for the antigen specificity of a TCR (Garcia et al., 1998).

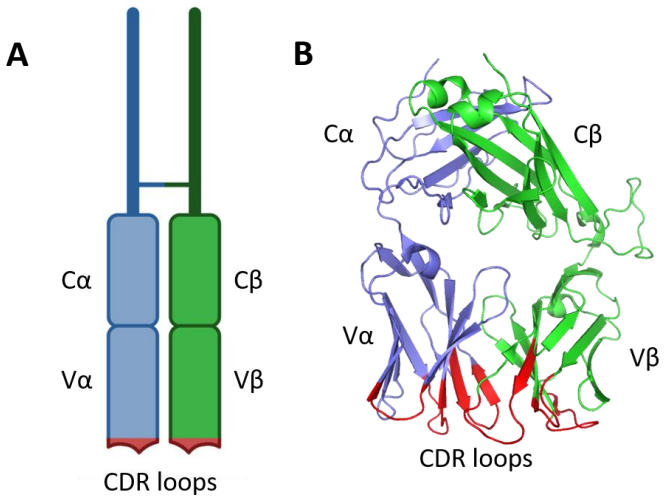

Figure 1.3. T-cell receptor structure.
The structure of a TCR shown as a schematic (**A**) and as a 3D crystal structure (**B**). TCRα chain (blue), TCRβ chain (green) and TCR CDR loops (red) are shown.

1.2.2. MHC antigen-processing

As discussed in **Section 1.1.2**, pathogen-derived peptides are presented to T-cells by MHC molecules in order to illicit an immune response. The process by which proteins are processed into suitable peptide fragments and loaded onto MHCs is known as antigen processing (**Figure 1.4**).

For loading onto MHC-I molecules (**Figure 1.4A**), intracellular proteins are first processed into small peptide fragments. This is achieved by proteases, or by the proteasome following ubiquitination (Rock et al., 2010). For the purpose of antigen processing, the standard proteasome works in tandem with a modified proteasome, known as the immunoproteasome (Rock et al., 2002). Conventionally the proteasome contains three catalytic subunits; β1, β2 and β5. However, under influence of IFN-γ, these subunits are replaced by LMP2, LMP7, and LMP10, resulting in the immunoproteasome (Ortiz-Navarrete et al., 1991). Proteasome cleavage results in peptide fragments of 11-14 amino acids in length. Peptides formed via the immunoproteasome have C-terminal anchors favourable to MHC binding (Schwarz et al., 2000). These peptide fragments are transported to the endoplasmic reticulum (ER) via the transporter associated with antigen processing (TAP) (Neefjes et al., 1993).

Once in the ER, peptide fragments are held by TAP and subjected to further trimming by endoplasmic reticulum aminopeptidase (ERAP) 1 and 2, which trim the N-terminal ends of the peptides to a more suitable length for MHC binding (Evnouchidou et al., 2014; Saric et

al., 2002). Prior to peptide loading onto the MHC, the peptide loading complex (PLC) is formed. The PLC consists of TAP, ERp57, tapasin, and the MHC-I (Koch et al., 2006). ERp57 is responsible for binding chaperones calnexin and calreticulin to the PLC (Morrice et al., 1998; Oliver et al., 1999). Tapasin is responsible for ERp57 association and stabilisation of the PLC. Tapasin also regulates MHC peptide loading by catalysing the release of sub-optimal peptides (Howarth et al., 2004). Once the peptide is loaded onto the MHC-I molecule, the now stable pMHC-I is transported through the Golgi network and presented on the cell surface.

The MHC-II presentation pathway differs from the MHC-I presentation, despite achieving a similar outcome. The MHC-II molecule is assembled in the ER and stabilised with the CD74 invariant chain (Ii). This MHC-II-Ii complex is transported via vesicles to the MHC-II compartment (MIIC), a late stage endosome (Blum et al., 1988). Meanwhile, extracellular proteins that are endocytosed into the cell are processed by aspartyl and cysteine proteases in endosomes, producing small peptide fragments (Norton et al., 2009). These peptide fragments are transported to the MIIC where they replace the Ii in the MHC-II binding groove (Mellins et al., 2014). Once peptide loading is complete the resulting pMHC is transported to the cell-surface.

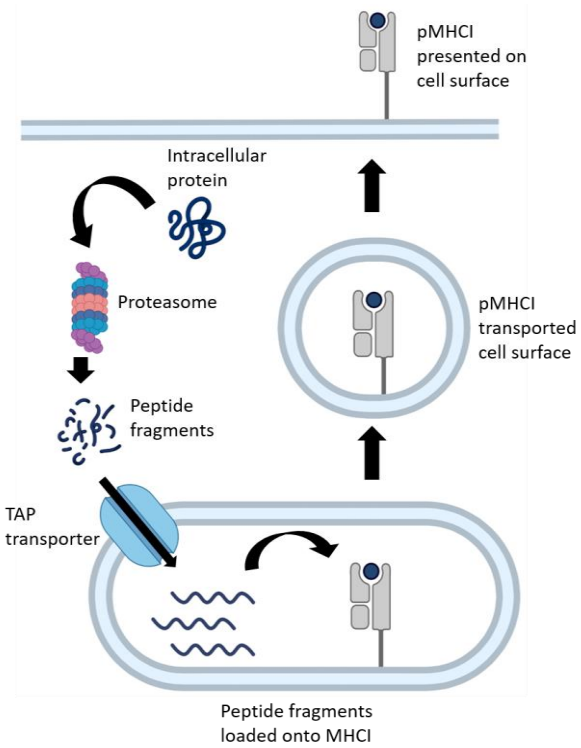

Figure 1.4. MHC class-I peptide presentation.
A schematic showing how peptides are processed and presented by class-I MHC.

1.2.3. MHC structure

Like the TCR, the MHC-I is a cell surface heterodimeric protein (**Figure 1.5A**). MHC-I consists of a heavy chain and a β_2 microglobulin (β_2M) chain. In humans, the MHC-I heavy chain is determined by expression of a human leukocyte antigen (HLA)-I gene. Each individual expresses both maternally and paternally inherited HLA-I alleles for three common HLA-I genes; *HLA-A*, *HLA-B*, and *HLA-C*. According to the European Bioinformatics Institute (EBI), at the time of writing there are 6,291 known alleles of *HLA-A*, 7,562 known alleles of *HLA-B*, and 6,223 known alleles of *HLA-C* (European Bioinformatics Institute, 2020). The large number of HLA-I alleles reflect the fact that the HLA-I genes are highly polymorphic. Conventionally, MHC molecules are named after their alleles. The earliest human MHC-I crystal structure in the PDB was published by Bjorkman *et al.*, and features a HLA-A*02:01 molecule (HLA-A2 henceforth), the most common HLA-I gene allele among the western population (Bjorkman et al., 1987; Krausa et al., 1995)

The MHC-I heavy chain is made up of α1, α2, and α3 domains, with the α1 and α2 domains located at the membrane distal end of the MHC-I, and the α3 domain and β_2M molecule located at the membrane proximal end. The α3 domain contains the transmembrane region, anchoring the MHC-I to the cell. The α1 and α2 domains form the peptide binding groove, made up of alpha helical structures which surround the presented peptide. In the case of MHC-I molecules, the binding groove generally accepts peptides between 8-12 amino acids in length. Peptides of 8 amino acids in length lie flat in the MHC-I binding groove; longer peptides can be accommodated but are forced to bulge out of the peptide-binding groove as the groove is closed at both ends (Speir et al., 2001). The peptide presented has a substantial impact on the MHC molecule as a whole, impacting its thermal stability and its molecular flexibility (Hawse et al., 2013; Fuller et al., 2017).

The first MHC-II structure (**Figure 1.5B**), published in 1993, demonstrated the differences and the similarities between class-I and class-II MHC molecules (Brown et al., 1993). Both molecules are cell surface proteins and have a cell membrane-distal peptide binding groove, composed of alpha helical structures. The MHC-II binding groove has an open conformation, allowing presentation of longer peptides than the MHC-I. This results in a peptide 'core' within the groove and peptide 'flanks' outside the groove. It has been demonstrated that both the core and the flanks of the peptide are important in TCR recognition (Maclachlan et al., 2019; Holland et al., 2020).

The MHC-II molecule is a heterodimer consisting of α and β chains, rather than the heavy chain-β_2M composition seen in MHC-I molecules. The MHC-II α and β chains are governed by expression of HLA-II genes. There are three common HLA-II types: *HLA-DP*, *HLA-DQ*, and *HLA-DR*, with *A* and *B* variants of each for expression of MHC-II α and β chains respectively. HLA-II alleles also highly polymorphic, with 1,681 *HLA-DP* alleles, 2,448 *HLA-DQ* alleles, and 3,565 *HLA-DR* alleles, according to the EBI (European Bioinformatics Institute, 2020).

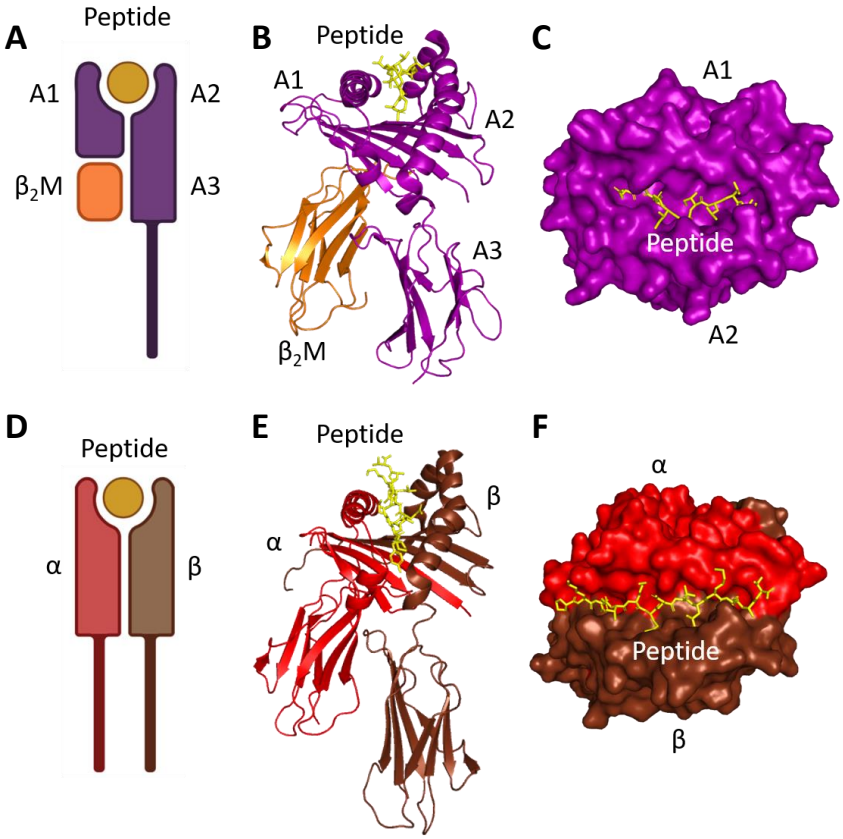

Figure 1.5. Class I and class II pMHC structures.
(**A-C**) The structure of a class I pMHC shown as a schematic (**A**), as a 3D crystal structure (**B**), and from a top-down perspective (**C**). Heavy chain subunits (magenta), β_2M subunits (orange) and peptide (yellow) are shown. (**D-F**) The structure of a class II pMHC shown as a schematic (**D**), as a 3D crystal structure (**E**), and from a top-down perspective (**F**). A-chain (red), β-chain (brown) and peptide (yellow) are shown.

1.2.4. CD4 and CD8 co-receptor structures

As well as binding the TCR, the pMHC has an important role facilitating the interaction with the T-cell co-receptors. As discussed in **Section 1.1**, conventional T-cells generally express either CD4 or CD8. The co-receptors have two principle functions: to deliver the src family tyrosine kinase Lck (see **Section 1.1.4**) to the CD3 complex, allowing the subsequent signalling pathway to occur (Artyomov et al., 2010); and to impose MHC restriction on the T-cell in the thymus (Laethem et al., 2012).

Each co-receptor also has its own unique functions. The CD8 co-receptor is a membrane-bound glycoprotein dimer, traditionally composed of two alpha subunits (CD8αα), or alpha and beta subunits (CD8αβ). The CD8αα co-receptor can regulate T-cell signalling by sequestering Lck away from the TCR, thus reducing signal transduction (Cheroutre et al., 2008), where CD8αβ has been shown to aid T-cell activation in the periphery (Moebius et al., 1991). Each CD8 subunit consists of an Ig-like domain and a long stalk structure which connects the Ig-like domain to the cell membrane (Gao et al., 1997) (**Figure 1.6A**). During TCR recognition, CDR3-like loops on the CD8αβ co-receptor bind the MHC-I molecule at the α3 domain with relatively weak affinity (Wang et al., 2009; Wyer et al., 1999). The stalk domain can exhibit a regulatory function in CD8αβ co-receptors. Once positive selection has occurred, the CD8αβ stalk is glycosylated with *O*-linked glycans via sialylation, which reduces its affinity for MHC-I molecules. This means the TCR must recognise peripheral antigens with a greater affinity than thymic antigens to activate an immune response, reducing the likelihood of autoreactivity (Daniels et al., 2001).

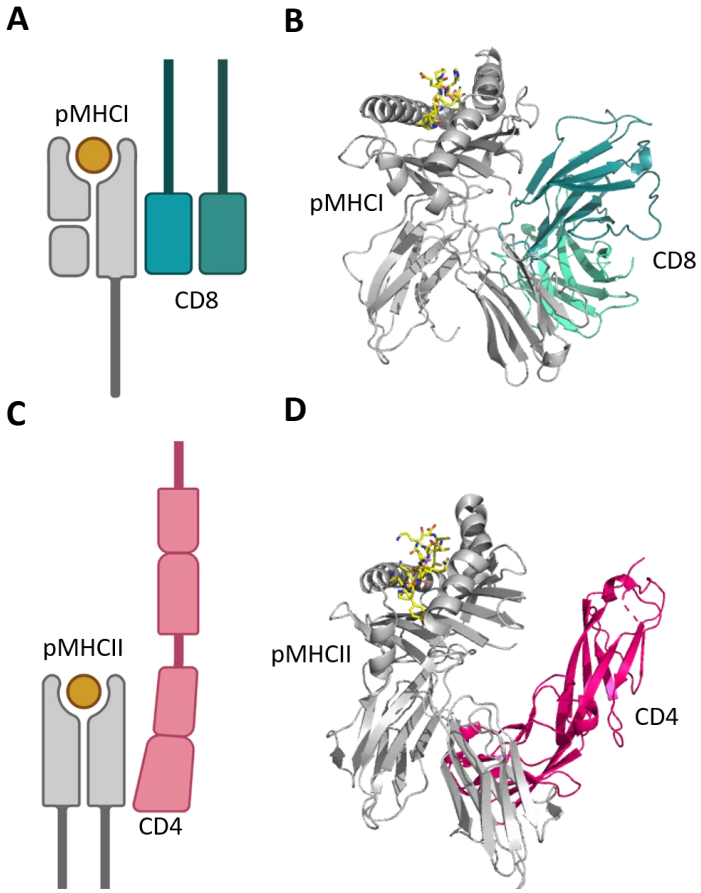

Figure 1.6. CD4 and CD8 co-receptor structures.
(**A-B**). The structure of a CD8 co-receptor in complex with a class-I pMHC molecule, shown as a schematic (**A**), as a 3D crystal structure (**B**). pMHC (grey), peptide (yellow) and CD8 co-receptor (blue) are shown. (**C-D**). The structure of a class II pMHC shown as a schematic (**C**), as a 3D crystal structure (**D**). pMHC (grey), peptide (yellow) and CD4 co-receptor (pink) are shown.

In contrast to CD8, CD4 is a monomeric membrane bound glycoprotein with a substantially weaker binding affinity to MHC-II than CD8 has to MHC-I (Davis et al., 2003). It has been suggested that this low affinity reduces autoimmune activity in the periphery (Li et al., 2013). CD4 comprises of four extracellular domains (D1, D2, D3, and D4) and a small stalk connecting to the transmembrane domain (**Figure 1.6b**). During TCR recognition, CD4 binds the α2 and β2 domains of MHC-II. The contact residues involved in both α and β chains of the MHC-II are conserved across HLA-II alleles, allowing universal binding of CD4 (Xiang et al., 2011).

1.2.5. TCR recognition of the pMHC complex

1.2.5.1. Structural mechanisms of TCR:pMHC recognition

The interaction between the TCR and the pMHC lies at the heart of T-cell biology (**Figure 1.7**). The 1996 TCR-pMHC crystal structure by Garboczi *et al.* demonstrated the core binding mechanisms involved in this interaction. The interaction typically involves the TCR docking over the pMHC at an angle which situates the TCR alpha chain above the MHC α2 domain and the TCR beta chain above the MHC α1 domain. Conventionally, the germline-encoded CDR1 and CDR2 loops of the TCR interact with the alpha helices of the MHC that form the peptide binding groove (Garboczi et al., 1996).

The TCR:pMHC binding mode remains largely conserved among different TCR:pMHC complexes, however, specific mechanical details differ between complexes. For example, when in complex with HLA-A2-presented Melan-A/MART1-derived epitope (EAAGIGILTV), the DMF5 TCR adopts a binding angle that favours germline interaction with the peptide. The DMF5 TCR tilts to such a degree that it leaves CDR3α further away from the peptide than the consensus binding mode would expect, resulting in CDR3α making very few contacts with either the peptide or the MHC molecule. Instead, it is the CDR1α loop that makes most of the peptide contacts (Borbulevych et al., 2011). In another example, when the G4 TCR binds an HLA-DR1-presented triose phosphate isomerase epitope (GELIGILNAAKVPAD), the CDR3α loop of the G4 TCR binds the peptide prior to the CDR1α interaction with the pMHC. Due to the steric interference caused by the relatively large CDR3α loop upon binding to the peptide, the G4 CDR1α is forced further away from the peptide than is conventionally observed (Deng et al., 2012).

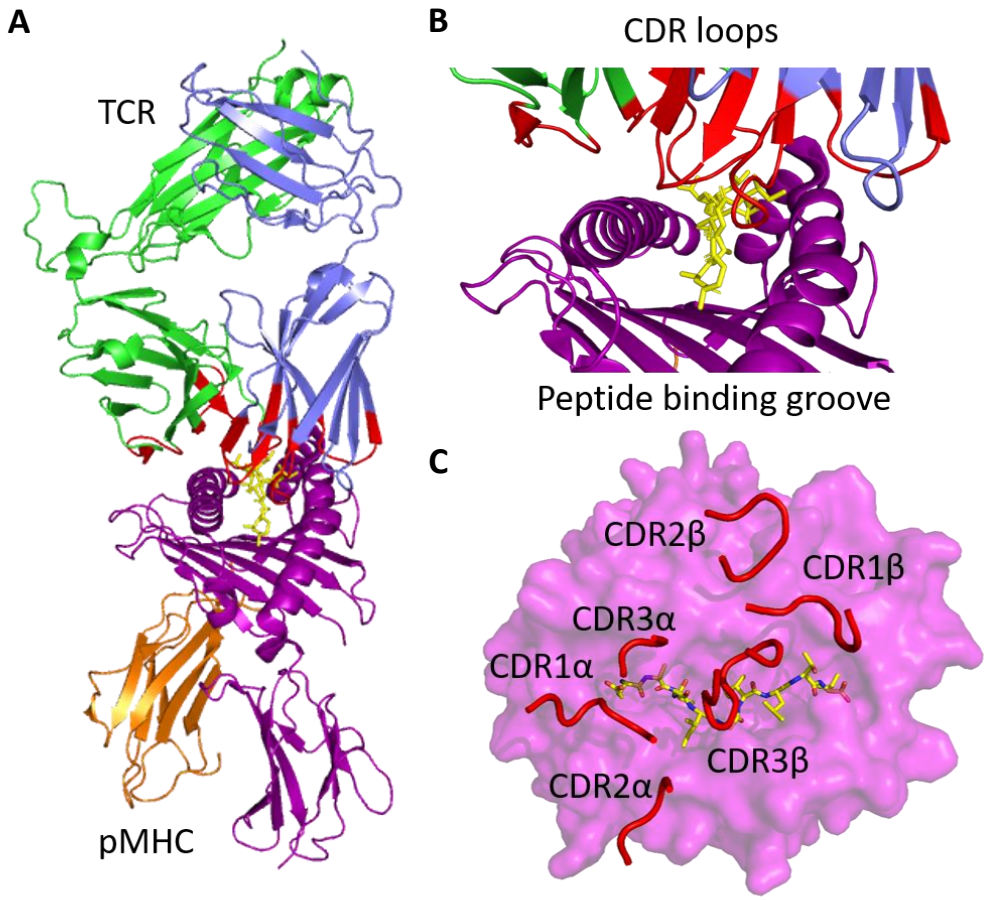

Figure 1.7. TCR:pMHC complex structure.
(**A**) The structure of a TCR:pMHC complex. (**B**) A close up of the TCR:pMHC interaction (**C)** Top-down view showing TCR CDR loops over a pMHC molecule. TCRα chain (blue), TCRβ chain (green), TCR CDR loops (red), pMHC heavy chain subunits (magenta), β_2M subunits (orange) and peptide (yellow) are shown.

CDR loops can retain flexibility after the TCR:pMHC binding event has occurred. The 2C TCR recognises the QL9 peptide in the context of H-2L^d, but NMR studies show that the flexibility of the 2C CDR3β loop is not quenched by the formation of the complex. The QL9 peptide was also shown to retain flexibility while in complex with the 2C TCR. Synchronised flexibility on the part of the peptide and the CDR3β results in a thermodynamically stable complex, as the 2C CDR3β loop can accommodate changes in the equally flexible QL9 peptide (Hawse et al., 2014).

Complex crystal structures published in the last decade have demonstrated just how far TCR:pMHC interactions can deviate from the consensus binding mode. Studies by Beringer *et al*. and Gras *et al.* describe TCRs that adopt reverse modes of binding to MHC-II and MHC-

I molecules respectively (Beringer et al., 2015; Gras et al., 2016). The TCRα and TCRβ chains of these TCRs are fixed over the α1 and α2 helices of the pMHC respectively, exhibiting a 180^{o} rotation compared to the consensus binding mode. Furthermore, the interactions highlighted by Gras *et al.* show CDR1α loops interacting with the peptide, whilst the CDR3α loop interacts with the MHC. While these TCRs are generally considered to be outliers, and exhibit relatively poor signalling capabilities, they demonstrate how just flexible the TCR:pMHC interaction can be (Beringer et al., 2015; Gras et al., 2016).

1.2.5.2. TCR germline bias

Despite the inherent flexibility of the TCR, its characteristics are heavily influenced by germline gene usage (**Section 1.1.1.1**). The gene exons selected for recombination for a particular TCR bias it towards certain peptide antigen by conferring biochemical properties on its germline-derived CDR1 and CDR2 loops. This is termed TCR germline bias (Garcia et al., 2009; Turner et al., 2006).

A 2003 study showed that almost all T-cells that recognise the Epstein-Barr virus (EBV)-derived peptide FLRGRAYGL in the context of HLA-B*08 share the same TCR gene usage across different individuals. TCRs that are present in multiple individuals are known as 'public' TCRs (Venturi et al., 2008). Most HLA-B*08-FLRGRAYGL-specific TCRs exhibited *TRAV26-2* and *TRAJ5-2* alpha chain gene usage, with *TRBV7-8* and *TRBJ2-7* beta chain usage (Kjer-Nielsen et al., 2003). A similar bias was also demonstrated in T-cells recognising the influenza-derived peptide GILGFVFTL in the context of HLA-A2. These T-cells exhibited *TRBJ17* usage, as well as a conserved IRSSY stretch in the germline encoded section of the CDR3β loop (Lehner et al., 1995; Stewart-jones et al., 2003). A bias towards *TRAV12-2* gene usage was observed in T-cells recognising the yellow fever-derived peptide LLWNGPMAV in the context of HLA-A2 (Bovay et al., 2018). *TRAV12-2* gene usage has also been observed in T-cells recognising a melanoma-derived peptide (Cole et al., 2009). Based on structural data, it would appear that this bias results in a binding interface where, unconventionally, the CDR1α chain often makes the majority of peptide contacts, rather than CDR3α (Cole et al., 2009). TCR germline bias is also present in TCRs that recognise class II MHC molecules. CD4^{+} T-cells recognising the influenza-derived PKYVKQNTLKLAT peptide in the context of HLA-DR1 have been shown to largely adopt *TRAV2* gene usage (Greenshields-Watson et al., 2020).

1.2.5.3. Structural basis of MHC restriction

TCR:pMHC interactions are governed by MHC restriction. It has been proposed that TCRs are MHC-restricted because they possess an intrinsic germline-encoded bias towards MHC molecules. A study by Tynan *et al.* described a 'restriction triad' on MHC-I molecules. The triad (composed of residues 65 and 69 on the MHC α1 helix and residue 155 on the MHC α2 helix) consistently interacted with the germline-encoded CDR1 and CDR2 loops of the TCR. This was observed in multiple TCR:pMHC structures, suggesting the triad was critical in MHC-I restriction and that TCRs are intrinsically biased for MHC (Tynan et al., 2005). Further evidence in support of the germline-encoded bias theory was reported by Feng *et al.* who observed the presence of certain amino acid residues on the TCR CDR1 and CDR2 loops which are required for MHC class II recognition (Feng et al., 2007).

In contrast to the theory of TCR germline bias is the belief that TCRs are not inherently MHC-restricted, but that this restriction is imposed upon them by the presence of the CD4/CD8 co-receptors. Van Laethem *et al.* showed that MHC-deficient mice lacking CD8 and CD4 co-receptors could produce functional T-cell repertoires. T-cells in these MHC-deficient mice could react to ligands independently of MHC molecules. This indicated that without the co-receptors, TCR antigen recognition is no longer MHC restricted (Laethem et al., 2007). Burrows *et al.* then showed that the proposed 'restriction triad' was not essential for TCR recognition of pMHC-I molecules, and that mutations in the restriction triad residues on the MHC did not always result in loss of T-cell activation. This is due to the formation of compensatory interactions between the TCR and pMHC, restoring TCR recognition. Furthermore, where mutations in the restriction triad did result in loss of T-cell activation, expression of the CD8 co-receptor was sufficient to restore T-cell activation (Burrows et al., 2010). Yin *et al.* demonstrated how the YAe62 TCR could recognise peptides in the context of both pMHC-I and pMHC-II molecules. This versatility was facilitated by conformational changes in the CDR loops of the TCR (Yin et al., 2011). The wide-ranging mechanisms by which a TCR can recognise multiple ligands are discussed further in **Section 1.3**. While there is still debate surrounding the role of the TCR germline sequence in MHC restriction, the above evidence suggests the CD4/CD8 co-receptors play an important role.

1.2.5.4. Biophysical properties of the TCR:pMHC interaction

Beyond imposing MHC restriction, the CD8 and CD4 co-receptors play a role in the affinity of the TCR:pMHC interaction. The binding affinity (K_D) of the TCR:pMHC interaction is measured

using the equation K_D = [TCR][pMHC]/[TCR:pMHC] and varies considerably between pMHC ligands. TCR binding affinity to viral-, bacterial-, and self-derived pMHCs conventionally measure at 1-10 µM, 10-100 µM, and >100 µM respectively (Bridgeman et al., 2011). Based on previous studies, it appears that TCRs on $CD8^+$ T-cells bind with higher affinities to their pMHC targets than those $CD4^+$ T-cells (Bridgeman et al., 2011; Davis et al., 2003). However, $CD8^+$ T-cell activation by lower affinity pMHCs (>200 µM) in culture usually critically depends on the CD8 co-receptor (Laugel et al., 2007). Furthermore, increasing the affinity between the CD8 co-receptor and the pMHC can allow the TCR to recognise lower affinity peptides (Wooldridge et al., 2010).

Another facet of the TCR:pMHC interaction is binding kinetics. The observation that TCRs with similar binding affinities to pMHC molecules can exhibit different activation potencies suggests other biophysical properties of such interactions are better determinants of T-cell activity (Kersh et al., 1998). TCR:pMHC interaction association rates (K_{on}) have a mean of approximately 3.8×10^4 M^{-s} s^{-1}, and the dissociation rates (K_{off}) have a mean of approximately 0.24 s^{-1}. MHC restriction has been shown to affect interaction kinetics, where the TCR:pMHC-I interaction exhibits a faster on-rate than the TCR:pMHC-II interaction (Cole et al., 2007; Willcox et al., 1999).

A function of K_{off} is the half-life of the TCR:pMHC interaction ($t_{1/2}$), which has been identified as a correlate of T-cell activation (Bridgeman et al., 2011). This correlation forms the basis of the 'kinetic proofreading' theory, which postulates that TCR:pMHC interaction has an optimal $t_{1/2}$ to allow sufficient contact time for T-cell signalling to occur, while allowing the T-cell to rapidly engage with subsequent targets (McKeithan, 1995). The kinetic proofreading theory has been supported by studies that demonstrate that TCR:pMHC interactions which fall outside of the optimum $t_{1/2}$ result in poor T-cell activity (Kalergis et al., 2001; Carreno et al., 2007; Limozin et al., 2019). However, there are recorded examples of TCR:pMHC interactions which do fall outside of the optimum $t_{1/2}$ that result in T-cell function, as well as examples where other biophysical properties correlate with TCR binding (Boulter et al., 2007; Bridgeman et al., 2011; Weber et al., 2005). As such, while $t_{1/2}$ is clearly an important factor in the TCR:pMHC interaction, a full grasp of its biophysical properties are required to fully understand the interaction.

It is worth noting that data relating to TCR:pMHC interaction biophysical properties are often based on experiments carried out at 25°C, rather than the more physiologically relevant temperature of 37°C. Willcox *et al.* highlighted the thermodynamic profile of the TCR:pMHC interaction and demonstrated how the biophysical properties are altered by temperature (Willcox et al., 1999). Furthermore, experiments measuring TCR:pMHC interaction biophysical properties involve monovalent interactions measured *in vitro* in three dimensions using soluble TCR and pMHC monomers (Stone et al., 2009). *In vivo* however, the TCR:pMHC interaction is multivalent within the two dimensional diffusion environment of two lipid bilayers (Stone et al., 2006). TCR clustering has been observed and has been shown to positively affect T-cell signalling (Pageon et al., 2016). The significance of this multivalence has been demonstrated by Li *et al.*, who showed that surface plasmon resonance (SPR), a monovalent technique, failed to detect the 3A6:DR2-VHFFKNIVTPRTP interaction, whereas pMHC tetramer staining, a multivalent technique, successfully detected the interaction (Li et al., 2005). T-cell activity *in vivo* is also affected many factors beyond the TCR:pMHC interaction, which complicates the task of correlating TCR:pMHC biophysics with T-cell activity.

1.3. T-cell cross-reactivity

In 1957 the 'clonal selection theory' was postulated by Frank MacFarlane Burnet, which states that a lymphocyte can only interact with a single antigen (Burnet, 1957). In the years that followed however, cases of T-cells recognising multiple peptide epitopes began to emerge. It was found that T-cells that recognise self-peptides can also recognise pathogenic peptides (Bhardwaj et al., 1993; Wucherpfennig et al., 1995). It was also found that a TCR may bind to multiple peptides, albeit with differing activation intensities, providing key residues were conserved (Reay et al., 1994).

In 1998, Don Mason calculated that the number of different T-cells required by a mouse to recognise all potential antigens would necessitate a spleen orders of magnitudes larger than the mouse itself. Mason's calculations, in conjunction with emerging evidence of T-cells recognising multiple peptide epitopes, resulted in his proposal of the 'Mason hypothesis'. This hypothesis suggests a lymphocyte can recognise multiple antigens, a characteristic termed cross-reactivity, thus allowing a smaller repertoire of lymphocytes to recognise all potential pathogens (Mason, 1998).

Further experimental evidence came from a 1999 study by Arstila *et al.* which predicted that the total number of different human TCRs is $<10^8$ and demonstrated that this would not be enough to recognise all potential pathogenic peptide sequences (Arstila et al., 1999). In 2012, my laboratory demonstrated that a single T-cell has the potential to recognise over one million different peptides, highlighting the extent of TCR degeneracy (Wooldridge et al., 2012). While the T-cell characteristic of cross-reactivity is now largely accepted, investigations into the mechanisms by which it occurs, as well as its consequences for immune function, are still ongoing.

1.3.1. Mechanisms of T-cell cross-reactivity

1.3.1.1. Molecular mimicry

Early evidence of TCR degeneracy emerged in 1996. Kersh *et al.* made single point mutations to the Asn9 residue of a peptide derived from murine haemoglobin (GKKVITAFNEGLK), which is recognised by the 3.L2 TCR when in complex with murine MHC I-K^E. Twelve altered peptide ligands (APLs) of the GKKVITAFNEGLK peptide were made, some of which contained non-natural amino acids. Of the twelve GKKVITAFNEGLK APLs, nine were recognised by the 3.L2 TCR, with varying degrees of reactivity. This study showed that TCR recognition would still occur despite peptide sequence differences (Kersh et al., 1996). The amino acid substitutions made in APLs successfully recognised by 3.L2 were structurally similar to the original Asn9 residue they were replacing, suggesting the 3.L2 TCR interacts with the APLs in a similar fashion. This phenomenon where a protein interacts with two different peptides which share structural characteristics is known as molecular mimicry (**Figure 1.8**).

An example of molecular mimicry was demonstrated by my laboratory using a selection of APLs derived from human telomerase. The APLs were recognised by the ILA TCR in the

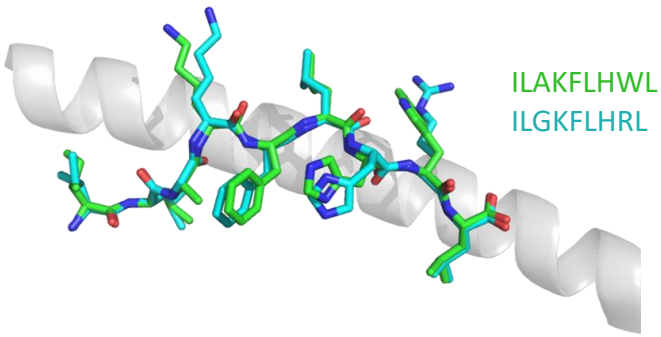

Figure 1.8. Example of molecular mimicry.
3D structures of ILAKFLHWL (green) and ILGKFLHRL (blue) peptides, both of which interact with the ILA TCR (Cole et al, 2017).

context of HLA-A2. The interaction of the ILA TCR with the 'wild-type' telomerase peptide (ILAKFLHWL) is highly focused on the Lys4 and Trp8 residues. However, substituting the Trp8 for threonine or tyrosine not only resulted in mechanically similar interactions, but increased binding affinity (Cole et al., 2017).

1.3.1.2. Hotspot binding

A key mechanism of T-cell cross-reactivity is 'hotspot' binding. This is where a T-cell can recognise multiple peptides based on conserved motifs within the peptide, termed recognition hotspots. Focused recognition on peptide motifs allows for extensive variability outside of the motif without loss of recognition (Wilson et al., 2004). A study by Adams *et al.* examined the 4F32 TCR, which recognises the artificial QL9 peptide (QLSPFPFDL) in the context of the murine MHC H-2L^{d}. Using yeast display, APLs were generated from the QL9 peptide with varying degrees of sequence homology and all were recognised by the 42F2 TCR with differing affinities. Structural data showed a conserved set of interactions for all APLs, where an Asp95-Ala-96-Pro97 stretch on the CDR3β chain interacts with residue 7 of the peptide, providing this residue is hydrophobic (Adams et al., 2016).

A 2016 study by my laboratory described cross-reactivity facilitated by hotspot binding. In this study, APLs were produced based on an HLA-A2-presented preproinsulin (PPI)-derived peptide (ALWGPDPAAA) which is recognised by the 1E6 TCR. Crystallography and SPR showed that 1E6 could bind to all seven APLs, along with the wild-type peptide, despite some APLs exhibiting only 30% sequence homology. The 3D structures of these interactions showed that the 1E6 TCR centred on a xxxGPDxxxx motif common in all peptides studied, suggesting this hotspot was essential for recognition (Cole et al., 2016). A study by Holland *et al*. shows that the use of hotspot binding positively correlates with TCR promiscuity (Holland, et al., 2020).

1.3.1.3. TCR recognition of dissimilar antigens

The studies highlighted above show examples of TCR degeneracy where the TCR:pMHC interaction mechanism is largely conserved across multiple ligands. However, there are also examples where a TCR or pMHC may undergo large structural changes to achieve recognition of different ligands (**Figure 1.9**). Riley *et al.* examined the interaction between the DMF5 TCR and two HLA-A2-restricted peptide ligands; a Melan-A-derived ligand (EAAGIGILTV), and a ligand produced via yeast display (MMWDRGLGMM) known as the DRG ligand (Gee et al.,

2018). Previous work had already highlighted the importance of the Melan-A xxxGIGxxxx motif for recognition via the DMF5 TCR (Borbulevych et al., 2011). Yet despite the DRG ligand lacking this motif, the DMF5 TCR recognised the DRG peptide. Further to this, HLA-A2 presents the Melan-A and DRG peptides in different ways. According to 3D structures, the DMF5-A2-DRG interaction causes the DRG peptide to undergo a conformation shift to allow binding. This is coupled with small changes in the CDR loops to accommodate the greater steric footprint of the DRG peptide (Riley et al., 2018).

Conformational shifts, in CDR3 loops in particular, have been implicated in TCR cross-reactivity. The Yin *et al.* study highlighted in **Section 1.2.5.3** demonstrates CDR3 flexibility. As briefly discussed, the YAe62 TCR can recognise two synthetic peptides, pWM (WIYVYRPM) and 3K (ASFEAQKAKANKAVD), in the context of H-2K^{b} and IA^{b} respectively. Structural data

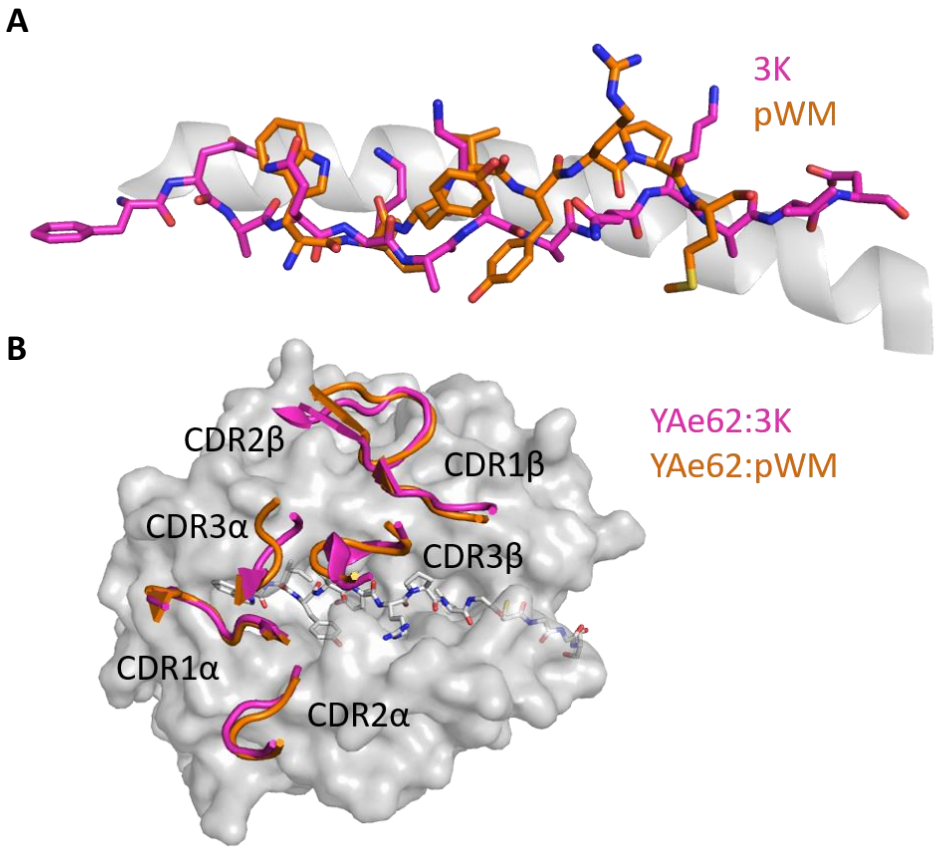

Figure 1.9. Example of peptide/CDR loop conformational shifts to enable cross-reactivity.
(**A**) 3D structures of 3K (magenta) and pMK (orange) peptides, both of which interact with the YAe62 TCR. (**B**) Top-down view showing YAe62 CDR loops (blue and red) when interacting with 3K and pMK respectively.

shows that when interacting with the pWM peptide, the YAe62 CDR3α loop makes multiple contacts with both the peptide and the H-2K^{b} molecule. However, when the YAe62 TCR interacts with the 3K peptide in the context of IA^{b} the CDR3α loop only makes minimal contacts with the IA^{b} molecule and makes no contacts with the peptide. These differences occur due to a conformational shift in the CDR3α backbone (Yin et al., 2011).

A study by Reiser *et al.* highlighted how the BM3.3 TCR can recognise two synthetic peptides, VS8 (RGYVYQGL) and pBM1 (INFDFNTI), which exhibit no sequence homology, in the context of murine H-2K^{b} (Reiser et al., 2000). The structural data showed how the CDR3α loop bends away from peptide in the BM3.3:pBM1 structure, resulting in contact with the α1 helix of the MHC. By contrast, the BM3.3:VS8 structure showed the CDR3α loop pointing towards the N-terminus of the peptide, thus creating contacts with the peptide (Reiser et al., 2003).

1.3.1.4. TCR recognition of multiple MHC alleles

The BM3.3 TCR can cross-react with different MHCs. As well as recognising the aforementioned VS8 and pBM1 peptides, BM3.3 can also recognise an endogenous RNA-binding protein-derived peptide, pBM8 (SQYYYNSL), in the context of H-2K^{bm8}, an allelic variant of H-2K^{b}. There are four polymorphisms between H-2K^{b} and H-2K^{bm8}, two of which are present in the peptide binding groove (Auphan-Anezin et al., 2006). Mazza *et al.* solved the structure of the BM3.3 TCR in complex with H-2K^{bm8}:pBM8 showing how the CDR3α undergoes a conformational shift to accommodate the different pMHC (Mazza et al., 2007).

The AGA1 TCR can recognise an HIV-1-derived peptide, KF11 (KAFSPEVIPMF), in the context of two HLA-B*35 alleles; *HLA-B*3501* and *HLA-B*3503*. These alleles differ by polymorphisms at positions 114 (Asp-Asn) and 116 (Ser-Tyr). While the polymorphisms between *HLA-B*3501* and *HLA-B*3503* only cause minor differences in peptide presentation, these differences result in slight adjustments in the AGA1 CDR loops to accommodate them. These AGA1 CDR loop rearrangements result in altered hydrogen bond networks between the TCR and positions 114 and 116 of the MHC. The AGA1 TCR also has a lower affinity for HLA-B*35:01-KF11 than HLA-B*35:03-KF11, demonstrating the impact just two MHC polymorphisms can make to TCR affinity (Stewart-Jones et al., 2012).

The 2C T-cell can recognise the aforementioned QL9 peptide (QLSPFPFDL) and a self-derived peptide, DEV8 (EQYKFYSV), in the context of H-2L^{d} and H-2k^{b} respectively. Structural data

shows similarities between the H-2L^d:DEV8 and H-2K^b:QL9 pMHC molecules, however the 'bulge' in the centre of the QL9 peptide protrudes further out of the peptide binding groove than the DEV8 peptide. Furthermore, the 2C TCR CDR3α loop adopts a different conformation depending on which pMHC it is bound to. When bound to H-2L^d:DEV8, the 2C TCR CDR3α loop primarily interacts with the central residues of the DEV8 peptide. Conversely, when bound to H-2K^b:QL9, the 2C TCR CDR3α loop shifts confirmation to interact predominantly with C-terminal QL9 peptide residues (Colf et al., 2007).

1.3.1.5. TCR germline influence of T-cell cross-reactivity

In **Section 1.2.6.2**, I discussed the theory of 'germline bias', where TCR recognition is influenced by germline-encoded CDR loops. Expanding upon this, studies have been conducted to determine how influential these germline-encoded regions are to the cross-reactive characteristics of a TCR. The 2016 study by Adams *et al.* discussed in **Section 1.3.1.1** uses structural data to demonstrate how the CDR1 and CDR2 loops of the 42F3 TCR use almost identical binding modes, irrespective of which peptide it is interacting with or the conformation of the CDR3 loops. Adams *et al.* suggest that these germline loops influence the specificity of the 42F3 TCR (Adams et al., 2016).

The role that germline-encoded CDR loops play in cross-reactivity was aptly demonstrated by a study involving three separate murine TCRs; B3K506, 2W20, and YAe62, which were known to be poorly cross-reactive, moderately cross-reactive, and very cross-reactive respectively (Huseby et al., 2005). These TCRs all express genes from the Vα4 family and all recognise the 3K peptide in the context of IA^b with similar affinities and kinetic profiles (Huseby et al., 2006). Structural analysis of all three TCRs in complex with IA^b-3k suggests that the more promiscuous TCRs exhibit fewer germline CDR loop contacts with the pMHC molecule (Dai et al., 2008).

More recently, Attaf *et al.* created two transgenic mouse strains. The first, ΔβCDR1-3, exhibited T-cells with 'simplified' CDR1β and CDR2β loops that consisted of predominantly glycine and alanine amino acid residues, and a CDR3β loop that was shortened to just three glycine residues. The second transgenic mouse strain, ΔβCDR3, only exhibited the shortened CDR3β loop. T-cells from the ΔβCDR1-3 mice were found to be more cross-reactive than the T-cells from the ΔβCDR3 mice, indicating that the germline encoded loops play a role in regulating cross-reactivity (Attaf et al., 2016).

1.3.1.6. The role of molecular dynamics in T-cell cross-reactivity

In many of the examples discussed in **Section 1.3.1**, TCR promiscuity is affected by the conformational adaptation of the TCR or pMHC. Thus, molecular flexibility is a key underlying determinant of cross-reactivity. Madura *et al.* investigated the MEL5 TCR which recognises a Melan-A-derived peptide (EAAGIGILTV) in the context of HLA-A2 (Cole et al., 2009). MEL5 also recognises the HLA-A2-presented heteroclitic peptide, ELAGIGILTV. Despite ELAGIGILTV having an optimal P2 anchor residue, it was recognised with lower affinity than the natural Melan-A peptide (Cole et al., 2010; Zweerink et al., 1992). Structural studies showed very similar modes of binding regardless of which peptide MEL5 TCR interacted with. However thermodynamic studies of the TCR:pMHC interactions show the MEL5:A2-EAAGIGILTV interaction is enthalpically favourable. This is due to the suboptimal P2 anchor (alanine) in the Melan-A peptide, which allows it to be 'pulled' from the binding groove towards the TCR. As such, the Melan-A peptide could shift into a more optimal conformation for TCR interaction than the heteroclitic peptide, resulting in a higher affinity interaction (Madura et al., 2015).

Borbulevych *et al.* investigated the cross-reactive properties of the A6 TCR which can recognise the Tax peptide (LLFGYPVYV) and the *Saccharomyces cerevisiae*-derived Tel1p peptide (MLWGYLQYV), in the context of HLA-A2. Both Tax and Tel1p are presented identically by HLA-A2. Despite this, A6 TCR interaction with Tel1p involves conformational shifts in the TCR, MHC, and peptide, that do not occur when A6 interacts with Tax. Molecular dynamics investigation showed that HLA-A2 exhibits greater flexibility when presenting Tel1p peptide than it does when presenting Tax peptide. HLA-A2-Tel1p was also shown to have lower thermal stability than HLA-A2-Tax, supporting the conclusions that HLA-A2-Tel1p is more flexible. This suggests that A6 TCR recognition of HLA-A2-Tel1p is facilitated by the increased flexibility of both the TCR and the pMHC (Borbulevych et al., 2009).

The link between CDR loop dynamics and TCR promiscuity was investigated by Tsuchiya *et al.*, who studied five different TCRs which exhibited varying degrees of cross-reactivity. Using molecular dynamics studies, they showed that the CDR3 loops of the more promiscuous TCRs predominantly formed non-specific bonds, such as CH-π and π-π bonds, resulting in a greater loss of entropy upon binding. By contrast, the CDR3 loops of less promiscuous TCRs predominantly formed specific hydrogen bonds with the pMHC molecule, resulting in a lesser

loss of entropy upon binding. It was therefore hypothesised that TCRs which exhibit a greater loss of entropy upon binding are more promiscuous (Tsuchiya et al., 2017).

1.3.2. Advantages of T-cell cross-reactivity

T-cells need to provide comprehensive immune coverage against pathogens, which requires T-cells to recognise a large array of pathogenic antigens. In this respect, T-cell cross-reactivity is advantageous, as greater immune coverage can be achieved with a smaller population of T-cells. T-cell cross-reactivity also confers a temporal and spatial advantage; if a greater number of T-cells are capable of responding to a particular pathogen an infection is likely to be recognised much more rapidly (Sewell, 2012). Another advantage is heterologous immunity (**Figure 1.10**), where memory T-cells that result from a particular pathogen response can also provide immunity to a second, previously not encountered, pathogen through cross-reactivity (Welsh et al., 2002).

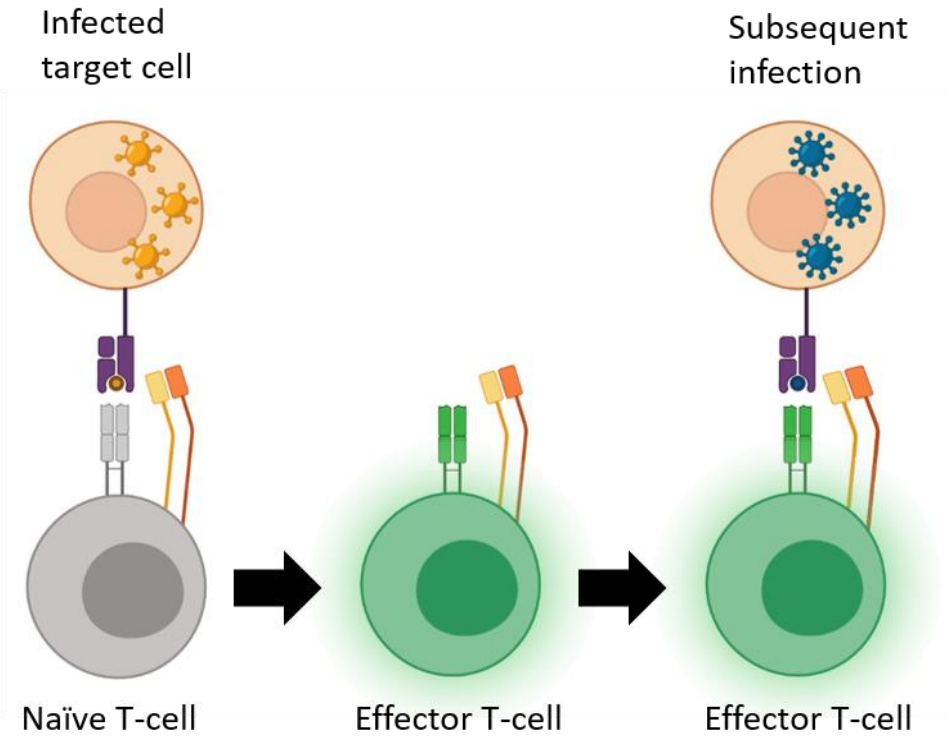

Figure 1.10. Heterologous immunity.
A schematic demonstrating heterologous immunity.

There have been numerous documented examples of heterologous immunity. Perhaps the earliest known example is how immunity to cowpox confers immunity to smallpox. This resulted in the world's first vaccine trial and has since led to the eradication of smallpox

(Stewart et al., 2006). Another well-known example is how the *Mycobacterium bovis* bacillus Calmette–Guérin (BCG) vaccine that aimed to provide protection against tuberculosis can also confer protection against leprosy, caused by *Mycobacterium leprae* (Setia et al., 2006). Many examples of T-cell cross-reactivity involve immunity across different but similar pathogens. T-cell cross-reactivity has been observed among strains of both influenza A and influenza B, which are responsible for seasonal flu epidemics (McMichael et al., 1983; Sandt et al., 2015). T-cell cross-reactivity has also been observed between avian and influenza A strains (Gras et al., 2010; Greenbaum et al., 2009; Wang et al., 2015). Cross-reactivity within influenza infections was investigated further by Koutsakos *et al.*, who not only observed T-cell cross-reactivity between a wide range of influenza B strains, but also observed T-cell cross-reactivity across influenza A, B, and C strains (Koutsakos et al., 2019).

Heterologous immunity has also been observed between flavivirus infections, specifically between Zika virus (ZIKV) and Dengue virus (DENV). These viruses share approximately 52%-57% amino acid homology, are prevalent in the same geographical locations, and have been found to co-infect humans (Barba-Spaeth et al., 2016; Dupont-Rouzeyrol et al., 2015). Wen *et al.* described ZIKV/DENV cross-reactivate epitopes, suggesting T-cell cross-reactivity can occur between the viruses (Wen et al., 2017a). Wen *et al.* then demonstrated how $CD8^+$ T-cells from DENV patients could protect against ZIKV infection (Wen et al., 2017b).

Another example of potential heterologous immunity concerns the 2019 SARS-CoV-2 pandemic. According to the European Center for Disease Control (ECDC), at time of writing the fatality rate of SARS-CoV-2 in Asia is lower than that in Europe and North America, despite the outbreak originating in Asia. While other external factors may influence the fatality rate, it has been hypothesised that the Asian population may possess pre-existing immunity due to previous coronavirus outbreaks in the region (Fouchier et al., 2003; Yaqinuddin, 2020). This hypothesis has been supported by data showing high amino acid homology between SARS-CoV-2 and other coronavirus strains (Wu et al., 2020).

T-cell cross-reactivity has been observed between different viral families. $CD8^+$ T-cells have been shown to cross-react with epitopes derived from the influenza neuraminidase (NA) protein and the hepatitis C NS3 protein. These epitopes share high sequence homology and elicit similar binding affinities to T-cells, suggesting molecular mimicry (Wedemeyer et al.,

2001). T-cells have also been found to cross-react with epitopes derived from influenza matrix protein and human immunodeficiency virus (HIV) Gag protein (Acierno et al., 2003).

T-cell cross-reactivity can provide the host with comprehensive immune coverage, preventing pathogen immune escape. Rapidly evolving pathogens, such as HIV, have been shown to 'escape' from the immune system (Klenerman et al., 2002). One mechanism by which this occurs is through mutation of T-cell-specific epitopes (Phillips et al., 1991). T-cell cross-reactivity can facilitate recognition of some viral escape mutants. Ladell *et al.* demonstrated $CD8^+$ recognition of both the KK10 epitope, a HIV Gag protein derivative, and a mutated 'escape' variant of KK10. The mechanism of interaction for both epitopes was determined to be almost identical (Ladell et al., 2013).

1.3.3. Disadvantages of T-cell cross-reactivity

1.3.3.1. Autoimmunity

While T-cell cross-reactivity is essential to provide comprehensive host immunity, it has also been linked to autoimmunity (**Figure 1.11**). As discussed in **Section 1.1.1.2**, T-cells are negatively selected in the thymus to prevent autoreactive T-cells from migrating to the periphery. Coupled with peripheral regulatory systems, such as the activity of Treg cells and co-inhibitory receptors, negative selection has evolved to limit autoimmunity. However, weakly autoreactive T-cells that pass thymic selection can be activated by pathogen

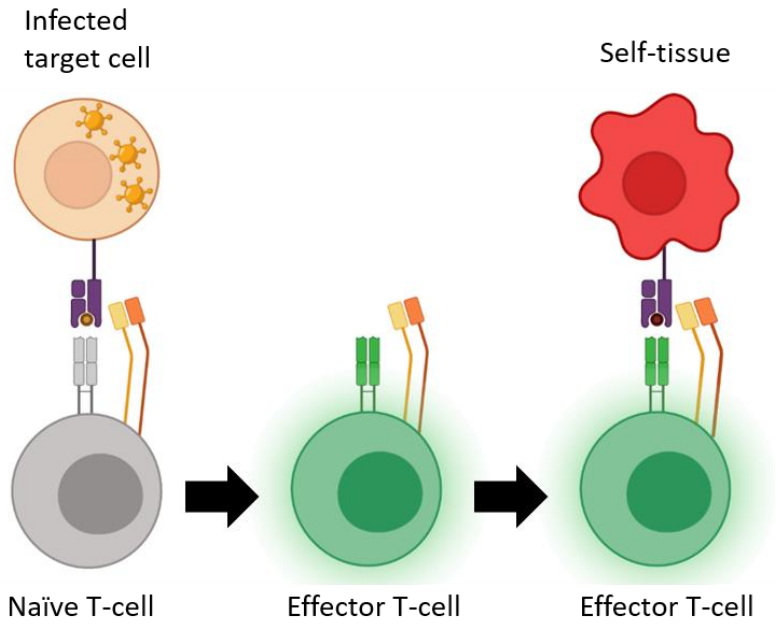

Figure 1.11. Autoimmunity.
A schematic demonstrating autoimmunity via cross-reactivity.

recognition in the periphery resulting in more sensitive effector T-cells that can recognise self-antigens through molecular mimicry (Oldstone, 1998).

Molecular mimicry has been shown to play a role in multiple sclerosis (MS), a prominent autoimmune disease. MS is characterised by demyelination of nerve cells. Bhardwaj *et al.* demonstrated how a $CD4^+$ T-cell specific for an epitope derived from myelin basic protein (MBP) could also recognise pathogen-derived peptides in a murine model (Bhardwaj et al., 1993). Wucherpfennig *et al.* supported this by demonstrating that another $CD4^+$ T-cell clone, Hy.1B11, which recognises MPB-derived epitopes in the context of HLA-DQ1, also recognises epitopes from herpes simplex virus (HSV), human papilloma virus, adenovirus, and *Pseudomonas aeruginosa*, highlighting the potential role of pathogen-driven molecular mimicry in MS (Wucherpfennig et al., 1995). The structural basis of Hy.1B11 cross-reactivity was elucidated by Sethi *et al*., who determined the structures of Hy.1B11 in complex with epitopes derived from MPB, HSV, and *Pseudomonas aeruginosa*. The structural data show a very similar binding mechanism to all three epitopes, despite differences in peptide sequence, with a single CDR3α loop residue being responsible for the majority of TCR:peptide contacts (Sethi et al., 2013). A role for pathogenic triggers in MS was further supported by Harkiolaki *et al*., who showed how injection of pathogenic peptides, which share homology with MPB epitopes, into humanised mice can cause central nervous system inflammation (Harkiolaki et al., 2006).

Parkinson's disease is characterised by accumulation of intra-neural protein aggregates called Lewy bodies, which are composed of α-synuclein (α-syn), and the death of dopaminergic neurons (Jakest et al., 1998). Certain HLA alleles have been associated with Parkinson's patients, suggesting autoimmune involvement (Wissemann et al., 2013). $CD8^+$ T-cells have also been shown to kill neuron cells (Zucca et al., 2014). In 2017, Sulzer *et al.* identified several α-syn-derived epitopes which were recognised by T-cells acquired from Parkinson's patients. While the link between the α-syn epitopes and $CD8^+$ T-cell killing of neurons has yet to be confirmed, there is strong evidence showing formation of Lewy bodies may act as an autoimmune trigger for the progression of Parkinson's disease (Sulzer et al., 2017).

A further, prominent example of an autoimmune disease is type 1 diabetes (T1D). This disease is discussed further in **Chapters 4 and 5**.

1.3.3.2. Alloreactivity

In **Section 1.3.1**, I discussed the phenomenon whereby a T-cell can cross-react with different MHC molecules. In practice, this usually occurs after a tissue transplant procedure, when the donor and recipient HLA types are mismatched. This is termed alloreactivity and is responsible for Graft-vs-Host Disease (GvHD), where the host immune system rejects the donor tissue (Medawar, 1944; Afzali et al., 2007). While evidence suggests both innate and adaptive immune mechanisms play a role in GvHD progression, only the role of T-cells will be considered here.

Graft rejection can be caused by both the killing of graft tissue, via $CD8^+$ T-cell activity, and by the recruitment of allo-antibodies, via $CD4^+$ T-cell activity (Moine et al., 2002). T-cells can react to graft tissue in two ways. 'Direct' alloreactivity involves T-cells recognising 'passenger' pMHC molecules expressed by the donor tissue graft (Lechler et al., 1982). 'Indirect' alloreactivity involves T-cells recognising peptide epitopes derived from donor tissue, which are presented by host MHC molecules (Jiang et al., 2004). Some examples of the structural mechanisms by which T-cell alloreactivity may occur are discussed in **Section 1.3.1**.

There has also been evidence suggesting a correlation between viral infection and incidence of GvHD post-transplantation (Cantoni et al., 2010). Antiviral drugs have been shown to reduce rates of GvHD in renal-transplant patients (Lowance et al., 1999). In 2002, Koelle *et al.* investigated the link between HSV-2 infection and GvHD incidence. Koelle *et al.* identified two $CD8^+$ T-cell lines that recognise HSV-2 epitopes in the context of HLA-A2 but can also recognise HLA-B*44 restricted epitopes (Koelle et al., 2002). A more recent study by Hall *et al.* investigated the link between GvHD and human cytomegalovirus (hCMV). Using *in silico* analysis, they identified multiple high-affinity CMV epitopes with sequence homology to known alloreactive epitopes, further supporting the hypothesis that molecular mimicry contributes to GvHD (Hall et al., 2017).

1.4. Therapeutic potential of T-cells

Beyond the immediate host benefits of broader immune coverage, T-cell cross-reactivity has a lot of potential in therapeutic design. *In vivo*, T-cell activity must compromise between the broad recognition of pathogenic antigens and maintaining self-tolerance. It stands to reason

then that the TCR:pMHC interaction can be rationally optimised to improve T-cell activity in patients.

1.4.1. T-cell ligand-based therapies

Perhaps the most obvious application of T-cell peptide ligands in therapy is in vaccination. In 1998, a peptide-based vaccine was used to prevent infectious mononucleosis, caused by EBV infection. It was hypothesised that administering a vaccine containing EBV-specific peptides, to EBV-seronegative patients, can promote the recruitment of EBV-specific T-cells in the patient. This would provide protection from subsequent EBV infections, reducing the likelihood of infectious mononucleosis (Moss et al., 1998). A phase-1 study determined the effectiveness of using a peptide derived from EBV nuclear antigen 3 (EBNA3) as a vaccine to prevent infectious mononucleosis. After vaccination, EBV-specific T-cells were found in eight out of nine of the vaccine recipients and in none of the placebo cohort. A 12 year follow up study showed that four of the vaccine recipients had become EBV sero-positive, but none had developed infectious mononucleosis. By contrast, two members of the placebo cohort had become EBV seropositive with one of those developing infectious mononucleosis (Elliott et al., 2008).

There is also potential for the use of peptide vaccines to protect against rapidly-evolving pathogens by recruiting cross-reactive T-cells, such as for use as a universal vaccine for seasonal influenza. Grant *et al.* identified several cross-reactive $CD8^+$ T-cell clones which can recognise multiple cross-strain influenza A-derived epitopes. Structural data indicate a conserved mechanism among these recognition events. As such, a peptide based vaccine targeting a cross-reactive $CD8^+$ T-cell may prove as effective as a universal influenza A vaccine (Grant et al., 2018).

There is much interest in the use of APLs as peptide vaccines. As discussed in **Section 1.3.1**, APLs can be designed with higher affinities for the TCR of interest than the wild-type peptide. A study by Ekeruche-Makinde *et al*. reported that APLs can promote T-cell receptor-optimised peptide skewing of the T-cell repertoire (TOPSORT), where by high affinity ligands can select for superior T-cells that wild-type ligands would be unable to select for (Ekeruche-Makinde et al., 2012). Much of the investigation into APL vaccines has focused on cancer vaccines, whereby high-affinity ligands may break self-tolerance to cancer tissue and illicit

tumour killing (Galloway et al., 2019). These investigations will be discussed further in **Chapter 3**.

APLs also show potential in the treatment of autoimmune disease. T-cell response to antigen can sometimes result in clonal deletion, due to IL-2 stimulated cell cycling and TCR re-engagement (Critchfield et al., 1994). In theory, the use of high affinity APLs would exacerbate this phenomenon, facilitating the removal of auto-reactive T-cells (Candia et al., 2016). A phase-I trial assessed the efficacy of ATX-MS-1467, a cocktail of 4 MBP-derived peptides, in the treatment of MS. ATX-MS-1467 was administered to six MS patients in doses ranging from 50 μg to 800 μg. Results showed that these doses were well tolerated by patients, with disease symptoms improving in one patient. While the study is too small to confirm the efficacy of this treatment, it does show the potential benefits of APL-based therapy in autoimmune disease (Streeter et al., 2015).

1.4.2. Adoptive T-cell therapy

Another avenue for T-cell therapy is adoptive cell therapy (ACT). ACT involves the transfer of T-cells into a patient to achieve a desired immune response. This technique has been utilised for the treatment of solid tumours in malignant melanoma patients. Patient T-cells from the melanoma tumour microenvironment are extracted and expanded *ex vivo*. These T-cells, known as tumour infiltrating lymphocytes (TILs), are then transferred back into the patient with the hope that the expanded TIL population will overcome tumour self-tolerance. This technique, in conjunction with IL-2 administration, has successfully cured melanoma in a number of patients (Ellebaek et al., 2012).

ACT has also been used for the treatment of autoimmune disease. Like TILs, Treg cells from patients with autoimmune diseases can be removed and expanded *ex vivo*. Expanded Tregs can then be transferred back into the patient to provide additional immune suppression to treat the autoimmune disease. Canavan *et al.* demonstrated the potential of this technique *in vitro* by suppressing activation of lamina propria T-cells, which had been linked to Crohn's disease progression (Canavan et al., 2016). Phase-I clinical trials using this technique have also been conducted. One trial involved administering endogenous Treg cells that have been expanded *ex vivo* to two patients suffering chronic and acute GvHD respectively. While this treatment was only partially effective in the case of acute GvHD, significant reduction in symptoms was achieved in the chronic GvHD patient (Trzonkowski et al., 2009). The same

technique was also used in a Phase-I clinical trial to treat T1D. A cohort of ten diabetic children was subjected to ACT. These patients exhibited a significant reduction in the amount of insulin required, with two patients no longer requiring insulin after 6 months compared to the control cohort (Trzonkowski et al., 2012).

ACT can be optimised by use of genetically enhanced T-cells. T-cells *in vivo* have to compromise between strong recognition of pathogenic antigens and weak recognition of self-antigens, resulting in potentially sub-optimal activity against aberrant self. To address this, TCRs can be engineered to recognise peptide ligands with greater affinities than their 'wild-type' counterpart (Crean et al., 2020). These high affinity TCRs can be genetically transferred to T-cells, which can then be expanded *ex vivo* and transferred into a patient. A 2006 clinical study modified peripheral blood lymphocytes of 15 patients by genetically encoding a melanoma-specific TCR. These modified lymphocytes were expanded *ex vivo* and administered back into the respective patients. Two patients exhibited significant regression of melanoma lesions (Morgan et al., 2006).

The use of genetically engineered T-cells to circumvent viral escape mutants has also been studied. Varela-Rohena *et al.* modified the 868 TCR, which recognises the SL9 peptide (SLYNTVATL) derived from HIV Gag protein. The enhanced 868 TCR exhibited improved binding affinity to wild-type SL9, broader recognition of common HIV escape mutants, and could control wild-type and mutant HIV strains *in vitro*, when genetically transferred into T-cells. This demonstrated the potential for modified TCRs to improve immune coverage (Varela-Rohena et al., 2008).

A further modification to ACT involves the use of chimeric antigen receptors (CARs). T-cells can be genetically engineered to express a CAR before undergoing *ex vivo* expansion and administration into patients. CARs consist of an extracellular binding domain to interact with the target, hinge and transmembrane regions, and a CD3ζ signalling region to activate the T-cell. The CAR binding domain is often a single-chain variable fragment (scFv) derived from an Ig specific to the target cell. Additional components can also be added to further improve T-cell function, such as CD28 co-stimulatory domains to improve proliferation and cytokine production (Hartmann et al., 2017). The role of CAR T-cell therapy, as well as other forms of ACT in the context of cancer immunotherapy, will be discussed further in **Chapter 3**.

1.4.3. Limitations of T-cell based therapies

While many T-cell based therapies have proven successful, there are limitations to consider. Firstly, conventional forms of T-cell therapy are governed by MHC restriction. A therapy which works in the context of HLA-A2 will be ineffective in patients who do not express HLA-A2. Given the large number of potential *HLA* genes, it is likely that any potential therapy would be effective in a minority of patients.

Another consideration is the potential of adverse TCR interactions. T-cell cross-reactivity can result in autoimmunity through the recognition of molecular mimics. The risk of negative cross-reactivity occurring increases with the use of engineered TCRs with artificially improved binding affinity, as they have not undergone thymic selection. This risk was highlighted in ACT clinical trials involving an engineered T-cell expressing the MAGE-A3^{a3a} TCR, which was affinity enhanced for recognition of the cancer epitope MAGE-A3. Pre-clinical studies indicated this engineered T-cell had potential as an anti-cancer therapeutic and that this T-cell would be safe to transfer into patients. However, two patients involved with the study suffered fatal cardiac toxicity (Linette et al., 2013). Subsequent investigation determined MAGE-A3^{a3a} TCR cross-reactivity between MAGE-A3 and titin, a protein present in striated heart muscle, which likely resulted in the cardiac toxicity. Structural data showed that MAGE-A3^{a3a} TCR cross-reactivity was caused by molecular mimicry (Raman et al., 2016). This unfortunate event demonstrated why thorough structural understanding of T-cell cross-reactivity is essential.

1.5. Aims

The study of T-cell cross-reactivity is crucial for our understanding of immune coverage, autoimmunity and the safe use of T-cell-based therapeutics. During my studies, I aimed to gain a structural and biophysical understanding of novel clinically relevant examples of TCRs that recognise multiple peptide epitopes in the context of a single HLA-I molecule. I hypothesised that the structural mechanisms governing T-cell cross-reactivity may be conserved within different biological contexts, thus allowing me to identify context-specific motifs. I initiated my studies with a cancer reactive TCR that was identified in a TIL population used to induce complete remission in a patient with Stage IV melanoma and found to persist after complete durable cancer remission. My colleagues had previously shown that T-cells bearing this TCR were potent cancer killers that could respond to a wide variety of other HLA-A2^{+} cancer types beyond melanoma. Unexpectedly, it was found that T-cells with this TCR

could respond to three different tumour-associated antigens: HLA-A2-EAAGIGILTV comprising residues 26-35 of Melan-A, HLA-A2-LLLGIGILVL comprising residues 22-31 of Bone Marrow Stromal antigen 2 (BST2), and HLA-A2-NLSALGIFST comprising residues 367-376 of insulin-like growth factor 2 mRNA binding protein 2 (IMP2). I aimed to understand how a TCR could structurally engage these three peptides in the context of HLA-A2.

I also aimed to understand how molecular mimicry might contribute to T1D through the two common T1D risk alleles, *HLA-A*0201* and *HLA*2402*, which are carried by >75% of T1D patients. As discussed in **Section 1.3.3.1**, a preferred model for the induction of autoimmune disease is molecular mimicry, which results from the pathogen priming of naïve T-cells that then respond to a self-epitope that is a structural mimic of the disease epitope. Specifically, I studied HLA-A2 and HLA-A*24:02 (HLA-A24 hereafter) restricted TCRs that were isolated from T1D patients and recognised HLA-A24-LWMRLLPLL (preproinsulin (PPI) residues 3-11), HLA-A2-VMNILLQYV (glutamic acid decarboxylase (GAD65) residues 495-503), and HLA-A2-HLVEALYLV (insulin B-chain residues 10-18). I aimed to understand how these TCRs might interact with pathogen-derived epitopes and provide structural and biophysical evidence of how such interactions might have potential to induce disease.

2. Materials and Methods

2.1. Protein production and purification

2.1.1. Reagents and buffers for protein production

Reagents	Composition
Psi Broth pH 7.6	5 g/L yeast extract (Sigma-Aldrich), 20 g/L tryptone (Sigma-Aldrich), 5 g/L magnesium sulphate (Fisher).
Transformation buffer (Tfb) I pH 5.8	30 mM potassium acetate (Fisher), 100 mM rubidium chloride (RbCl, Fisher), 10 mM calcium chloride ($CaCl_2$, Sigma), 50 mM magnesium chloride ($MgCl_2$, Acros organics), 15% v/v glycerol (Fisher).
TfbII pH 6.5	10 mM 3-(N-morpholino) propanesulfonic acid (MOPS, Sigma-Aldrich), 75 mM $CaCl_2$, 10 mM RbCl, 15% v/v glycerol.
Luria broth (LB) agar	10 g/L tryptone, 5 g/L yeast extract, 10 g/L sodium chloride ($NaCl_2$, Fisher) 15 g/L bacteriological agar (Oxoid).
TYP media	16 g/L tryptone, 16 g/L yeast extract, 5 g/L $NaCl_2$, 3.3 g/L potassium phosphate dibasic (Merck).
Lysis buffer	10 mM tris(hydroxymethyl)aminomethane (TRIS) pH 8.1 (Sigma), 10 mM $MgCl_2$, 150 mM $NaCl_2$, 10% v/v glycerol.
Triton wash	50mM TRIS pH 8.1, 100 mM $NaCl_2$, 2 mM Ethylenediaminetetraacetic acid (EDTA, Sigma-Aldrich), 0.5% v/v Triton X (Sigma).
Resuspension buffer	50mM TRIS pH 8.1, 100mM $NaCl_2$, 2mM EDTA.
Guanidine buffer	50 mM TRIS pH 8.1, 100mM $NaCl_2$ 2mM EDTA, 6 M guanidine (Fisher).
pMHC refold buffer pH 8.1	50mM TRIS pH 8.1, 2 mM EDTA, 400 mM L-arginine (Sigma-Aldrich).
TCR refold buffer pH 8.1	50mM TRIS pH 8.1, 2 mM EDTA, 2.5 M urea (Sigma).
Buffer A	10 mM TRIS, filtered 0.45 µm.
Buffer B	10 mM TRIS, 1 M $NaCl_2$, filtered 0.45 µm.
Hydrophobicity interaction column (HIC) buffer A	10 mM TRIS, 3 M $NaCl_2$, filtered 0.45 µm.
HIC buffer B	10 mM TRIS, filtered 0.45 µm.
Phosphate buffered saline (PBS, Oxoid)	Tablets containing 8 g/L $NaCl_2$, 0.2 g/L potassium chloride, 1.15 g/L di-sodium hydrogen phosphate, 0.2 g/L potassium dihydrogen phosphate. One tablet was dissolved in 100 mL of ddH_2O.
Crystal buffer	10 mM TRIS, 10 mM $NaCl_2$.
Biacore Buffer	10x HBS-P buffer (GE healthcare), containing 0.1 M 4-(2-hydroxyethyl)-1-piperazine ethane

	sulfonic acid (HEPES), 1.5 M $NaCl_2$, 0.2% v/v Surfactant P20.

Table 2.1. Reagent compositions used for protein production.

2.1.2. Expression vectors and protein constructs

The expression vector pGEM-T7 (Promega, **Figure 2.1**) was used for soluble protein expression in *Escherichia coli* (*E. coli*) cells (Roger et al., 1998). The pGEM-T7 vector uses an f1 origin of replication and allows for negative selection via ampicillin resistance, enabled by the *AmpR* gene, as well as positive selection via blue/white selection, enabled by the lac operon. The lac operon also allows protein production to be regulated by the lac promotor, induced by Isopropyl β-D-1-thiogalactopyranoside (IPTG). The pGEM-T7 vector was used to produce all soluble protein during this thesis.

The protein sequences used in this thesis are shown below (**Table 2.2**). The constructs used are the extracellular domains of their respective proteins. Non-natural cysteine residues are present in position 48 of each TCRα constant region and position 57 of each TCRβ constant region. These result in artificial di-sulphide bond formation, improving the stability of the refolded TCR proteins (Boulter et al., 2003).

Construct	Amino acid sequence
MEL8 α-chain	MQKEVEQNSGPLSVPEGAIASLNCTYSDRGSQSFFWYRQYSGKSPELIMSIYSNGDKE DGRFTAQLNKASQYVSLLIRDSQPSDSATYLCAVQKLVFGTGTRLLVSPNIQNPDPAVY QLRDSKSSDKSVCLFTDFDSQTNVSQSKDSDVYITDKCVLDMRSMDFKSNSAVAWSN KSDFACANAFNNSIIPEDTFFPSPESS
MEL8 β-chain	MNAGVTQTPKFQVLKTGQSMTLQCAQDMNHEYMSWYRQDPGMGLRLIHYSVGAG ITDQGEVPNGYNVSRSTTEDFPLRLLSAAPSQTSVYFCASSYSFTEATYEQYFGPGTRLTV TEDLKNVFPPEVAVFEPSEAEISHTQKATLVCLATGFYPDHVELSWWVNGKEVHSGVC TDPQPLKEQPALNDSRYALSSRLRVSATFWQDPRNHFRCQVQFYGLSENDEWTQDRA KPVTQIVSAEAWGRAD
MEL5 α-chain	MRKEVEQNSGPLSVPEGAIASLNCTYSDRGSQSFFWYRQYSGKSPELIMFIYSNGDKED GRFTAQLNKASQYVSLLIRDSQPSDSATYLCAVNVAGKSTFGDGTTLTVKPNIQNPDPA VYQLRDSKSSDKSVCLFTDFDSQTNVSQSKDSDVYITDKCVLDMRSMDFKSNSAVAWS NKSDFACANAFNNSIIPEDTFFPSPESS
MEL5 β-chain	MSQTIHQWPATLVQPVGSPLSLECTVEGTSNPNLYWYRQAAGRGLQLLFYSVGIGQIS SEVPQNLSASRPQDRQFILSSKKLLLSDSGFYLCAWSETGLGTGELFFGEGSRLTVLEDLK NVFPPEVAVFEPSEAEISHTQKATLVCLATGFYPDHVELSWWVNGKEVHSGVCTDPQP LKEQPALNDSRYALSSRLRVSATFWQDPRNHFRCQVQFYGLSENDEWTQDRAKPVTQ IVSAEAWGRAD

4C6 α-chain	MGEDVEQSLFLSVREGDSSVINCTYTDSSSTYLYWYKQEPGAGLQLLTYIFSNMDMKQ DQRLTVLLNKKDKHLSLRIADTQTGDSAIYFCAEPSGNTGKLIFGQGTTLQVKPIQNPDP AVYQLRDSKSSDKSV**C**LFTDFDSQTNVSQSKDSDVYITDKCVLDMRSMDFKSNSAVA WSNKSDFACANAFNNSIIPEDTFFPSPESS
4C6 β-chain	MDTGVSQDPRHKITKRGQNVTFRCDPISEHNRLYWYRQTLGQGPEFLTYFQNEAQLE KSRLLSDRFSAERPKGSFSTLEIQRTEQGDSAMYLCASSLHHEQYFGPGTRLTVTEDLKN VFPPEVAVFEPSEAEISHTQKATLV**C**LATGFYPDHVELSWWVNGKEVHSGVCTDPQPL KEQPALNDSRYALSSRLRVSATFWQDPRNHFRCQVQFYGLSENDEWTQDRAKPVTQI VSAEAWGRAD
Clone 29 α-chain	MMILNVEQSPQSLHVQEGDSTNFTCSFPSSNFYALHWYRWETAKSPEALFVMTLNGD EKKKGRISATLNTKEGYSYLYIKGSQPEDSATYLCARNTGNQFYFGTGTSLTVIPIQNPDP AVYQLRDSKSSDKSV**C**LFTDFDSQTNVSQSKDSDVYITDKCVLDMRSMDFKSNSAVA WSNKSDFACANAFNNSIIPEDTFFPSPESS
Clone 29 β-chain	MNAGVTQTPKFQVLKTGQSMTLQCAQDMNHEYMSWYRQDPGMGLRLIHYSVGAG ITDQGEVPNGYNVSRSTTEDFPLRLLSAAPSQTSVYFCASSLQTGTGNYGYTFGSGTRLT VVEDLKNVFPPEVAVFEPSEAEISHTQKATLV**C**LATGFYPDHVELSWWVNGKEVHSGV CTDPQPLKEQPALNDSRYALSSRLRVSATFWQDPRNHFRCQVQFYGLSENDEWTQDR AKPVTQIVSAEAWGRAD
InsB4 α-chain	MQKEVEQNSGPLSVPEGAIASLNCTYSDRGSQSFFWYRQYSGKSPELIMFIYSNGDKE DGRFTAQLNKASQYVSLLIRDSQPSDSATYLCAVSSSYKLIFGSGTRLLVRPDIQNPDPAV YQLRDSKSSDKSV**C**LFTDFDSQTNVSQSKDSDVYITDKCVLDMRSMDFKSNSAVAWS NKSDFACANAFNNSIIPEDTFFPSPESS
InsB4 β-chain	MEAGVTQFPSHSVIEKGQTVTLRCDPISGHDNLYWYRRVMGKEIKFLLHFVKESKQDE SGMPNNRFLAERTGGTYSTLKVQPAELEDSGVYFCASSAGGALTGELFFGEGSRLTVLE DLKNVFPPEVAVFEPSEAEISHTQKATLV**C**LATGFYPDHVELSWWVNGKEVHSGVCTD PQPLKEQPALNDSRYALSSRLRVSATFWQDPRNHFRCQVQFYGLSENDEWTQDRAKP VTQIVSAEAWGRAD
HLA-A2 chain (**with biotin tag**)	MGSHSMRYFFTSVSRPGRGEPRFIAVGYVDDTQFVRFDSDAASQRMEPRAPWIEQEG PEYWDGETRKVKAHSQTHRVDLGTLRGYYNQSEAGSHTVQRMYGCDVGSDWRFLR GYHQYAYDGKDYIALKEDLRSWTAADMAAQTTKHKWEAAHVAEQLRAYLEGTCVEW LRRYLENGKETLQRTDAPKTHMTHHAVSDHEATLRCWALSFYPAEITLTWQRDGEDQ TQDTELVETRPAGDGTFQKWAAVVVPSGQEQRYTCHVQHEGLPKPLTLRWEP**GLNDI FEAQKIEWHE**
HLA-A24 chain (**with biotin tag**)	MGSHSMRYFSTSVSRPGRGEPRFIAVGYVDDTQFVRFDSDAASQRMEPRAPWIEQEG PEYWDEETGKVKAHSQTDRENLRIALRYYNQSEAGSHTLQMMFGCDVGSDGRFLRGY HQYAYDGKDYIALKEDLRSWTAADMAAQITKRKWEAAHVAEQQRAYLEGTCVDGLR RYLENGKETLQRTDPPKTHMTHHPISDHEATLRCWALGFYPAEITLTWQRDGEDQTQ DTELVETRPAGDGTFQKWAAVVVPSGEEQRYTCHVQHEGLPKPLTLRWEP**GLNDIFE AQKIEWHE**
B_2M chain	MIQRTPKIQVYSRHPAENGKSNFLNCYVSGFHPSDIEVDLLKNGERIEKVEHSDLSFSKD WSFYLLYYTEFTPTEKDEYACRVNHVTLSQPKIVKWDRDM

Table 2.2. Protein constructs used during this thesis. Artificial cysteine residues present in TCR chains are highlighted in red.

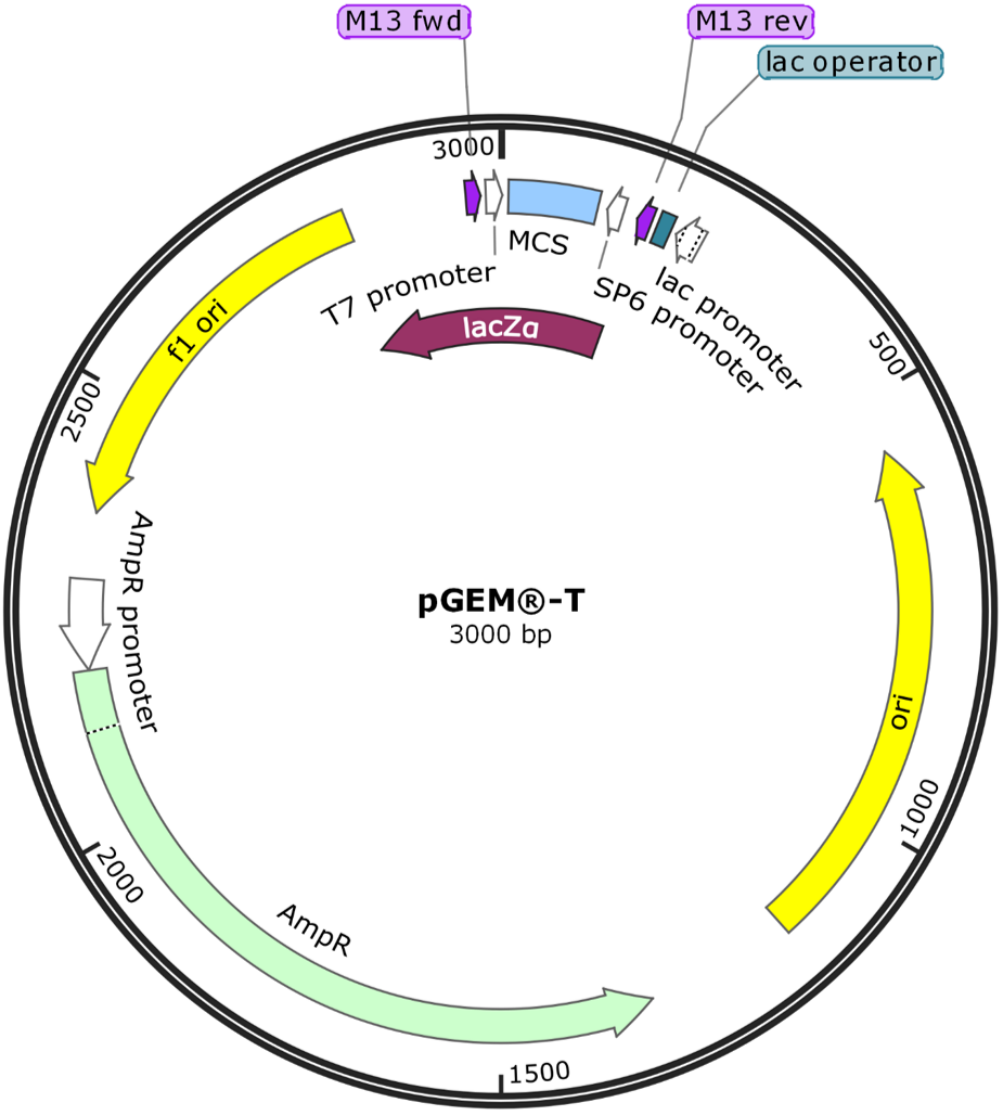

Figure 2.1. pGEM-T7 plasmid map.
A map detailing the features of the pGEM-T7 bacterial expression plasmid. Map made using SnapGene.

2.1.3. Inclusion body production

2.1.3.1. Competent E. coli cell production

Competent *E. coli* cells were required for vector transformation. Two strains of competent *E. coli* were used during this thesis. The first are BL21 cells (Lifetech), which were used for soluble protein production. BL21 cells lack T7 promotors so are optimised for T7 vector usage, allowing for more controlled protein expression. The second competent cell type are TOP10 cells (Lifetech), which were used for DNA amplification procedures due to the higher vector uptake compared to BL21 cells.

An initial aliquot of pre-bought competent *E. coli* cells were cultured in 50 mL of psi broth and incubated at 37°C, 100RPM overnight. 100 mL of psi broth was inoculated with 1 mL of the overnight competent cell culture at 37°C, 100RPM until culture optical density (OD_{450}) measured 0.45. OD_{450} measurements were made using a CO800 cell density meter (WPA Biowave). The competent cell culture was incubated on ice for 15 minutes, then centrifuged at 4353 x g (Beckman Caulter Aventi JE) for 10 minutes. The supernatant was discarded and the pellets were resuspended in 40 mL TFBI. The cells were incubated again on ice for 15 minutes, before centrifugation at 4353 x g for 10 minutes. The supernatant was discarded and the pellet was resuspended in 4 mL of TFBII. The cells were incubated on ice for 15 minutes before aliquoting and snap freezing in isopropanol/dry ice slurry.

2.1.3.2 Inclusion body expression

The pGEM-T7 plasmid containing the protein of interest was transformed into competent cells via heat shock. A 50 µL aliquot of competent cells was removed from -80°C storage and incubated on ice for 5 minutes. 1 µL of plasmid was added to the cells, gently mixed, then incubated on ice for 5 minutes. The cells were then incubated at 42°C for 1 minute and then incubated on ice for 5 minutes. The cells were then plated onto LB agar plates containing 50 µg/mL of carbenicillin (Fisher) and incubated at 37°C overnight.

Colonies present on the agar plate, indicating successful transformation, were used to inoculate 20 mL of TYP media to form a 'starter culture' in a 50 ml falcon tube. The starter culture was incubated at 37°C, 220 RPM in an orbital shaking incubator until its OD_{450} measured 0.5. The starter culture was used to inoculate 1 L of TYP media in a 2 L conical flask, which was incubated at 37°C, 200 RPM until the OD_{450} measured 0.5. The cultures were then induced with 0.5 µg/mL of IPTG and incubated at 37°C, 220 RPM for 3 hours. The cultures were centrifuged at 2786 x g (Eppendorf 5810R) for 20 minutes and the subsequent pellet was resuspended in 40 mL of lysis buffer before freezing.

2.1.3.3 Purification of inclusion bodies

The frozen bacterial pellet resuspensions were thawed and sonicated (Sonoplus, Bandelin) for 20 minutes at approximately 50% power. 100 µg/mL of DNAse was added to the bacterial resuspensions, before incubation at 37°C for 1 hour. The resuspension was then centrifuged at 17696 x g (Beckman Caulter Aventi JE) for 20 minutes, forming a protein pellet. The protein pellet was resuspended in 200 mL of triton wash and this step was repeated until the pellet

was white and dry. The protein pellet was then resuspended in 200 mL of resuspension buffer, where 1 mL samples were taken for quality control by sodium dodecyl sulphate–polyacrylamide gel electrophoresis (SDS-PAGE). The inclusion body resuspension was then centrifuged at 17696 x g for 20 minutes. The protein pellet was then resuspended in 20 mL of guanidine buffer, forming a soluble inclusion body. The absorbance of the inclusion body at the 280 nm wavelength (A_{280}) was measured using an Implen nanophotometer (Geneflow). Beers Law ($A = \varepsilon cl$) was used to determine protein concentration, with the extinction coefficient (ε) determined theoretically using ProtParam. The A_{260}/A_{280} value was also recorded. If the A_{260}/A_{280} was above 1, indicating DNA contamination, the inclusion body was centrifuged at 12069 x g (Beckman Caulter Aventi JE) for 30 minutes. The supernatant, containing the soluble inclusion bodies, was retained and the DNA pellet was discarded.

2.1.4. SDS-PAGE

SDS-PAGE was used to analyse the protein components of a sample by separating them by molecular weight. 10 µL of protein sample was mixed with 20% v/v SDS sample buffer (Lifetech) to produce a 'non-reduced' sample. A duplicate of each sample was mixed with 10% v/v SDS sample buffer and 200 mM dithiothreitol (DTT, Fisher) to produce 'reduced' samples. All samples were incubated at 95°C for 15 minutes. A pre-cast 4-20% polyacrylamide gel (Lifetech) was placed into a Lifetech Bolt gel tank and submerged in 1x Bolt SDS running buffer (Lifetech). Protein samples were loaded onto the gel, along with an elite pre-stained protein ladder (Protein Ark) for reference. The gel was run at 165 V for 35 minutes. Once finished, the gel was removed from its plastic casing and washed with ddH_2O. The gel was then submerged in 25 mL of quick coomassie blue stain (Generon) and microwaved for 1 minute. The gel was left to develop for an hour, before de-staining overnight in ddH_2O.

2.1.5. Soluble protein refolding

Due to the size and dimeric nature of TCR and pMHC molecules, it was not possible to express fully folded protein in *E. coli*. Instead, inclusion bodies of the relevant components, either TCRα and TCRβ chain pairs, or pMHC heavy subunit, β_2M, and peptide, were refolded together by dilution of denaturing conditions (Boulter et al., 2003). Soluble TCR molecules were refolded by incubating 30 mg of TCRα chain inclusion bodies with 10 mM DTT at 37°C for 30 minutes. 30 mg of TCRβ chain inclusion bodies were also incubated with 10 mM DTT for 30 minutes, with incubation beginning 15 minutes after the TCRα chain incubation began.

0.74 g of cysteamine (Sigma) and 0.83 g of cystamine (Aldrich) were added to 1 L of TCR refold buffer (50mM TRIS pH 8.1, 2 mM EDTA, 2.5 M urea) at 4°C whilst the TCR chains were incubating at 37°C. After incubation the TCR chains were added to the 1 L of TCR refold buffer, with the α-chain added 15 minutes before the β-chain. Once the chains were added, the TCR refold buffer was continually stirred at 4°C for 6 hours. Soluble pMHC were refolded in much the same way. 30 mg of MHC heavy chain, 30 mg of β_2M, 4 mg of peptide and 10 mM DTT were added together and incubated at 37°C for 30 minutes. 0.74 g of cysteamine and 0.83 g of cystamine was added to 1 L of pMHC refolding buffer (50mM TRIS pH 8.1, 2 mM EDTA, 400 mM L-arginine) whilst the heavy chain, β2M and peptide were incubating at 37°C. After incubation, the mixture of heavy chain, β2M and peptide was then added to the 1 L of pMHC refold buffer. The pMHC buffer was continually stirred at 4°C for 6 hours. Once the 6-hour incubation for the TCR or pMHC refold buffers was complete, the buffer was dialysed (Cellulose dialysis membrane, Sigma-Aldrich) in 10 mM TRIS buffer until the conductivity measured below 2 mS/cm.

2.1.6. Fast Protein Liquid Chromatography (FPLC) refold purification

2.1.6.1. Anion exchange chromatography

Once dialysed, the refolds were filtered through a 0.45 µm cellulose membrane (Sartorius) in preparation for FPLC purification. Ion exchange chromatography was usually the first purification step conducted on a newly refolded protein, which would separate proteins based on their isoelectric point. The isoelectric point of TCR and pMHC molecules is approximately pH 5 and the buffers used for purification are pH 8.1, so anion exchange was used due to the basic nature of the proteins in the selected buffer.

A Porus 50HQ (Applied Bioscience) anion exchange column was attached to an AKTA pure FPLC machine (GE healthcare), washed with 50 mL of buffer B and equilibrated in buffer A. Refolded protein was loaded into the column and subsequently eluted into 1 mL fractions by introducing buffer B in a linear gradient. A chromatogram was formed by measuring A_{280} of the refolded protein as it was eluted. Fractions exhibiting A_{280} absorbance were analysed by SDS-PAGE and those containing the protein of interest were combined and concentrated to a volume of 1 mL using Amicon ultra 10,000 kDa spin columns (Milipore).

2.1.6.2 Size exclusion chromatography

Size exclusion chromatography (SEC) separates proteins by molecular weight and was conducted after anion exchange chromatography to provide two-step protein purification. SEC was also used to buffer exchange refolded protein into an appropriate buffer for downstream experiments. A Superdex 200 SEC column (GE healthcare) was attached to an AKTA pure FPLC and equilibrated into either PBS buffer (for tetramer staining or circular dichroism), crystal buffer (for crystallisation experiments), or biacore buffer (for surface plasmon resonance (SPR) experiments). The 1 mL sample of protein was loaded onto the column and eluted by flowing the selected buffer through the column. Fractions were analysed as per the anion exchange protocol (**Section 2.1.6.1**). Fractions containing refolded protein were combined and stored for subsequent downstream experiments.

2.1.6.3 Hydrophobicity interaction chromatography

Hydrophobicity interaction chromatography (HIC) was used for purifying particular TCR refolds, where anion exchange chromatography was ineffective at purifying a refolded protein. HIC separates proteins based on the number of hydrophobic amino acid residues it possesses. A HiTrap Capto Butyl Impres column (GE healthcare) was attached to an AKTA pure FPLC machine, washed with 20 mL of HIC buffer B and equilibrated in HIC buffer A. Refolded protein was buffer exchanged into HIC buffer A and loaded onto the HIC column. The flow through from the loading procedure, which contained our protein of interest, was retained. The flow through was concentrated down to 1 mL using Amicon ultra 10,000kDa spin columns in preparation for further purification.

2.1.7. Biotinylation of refolded pMHC molecules

Some pMHC molecules needed to be biotinylated for certain downstream experiments, such as tetramer staining and SPR. To do this, MHC heavy chains containing a biotin tag were used for pMHC refolds where biotinylated protein was required. Once these refolds were purified by anion exchange chromatography, they were concentrated to 700 µL using Amicon ultra 10,000 kDa spin columns. 100 µL of Biomix A (Avidity), 100 µL of biomix B (Avidity), 100 µL of Bio200 (Avidity), and 1 µL of BirA enzyme (Avidity) were added to the refold. The refold was then incubated at room temperature overnight. The excess biotin was then washed out by buffer exchanging into PBS using Amicon ultra 10,000 kDa spin columns and the refold proceeded to SEC purification.

2.2. Protein crystallisation

2.2.1. Sitting drop crystallisation

Crystals were grown as described by Bulek *et* al. (Bulek et al., 2012). Refolded TCR or pMHC protein of interest was concentrated to 10 mg/mL using Amicon ultra 10,000 kDa spin columns and Cercon 0.5 mL 10,000 kDa spin columns (Generon). For crystallisation experiments involving TCR:pMHC complexes, both components were concentrated to approximately 10 mg/ml and then mixed in a 1:1 molar ratio. The protein sample was loaded onto a Griffin (Art Robins) crystallography robot, along with a 96-condition crystallisation screen. The crystallisation screens used in this thesis were the T-cell optimisation screen (Bulek et al., 2012), the PACT screen (Molecular Dimensions), and the Proplex screen (Molecular Dimensions). Sitting drop crystallisation took place on 96-3 well low profile intelliplates, which consist of 96 wells each containing a mother liquor and three smaller wells (Molecular Dimensions). For each well, 200 µL of crystallisation screen was placed into the mother liquor and 0.2 µL was placed in 'smaller' wells one and two. 0.2 µL of protein sample was then added to the first 'smaller' well. The plates were sealed and stored at 18°C. Plates were periodically imaged using Rock Imager (Formulatrix, **Figure 2.2a**).

2.2.2. Seeding protein crystals

To improve the odds of successful protein crystallisation, crystal seeding was sometimes used (D'arcy et al., 2007). Crystals of protein with similar sequence homology to the protein of interest that have successfully diffracted were crushed into sub-microscopic fragments, known as a seed mixture, using a Qiagen crystal seeding kit (Qiagen). The seed mixture was then added to a homologous protein sample to aid the formation of protein crystals. 1 µL of protein sample, 0.5 µL of seed mixture, and 1 µL of crystallisation buffer were added to a hanging drop well by hand. The well was suspended above a 500 µL reservoir of crystallisation buffer. Seeding plates were imaged under a microscope (Leica).

2.2.3. Crystal data collection and structure determination

2 µL of mother liquor solution containing 10% v/v ethyleneglycol (Molecular Dimensions) was added to the drop containing the protein crystals. The crystals were then fished out of the drop using a magnetic cryo-loop (Molecular Dimensions) and stored in liquid nitrogen. The collected crystals were then taken to the Diamond Light Source synchrotron in Oxfordshire, UK. X-ray datasets were collected using a wavelength of 0.98 Å and consisted

of 3600 images, with 0.1 second exposure and 0.1° oscillation (**Figure 2.2b**). Datasets were processed to produce reflection intensities and to determine unit cell dimensions and symmetry space group. The processing software used for each structure will be highlighted in their respective statistics table.

The resulting x-ray diffraction data were used to 'solve' the 3D crystal structure using the CCP4 software suite. Matthews Coefficient was used to determine the number of asymmetrical units in each unit cell of the reflection intensities (Winn et al., 2011). Phaser was then used to conduct molecular replacement , which uses an existing 3D structure with high structural homology to the protein of interest as a model, to produce a 3D structure solution (Mccoy et al., 2007). Win-Coot was used to adjust the amino acid sequence of the model to match the protein of interest and add relevant solvent molecules to the 3D structure (**Figure 2.2c**) (Emsley et al, 2004). Finally, REFMAC5 was used to refine the 3D structure to publication quality (Murshudov et al., 2011).

2.2.4. 3D structural analysis

Refined 3D structures were analysed using Pymol version 2.3.4 to identify points of interest. Contacts between TCR and pMHC chains were identified using CCP4 and imaged using Pymol. TCR crossing angles were determined using Pymol and Microsoft Excel.

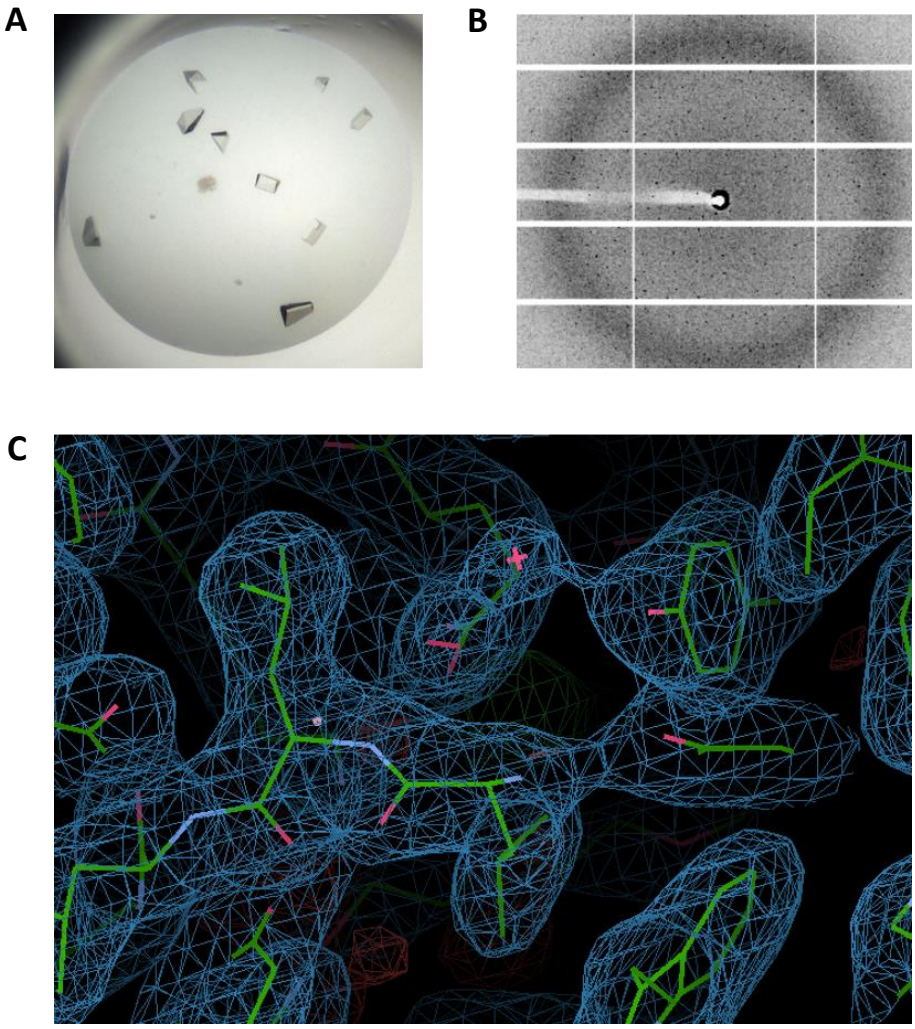

Figure 2.2. Structural determination workflow.
(**A**) Example of protein crystals to be taken to the Diamond Light Source synchrotron. (**B**) Example of an x-ray diffraction pattern acquired from the synchrotron. (**C**) Example of an electron density map formed using WinCoot.

2.3. Homology modelling

Due to difficulties experienced crystallising certain TCR:pMHC complexes and the poor diffraction exhibited by some crystals, some TCR:pMHC 3D structures were unobtainable using x-ray diffraction. In these cases, homology modelling was used to provide a theoretical structure of the protein of interest. Homology modelling was conducted using the Modeller software suite (Webb et al., 2014). 3D structures with strong homology to the protein of interest were aligned with the amino acid sequence of the protein of interest. The software used this alignment to form a theoretical 3D protein model which obeys known constraints of protein folding. The theoretical model was analysed as described in **Section 2.2.4**.

2.4. Biophysical analysis

2.4.1. Surface plasmon resonance (SPR)

TCR:pMHC binding kinetics were determined by SPR as described (Whalley et al., 2020) (**Figure 2.3**). SPR experiments were conducted using a BIAcore T200 (GE healthcare). Approximately 500 response units (RU) of biotinylated pMHC molecules was immobilised onto a CM5 sensor chip (GE Healthcare). A negative control was bound to flow cell 1 and samples bound to flow cells 2-4. Equilibrium binding analysis was performed at 25°C. Ten serial dilutions of the TCR were made and 100 mL of each dilution was injected onto the chip. Data was analysed using Graphpad Prism and fitted to a global fit algorithm. K_D values were calculated assuming 1:1 binding and Michaelis–Menten kinetics ($AB = B*AB_{MAX}/(K_D+B)$)

SPR was also used to determine thermodynamic parameters, as described (Willcox et al., 1999) The SPR method above was repeated at 8, 15, 21, 25, 35, and 40°C. Thermodynamic parameters were calculated using the non-linear Van't Hoff equation ($RT \ln K_D = \Delta H° - T\Delta S° + \Delta Cp°(T - T^0) - T\Delta Cp° \ln (T/T^0)$) with $T^0 = 298$ K.

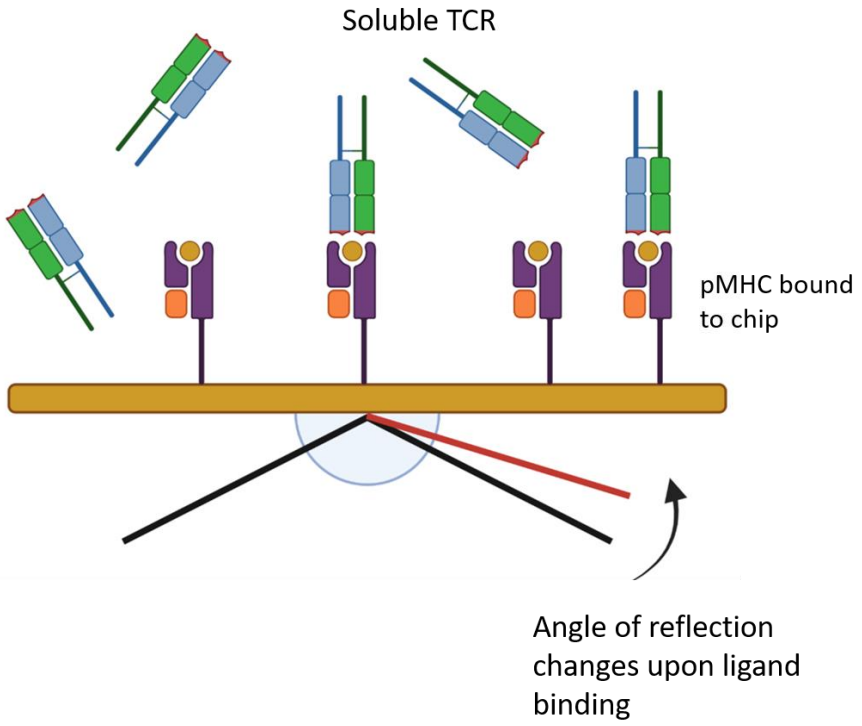

Figure 2.3. Surface plasmon resonance.
A diagram showing a surface plasmon resonance experiment.

2.5. Molecular biology

2.5.1. Protein construct design

TCR expression constructs of interest were designed based on in-house T-cell repertoire sequencing data. These data were used in conjunction with the International Immunogenetics Information System (IMGT) to assemble the amino acid sequence. Two stop codons were added to the 3' end of the construct. NdeI (CATATG) and EcoRI (GAATTC) restriction sites were placed at the 5' and 3' ends respectively of the construct. Constructs were ordered from GeneArt (ThermoFisher), with nucleotide sequences optimised for *E. coli* expression.

2.5.2. Molecular cloning

2.5.2.1. Restriction digest

Protein constructs ordered from GeneArt were shipped in a pMK transport plasmid and needed to be cloned into the pGEM-T7 *E. coli* expression vector. 2 µg of pMK plasmid containing the construct was mixed with 1 µL of NdeI enzyme (Thermo Scientific), 1 µL of EcoRI enzyme (Thermo Scientific), 2 µL of 10x green Fast Digest buffer (Thermo Scientific) and made to 20 µL using nuclease-free water (Ambion). This process was repeated using 'empty' pGEM-T7 vector. Both plasmids were incubated overnight at 37°C. After incubation, digested pGEM-T7 was treated with 1 µL FastAP enzyme (Thermo Scientific) and incubated at 37°C for 15 minutes. The pGEM-T7 was then incubated at 65°C for 5 minutes to deactivate FastAP. FastAP treatment was not needed for the pMK plasmid.

Agarose gel electrophoresis was used to confirm digestion was successful. 0.5 g of agarose (Sigma) was added to 50 mL of 1x TAE buffer, diluted from a 50x stock (2 M Tris, 1 M acetic acid (Fisher), 50 mM EDTA). The mixture was heated to dissolve the agarose, then 2.5 µL of Midori Green was added once the mixture was cool enough to handle. The agarose mixture was poured into a gel tank and left to set. The resulting gel was submerged in 1x TAE buffer. Digested plasmids were loaded onto the gel along with pre-stained molecular marker (Thermo Scientific). The gel was run at 45V for 90 minutes. Once the gel had finished running it was imaged under UV light. Successful pMK digestion showed two bands, a larger band (pMK vector) and a smaller band (protein construct) at approximately 3000 base pairs and 700 base pairs respectively. Successful 'empty' pGEM-T7 digestion would just show one band (pGEM-T7 vector) at approximately 3000 base pairs.

2.5.2.2. DNA extraction and ligation

Once the protein construct has been 'cut' from the pMK vector, it was ligated into the 'empty' pGEM-T7 vector. The bands indicating protein construct and pGEM-T7 vector were cut out of the gel and subjected to gel extraction using the Wizard® SV Gel and PCR Clean-Up System (Promega). Membrane binding solution was added to each gel fragment in a 1:1 w/v ratio. The fragments were incubated at 65°C until the gel fragments had dissolved, forming DNA solutions. The DNA solutions were transferred to SV Minicolumn, incubated for 1 minute at room temperature and centrifuged at 16,000 x g (Eppindorf 5424) for 1 minute. 700 µL of membrane wash buffer was added to the SV minicolumns and centrifuged at 16,000 x g for 1 minute. A further 500 µL of membrane wash buffer was added and centrifuged at 16,000 x g for 5 minutes, before a dry centrifugation at 16,000 x g for 1 minute. Finally, the SV minicolumn was transferred to a clean 1.5 mL tube, 50 µL of nuclease-free water was added, incubated at room temperature for 1 minute and centrifuged at 16,000 x g for 1 minute. The resulting flow through contained extracted DNA.

For DNA ligation, 30 fmol of 'empty' pGEM-T7 DNA, 150 fmol of protein construct DNA, 1 µL of DNA ligase enzyme (Thermo Scientific) and 2 µL of 10x DNA ligase buffer (Thermo Scientific) were mixed together and made up to 20 µL using nuclease-free water. The mixture was incubated at room temperature overnight. Following ligation, the DNA was transformed into TOP10 competent *E. coli* cells and plated into ampicillin LB agar plates.

2.5.3. Colony PCR

Colony PCR was conducted to confirm ligation was successful. A mixture consisting of 12.5 µL DreamTAQ mastermix (Thermo Scientific), 1 µL T7 forward primer (5´-TAATACGACTCACTATAGGG- 3´) at 50 pmol, and 1 µL SP6 primer (5'-ATTTAGGTGACACTATAG- 3') at 50 pmol, was made up to 25 µL with nuclease-free water. A colony from the post-ligation transformation was added. Mixtures were placed in a thermal cycler, set to the following program:

94°C – 10 minutes
94°C – 20 seconds
57°C – 20 seconds
72°C – 1 minute
x 20 cycles
72°C – 7 minutes

PCR mixtures were analysed by agarose gel electrophoresis (as described in **Section 2.5.2.1**). Bands of appropriate size (approximately 700 base pairs) indicated successful ligation.

2.5.4. DNA amplification

Successfully ligated DNA was amplified for sequencing and protein expression. Colonies containing ligated DNA (as shown by colony PCR) were cultured in 5 mL of LB media (10 g/L tryptone, 5 g/L yeast extract, 10 g/L $NaCl_2$), containing 50 µg/mL carbenicillin and incubated overnight at 37°C, 220 RPM. Cultures were then centrifuged at 2786 x g (Eppindorf 5810R) for 20 minutes, and the supernatant removed, leaving the bacterial pellet.

A PureLink Quick Plasmid Miniprep kit (Invitrogen) was used to amplify the DNA. Bacterial pellets were homogenised in 250 µL of R3 buffer. 250 µL of L7 buffer was added, mixed gently and incubated at room temperature for 5 minutes. 350 µL N4 buffer was then added. The mixture was mixed vigorously and centrifuged at 16,000 x g for 10 minutes (Eppendorf 5424). The supernatant, which contained the desired DNA, was transferred to a spin column, incubated at room temperature for 1 minute and centrifuged at 12,000 x g for 1 minute. 500 µL of W10 buffer was added to the spin column and centrifuged at 12,000 x g for 1 minute. 700 µL of W9 was then added, incubated for 1 minute at room temperature, then centrifuged at 12,000 x g for 1 minute. The 'dry' spin column was centrifuged again at 12,000 x g for 1 minute. The spin column was then transferred to a 1.5 mL tube, 30 µL of nuclease-free water added and was incubated at room temperature for 1 minute. The spin column was centrifuged at 12,000 x g for 2 minutes and the resulting flow through contained the amplified DNA.

2.5.5. DNA sequencing

Amplified DNA was sequenced to confirm the ligated DNA construct was correct before expression. Sanger sequencing was conducted using the TubeSeq service (Eurofins). 15 µL of sample DNA at 50-100 ng/µL was mixed with 2 µL of T7 forward primer at 10 pmol in a 1.5

mL tube. A barcode supplied by Eurofins was used to send the DNA samples for sequencing. Sequencing results were checked against the protein sequencing using nBLAST.

2.6. Cell culture

2.6.1. Reagents and buffers for cell culture and cell assays

Reagent	Composition
200IU T-cell culture media	R10 supplemented with 200 IU/mL Interleukin (IL)-2 (Proleukin), 25 ng/mL IL-15 (Miltenyi Biotech), 1 x non-essential amino acids solution (Sigma-Aldrich), 1 mM sodium pyruvate (Sigma-Aldrich), 10 mM HEPES (Sigma-Aldrich).
20IU T-cell expansion media	R10 supplemented with 20 IU/mL Interleukin (IL)-2, 25 ng/mL IL-15, 1 x non-essential amino acids solution, 1 mM sodium pyruvate, 10 mM HEPES.
Red blood cell (RBC) lysis buffer pH 7.2 – 7.4	10 mM potassium bicarbonate (Sigma-Aldrich), 155 mM ammonium chloride (Acros Organics), 0.1 mM EDTA pH 8.0.
R10	RPMI 1640 (Sigma-Aldrich), 10% v/v FBS (Gibco Life Technologies), 100 U/mL penicillin (Sigma-Aldrich), 100 µg/mL streptomycin (Sigma-Aldrich), 2 mM L-glutamine (Sigma-Aldrich).
R0	RPMI 1640, 100 U/mL penicillin, 100 µg/mL streptomycin, 2 mM L-glutamine.
R5	RPMI 1640, 5% v/v FBS, 100 U/mL penicillin, 100 µg/mL streptomycin, 2 mM L-glutamine.
Red blood cell (RBC) lysis buffer pH 7.2 – 7.4	10 mM potassium bicarbonate (Sigma-Aldrich), 155 mM ammonium chloride (Acros Organics), 0.1 mM EDTA pH 8.0.
Freezing buffer	90% v/v FBS, 10% v/v dimethyl-sulfoxide (DMSO) (Sigma-Aldrich).
Fixing buffer	PBS supplemented with 4% v/v paraformaldehyde (PFA) (Fisher Chemicals).
FACS buffer	PBS supplemented with 2% v/v FBS.
Wash buffer	PBS supplemented with 0.05% v/v Tween-20 (Merck).
Reagent diluent (RD) buffer	PBS supplemented with 1% v/v BSA.
TAPI-0 mix	30 µM TAPI-0 (Chem Cruz), 1.5 µL anti-TNFα-PE-Vio770 (clone cA2), 1.5 µL anti-CD107a-FITC (clone H4A3), 65% R5.

Table 2.3. Buffer compositions used for T-cell culture.

2.6.2. $CD8^+$ T-cell culture

$CD8^+$ T-cells, isolated from donor blood by my colleagues, were cultured in 200IU T-cell media and plated into 24-well plates (Greiner). Plates were incubated at 37°C, 5% CO_2. Half of the $CD8^+$ T-cell culture media was removed on Mondays, Wednesdays and Fridays and replaced with fresh 200IU T-cell media.

2.6.3. $CD8^+$ T-cell expansion

2.6.3.1. Isolation of peripheral blood mononuclear cells (PBMC)

A primary component of $CD8^+$ T-cell expansion is an allogenic mix of PBMCs (referred to as feeder mix cells henceforth), which are isolated from EDTA-treated buffy coats provided by the welsh blood service and non-lethally irradiated to prevent cell division. The following procedures were conducted in accordance with the Human Tissue Act (HTA). Donor blood was diluted 1:2 v/v with R10, aliquoted into 50 mL tubes and incubated at room temperature overnight on a rolling mixer. 13 mL of Histopaque (Stemcell Technologies) was added to the bottom compartment of a SepMate tube (Stemcell Technologies). 25 mL of diluted blood was transferred slowly to a SepMate tube and diluted to 50 mL with R0. SepMate tubes were centrifuged at 1200 x g (Eppindorf 5810R) for 10 minutes. The top layer of primary lymphocytes was transferred to a new 50 mL tube and diluted to 50 mL with R0. The tube was centrifuged at 800 x g for 10 minutes, the supernatant was discarded and the pellet was resuspended in 25 mL of RBC lysis buffer to remove any potential RBC contamination. The resuspension was incubated at 37°C for 10 minutes, diluted to 50 mL with R0 and centrifuged at 400 x g for 5 minutes. If the resulting pellet was red, the RBC lysis buffer wash was repeated. If the pellet was clear, it was resuspended in 25 mL of R10 and counted (see **Section 2.6.5**). The resulting resuspension contained isolated allogenic PBMCs.

2.6.3.2. $CD8^+$ T-cell culture expansion

After successful isolation, the aforementioned allogenic PBMCs were non-lethally irradiated at 3000-3100 cGy. 15 million of these feeder mix cells were incubated in a T25 flask (Greiner), with up to 1 million $CD8^+$ T-cells and 1 µg/mL phytohemagglutinin (PHA) (PAN biotech). The flask was made up to 15 mL with 20IU cell expansion media.

Flasks were incubated at 37°C, 5% CO_2 for five days. 7.5 mL of media was then removed and replaced with 7.5 mL of fresh 20IU cell expansion media, then incubated for a further two days at 37°C, 5% CO_2. $CD8^+$ T-cells were then harvested and plated at the appropriate density (generally 3-4 million cells in 2 mL in a 24 well plate) in 200UI cell culture media. $CD8^+$ T-cells were then cultured as discussed in **Section 2.6.2**.

2.6.4. Culture of suspension cell lines

Two suspension cell lines were used in this thesis. A T2 cell line, a lymphoblast line, was used for expression of HLA-A2 proteins, while a C1R cell line, a β-cell lymphoblast line, was used for expression of HLA-A24 proteins. Suspension cell lines were incubated in R10 media at 37°C, 5% CO_2. Cells were sourced from the American Type Cell Collection. Suspension cell cultures were split every Monday and Friday by removing half of the media and replacing with fresh R10. For expansion, cells were split over multiple flasks and supplemented with fresh R10 media.

2.6.5. Cell counting

Cells to be counted were harvested and resuspended in 1-5 mL of R10, depending on cell density. 10 µL of resuspended cells were mixed with 10 µL of 0.4% Trypan Blue solution (Sigma Aldrich). Cells were added to a haemocytometer and 'bright' cells were counted on the assumption that only dead cells would uptake Trypan Blue. The average number of cells per grid were multiplied by the dilution factor, then multiplied by 10^4 to determine cells per mL.

2.6.6. Long term cell storage

Cells bound for storage were centrifuged at 400 x g for 5 minutes and the supernatant was discarded. The resulting pellet was resuspended in freezing buffer and split into 1 mL aliquots. Cells were incubated at -80°C in Mr Frosty isopropanol-filled controlled-rate freezing pots (Nalgene) for at least 24 hours. Cells were then transferred to liquid nitrogen for long term storage.

Cells were removed from storage by incubating at 37°C until thawed. Cells were then transferred into 10 mL of R10 media, which was pre-warmed to 37°C. Cells were centrifuged at 400 x g for 5 minutes, the supernatant was discarded and the pellet was resuspended in appropriate media. The cell resuspension was then cultured according to cell type.

2.7. CD8$^+$ T-cell assays

2.7.1. CD8$^+$ peptide activation assay

2.7.1.1. CD8$^+$ peptide co-incubation

To determine activation in response to exogenously-applied peptide, CD8$^+$ T-cells were harvested and washed in R0 media and incubated at 37°C, 5% CO_2 overnight to 'rest' them. CD8$^+$ T-cells were then plated at a density of 30,000 cells per well in a 96-well plate (Greiner), along with 60,000 antigen presenting cells (HLA-A2$^+$ T2 or HLA-A24$^+$ C1R cell lines) per well and 10 µL of peptide at the appropriate concentration for the assay. Plates were incubated at 37°C and 5% CO_2 overnight. The following morning, the plates were centrifuged at 400 x g for 5 minutes. 50 µL of supernatant was harvested, transferred to a fresh 96-well plate and diluted in 70 µL of R5 media.

2.7.1.2. Enzyme-linked immunosorbent assay (ELISA)

A DuoSet human ELISA assay kit (R + D Systems) was used to measure CD8$^+$ T-cell activation. Half-area flat-bottomed 96-well plates (Greiner) were coated in 50 µL of 1 µg/mL anti-human MIP-1β antibodies (R + D Systems), sealed with Clingfilm and incubated at room temperature overnight.

The plates were then washed with 190 µL Wash buffer three times using a Wellwash Versa plate washer (Thermo Fisher). 150 µL of RD buffer was then added and the plates were sealed and incubated for 1 hour. The plates were then washed before 50 µL of CD8$^+$ supernatant was added and the plates were incubated for 75 minutes. Recombinant human standards were added at this point at a serial dilution, starting at 2000 pg/mL, which were used to create a standard curve (**Figure 2.4**). The plates were washed again as before 50 µL of MIP-1β detection antibody was added to the plates, which were then incubated at room temperature for 1 hour 15 minutes. The plates were washed again as described.

50 µL of streptavidin-conjugated horseradish peroxidase (R + D Systems) was added to the plates before incubation at room temperature in the dark for 20 minutes. The plates were then washed. 50 µL of 1:1 Colour A and B mixture (R + D Systems) was added to the plates before incubation for 5-10 minutes to allow the plates to develop, then 25 µL of STOP solution (R + D systems) was added to halt development. OD_{450} of the wells were recorded using an iMark microplate reader (BioRad). Data was analysed using Microsoft Excel.

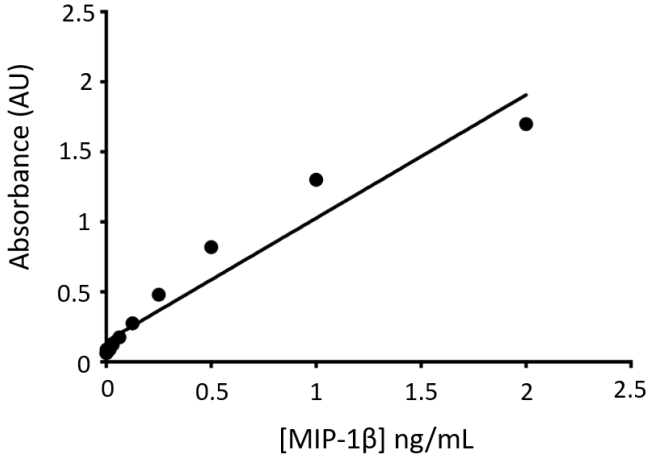

Figure 2.4. MIP-1β ELISA standard curve.
An example of a standard curve used during a MIP-1β ELISA experiment.

2.7.2. Combinatorial peptide library (CPL) screening

CPLs were performed using an ELISA assay, as described (Whalley et al., 2020). 60,000 antigen presenting cells were pulsed with 100 µM peptide mix from a CPL screen (Pepscan Presto Ltd.) by incubating for 2 hours at 37°C, 5% CO_2. 30,000 rested T-cells were then co-incubated with the antigen presenting cell:peptide mixture as described in **Section 2.7.1**. MIP-1β expression was measured by ELISA as described in **Section 2.7.1**.

2.7.3. Chromium-51 (^{51}Cr)- release cytotoxicity assay

Cytotoxicity assays were performed as described (Tungatt et al., 2015). Target cells were harvested and labelled with 30 µCi of ^{51}Cr (Perkin Elmer) per 1 x 10^6 cells. Target cells were then incubated at 37°C for 1 hour. Target cells were then washed with D-PBS, resuspended in R10 and incubated at 37°C for 1 hour. Target cells were then washed with D-PBS and resuspended in R10, before plating at 2000 cells per well in a 96-well plate. Some target cells were incubated with 5% Triton X-100 to determine maximum ^{51}Cr release, while some other target cells were incubated with R10 to determine spontaneous ^{51}Cr release. The remaining cells were incubated with effector $CD8^+$ cells at a 3:1 $CD8^+$:target cell ratio in 150 µL of R10. Cells were co-incubated for 4 hours at 37°C, 5% CO_2. Cell supernatants were then harvested and measured for radioactivity using a 1450-Microbeta™ counter (Perkin Elmer). The following equation was used to calculate T-cell cytotoxicity:

$$\%\ \text{Specific lysis} = \frac{\text{Experimental } ^{51}\text{Cr release} - \text{Spontaneous } ^{51}\text{CR release}}{\text{Maximum } ^{51}\text{Cr release} - \text{Spontaneous } ^{51}\text{CR release}} \times 100$$

2.7.4. pMHC multimer staining

2.7.4.1. pMHC multimer assembly

Fluorochrome-conjugated pMHC tetramers were assembled in the dark from biotinylated pMHC monomers refolded as described in **Section 2.1**. The pMHC monomers were mixed with PE-conjugated streptavidin at a 4:1 ratio, with pMHC monomers at a molar excess (Invitrogen, Thermo Fisher). PE-conjugated streptavidin was added to pMHC monomer over 5 stepwise increments, each separated by incubation on ice for 20 minutes. 1 µL of protease inhibitor was added and the tetramer solution was diluted to 0.1 µg/µL in PBS. The stepwise addition of pMHC monomer allowed exploitation of the cooperative nature of biotin-avidin interaction (Dolton et al., 2015).

2.7.4.2. In vitro $CD8^+$ T-cell staining with pMHC multimers

Multimer staining (**Figure 2.5**) was performed as described by Dolton *et al*. (Dolton et al., 2015). 50,000 $CD8^+$ T-cells were harvested and transferred to 5 mL fluorescence-activated cell sorting (FACS) tubes (Elkay Labs). $CD8^+$ cells were washed twice with 3 mL of FACS buffer, centrifuged at 800 x g for 2 minutes and the supernatant discarded. 50 µL of 100 nM Dasatinib protein kinase inhibitor (Axon Medchem) was added and the tubes were incubated at 37°C for 10 minutes.

The following steps were conducted in the dark: 0.5 µg of fluorochrome-conjugated pMHC multimer was added to the tube containing $CD8^+$ cells, mixed and incubated on ice for 30 minutes. The cells were washed with PBS twice and 0.5 µg of fluorochrome-unconjugated anti-PE antibody (Miltenyi) was added. $CD8^+$ Cells were incubated on ice for 20 minutes, then washed in PBS. $CD8^+$ Cells were then stained with 2 µL of Fixable Violet Dead Stain (Thermo Fisher) before incubation for 5 minutes on ice for 5 minutes. Relevant primary fluorochrome-conjugated antibodies were added to stain for cell-surface markers, before incubation on ice for 20 minutes. If staining was to be analysed the next day, 50 µL of fixing buffer was added to each tube, followed by incubation in ice for 20 minutes. The tubes were washed twice in PBS.

Staining was analysed using a FACS Canto II (BD Bioscience). A typical gating strategy involved using forward and side scatter to isolate lymphocytes and removing doublets by gating on single cells. Vivid stain was used to remove dead cells, then cell surface marker staining was

used to isolate phenotypically relevant cells. Data was analysed and presented using FlowJo (Tree Star Inc.).

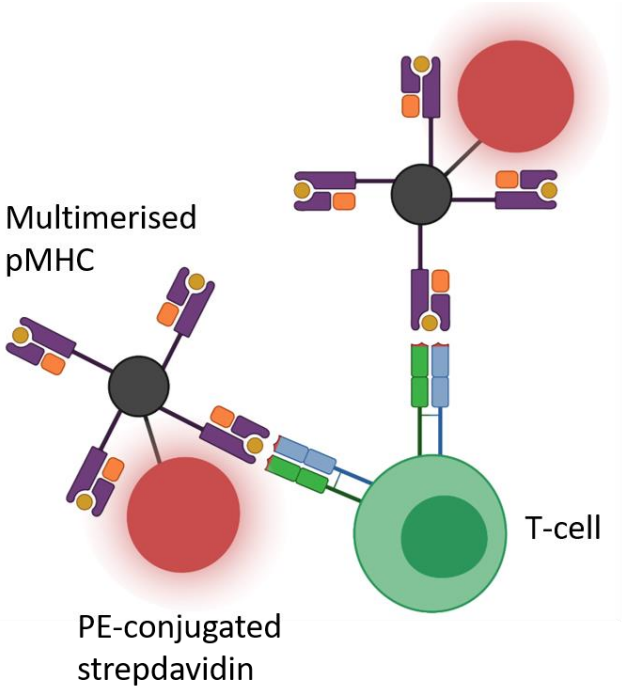

Figure 2.5. pMHC multimer staining.
A diagram showing a pMHC multimer staining experiment.

2.7.4.3. T-Cell purification via pMHC multimer specificity.

$CD8^+$ T-cells were purified based on pMHC-specificity using the miniMACS (Miltenyi) separation protocol, as per the manufacturer's instructions. T-cells were harvested and washed with 15 mL of MACS buffer (0.5% bovine serum albumin (Sigma), 2 mM EDTA in D-PBS), before centrifugation for 400 x g at 5 minutes. The cells were resuspended in 50 µL MACS buffer and 1 nM Dasatinib protein kinase inhibitor and incubated at 37°C for 10 minutes. 5 µg of pMHC multimer, relative to the pMHC component, was added to the cells before incubation on ice for 30 minutes. All buffers and cells were kept on ice from this point on, with all centrifugation steps conducted at 4°C.

Cells were washed with 15 mL of MACS buffer, centrifuged at 400 x g for 5 minutes and resuspended in 80 µL of MACS buffer and 20 µL anti-PE microbeads (Miltenyi) per 10^7 cells, before incubation at 4°C for 15 minutes. Cells were washed in 15 mL of MACS buffer, centrifuged at 400 x g for 5 minutes and resuspended in 500 µL of MACS buffer. The cells were filtered through a 30 µM membrane (Celltrics, Wolf Labs) and loaded onto pre-equilibrated miniMACS separation columns (Miltenyi). The miniMACS columns were washed three times with 500 µL of MACS buffer. The columns were then removed from the magnetic holder and the cells were eluted in 500 µL 200 IU T-cell media. The $tetramer^+$ cells were counted and plated in 24-well plates. T-cell purification was conducted by Dr Garry Dolton.

2.7.4.4. In situ $CD8^+$ T-cell staining with pMHC multimers

Cadaveric donor 6025 was sourced from the network for Pancreatic Organ donors with diabetes (nPOD). *In situ* multimer staining was performed as previously reported (Coppieters et al., 2012). Unfixed, frozen tissue sections were dried for 2 h and loaded with 1 µg (with respect to pHLA component) of PE conjugated tetramers overnight at 4°C. After one wash with PBS, sections were fixed in 2% paraformaldehyde solution for 10 min. After washing, endogenous peroxidase activity was blocked by incubation in 0.3% H_2O_2. Rabbit anti-PE antibody was added for 1.5 h at room temperature. Swine-anti-rabbit antibody coupled to horseradish peroxidase (HRP) was added and then, after 3 washes in PBS, DAB enzymatic substrate (Thermo Scientific) was applied for 3 min for detection. After washing, sections were counterstained with hematoxylin and dehydrated with sequential passages in ethanol (95%, 100%) and xylene. Tissue sections were then mounted and analyzed. *In situ* staining was conducted by Dr Garry Dolton.

2.7.5. TNF processing inhibitor-0 (TAPI-0) assay

TAPI-0 assays were used to assess T-cell functionality by measuring antigen-specific TNF production (Haney et al., 2011). This flow cytometry assay was often used in conjunction with an assay measuring cell surface expression of CD107a, a surrogate marker of lytic granule release (Betts et al., 2003). Target cells were rested overnight in R5 media. 60,000 'rested' target cells were plated at a density of 60,000 cells/well in 50 µL in a 96 U-well plate (Greiner). 'Rested' T-cells were harvested and added to the wells at a density of 30,000 cells/well in 40 µL. 10 µL of TAPI-0 mix was added to the well, resulting in a final volume of 100 µL per well.

Plates were incubated in the dark at 37°C, 5% CO_2 for 4 hours. Cells were then washed in PBS and stained with Fixable Violet Dead Stain and relevant surface antibodies as described in **Section 2.7.4**. Staining was analysed by flow cytometry as described in **Section 2.7.4** and data was analysed and presented using FlowJo. The TAPI-0 assay was performed by Dr Garry Dolton, Dr Cristina Rius Rafael and Dr Jade Hopkins.

2.8 Data and statistical analysis

All plots were generated using GraphPad Prism Version 9 (GraphPad Software) and all flow cytometry data were analysed using FlowJo (Tree Star Inc). Standard deviation (SD) was shown as error bars in data where N > 2. Where appropriate, an unpaired two-step T-test was used to determine statistical significance.

2.9 Clarification of experiments performed

Several experiments highlighted in this thesis were carried out by my colleagues. For clarity, all experiments that involved the production and analysis of soluble protein, including SPR, crystallography, and molecular biology were performed and analysed by myself. Experiments that involved cell culture and T-cell assays, with the exception of **Figure 5.8** and **Figure 5.13**, were performed by either Dr Garry Dolton, Dr Cristina Rius Rafael, or Dr Jade Hopkins. Any work contributed by my colleagues has been noted in both the thesis text and figure legends.

3. Dominant persistent T-cell receptors following successful immunotherapy can engage multiple different cancer antigens

3.1. Introduction: Cancer immunotherapy

While T-cells primarily respond to pathogens they can also respond to aberrant-self, including dysregulated or mutated self in cancer cells. Anti-cancer T-cells recognise tumour-associated antigens (TAAs) and mount immune responses against them (Bianchi et al., 2016). However, the tumour microenvironment suppresses T-cell activity via a number of mechanisms including; a lack of nutrients, overexpression of ligands for T-cell checkpoint molecules, and through secretion of immunosuppressive cytokines by the tumour (Frey, 2015). These factors, coupled with the fact that TCRs directed against TAAs tend to have low affinities (Aleksic et al., 2012) result in poor tumour immunity. This presents a substantial challenge to the endogenous anti-cancer T-cell immune response. However, there are ongoing efforts to overcome T-cell tolerance to tumour cells. These so-called 'cancer immunotherapies' represent the biggest development in cancer treatment since radiotherapy and chemotherapy. Whilst there have been studies that show potential in using $CD4^+$ T-cells (Wang et al., 2018; Xhangolli et al., 2019) and γδ T-cells (Alexandra et al., 2016; Parente-pereira et al., 2014), this thesis will mainly discuss $CD8^+$ T-cells as these cells are currently the preferred immune cells for targeting cancer (Farhood, 2019).

3.1.1. Checkpoint blockade therapy

A key cancer immunotherapy approach is checkpoint blockade therapy. As mentioned in **Section 3.1**, overexpression of immune checkpoint molecule ligands presents a barrier to immune targeting of tumours. One strategy to overcome this is to use antibodies to block these checkpoint molecules, preventing ligand binding and thus improving T-cell function within the tumour microenvironment (Sharma et al., 2015). Two commonly targeted checkpoint molecules are CTLA-4 and PD-1. CTLA-4 is expressed on T-cells and regulates T-cell activity by inhibiting T-cell proliferation in response to CD80 and CD86 molecules present on target cells (Walunas et al., 1994). PD-1 is also expressed on T-cells and inhibits proliferation and cytokine production in response to PD-L1 expressed by target cells (Freeman et al., 2000). Blocking either CTLA-4, PD-1, or their respective ligands, has been shown to be a viable strategy for overcoming the immune-suppressive tumour microenvironment.

The first checkpoint blockade therapy approved by the US food and drug association (FDA) was ipilimumab in 2011. Ipilimumab is a recombinant immunoglobulin molecule which disrupts the CTLA-4:CD80/CD86 interaction by binding to CTLA-4. Ipilimumab was approved for the treatment of melanoma, a disease where the only prior treatment was chemotherapy (Sondak et al., 2011). In 2014, two further checkpoint inhibitors, pembrolizumab and nivolumab, were approved by the FDA. Both pembrolizumab and nivolumab are antibody based-therapies and both bind PD-1 (Guo et al., 2017; Khoja et al., 2015). There are currently seven checkpoint inhibitor therapies approved by the FDA. Due to the mechanical differences by which CTLA-4 and PD-1 regulate T-cell activity, it is possible to use multiple checkpoint inhibitors simultaneously. Phase III trials suggest combinatorial therapy using both ipilimumab and nivolumab results in greater progression-free survival than either therapy alone (Hellmann et al., 2019; Hodi et al., 2018).

While immune checkpoint blockade therapy has shown efficacy in the treatment of cancer, it can also produce immune related adverse effects (IRAEs) in some patients, particularly those with underlying autoimmune conditions, due to the disruption of immune regulation (Kostine et al., 2017). The occurrence of autoimmune disease following immune checkpoint blockade has also been observed in patients with no underlying autoimmune symptoms (Belkhir et al., 2017). The use of immunosuppressive therapy to treat IRAEs has been studied, however findings have shown that this may reduce the effectiveness of immune checkpoint blockade therapy (Tison et al., 2019).

3.1.2. Cancer vaccines

Another promising cancer immunotherapy approach is the use of TAAs as vaccines. In theory, the use of TAAs as vaccines could promote the proliferation of cancer-specific T-cells and result in an improved anti-cancer immune response. Vaccines can also take the form of HLA-restricted peptides. TAA vaccine candidates that have been explored include the Melan-A- (Reynolds et al., 1997) and the GP100-derived (Salgaller et al., 1996) peptide vaccines. High affinity APLs derived from TAAs could theoretically break T-cell tolerance to tumour cells. A study from my laboratory described an APL (MTSAIGILPV) as a super-agonist ligand for a melanoma patient-derived CD8 T-cell that responded to the well-studied HLA-A2-restricted Melan-A epitope (EAAGIGILTV). MTSAIGILPV was shown to induce a more effective T-cell response in healthy donors, as well inducing T-cells with superior anti-cancer response from melanoma patient blood, when compared to the EAAGIGILTV epitope (Galloway et al., 2019).

Cancer neoantigens have also been studied for use as cancer vaccines. Neoantigens are peptides encoded by mutations exclusively present in tumour cells. As neoantigens are non-self-antigens, T-cells are not tolerised to them. Tumours with greater mutational loads and subsequently greater numbers of neoantigens have been shown to generate more effective anti-cancer T-cell responses (Brown et al., 2014). A phase 1 clinical study by Ott *et al*. used whole-exome sequencing to identify novel somatic mutations present in the tumour DNA of individual patients. RNA-seq was used to confirm expression of mutated alleles and netMHCpan was used to predict which mutated peptides would bind to HLA-A and HLA-B. Vaccine candidates were synthesised using this data. These vaccine candidates successfully induced T-cell responses to 76% of neoantigens identified among the patient cohort (Ott et al., 2017). However, whilst neoantigens vaccines can clearly be effective, the individual nature of tumour mutations means this treatment is highly personalised, requiring costly whole-exome screening of each patient to identify potential neoantigens that can be used as vaccine targets (Yadav et al., 2014).

Vaccines can also be used as cancer prophylaxis, where patients are vaccinated against oncogenic viruses to help prevent the cause of cancer. Two prominent examples of prophylactic cancer vaccines are Heptabax-B, which prevents hepatocellular carcinoma by vaccinating against hepatitis B (Maugh, 1981) and Gardasil, which prevents cervical cancer by vaccinating against human papillomavirus (Siddiqui et al., 2006). More recent studies have also suggested CMV may have an oncolytic role, specifically in breast and colorectal cancer, implying a use for CMV vaccines as cancer prophylactics (Ardakani et al., 2019; Richardson et al., 2020).

3.1.3. Adoptive cell therapy in cancer

3.1.3.1. Tumour infiltrating lymphocyte therapy

As discussed in **Section 1.4.1**, ACT has shown promise in the field of cancer immunotherapy through the use of TILs, which are T-cells taken from a patient's tumour-microenvironment, expanded *ex vivo* and infused back into the patient to illicit immune killing of the tumour. A study by Dudley *et al.* showed how a TIL-based therapy can produce tumour regression in patients with metastatic melanoma (Dudley et al., 2002). Further studies optimised TIL therapy in metastatic melanoma by subjecting patients to chemoradiation prior to TIL infusion, as well as combining TIL therapy with IL-2 infusion to promote the activity of the TILs (Dudley et al., 2008; Rosenberg et al., 2011). A modification of the standard TIL therapy

involves the use of 'young' TILs, which are TILs that are taken from tumour fragments, pooled, then infused into the patient with minimum screening. Young TILs exhibit greater expression of co-stimulatory molecules due to requiring less time in culture, allowing for a more effective T-cell response against the tumour (Donia et al., 2012).

TIL therapy has proven effective in the treatment of other forms of cancer including colorectal, ovarian, pancreatic, and urothelial cancer (Huang et al., 2018; Meng et al., 2019; Naito et al., 1998; Stumpf et al., 2009). However, the success of TIL therapy is dependent on the accessibility of the tumour, as the TILs need to be surgically removed. 'Young' TIL therapy is particularly dependent on tumour accessibility, as enough TILs need to be safely and quickly extracted to prevent them spending too long in culture.

3.1.3.2. TCR-T therapy

TIL therapy relies on adoptive transfer of exogenous anti-cancer T-cells to kill tumours. As discussed in **Section 3.1**, T-cells possess a naturally low affinity for TAAs and are thus suboptimal for tumour killing. In **Section 1.4.2**, I discussed how TCRs can be transduced into T-cells to improve their ability to recognise target cells. This is known as 'TCR-T' therapy and has been studied for use in cancer immunotherapy. The Morgan *et al*. study described in **Section 1.4.2**, where adoptive transfer of T-cells transduced with known cancer specific TCRs resulted in melanoma tumour regression, was among the first TCR-T clinical trials for use in cancer patients (Morgan et al., 2006). Since then, clinical trials have been conducted to assess TCR-T therapy viability in other forms of cancer, such as oesophageal cancer and acute myeloid leukaemia (Chapuis et al., 2019; Kageyama et al., 2015).

TCR-T therapy can be optimised by transducing modified TCRs into T-cells to further improve target recognition. TCRs can be modified to improve their affinity for a given TAA, or to increase their density on the cell surface, thus improving T-cell recognition of tumour cells (Cole et al., 2013; Spear et al., 2017). However, as discussed in **Section 1.4.3**, engineered TCRs are at increased risk of interacting with self-antigens, as the mutations in the TCRs have not undergone thymic selection. This was highlighted in the previously discussed Linette *et al.* study (**Section 1.4.3**), where patients administered T-cells transduced with the affinity-enhanced MAGE-A3^{a3a} TCR suffered cardiac arrest, due to TCR cross-reactivity between the targeted melanoma antigen and titin (Linette et al., 2013; Raman et al., 2016). A study by Morgan *et al.* also demonstrated the risk of using enhanced TCRs in therapy, where T-cells

transduced with another enhanced MAGE-A3-specific TCR caused neurological toxicity in patients due to the enhanced TCR recognising a MAGE family protein expression in the brain (Morgan et al., 2013).

Another potential risk associated with TCR-T therapy is aberrant chain pairing between the exogenous TCR and the transduced TCR, which can result in expression of 'mixed' TCR dimers on the cell surface as the result of mispairing of the endogenous and transduced TCR α and β chains. It has been shown that these mixed TCRs can potentially exhibit allo- and self-reactive properties, which would result in off target effects in patients (Loenen et al., 2010). There have been attempts to prevent expression of mixed TCRs, including using CRISPR/Cas9 knockout to remove exogenous TCR expression, as well as transducing target TCRs into hematopoietic stem cells to reduce exogenous TCR expression via allelic restriction (Legut et al., 2018; Stärck et al., 2014).

3.1.3.3. CAR-T therapy

Another form of ACT involves the use of chimeric antigen receptor transduced (CAR-T) cells. As discussed in **Section 1.4.2**, a CAR consists of a CAR binding region (an scFvs derived from a target-specific Ig molecule), which is linked to a CD3ζ signaling domain that recruits ZAP70, resulting in T-cell activation in response to the target. Such CARs are known as 1st generation CARs. CARs can also incorporate either a single co-stimulatory molecule (2nd generation CAR) or multiple co-stimulatory molecule (3rd generation CAR), such as CD28 and 4-1BB, which improve T-cell proliferation, survival, and cytokine secretion (Hartmann et al., 2017). Further modifications that have been made to CARs include the addition of 'suicide' genes that kill the CAR T-cells in response to a small molecule (smart CARs) and the addition of ligand binding sites which prevent T-cell activation in the absence of a particular ligand (convertible CARs) (Landgraf et al., 2020; Zhou et al., 2020). Both smart CARs and convertible CARs allow for regulation of CAR T-cell activity, reducing the risk of adverse effects such as of cytokine release syndrome and neurotoxicity (Locke et al., 2019).

CAR-T therapy has proven particularly effective in the treatment of B-cell lymphomas, specifically through the targeting of CD19, a B-cell marker (Brentjens et al., 2003; D. Li et al., 2019). The first CAR-T therapy approved by the FDA was Axicabtagene Ciloleucel, which targeted CD19 and was approved for the treatment of B-cell lymphoma in 2017 (Neelapu et al., 2017). CAR-T therapy targeting of CD22, another B-cell marker, has also been used,

resulting in B-cell lymphoma regression (Fry et al., 2018). However, despite the success of CAR-T therapy in haematological malignancies, it has proven less effective in the treatment of solid tumours (Watanabe et al., 2018). While there has been some success, for example CAR-T targeting of interleukin-13 receptor alpha 2 (IL13Rα2) has resulted in glioblastoma tumour regression (Brown et al., 2016), or the use of T-cell receptor fusion constructs (TRuCs) which can target tumour surface antigens without an additional co-stimulatory domain (Baeuerle et al., 2019), more research is required to improve CAR-T success in solid tumour therapy.

3.1.4. TIL therapy studies at Cardiff University

The therapeutic benefits of TIL-based therapy in combination with IL-2 infusion were demonstrated in a clinical study conducted by the Centre for Cancer Immune Therapy (CCIT), at the Copenhagen university hospital (clinical trial NCT00937625) (Borch et al., 2020).

Our laboratory has previously characterised the TIL populations infused into the NCT00937625 patients that subsequently underwent a complete, durable remission. An HLA-A2-restricted T-cell clone called MEL8 was identified within the TIL infusion product given to complete remission patient MM909.24. MEL8 was also found to persist in the blood of patient MM909.24 long after the patient had cleared their tumour and may therefore have played a prominent role in the clearance of cancer in this patient. The MEL8 T-cell clone recognises an epitope (EAAGIGILTV) derived from the Melan-A protein, which is preferentially expressed in melanoma (Coulie et al., 1996). Further study of MEL8 showed that it killed many other HLA-$A2^{+}$ cancer cell types that did not express Melan-A. My colleagues than set about trying to find how MEL8 T-cells were recognising other cancer types and discovered that it recognised at least two other new T-cell epitopes in addition to EAAGIGILTV. These new epitopes, LLLGIGILVL and NLSALGIFST, were derived from BST2 (also known as tetherin and CD137) and IMP2 respectively. Importantly, BST2 and IMP2 have been shown to be overexpressed in several forms of cancer (Kawakami et al, 1994, Sayeed et al, 2013, Ribeiroet al, 2012). Individual T-cells that can recognise multiple tumour-associated peptides could be advantageous in cancer immunotherapy as such T-cells would be especially difficult for the cancer to escape from. This finding warranted further investigation.

3.2. Aims and objectives

I aimed to characterise how the MEL8 TCR allowed T-cells expressing it to respond to at least three, seemingly unrelated, tumour-associated peptide antigens (HLA-A2-EAAGIGILTV, HLA-A2-LLLGIGILVL and HLA-A2-NLSALGIFST). To achieve this, I aimed to produce 3D structure data of MEL8 in complex with these respective ligands and to conduct biophysical studies on each TCR:pMHC complex.

3.3. Results

3.3.1. The MEL8 T-cell clone responds to multiple tumour-associated antigens

Previous work undertaken in my laboratory isolated the Melan-A-specific MEL8 T-cell clone from the TIL infusion product used to induce a complete durable remission in stage IV melanoma patient, MM909.24 at CCIT Copenhagen. Over 80% of the response to the autologous melanoma line in the TIL infusion product used to successfully treat patient MM909.24 was shown to be HLA-A2-restricted by former Sewell laboratory PhD student Dr Cristina Rius Rafael, under the supervision of Dr Garry Dolton (Rius Rafael, 2019) (**Figure 3.1**). The dominance of HLA-A2-restricted anti-cancer responses in the TIL used to successfully treat patient MM909.24 was confirmed by comparing the response to the autologous MM909.24 melanoma line with and without CRISPR-Cas9-generated knockout of the HLA-A2 heavy chain. The MEL8 TCR was observed in the TIL infusion product used to treat patient MM909.24 and was then found to be expanded in the patient blood following complete cancer remission suggesting that it may have played a role in the cancer remission. Such T-cell clones are described as being 'persistent'. MEL8 was one of 16 HLA-A2-restricted T-cell clonotypes found after the successful treatment of patient MM909.24. The persistence of the MEL8 T-cell during and after complete cancer remission made it of particular interest.

During further study the MEL8 T-cell clone was found to respond to many other HLA-A2$^+$ non-melanoma cancer cell lines that do not express Melan-A, suggesting MEL8 could recognise a further TAA (**Figure 3.2A-B**). In order to discover what this other TAA-derived antigen might be my colleagues examined the peptide recognition landscape of the MEL8 TCR. Although HLA-I-restricted T-cells can recognise huge number of different peptides, CD8$^+$ T-cells tend to exhibit a preference for agonists of a specific length (Ekeruche-Makinde et al., 2013). A peptide sizing scan using peptides of 8-13 amino acids in length with degenerate sequence at each position (Ekeruche-Makinde et al., 2013) showed that the MEL8 TCR exhibited a clear preference for peptides of 10 amino acids in length (**Figure 3.3A**). The data from a 10-mer combinatorial library screen using MEL8 T-cells (**Figure 3.3B**) showed that recognition at position 6 was restricted to glycine while there was some flexibility at other positions. These data were input into the webtool designed by Dr Szomolay (Szomolay et al, 2016) and used to search a cancer proteome database (unpublished) for likely agonists of the MEL8 T-cell ranked by likelihood of recognition. The 15 highest scoring cancer-derived likely agonists for the MEL8 TCR are shown in **Table 3.1**.

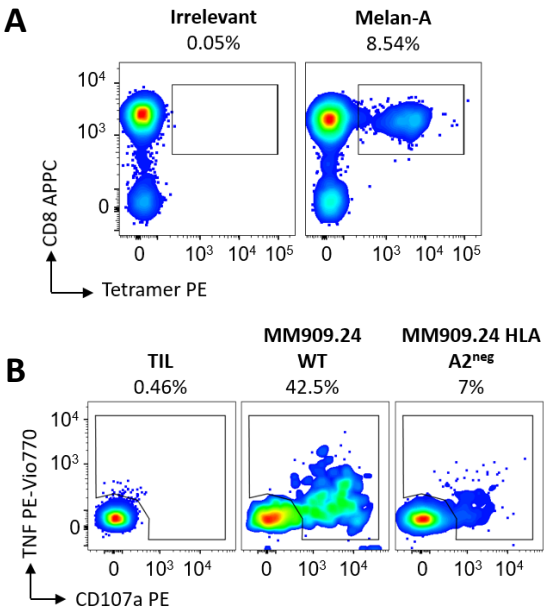

Figure 3.1. The majority of the tumour-specific T-cell response in patient MM909.24 TIL is HLA-A*02:01-restricted.

(**A**) HLA-A2-EAAGIGILTV (Melan-A) tetramer staining of TIL infusion product from patient MM909.24. Gates were set on single lymphocytes and live $CD3^+$ cells. The percentage of $CD8^+Tet^+$ T-cells is shown for each gate. Irrelevant tetramer made with human telomerase reverse transcriptase ($hTERT_{540–548}$, ILAKFLHWL) was used to set the gates. (**B**) TAPI-0 staining of tumour reactive T-cells from autologous TIL population co-incubated for 5 hours with the indicated tumour lines followed by viable sorting based on expression of CD107a and TNF on live $CD8^+CD3^+$ cells. Percentage of tumour-reactive cells found within the population is indicated above each panel. Data reproduced from the PhD thesis of Dr Cristina Rius Rafael.

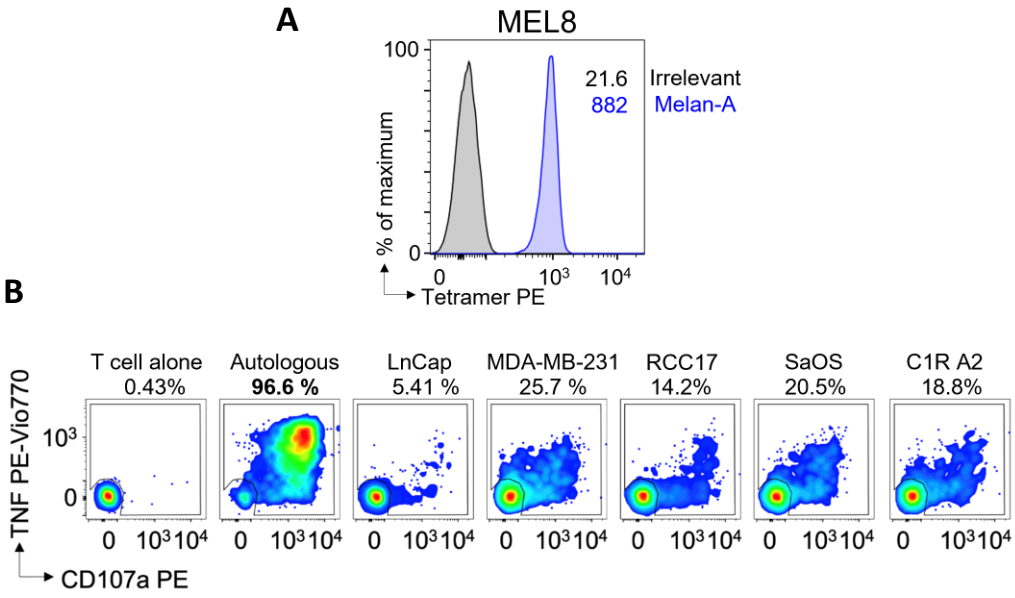

Figure 3.2. Patient MM909.24 derived Melan-A-specific $CD8^+$ T-cell clone MEL8 shows broad recognition of HLA-A2 cancer lines.

(**A**) MEL8 T-cell clone staining with HLA-A2-restricted Melan-A_{25-35} (EAAGIGILTV, in blue) and Irrelevant HLA*A02:01-restricted $hTERT_{540-548}$ (ILAKFLHWL, in grey) tetramers. MFI values are displayed. (**B**) TAPI-0 assay of MEL8 T-cell clone following 5-hour co-incubation with a panel of $HLA\text{-}A2^+$ tumours from diverse tissue origin. Gates were set on single lymphocytes and live $CD8^+CD3^+$ cells. Percentage of tumour-reactive cells based on TNF and CD107a outputs is indicated in each panel. Data adapted from PhD thesis of Dr Cristina Rius Rafael.

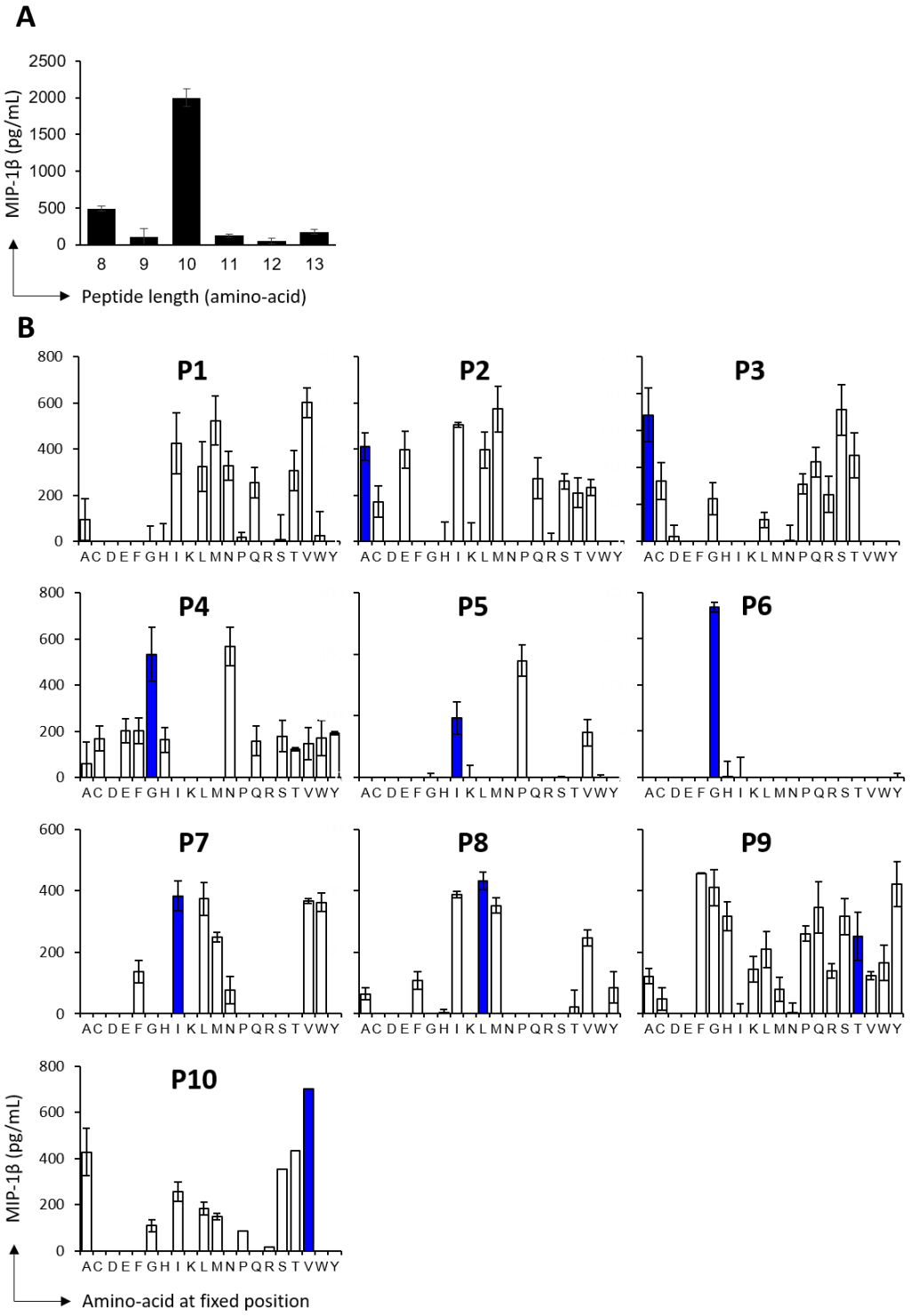

Figure 3.3. Decamer CPL-screening of Melan-A-specific T-cell clone MEL8.
(**A**) Peptide size-scan using MIP-1β (pg/mL) output measured using ELISA following overnight co-incubation of T-cells with peptide-pulsed T2 shows a strong preference for decamer peptides. (**B**) Decamer PS-CPL library (10^{-4} M) using MIP-1β ELISA as a readout. Results are displayed as histogram plots of the L-amino acid residue landscape (shown in single-letter code format) and SD from the mean of two replicates is shown. The index Melan-A peptide sequence (EAAGIGILTV) is shown in blue. Y axis marks indicate increments of 200 pg/mL. Data reproduced from PhD thesis of Dr Cristina Rius Rafael.

Rank	*Peptide sequence*	*Protein*	
-22.065	ELAGIGILTV	Melanoma antigen recognized by T-cells 1	Melan-A
-22.488	NLAAVGLFPA	Insulin-like growth factor 2 mRNA-binding protein 1	IF2B1
-22.659	EAAGIGILTV	Melanoma antigen recognized by T-cells 1	Melan-A
-22.969	LLLGIGILVL	Bone marrow stromal antigen 2	BST2
-23.128	NLSALGIFST	Insulin-like growth factor 2 mRNA-binding protein 2	IF2B2
-23.301	VYAALGILQG	Canalicular multispecific organic anion transporter 2	MRP3
-23.373	LILNIAIFFV	Dermatan-sulfate epimerase	DSE
-23.418	ATSAMGTISI	Mucin-16	MUC16
-23.435	ISAVVGILLV	Receptor tyrosine-protein kinase erbB-2	ERBB2
-23.477	TSSAIPIMTV	Mucin-16	MUC16
-23.530	TYSCVGVFQH	Heat shock 70 kDa 1A	HS71A
-23.530	LRLALGLLQL	G-protein coupled receptor 143	GP143
-23.592	MVSCIIFFFV	ATP-binding cassette sub-family C member 11	ABCC11
-23.692	QLLAEGVLSA	Anoctamin-7	ANO7
-23.695	TTLAICLLYV	Canalicular multispecific organic anion transporter 2	MRP3
-23.794	GVSGIGVTLF	Tyrosine-protein kinase Fgr	FGR
-23.820	LIAARGIFYG	Canalicular multispecific organic anion transporter 2	MRP3
-23.836	TSSAIPTLPV	Mucin-16	MUG16
-23.840	TIPSMGITSA	Mucin-16	MUG16
-23.843	TTQSLGVMSS	Mucin-16	MUG16

Table 3.1. Top 15 cancer-associated peptide sequences predicted to activate T-cell clone MEL8 by webtool designed by Barbara Szomolay and colleagues (Szomolay et al. 2016).

3.3.2. The MEL8 T-cell responds to Melan-A, BST2 and IMP2 peptides presented HLA-A2

The peptides listed in **Table 3.1** were purchased in crude form and used in T-cell recognition assays with the MEL8 T-cell. Recognition of the top five scoring peptides is shown (**Figure 3.4A**). In total, the MEL8 T-cell responded to three different cancer associated peptides; the Melan-A epitope (EAAGIGILTV), the BST2 epitope (LLLGIGILVL), and the IMP2 epitope (NLSALGIFST). The BST2 and IMP2 epitopes have not been previously described in the scientific literature. These three peptides were purchased in pure form and used in a peptide titration assay (**Figure 3.4B**). All three peptides were recognised by the MEL8 T-cell with the Melan-A peptide acting as the strongest agonist. Data provided by Dr Cristina Rius Rafael.

Dr Rius Rafael further went on to demonstrate that MEL8 still recognised the M909.24 melanoma cell line when Melan-A was knocked out using CRISPR (**Figure 3.5**) and the use of all three peptides at 10^{-8} M, a concentration likely to give a physiological antigen density at the cell surface, showed that each peptide had an additive effect in terms of target recognition by the MEL8 T-cell (**Figure 3.6**). These experiments suggested that the MEL8 T-cell could recognise cancer cells via at least three different cancer-associated epitopes.

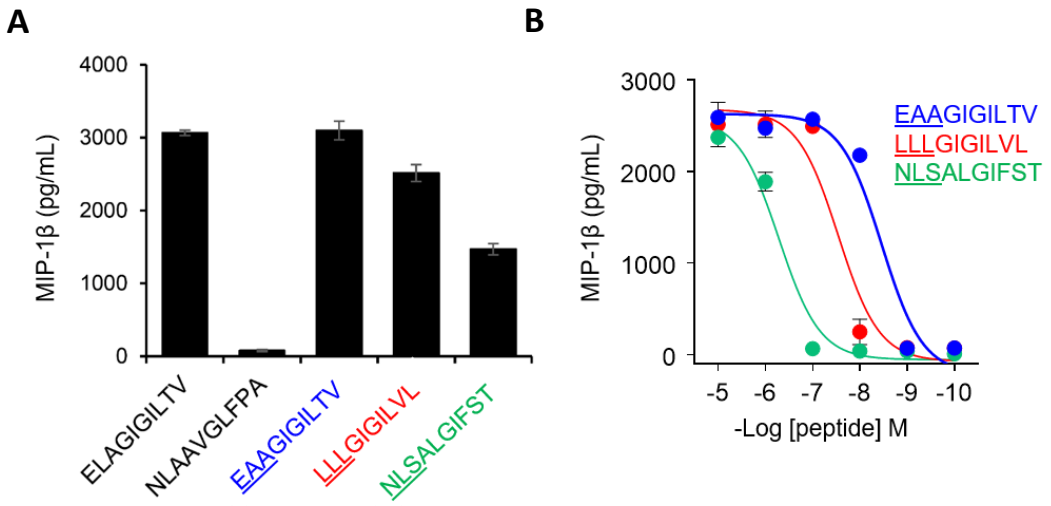

Figure 3.4. The MEL8 T-cell clone recognises multiple tumour-associated antigens.
(**A**) Activation to peptide was assessed by MIP-1β (pg/mL) release measured by ELISA after overnight co-incubation with 10^{-6} M candidate crude peptides (>40% manufacturing purity). Data courtesy of Dr Valentina Bianchi. (**B**) Peptide sensitivity of the T-cell clone was assessed by MIP-1β (pg/mL) release measured by ELISA after overnight co-incubation with EAAGIGILTV peptide (Melan-A, blue), LLLGIGILVL (BST2, red) and NLSALGIFST (IMP2, green) peptides. Mean and standard experimental error from duplicate samples is shown. Non-linear curves of best-fit are shown. Data courtesy of Dr Cristina Rius Rafael.

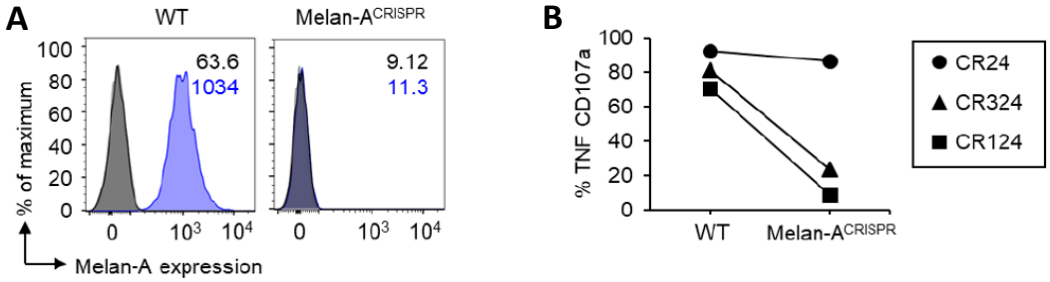

Figure 3.5. MM909.24 TIL-derived T-cell clones recognise autologous melanoma regardless of Melan-A expression.
(**A**) Melan-A expression in patient MM909.24 autologous melanoma measured by intracellular antibody staining in Wild Type (WT) and CRISPR transduced patient-autologous tumour (Melan-A^{CRISPR}). Mean Fluorescence Intensities (MFI) for Isotype (black) and Melan-A (blue) are shown. (**B**) T-cell clones MEL8 (shown in the figure as CR24 (●)), CR324 (▲) and CR124 (■) were subjected to a TAPI assay following 4-hour co-incubation with Wild Type (WT) or CRISPR transduced (Melan-A^{CRISPR}) autologous melanoma. Gates were set on single lymphocytes and live $CD8^+CD3^+$ cells. Percentage of reactive cells (%TNF^+ $CD107a^+$) is shown. Data courtesy of Dr Cristina Rius Rafael.

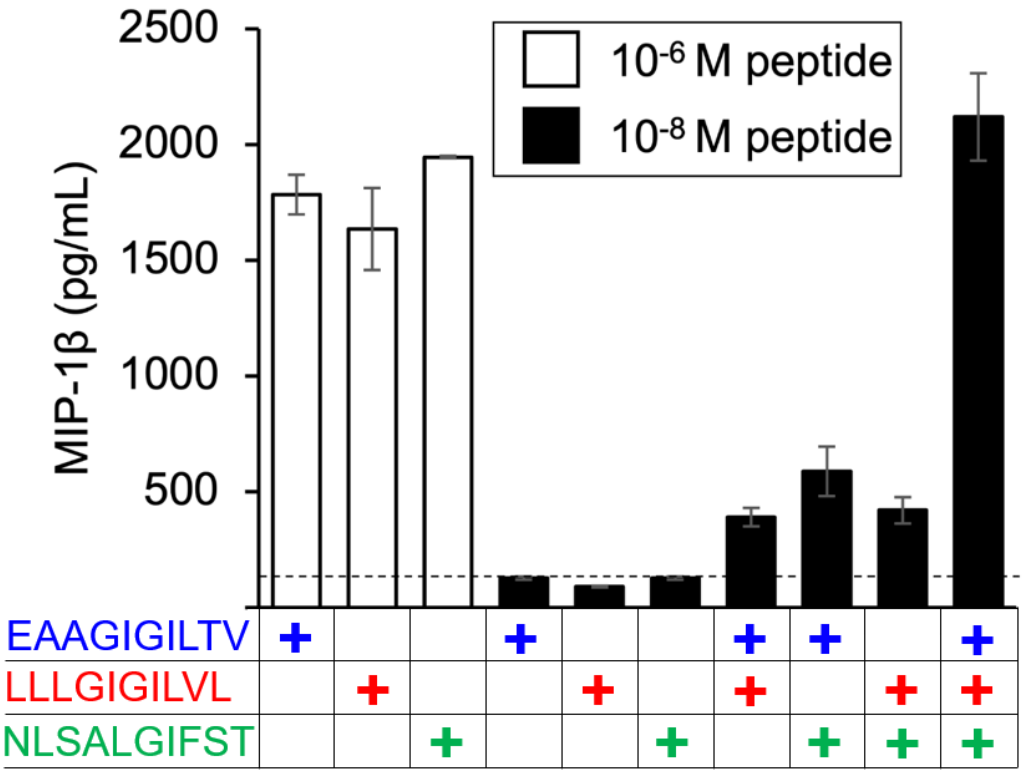

Figure 3.6. Recognition of three cancer epitopes by the MEL8 T-cell is additive.
Overnight activation of MEL8 T-cell clone co-incubated with peptide-pulsed T2 cells was assessed by MIP-1β (pg/mL) release measured by ELISA. EAAGIGILTV (Melan-A), LLLGIGILVL (BST2) and NLSALGIFST (IMP2, green) peptides were used alone or combined at the indicated concentrations. Standard deviation from the mean of two duplicate samples is shown. Data provided by Dr Cristina Rius Rafael.

3.3.3. The MEL8 T-cell binds to Melan-A, BST2 and IMP2 peptides presented by HLA-A2

Confirmation that the MEL8 T-cell clone could bind to the HLA-A2-EAAGIGILTV, HLA-A2-LLLGIGILVL, and HLA-A2-NLSALGIFST required I manufacture biotinylated versions of these pMHC monomers for use in staining experiments using fluorochrome-conjugated pMHC multimers (**Figure 3.7A-B**). The pMHC monomers were assembled into pMHC tetramers. Tetrameric pMHC molecules were used to successfully stain the MEL8 T-cell clone by Dr Cristina Rius Rafael, confirming MEL8 recognition of the Melan-A, BST2, and IMP2 epitopes (**Figure 3.7C**).

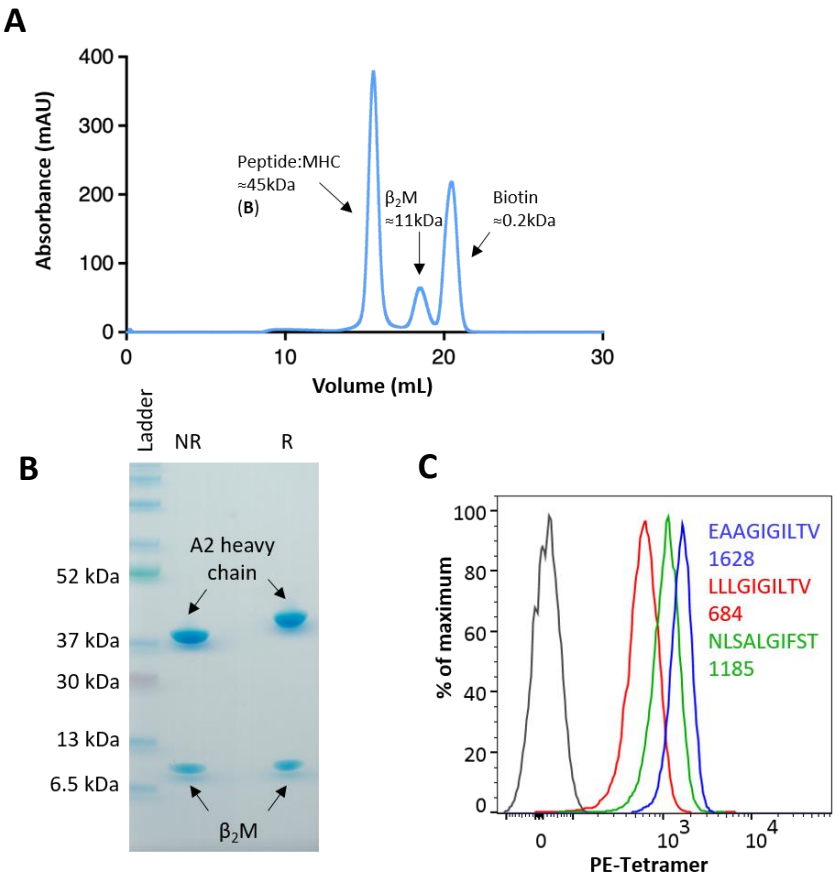

Figure 3.7. MEL8 T-cell stains with pMHC tetramer presenting cancer-derived epitopes.
(**A**) Biotinylated HLA-A2-NLSALGIFST size exclusion chromatogram (**B**) SDS-PAGE gel of the first peak of the size exclusion sample, as indicated in **A**. Sample was analysed in reduced (R, with DTT) and non-reduced (NR, without DTT) conditions. (**C**) MEL8 was stained with R-Phycoerythrin conjugated HLA-A2 tetramers assembled with peptides: EAAGIGILTV, LLLGIGILVL and NLSALGIFST from Melan A (blue), BST2 (red) and IMP2 (green) respectively. MEL8 did not stain with HLA-A*02:01 irrelevant tetramers (data not shown). Data provided by Dr Garry Dolton and Cristina Rius Rafael.

3.3.4. Production of soluble MEL8 TCR

The above data indicate that the MEL8 T-cell can recognise cancer cells via epitopes from three different TAAs. This type of 'multipronged' T-cell recognition has never previously been observed and warranted further investigation through biophysical and structural studies. I engaged on the task of generating these data and set about trying to make soluble MEL8 TCR. MEL8 TCR α- and β-chain *E. coli* expression constructs were designed and cloned into the pGEM-T7 expression vector. The individual MEL8 TCR chains were expressed, solubilised and refolded together by dilution of denaturing conditions as described in **Section 2.1.5**. Refolded MEL8 TCR was purified by anion exchange and size exclusion chromatography (**Figure 3.8A)**. SDS-PAGE analysis of the purified MEL8 TCR indicated successful refolding, however there were multiple impurities which would hinder accurate measurement of ligand binding and crystallisation (**Figure 3.8B**). These impurities persisted through multiple repeats of purification and were present in subsequent refold attempts.

Before attempting to optimise the MEL8 TCR production protocols, the functional ability of the refolded MEL8 TCR needed to be assessed. SPR analysis was conducted and showed positive interaction between the impure MEL8 TCR and HLA-A2-ITSGIGILTV, a high affinity artificial super-agonist of the MEL8 T-cell that was identified by an early CPL screen (Galloway et al., 2019) (**Figure 3.8C**). No interaction was observed between the MEL8 TCR and HLA-A2-FATGIGIITV a ligand that the MEL8 T-cell fails to respond to (Galloway et al., 2019) (**Figure 3.8D**). Due to the impurities present in the MEL8 TCR sample, it was not possible to accurately determine the binding affinity of the MEL8:A2-ITSGIGILTV interaction, as it was impossible to accurately measure the MEL8 TCR concentration. Nevertheless, the obvious binding of my sample to the HLA-A2-ITSGIGILTV super-agonist ligand was encouraging so I next attempted to produce better quality protein.

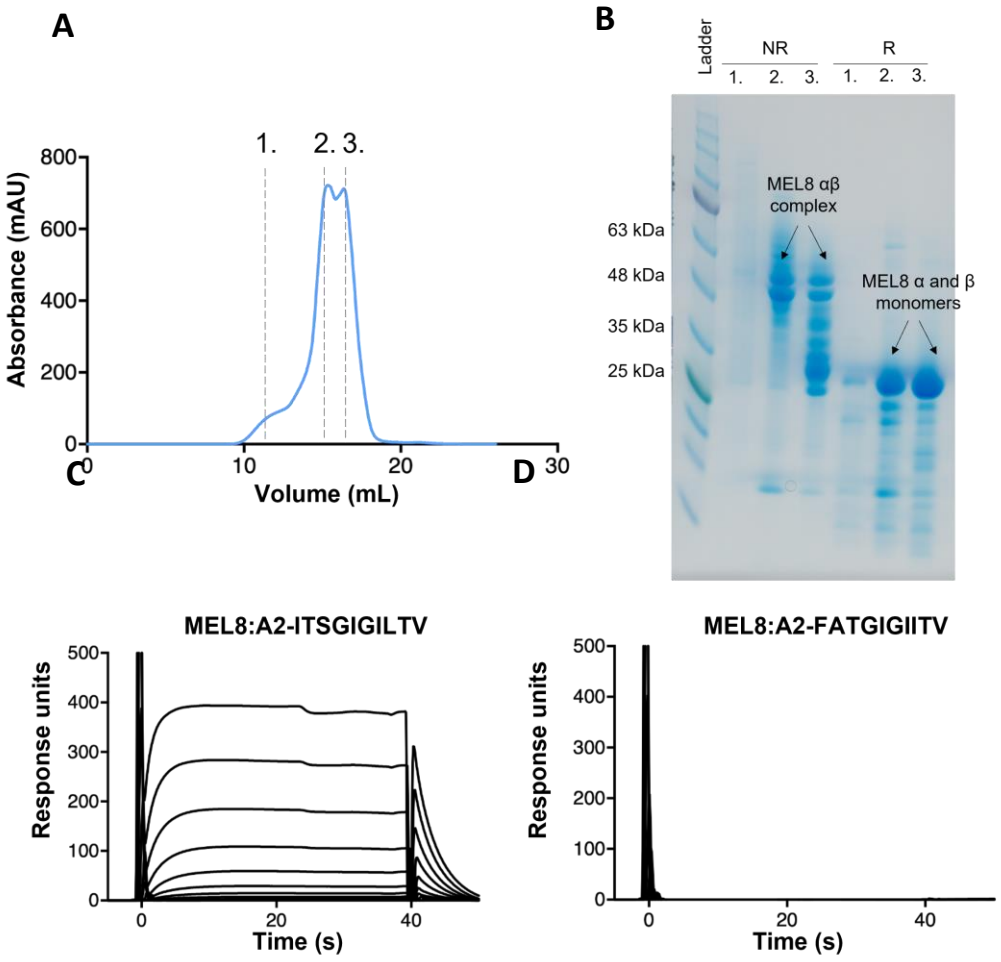

Figure 3.8. Soluble MEL8 TCR protein was successfully produced.
(**A**) MEL8 size exclusion chromatogram, showing MEL8 absorbance. Samples selected for SDS-PAGE analysis indicated by numbers and dotted lines. (**B**) SDS-PAGE gel of size exclusion samples, as indicated in **A**. Samples were analysed in reduced (R, with DTT) and non-reduced (NR, without DTT) conditions. (**C**) SPR responses of MEL8 against HLA-A2-ITSGIGILTV and HLA-A2-FATGIGIITV. Responses against the irrelevant HLA-A2-HLVEALYLV protein were subtracted to remove background response. Ten serial dilutions of MEL8 were injected, with a maximum concentration of 236.2 µM.

3.3.5. Optimising production and purification of soluble MEL8 TCR

There were two recurring impurities in my soluble MEL8 TCR preparation indicated by SDS-PAGE which needed to be removed (**Figure 3.9A**). The first was a 'smear' between 35kDa and 63kDa indicating protein aggregation, the second was a protein of roughly 16kDa mass which persisted despite size exclusion chromatography, suggesting that it interacted with the refolded MEL8 TCR.

The first optimisation step I employed was to add 1 M L-arginine to the refold buffer. The -NH_2 groups present on L-arginine form hydrogen bonds with the MEL8 TCR chains during the refold procedure, theoretically reducing aberrant hydrogen bond formation between the TCR chains and reducing aggregation. I also employed a vivaflow 200 cassette (Sartorias) to rapidly concentrate the refold buffer following the 6-hour incubation of the TCR chains in refold buffer before diluting in 10 mM Tris. The standard refold protocol instead slowly dialyses the refold buffer out in 10 mM Tris. I hoped that this faster rate of buffer exchange afforded by the vivaflow cassette (approximately 6 hours compared to approximately 2 days by dialysis) would reduce the chance for aberrant interactions occurring between the TCR chains. Finally, I opted to use hydrophobic exchange chromatography instead of anion exchange, to determine if changing the purification parameters would remove the MEL8 TCR impurities. Implementation of these optimisations resulted in purer MEL8 TCR production as shown in **Figure 3.9B**).

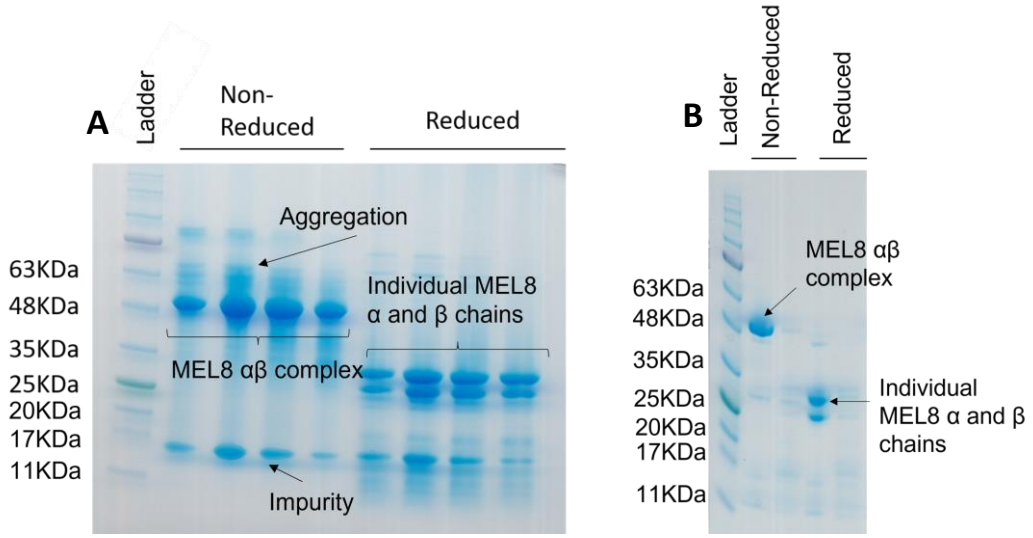

Figure 3.9. MEL8 was successfully purified using optimised refold protocol.
SDS-PAGE gels of MEL8 when purified by conventional (**A**) and optimised (**B**) purification protocols. Samples analysed in reduced (with DTT) and non-reduced (without DTT) conditions.

3.3.6. MEL8 CDR1α and CDR3β loops are instrumental in Melan-A peptide recognition.

Using the optimised refold protocol to produce pure MEL8 TCR, I was able to solve the 3D structure of the MEL8-A2-EAAGIGILTV complex at a resolution of 2.8 Å (**Table 3.2**, **Appendix Table 1**). The 3D structure shows that EAAGIGILTV peptide residues Glu1, Ile5 and Leu8 protrude upwards towards the TCR (**Figure 3.10A**), with CDR1α and CDR3β loops of the MEL8 TCR in close proximity to the EAAGIGILTV peptide (**Figure 3.10B**)**.** Peptide residues 1-5 form a 'pocket' which is occupied by MEL8 TCR residue Glu31α (**Figure 3.10C**).

3.3.7. MEL8 CDR loop interactions primarily focus on peptide residues 4 and 7

Further examination of contacts between the MEL8 TCR CDR loops and the EAAGIGILTV peptide revealed that a sizable proportion of the interactions were focused on peptide residues Gly4 and Ile7 (**Figure 3.11A**). There were 46 van der waals interactions and 6 hydrogen bonds between the MEL8 CDR loops and the EAAGIGILTV peptide, with 22 van der waals interactions and 3 hydrogen bonds involving peptide residues Gly4 and Ile7 alone, demonstrating their importance to the interaction. CDR loop residues spanning both CDR1α (Gln31α, Ser32α) and CDR3β (Thr98β) surrounded peptide residue Gly4 (**Figure 3.11B**), whereas CDR3β loop residue Thr98β was solely responsible for numerous interactions with peptide residue Ile7. (**Figure 3.11C**). Despite the protrusion of peptide residues Glu1, Ile5 and Leu8, they contributed far less interactions with the MEL8 TCR than Gly4 and Ile7.

CDR loop	TCR residue	Peptide residue	MHC residue	Number of VdW (≤4 Å)	Number of H-bonds (≤3.4 Å)	Number of Salt Bridges
CDR1α	Gly29		Trp167	2		
		Glu1		2		
	Gln31		Tyr159	2		
			Thr163	4	1	
		Glu1		1		
		Ala2			1	
		Ala3		2		
		Gly4		3	1	
		Ile5		3		
	Ser32	Gly4		1		
		Ile5		1		
CDR2α	Tyr51		Glu154	5		
			Gln155	3		
			Ala158	1		
		Ile5		1		
FWα	Lys67		Thr163		1	
CDR3α	Lue94		Arg65	1		
CDR1β	Glu30		Gln72	3	1	
			Val76	2		
CDR2β	Tyr48		Arg65	7	1	
	Val50		Ala69	3		
			Gln72	2		
	Gly51		Gln72	4		
	Ala52		Gln72	1		
			Arg75	1		
	Ile54		Lys68	2		
	Asp56		Lys68	2		2
CDR3β	Tyr95	Thr9		3	1	
	Phe97		Ala69	3		
			Thr73	4		
	Thr98		Ala69	1		
		Gly4		7	1	
		Ile5		3		
		Gly6		1		
		Ile7		11	2	
	Glu99		Gln155	2	1	
		Gly6		1		
	Ala100		Ala150	1		
			Gln155	7	1	
		Lue8		3		
	Thr101		Ala150	1		
			Gln155	4	1	
	Tyr102		Ala150	1		
		Lue8		1		

Table 3.2 Contacts between the MEL8 TCR and HLA-A2-EAAGIGILTV.

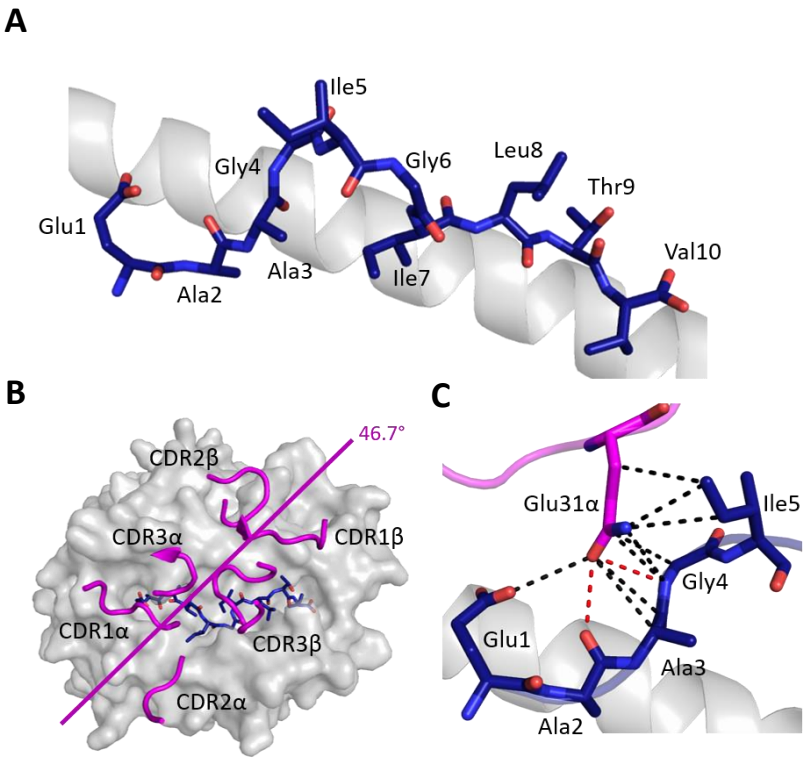

Figure 3.10. 3D structure of MEL8 in complex with HLA-A2-EAAGIGILTV.
(**A**) EAAGIGILTV peptide (blue) shown as sticks. MHC alpha helix (grey) shown as cartoon for orientation. (**B**) Top down view of EAAGIGILTV peptide (blue sticks) presented by HLA-A2 (grey, shown as surface). MEL8 CDR loops (magenta) are shown as cartoon. Crossing angle is indicated by the magenta line. (**C**) Close-up of Gln31α (magenta) interacting with the EAAGIGILTV peptide (blue). Van Der Waals forces (black dotted lines) and hydrogen bonds (red dotted lines) are shown.

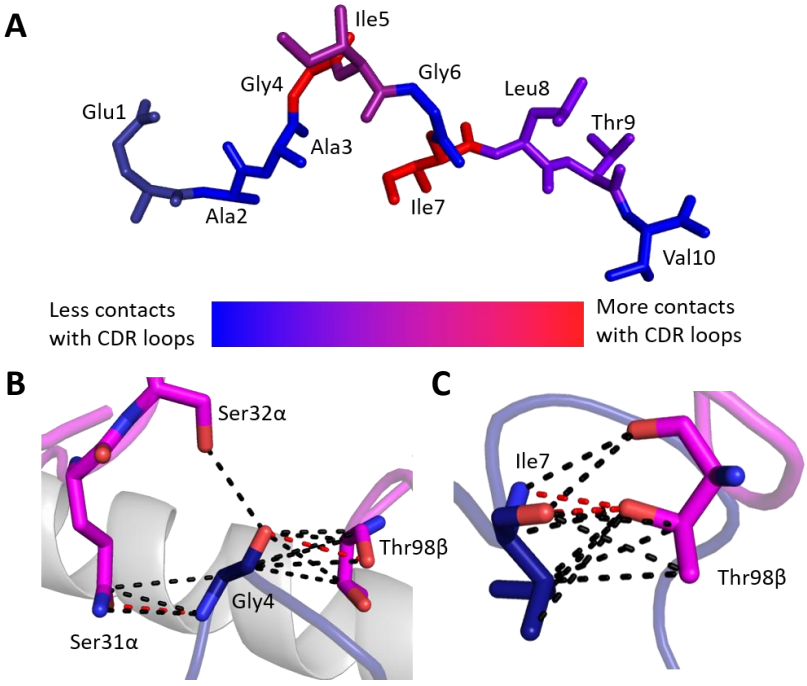

Figure 3.11. Peptide residues Gly4 and Ile 7 are crucial for the MEL8:HLA-A2-EAAGIGILTV interaction.
(**A**) Heat map of EAAGIGILTV peptide showing number of interactions each residue make with MEL8 CDR loops. (**B-C**) Interactions between Gly4 and Ile7 of EAAGIGILTV peptide (blue) respectively. Van der Waals forces (black dotted line) and hydrogen bonds (red dotted lines).

3.3.8. MEL8 interacts with Melan-A peptide using a similar mechanism to the MEL5 TCR

The Melan-A-derived EAAGIGILTV peptide has previously been shown to be recognised by a TCR known as MEL5 (Borbulevych et al., 2011; Madura et al., 2015; Cole et al., 2009). In addition to their shared recognition of the EAAGIGILTV peptide, both MEL8 and MEL5 exhibit *TRAV12-2* gene usage. As such, I thought it interesting to compare their mechanism of binding to EAAGIGILTV using the previously reported MEL5:A2-EAAGIGILTV structure (PDB:4OQK) (Madura et al., 2015). Apart from the *TRAV12-2* gene, both MEL8 and MEL5 TCRs exhibit different gene usage. MEL8 also has a shorter CDR3α loop than MEL5, as well as a dissimilar CDR3β loop (**Figure 3.12A**). Analysis of the CDR loop structure revealed differences between MEL5 and MEL8 CDR loop conformation, however the proximity of CDR1α and CDR3β to EAAGIGILTV was maintained (**Figure 3.12B**). Differences in CDR3α and CDR3β loop compositions between the MEL5 and MEL8 TCRs mean MEL5 TCR residues Leu98β and Asn92α interact with peptide reside Gly4 and MEL5 TCR residues Thr96β, Leu98β, and Gly99β interact with peptide residue Ile7. However, the conserved CDR1α loop results in MEL5 TCR residue Gln31α interacting with peptide residue Gly4 in a similar fashion to the MEL8:A2-EAAGIGILTV complex (**Figure 3.12C-D**). The conserved Gln31α residue also means interactions with the pocket formed by peptide residues P1-P5 are observed in both the MEL8:A2-EAAGIGILTV and MEL5:A2-EAAGIGILTV structures (**Figure 3.12E**). Thus, despite the differences in amino acid composition, the MEL5 and MEL8 TCRs use a similar mode of binding to HLA-A2-EAAGIGILTV.

A

TCR	*TRAV*	CDR3α	*TRAJ*	*TRBV*	CDR3β	*TRBJ*
ST8	12-2	CAVQKLVF	8	6-5	CASSYSFTEATYEQYF	3
MEL5	12-2	CAVNVAGKSTF	27	30	CAWSETGLGTGELFF	2-2

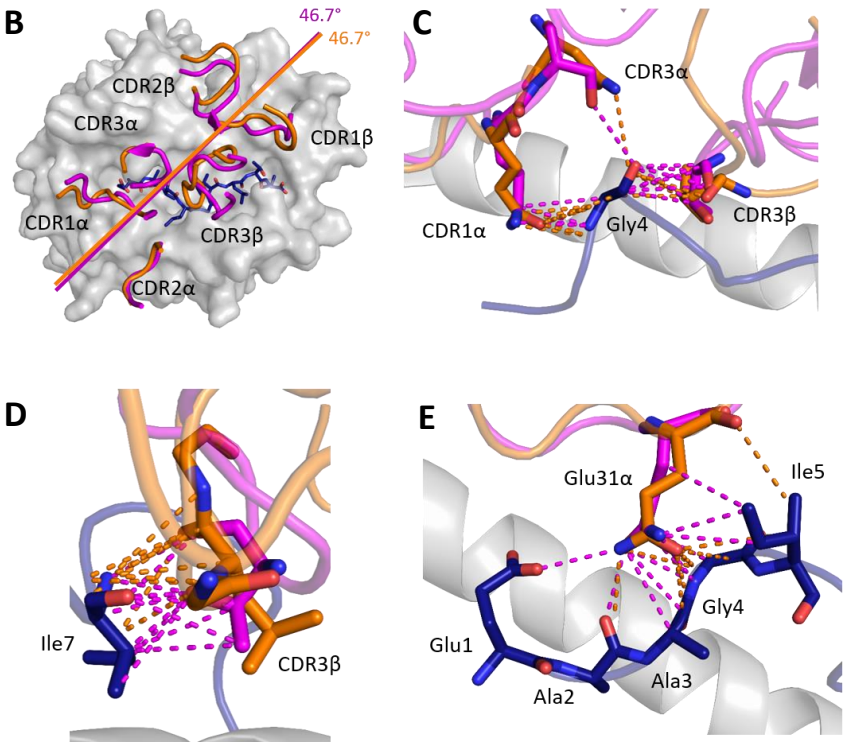

Figure 3.12. MEL5 and MEL8 interact with HLA-A2-EAAGIGILTV in similar manners.
(**A**) Comparison of MEL8 and MEL5 (PDB:4QOK) gene usage and CDR3 loop sequences. (**B**) Comparison of MEL8 (magenta) and MEL5 (orange) CDR loops in relation to the EAAGIGILTV peptide (blue). MEL8 and MEL5 crossing angles are indicated by the magenta and orange lines respectively. (**C-D**) Comparison between MEL8 (magenta) and MEL5 (orange) residues which interact with Gly4 and Ile7 of EAAGIGILTV peptide (blue) respectively. (**C**) Close-up of MEL8 and MEL5 Gln31α (magenta and orange respectively) interacting with the EAAGIGILTV peptide (blue). Bonds shown in figures **C-E** involve the MEL8 TCR (magenta) or the MEL5 TCR (orange) respectively.

3.3.9. MEL5 also recognises the BST2 and IMP2 epitopes in the context of HLA-A2

Despite multiple attempts, crystal structures of MEL8 in complex with HLA-A2-LLLGIGILVL and HLA-A2-NLSALGIFST were not acquired. The lack of successful MEL8 crystallisation was compounded by the low yields of pure MEL8 production which reduced the rate by which I could conduct crystallography experiments. As a result, I began to study the MEL5 T-cell as previous investigations within our laboratory indicated that the MEL5 TCR would be easier to work with than the MEL8 TCR. As both MEL8 and MEL5 TCRs adopt a similar binding mechanism to engage the Melan-A epitope, I hypothesised that the MEL5 TCR might also bind to the BST2 and IMP2 epitopes. In order to test this hypothesis, the MEL5 T-cell was stained with pMHC tetramers of HLA-A2-EAAGIGILTV, HLA-A2-LLLGIGILVL and HLA-A2-NLSALGIFST by Drs Garry Dolton and Cristina Rius Rafael, using an optimised staining protocol (Dolton et al., 2018) (**Figure 3.13A**). All three tetramers stained the MEL5 T-cell

clone confirming that the MEL5 TCR, like the MEL8 TCR, can engage epitopes from at least three different cancer antigens.

I next produced soluble MEL5 TCR for use in SPR experiments. While I was able to confirm the interaction between MEL5 and the Melan-A epitope, as had been previously reported (Madura et al., 2015), the response with HLA-A2-LLLGIGILVL or HLA-A2-NLSALGIFST was too low to determine accurate binding affinities. These results suggest that the MEL5 has a weak binding affinity for the BST2 and IMP2 epitopes (**Figure 3.13B-D)**.

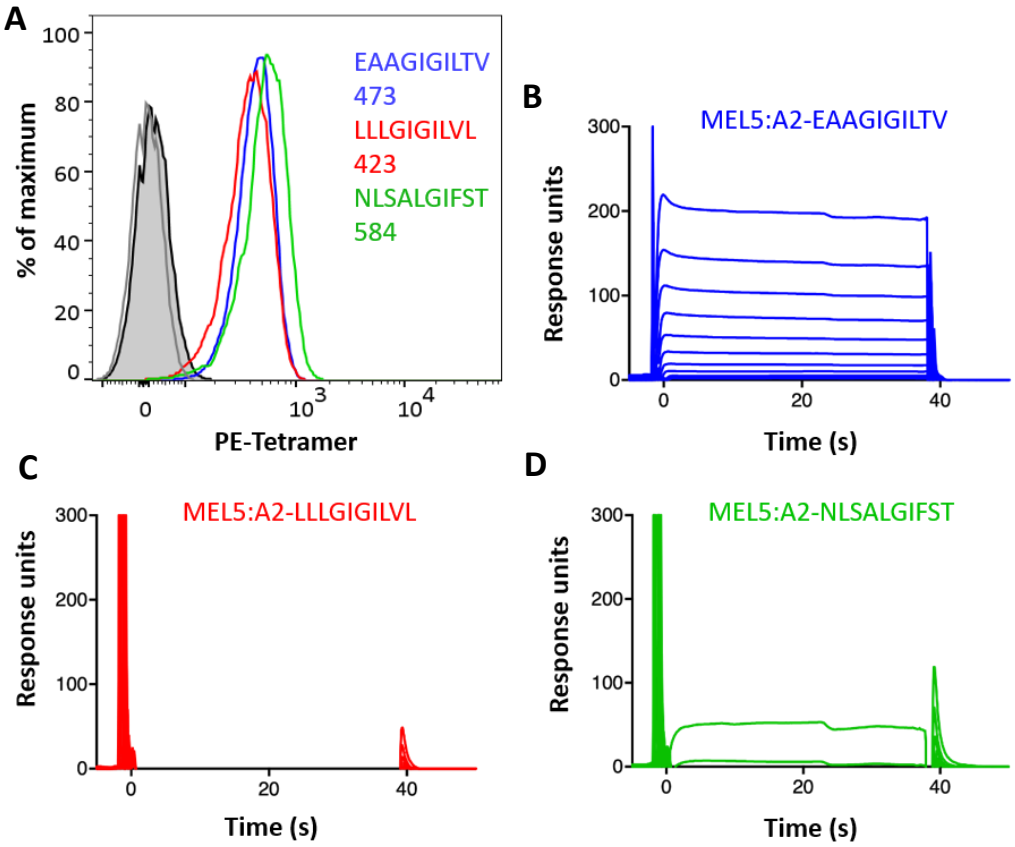

Figure 3.13. The MEL5 TCR interacts with Melan-A, BST2 and IMP2 epitopes.
(**A**) MEL5 was stained with R-Phycoerythrin conjugated HLA-A2 tetramers assembled with peptides: EAAGIGILTV, LLLGIGILVL and NLSALGIFST from Melan A (blue), BST2 (red) and IMP2 (green) respectively. MEL5 did not stain with HLA-A*0201 irrelevant tetramers (grey). Data provided by Dr Garry Dolton and Cristina Rius Rafael. (**B-D**) SPR responses of MEL5 against HLA-A2-EAAGIGILTV (blue, **B**), HLA-A2-LLLGIGILVL (red, **C**), and HLA-A2-NLSALGIFST (green, **D**). Responses against the irrelevant HLA-A2-GLGGGGGGL irrelevant protein were subtracted to remove background response. Ten serial dilutions of MEL5 were injected, with a maximum concentration of 160 µM.

3.3.10. The MEL5 TCR interacts with all three cancer epitopes with near-identical structural mechanism

The MEL5 TCR was far easier to produce and purify than the MEL8 TCR so I next attempted to crystallise these interactions. 3D crystal structures of MEL5:A2-LLLGIGILVL and MEL5:A2-NLSALGIFST were solved at 2.10 Å and 2.55 Å resolution respectively (**Table 3.3, Table 3.4, Appendix Table 1)**. Examination of these two novel 3D structures and the previously solved MEL5:A2-EAAGIGILTV structure (Madura et al., 2015) shows that all three peptides are presented by HLA-A2 in a similar manner (**Figure 3.14A**). Furthermore, the MEL5 CDR loops adopt similar conformations when bound to either EAAGIGILTV, LLLGIGILVL, or NLSALGIFST (**Figure 3.14B**). As observed above for the MEL8:A2-EAAGIGILTV structure, when interacting with MEL5 all three peptides form a 'pocket' using peptide residues P1-P5 which is occupied by the MEL5 Glu31α residue (**Figure 3.14C**). Additionally, analysis of the three structures showed that peptide residues P4 and P7 are key contact points mechanisms irrespective of which cancer epitope MEL5 is bound to (**Figure 3.14D-E**). These observations suggest that MEL5 cross-reactivity is driven by molecular mimicry between the three cancer epitopes.

3.3.11. Homology modelling suggests that the MEL8 binding mechanism is conserved between Melan-A, BST2 and IMP2 epitopes

With the determination of the MEL8:A2-EAAGIGILTV complex structure highlighted in **Section 3.3.6** and the MEL5 complex structures highlighted in **Section 3.3.10**, it was possible to use homology modelling to predict the theoretical structures of the MEL8:A2-LLLGIGILVL and MEL8:A2-NLSALGIFST complexes. Analysis of the homology models suggests the mode of HLA-A2 peptide presentation and the arrangement of the TCR CDR loops in the MEL8:A2-LLLGIGILVL and MEL8:A2-NLSALGIFST complexes are very similar to those found in the MEL8:A2-EAAGIGILTV complex (**Figure 3.15A-B**). The key role of peptide residues P4 and P7 is also observed in the modelled structures (**Table 3.5, Table 3.6, Figure 3.15C-D**).

In summary, the similarities of the homology models to MEL8:A2-EAAGIGILTV, coupled with the mechanical similarities between MEL5 and MEL8 recognition of EAAGIGILTV (**Section 3.3.7**) and the structural evidence presented here that MEL5 recognition of the Melan-A, BST2, and IMP2 epitopes is driven by molecular mimicry (**Section 3.3.10**), support the hypothesis that MEL8 recognition of multiple cancer epitopes is also driven by molecular mimicry.

CDR loop	TCR residue	Peptide residue	MHC residue	Number of VdW (≤4 Å)	Number of H-bonds (≤3.4 Å)	Number of Salt Bridges
CDR1α	Arg28		Glu166	5	2	
			Trp167	2		
	Gly29		Trp167	3		
		Lue1		2		
	Gln31		Lys66	1		
			Tyr159	2		
			Thr163	2		
		Lue1		1		
		Lue2			1	
		Lue3		3		
		Gly4		5	2	
		Ile5		3		
CDR2α	Tyr51		Glu154	3		
			Gln155	5		
			Ala158	1		
FWα	Lys67		Thr163	1		
CDR3α	Asn92	Gly4		2	1	
		Ile5		1		
	Ala94		Gly62	6		
			Arg65	5	1	
	Gly95		Lys66	3		
	Lys96		Arg65	7		
CDR1β	Asn30		Val76	2		
CDR2β	Tyr49		Arg65	4		
	Val51		Lys68	1		
			Ala69	1		
			Gln72	3		
	Gln55		Gln72	1		
			Arg75	1		
	Glu59		Arg65	2	2	
CDR3β	Thr96	Val9		2		
	Gly97		Ala69	2		
			Thr73	2		
		Ile7		2		
	Leu98		Lys66	1		
			Ala69	2		
			His70	2		
		Leu3		1		
		Gly4		2		
		Ile5		5		
		Gly6		2	1	
		Ile7		8	2	
	Gly99	Gly4		1		
		Ile5		3		
		Ile7		1		
		Lue8		1		
	Thr100		Gln155	2		

Table 3.3. Contacts between the MEL5 TCR and HLA-A2-LLLGIGILVL.

CDR loop	TCR residue	Peptide residue	MHC residue	Number of VdW (≤4 Å)	Number of H-bonds (≤3.4 Å)	Number of Salt Bridges
CDR1α	Arg28		Glu166	1		
			Trp167	4		
	Gly29		Trp167	2		
	Gln31		Tyr159	1		
			Thr163	3		
		Asn1		1		
		Leu2			1	
		Ser3		2		
		Ala4		7	1	
		Leu5		2		
CDR2α	Tyr51		Glu154	2		
			Gln155	6		
			Ala158	1		
CDR3α	Gln92	Ala4		2	1	
	Ala94		Gly62	1		
			Arg65	5		
			Lys66	1		
	Lys96		Arg65	1		
CDR1β	Asn30		Val76	4		
CDR2β	Tyr49		Arg65	2		
			Ala69	1		
	Val51		Ala69	1		
			Gln72	3		
	Gln55		Gln72	3		
			Arg75	2	1	
	Glu59		Arg65	1	1	
CDR3β	Glu95	Phe8		1		
	Thr96	Ser9		1		
	Gly97		Thr73	1		
		Ile7		2		
	Leu98		Lys66	1		
			Ala69	2		
			His70	2		
		Ser3		1		
		Ala4		6		
		Lue5		3		
		Gly6			1	
		Ile7		5	3	
	Gly99		Gln155	3		
		Ala4		1		
		Lue5		2		
		Ile7		1		
	Thr100		Gln155	5		
		Leu5		1		

Table 3.4. Contacts between the MEL5 TCR and HLA-A2-NLSALGIFST.

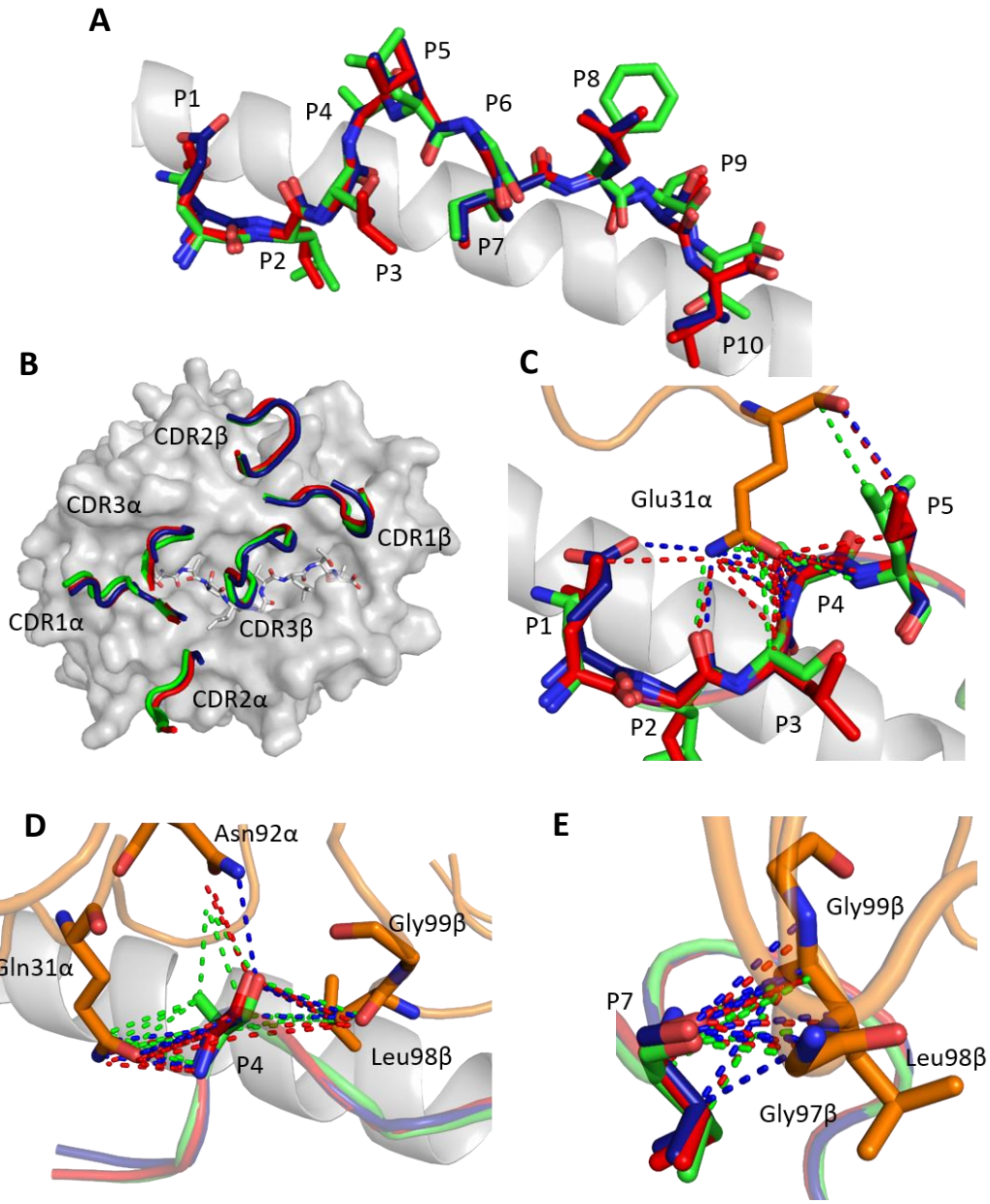

Figure 3.14. MEL5 recognises all three cancer derived epitopes via molecular mimicry.
(**A**) EAAGIGILTV (blue), LLLGIGILVL (red), and NLSALGIFST (green) peptides shown as sticks. MHC alpha helix (grey) shown as cartoon for orientation. (**B**) Top down view showing MEL5 CDR loops in complex with EAAGIGILTV (blue), LLLGIGILVL (red) and NLSALGIFST (green) peptides. Representative peptide shown in white. (**C**) Close-up of MEL5 Gln31α (orange) interacting with the EAAGIGILTV (blue), LLLGIGILVL (red) and NLSALGIFST (green) peptides. (**D-E**) MEL5 (orange) residues which interact with P4 and P7 of EAAGIGILTV (blue), LLLGIGILVL (red), and NLSALGIFST (green) peptides respectively. Bonds shown in figures **C-E** involve the EAAGIGILTV (blue), LLLGIGILVL (red), and NLSALGIFST (green) peptides respectively.

CDR loop	TCR residue	Peptide residue	MHC residue	Number of VdW (≤4 Å)	Number of H-bonds (≤3.4 Å)	Number of Salt Bridges
CDR1α	Gly29		Trp167	1		
	Gln31		Tyr159	4		
		Lue1		1		
		Lue2		2	1	
		Lue3		3		
		Gly4		4	2	
	Ser32	Gly4		1		
		Ile5		2		
CDR2α	Tyr51		Glu154	7		
			Gln155	4		
			Ala158	2		
		Ile5		2		
	Ser52		Ala158	1		
FWα	Lys67		Thr163		1	
CDR3α	Gln92	Gly4		1		
CDR1β	Glu30		Gln72	3	1	
			Val76	3		
CDR2β	Tyr48		Arg65	7	1	
	Val50		Lys68	1		
			Gln72	2		
	Gly51		Gln72	6		
	Ala52		Gln72	1	1	
			Arg75	1		
	Asp56		Lys68	1		2
	Gly58		Arg65			
CDR3β	Tyr95		Lys146	2	1	
		Val9		8		
	Ser96	Ile7			1	
		Lue8		2		
	Phe97		Ala69	6		
			Thr73	5		
	Thr98	Gly4		4		
		Ile5		5		
		Gly6			1	
		Ile7		10	2	
	Glu99		Gln155	2	1	
		Ile5		2		
		Gly6		1		
	Ala100		Val152	1		
			Gln155	10		
		Lue8		9		
	Thr101		Gln155	2	1	
	Tyr102		Lys146	3		
		Lue8		7		

Table 3.5. Theoretical contacts between the MEL8 TCR and HLA-A2-LLLGIGILVL as determined by homology modelling.

CDR loop	TCR residue	Peptide residue	MHC residue	Number of VdW (≤4 Å)	Number of H-bonds (≤3.4 Å)	Number of Salt Bridges
CDR1α	Gly29		Trp167	4		
		Asn1		1		
	Gln31		Tyr159	3		
			Thr163	3		
		Asn1		1		
		Lue2		2	1	
		Ser3		6		
		Ala4		4	1	
		Lue5		2		
	Ser32	Ala4		1		
		Lue5		2		
CDR2α	Tyr51		Glu154	2		
			Ala158	3		
		Lue5		6		
FWα	Lys67		Thr163		1	
CDR3α	Gln92	Ala4		2		
CDR1β	Glu30		Gln72	5	1	
	Glu30		Val76	1		
CDR2β	Tyr48		Arg65	5	1	
	Val50		Lys68	2		
			Ala69	1		
			Gln72	2		
	Gly51		Gln72	4		
	Ala52		Gln72	1		
			Arg75	1		
	Ile54		Lys68	4		
	Asp56		Lys68	1		2
CDR3β	Tyr95	Phe8		4		
		Ser9		3		
	Ser96	Phe8		2		
	Phe97		Ala69	9		
			Gln72	2		
			Thr73	4		
	Thr98		Ala69	1		
		Ala4		4	1	
		Lue5		2		
		Gly6		1		
		Ile7		12	1	
	Glu99		Gln155	2	1	
		Ala4		1		
		Lue5		1		
	Ala100		Gln155	11		
		Phe8		3		
	Thr101		Gln155	4	2	
	Tyr102	Phe8		11		

Table 3.6. Theoretical contacts between the MEL8 TCR and HLA-A2-NLSALGIFST as determined by homology modelling.

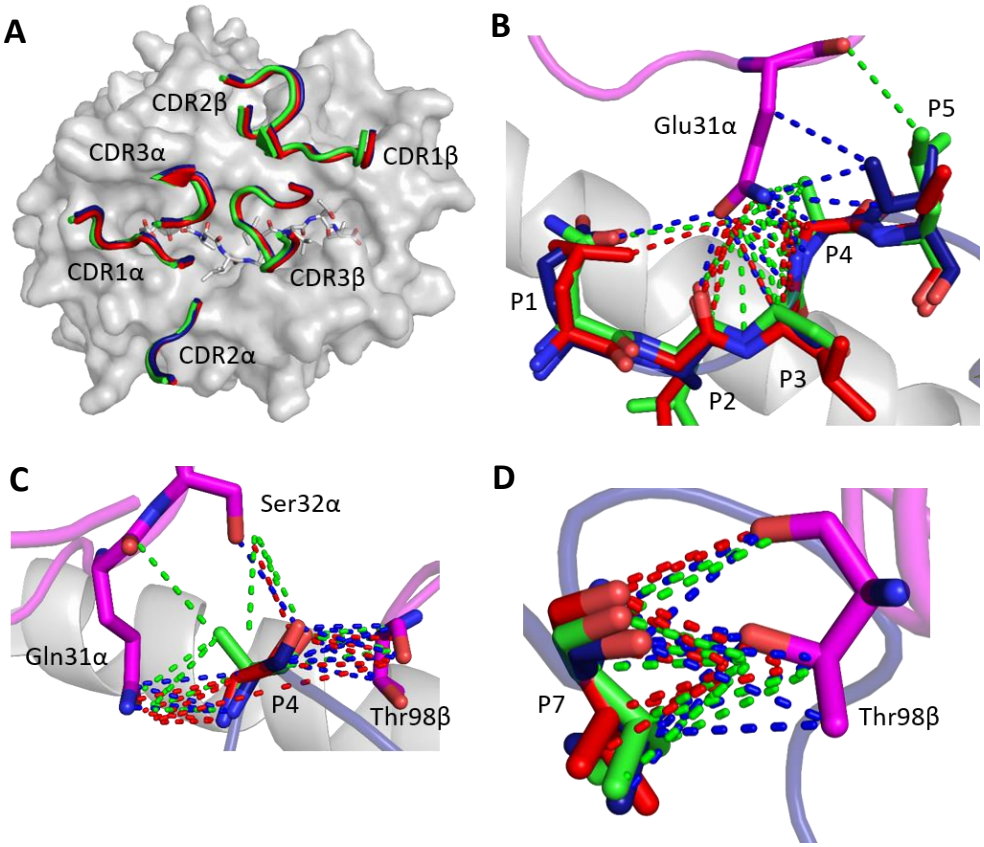

Figure 3.15. Homology modelling suggests MEL8 cross-reactivity is driven by molecular mimicry.

(**A**) Top down view showing MEL8 CDR loops in complex with EAAGIGILTV (blue), LLLGIGILVL (red) and NLSALGIFST (green) peptides. Representative peptide shown in white. (**B**) Close-up of MEL8 Gln31α (magenta) interacting with the EAAGIGILTV (blue), LLLGIGILVL (red) and NLSALGIFST (green) peptides. (**C-D**) MEL8 (magenta) residues which interact with P4 and P7 of EAAGIGILTV (blue), LLLGIGILVL (red), and NLSALGIFST (green) peptides respectively. Bonds shown in figures **B-D** involve the EAAGIGILTV (blue), LLLGIGILVL (red), and NLSALGIFST (green) peptides respectively.

3.4. Discussion

The aim of this chapter was to investigate the structural and biophysical characteristics by which the MEL8 TCR interacts with epitopes from Melan-A (EAAGIGILTV), BST2 (LLLGIGILVL), and IMP2 (NLSALGIFST). To my knowledge, this is the first description of a single T-cell that can recognise multiple cancer-derived eptiopes and, by extension, can recognise multiple different cancer cell lines. The therapeutic potential of such a TCR, along with historic examples of aberrant T-cell activity in immunotherapy, necessitated greater understanding of how MEL8 achieved this potentially 'multipronged' recognition.

3.4.1. The advantages of 'multipronged' cancer-specific T-cells in autologous anti-cancer immunity

As discussed in **Section 3.1**, several factors result in suboptimal immune response to cancer cells, including; the suppression of T-cells via the tumour microenvironment, T-cells traditionally exhibiting a low affinity to TAAs, and high tumour mutation rates that can lead to immune escape. The data presented in this chapter indicate that T-cell cross-reactivity, particularly between different TAAs, could help overcome the challenges in the immune clearance of cancer cells.

The MEL8 T-cell was isolated from the TIL infusion product of a melanoma patient and shown to respond to a Melan-A derived peptide. It was also shown to recognise multiple different cancer cell lines that do not express Melan A, suggesting that it may respond to a further TAA (**Figure 3.2**). By using a CPL screen and Dr Szomolay's webtool we identified two further TAA-derived MEL8 T-cell agonists: BST2 and IMP2 derived-peptides (**Figure 3.3-3.7**).

Further data generated by my colleague, Dr Cristina Rius Rafael, demonstrated that the MEL8 T-cell clone still killed the autologous melanoma line from patient MM909.24 even when the Melan A gene had been removed by CRISPR/Cas9. Dr Rius Rafael also showed that the response of MEL8 to these three cancer epitopes can be synergistic, as recognition of multiple epitopes resulted in a more potent T-cell response than recognition of a single epitope (**Figure 3.6**) (Rius Rafael, 2019). It is interesting to speculate that the simultaneous recognition of three TAA by the MEL8 T-cell clone played a role in allowing patient MM909.24 to clear their cancer.

While the data presented in this chapter suggest the MEL8 T-cell is capable of multipronged recognition, further data are required to prove this hypothesis. **Figure 3.6** indicates that MEL8 T-cell recognition of the Melan-A, BST2, and IMP2 epitopes is synergistic; however, it does not exclude the possibility that one of the epitopes is the primary driver of recognition. To support the multipronged hypothesis, MEL8 T-cell recognition of both BST2 knockout and IMP2 knockout variants of the autologous tumour will have to be assessed to confirm that no single epitope is primarily responsible for recognition. Furthermore, the data presented in this chapter concerns a single T-cell clone isolated from a single melanoma patient. Identifying potential multipronged recognition by additional T-cells, ideally across multiple patients, will be required to prove the significance of multipronged recognition in cancer immunity.

3.4.2. MEL8/MEL5 structural analysis

3.4.2.1. TRAV12-2 gene usage has been associated with optimal Melan-A epitope recognition

I successfully solved the crystal structure of the MEL8 TCR in complex with the Melan-A derived EAAGIGILTV epitope (**Figure 3.10-3.11**). When comparing this MEL8:A2-EAAGIGILTV complex to the MEL5:A2-EAAGIGILTV complex, it was noted that in both complexes TCR residue Gln31α occupies a peptide 'pocket' formed by peptides residues P1-P5, this facilitates the formation of numerous bonds between the peptide and the TCR. The Gln31α residue is present in the *TRAV12-2* gene, use of which is shared between MEL5 and MEL8. There are further examples of Melan-A-specific TCRs that exhibit *TRAV12-2* gene usage, including DMF5 (Borbulevych et al., 2011) and 199.16 (PDB:5NQK, unpublished), which have the same Gln31α residue occupying a pocket formed by the EAAGIGILTV peptide.

An example of a Melan-A specific TCR that does not exhibit *TRAV12-2* usage is DMF4, which is instead encoded using the *TRAV35* gene. Structural analysis showed that the DMF4 CDR1α loop does not have an analogue to the Gln31α residue found in the *TRAV12-2* CDR1α loop and thus no TCR residue occupies the 'pocket' formed by the EAAGIGILTV peptide (Borbulevych et al., 2011). Functional comparison between DMF4 and DMF5 showed how DMF5 exhibits greater avidity for the Melan-A epitope than DMF4, with the study linking higher avidity Melan-A recognition to the *TRAV12-2* gene usage of DMF5 (Johnson et al., 2006). As such, while Melan-A recognition can occur in *TRAV12-2* negative TCRs, *TRAV12-2*

gene usage appears to result in optimal Melan-A recognition compared to other *TRAV* genes, possibly due to the extra bonds formed when Gln31α occupies the P1-P5 'pocket'.

3.4.2.2. Molecular mimicry is a key driver of MEL8/MEL5 cross-reactivity

Analysis of the MEL8:A2-EAAGIGILTV complex structure showed that many bonds between the TCR and peptide involved peptide residues Gly4 and Ile7 (**Figure 3.10**, **Figure 3.11**, **Table 3.2**). While some interactions occur across the whole peptide, 52% of TCR:peptide contacts involve Gly4 and Ile7. This focused manner of binding can also be found in the MEL5:A2-EAAGIGILTV structure (**Figure 3.12**) where contacts involving Gly4 and Ile7 also account for 52% of total contacts between the TCR and peptide. These data demonstrate that MEL8 and MEL5 binding to HLA-A2-EAAGIGILTV is structurally similar. Despite both MEL8 and MEL5 exhibiting different CDR3β loop structures and amino acid compositions, CDR3β produced the same number of interactions (50) with the peptide, with both TCRs exhibiting similar focus on Gly4 and Ile7.

The analysis of the MEL8:A2-EAAGIGILTV and MEL5:A2-EAAGIGILTV complex structures highlight peptide residues Gly4 and Ile7 as potential binding hotspot residues (**Figure 3.12**). A comparison between the MEL5 TCR in complex with Melan-A, BST2, and IMP2 epitopes supports the notion of hotspot binding (**Figure 3.14**), as while peptide N- and C-termini sequence differ, resulting in differing chemical and steric properties, these hotspot residues are either highly conserved (all P4 residues are small, hydrophobic residues) or identical (all P7 residues are Ile). Indeed, the MEL5:A2-LLLGIGILVL and MEL5:A2-NLSALGIFST complex structures showed that 51% and 58% of interactions with these peptides involved P4 and P7 respectively.

Examination of the role of the TCR residue Gln31α in each complex structure suggests further molecular mimicry, as EAAGIGILTV, LLLGIGILVL, and NLSALGIFST can all form the P1-P5 'pocket', despite differences in amino acid composition. Observations regarding the P4/P7 hotspots and molecular mimicry involved in Gln31α interactions were supported further by the homology models of MEL8:A2-LLLGIGILVL and MEL8:A2-NLSALGIFST (**Figure 3.15**).

With the mechanism of recognition established for each interaction, the next step was to determine how the binding modes of the TCR:pMHC complexes affect TCR function. SPR data suggested that MEL5 recognises EAAGIGILTV with greater affinity than LLLGIGILVL and

NLSALGIFST (**Figure 3.13**). However, analysis of TCR:pMHC interactions suggests more bonds form between MEL5 and HLA-A2-LLLGIGILVL than either HLA-A2-EAAGIGILTV or HLA-A2-NLSALGIFST. A potential reason for the differences in binding affinity between the three complexes could be differing thermodynamic properties between the complexes, driven by differences in the P2 anchor. Madura *et al* showed how a 'suboptimal' anchor residue, such as alanine, can result in greater binding affinity than an optimal anchor residue like leucine, due to the suboptimal anchor exhibiting favourable binding thermodynamics (Madura et al., 2015). This hypothesis could apply to this study, as LLLGIGILVL and NLSALGIFST exhibit a more optimal P2 anchor than EAAGIGILTV and appear to have lower binding affinities. Confirmation of this hypothesis would require thermodynamic data on the MEL5:A2-LLLGIGILVL and MEL5:A2-NLSALGIFST interactions.

Determining the relationship between MEL8:A2-EAAGIGILTV interactions and MEL8 function is more difficult, as there is currently no biophysical data concerning MEL8. As such, it is difficult to compare MEL8 and MEL5 interactions as differences in binding modes cannot be correlated with affinity, kinetics or thermodynamics.

3.4.3 'Multipronged' anti-cancer T-cells in immunotherapy

As discussed in **Section 3.1.3**, studies are ongoing to improve the effectiveness of ACT, with one area of study aiming to identify optimal anti-cancer TCRs that can be used for TCR-T therapy. While affinity-enhanced artificial TCRs have been used, they are not subject to thymic selection and can exhibit cross-reactive properties that have fatal adverse effects (Linette et al., 2013). Therefore, identifying naturally occurring TCRs with enhanced anti-cancer properties is desirable. MEL8 and MEL5 could potentially serve as ideal candidates for TCR-T therapy. The potential success of MEL8 in TIL therapy, coupled with the fact that MEL8 has successfully undergone thymic selection and that other multipronged anti-cancer T-cells (like MEL5) can be safely present in healthy individuals, supports the hypothesis that MEL8 may be a safer alternative to affinity enhanced TCR-T therapy in HLA-$A2^+$ individuals.

In **Section 3.1.2**, the use of single APLs as vaccines to break immune tolerance to cancer was discussed. The use of multiple cancer-derived epitopes in combination as a multi-epitope vaccine has also been studied. Dominguez-Romero *et al* used a multi-epitope vaccine containing a library of APLs derived from the survivin protein, which resulted in breast cancer tumour growth inhibition in mice (Dominguez-Romero et al., 2020). The Melan-A, BST2, and

IMP2 epitopes could potentially be used in conjunction as a combinatorial peptide vaccine to produce a stronger, potentially pan-cancer, anti-cancer T-cell response than a vaccine based on a single epitope. The safety and potential success of MEL8 in TIL therapy, coupled with the fact that MEL8-like multipronged TCRs may be a safer alternative to affinity enhanced TCR-T therapy in HLA-$A2^+$ individuals.

The structural data presented in **Section 3.3.10** may also have implications on vaccine design. These data show how MEL5 recognises three separate cancer-derived epitopes via molecular mimicry and the conservation of particular hotspot residues within the peptides. It could therefore be hypothesised that further cancer specific T-cells may also recognise multiple cancer epitopes via molecular mimicry. Therefore, in future, published structures of anti-cancer TCRs could be analysed for identification of peptide recognition motifs or hotspots that could then be used in the rational design of APLs for combinatorial anti-cancer peptide vaccines.

3.4.5. Conclusions

In this chapter, I report what is, to my knowledge, the first structural evidence of a TCR recognising multiple cancer-derived epitopes. I show how the MEL5 TCR uses molecular mimicry to recognise epitopes from Melan-A, BST2, and IMP2. Homology modelling suggests that the same mechanism is used by the MEL8 TCR to recognise the three epitopes. Future work will aim to prove the multipronged hypothesis by demonstrating MEL8 T-cell recognition of multiple cancer epitopes in the absence of the BST2 and IMP2 epitopes, as well as identifying further examples of multipronged recognition in T-cells isolated from other donors. Structural data regarding the remaining MEL8 interactions will also need to be acquired and SPR will be used to achieve a greater understanding of these multipronged anti-cancer T-cells. The structural data reported here, along with data reported by my colleagues (Galloway et al., 2019; Rius Rafael, 2019), highlight the role that multipronged T-cell recognition may play in autologous cancer immunity, as well as the potential for the use of multipronged anti-cancer TCRs and their epitopes in cancer immunotherapy.

4. Structural characterisation of TCR recognition of an insulin-derived peptide in the context of HLA-A*24:02

4.1. Introduction

4.1.1. Type 1 diabetes mellitus

Diabetes mellitus is a disease characterised by an inadequate insulin response, resulting in hyperglycaemia (Blair, 2016). Low insulin can cause mild symptoms such as thirst or drowsiness, but if left unmanaged can cause renal failure, neuropathy, cardiovascular damage, and eventually death. There are two broad classifications of diabetes mellitus; type 1 diabetes (T1D), characterised by impairment in insulin secretion, and type 2 diabetes, characterised by insulin resistance (Alberti et al, 1998).

T1D is an autoimmune disease which typically manifests in early life and was historically referred to as juvenile diabetes. T1D is caused by the autoimmune destruction of pancreatic β-cells, which secrete insulin. Insulin loss prevents excess glucose from being stored as glycogen, thus resulting in hyperglycaemia (Gepts, 1965). Despite reports of some success using pancreatic cell transplants (Shapiro et al, 2000) and regulatory T-cells (Tang et al, 2004), the most common form of treatment remains management of glucose levels via life-long diet control and administration of insulin (Petry et al, 2015). Management of T1D costs a sizeable fraction of the NHS budget in the UK (Stedman et al., 2020), with male and female patients having a life expectancy of 7 and 8.5 years shorter than their non-diabetic counterparts (Heald et al., 2020). It is important that more effective treatments for T1D are found and this will require a better understanding of the mechanism of disease.

4.1.2. The role of $CD8^+$ T-cells in type 1 diabetes

It is now well established that $CD8^+$ T-cells play a key role in T1D. Early studies provided evidence of $CD8^+$ T-cell infiltration and activation in the pancreas of T1D patients (Hanninen et al, 1992; Somoza et al, 1994). In 1995, Panina-Bordignon *et al.* showed that a polyclonal population of $CD8^+$ T-cells specific for a GAD65-derived peptide were present in T1D patients and could kill pancreatic β-cells upon activation (Panina-Bordignon et al, 1995).

In 2008, Skowera *et al.* isolated a $CD8^+$ T-cell clone that could kill pancreatic β-cells. This study identified an HLA-A2 restricted peptide (ALWGPDPAAA) derived from amino acid residues 15-24 of PPI, an insulin precursor. The $CD8^+$ T-cell clone, 1E6, was shown to recognise the

PPI_{15-24} peptide in the context of HLA-A2 and exhibited glucose-regulated destruction of pancreatic β-cells (Skowera et al, 2008). Bulek *et al.*, solved a 3D crystal structure of the 1E6 TCR in complex with the HLA-A2-ALWGPDPAAA pMHC to provide the first ever structure of a human TCR bound to an HLA-I-restricted autoantigen (Bulek et al, 2012). Other HLA-I-restricted diabetes-specific $CD8^+$ T-cell epitopes have also been identified, including epitopes in the insulin B-chain (InsB) and the islet-specific glucose-6-phosphatase catalytic subunit-related protein (IGRP) (Jarchum et al, 2008; Pinkse et al, 2005).

Less well understood is how T1D autoreactive T-cells, which theoretically should have been deleted during thymic selection, are able to survive selection and recognise these self-derived epitopes. A hypothesis discussed in the Skowera *et al.* study suggests that T-cell activation may occur as a result of high glucose levels; as this would result in high levels of insulin secretion, followed by high levels of T1D epitope presentation. This would increase avidity between autoreactive T-cells and presenting cells, potentially allowing TCRs with weaker affinities to become activated and break self-tolerance (Skowera et al, 2008). However, this proposed mechanism of disease initiation does not provide naïve T-cells with essential signalling provided by professional antigen presenting cells or $CD4^+$ T-cell help so seems unlikely. It also fails to explain why only a small minority of individuals with disease-risk HLA alleles develop disease.

Alternatively, as discussed in **Section 1.3.3**, T1D autoreactive T-cells could cross-react with a high affinity pathogenic epitope, with the resulting activation allowing these T-cells to break self-tolerance and respond to weaker T1D-relevant self-epitopes. A number of human pathogens have been associated with T1D, including cytomegalovirus, human enterovirus, and human endogenous retrovirus (Levet et al, 2019; Pak et al, 1988; Tracy et al, 2011). The notion of pathogenic triggers was explored by Cole *et al.* who used a CPL screen to identify alternative epitopes for the 1E6 autoreactive T-cell clone. One such epitope was found to be present in the proteasome of *Clostridium asparagiforme* and reacted more potently with 1E6 than the PPI_{15-24} self-peptide (Cole et al, 2016). Subsequently, this technique was utilised by Whalley *et al.* to identify peptides derived from *Candida albicans* and *Helicobactor pylori* which interact with the InsB4 T-cell clone, another T1D-relevant autoreactive T-cell clone which recognises an insulin B-chain-derived peptide in the context of HLA-A2 (Whalley et al, 2020).

4.1.3. The role of HLA class I in type 1 diabetes

HLA-associations are a hallmark of autoimmune disease and a number have been observed for T1D. The link between T1D and certain class II HLA-DR and HLA-DQ alleles was established as early as the 1980s (Todd et al, 1987. Wolf et al, 1983). In 2007, a study by Nejentsev *et al.* identified a number of HLA class I alleles linked to T1D. Specifically, *HLA-B*39* and *HLA-A*24* were found to predispose T1D, while *HLA-B*27* and *HLA-A*11* were found to protect against T1D (Nejentsev et al, 2007). T-cells specific for T1D-relevant epitopes in the context of these HLA risk alleles have been observed in T1D patients (Yeo et al, 2020). Subsequent studies at showed that *HLA-B*3906*, *HLA-A*2402*, *HLA-A*0201*, *HLA-B*1801* and *HLA-C*0501* predispose towards disease (Noble et al., 2010). *HLA-A*0201* and *HLA-B*3906* are both able to mediate T1D in mouse models (Marron et al., 2002; Schloss et al., 2018).

The predisposition to T1D afforded by *HLA-A*2402* is of particular interest to this thesis. *HLA-A*2402*, whilst widely present across the global population, is the most frequent HLA-A allele across the Asian population (Middleton et al, 2000). This makes it a highly relevant candidate to study. In 2012, Kronenberg *et al.* identified a peptide (LWMRLLPLL) composed of PPI residues 3-11. The epitope is naturally processed and presented at the cell surface in the context of HLA-A24. This group also isolated a T-cell clone (4C6) from a T1D patient which recognises the PPI_{3-11} peptide and can kill pancreatic β-cells (Kronenberg et al, 2012). Recently, Yeo *et al.* demonstrated that young T1D patients possess effector memory T-cell populations specific for the PPI_{3-11} peptide, making it an ideal model system for the present investigation (Yeo et al., 2020).

4.2. Aims

I had access to the T1D patient-derived 4C6 PPI_{3-11}-specific T-cell and its TCR so aimed to examine the preferred peptide recognition landscape of this T-cell and generate an atomic resolution structure of the 4C6 TCR in complex with its cognate PPI-derived epitope. I hypothesised that the 4C6 T-cell would be very cross-reactive and respond to a large number of different peptides. I hoped to understand the structural underpinning of any crossreactivity and use this to identify pathogen-derived epitopes which may have allowed the 4C6 T-cell to break self-tolerance.

4.3. Results

4.3.1. Generating a peptide recognition landscape for the 4C6 T-cell

We wished to use CPL screening in order to better understand peptide recognition by the 4C6 T-cell. A peptide sizing scan (Ekeruche-Makinde et al., 2013) showed that the 4C6 T-cell exhibited a strong preference for peptides of 9 amino acids in length (**Figure 4.1A**). The 4C6 T-cell was screened with a 9-mer CPL in order to generate a preferred peptide recognition landscape (**Figure 4.1B-C**). These data show that peptide recognition is quite limited at positions 4-8 across the centre of the peptide. There appeared to be more flexibility at positions 1-3 and position 9 where several peptide sub-libraries were recognised. Amino acid recognition was most restricted at position 5 where only the leucine sub-library was recognised. The amino acid present in the natural HLA-A24-LWMRLLPLL epitope is indicated using green bars in **Figure 4.1B**. CPL data was provided by Dr Garry Dolton.

4.3.2. The 4C6 T-cell exhibits a stronger response to the QLPRLFPLL super-agonist than the T1D epitope

The CPL data in **Figure 4.1B** were input into a webtool designed by Dr Szomolay (Szomolay et al, 2016). As discussed in **Chapter 3**, Dr Szomolay's webtool uses the CPL data to search proteome databases and provides lists of potential epitopes, ranked by likelihood of recognition. Ten peptides from the top 500 predicted 4C6 T-cell agonists were generated at random using the biased sampling technique previously applied to the HLA-A*0201-restricted 1E6 T-cell (**Appendix Figure 1**) (Wooldridge et al., 2012). The two best recognised peptides were NMPRLFPIV and QLPRLFPLL in MIP1-β ELISA assays (**Figure 4.2A**). The QLPRLFPLL was almost 10,000 times more potent than the 'index' LWMRLLPLL sequence as a pure peptide (>95% purity) in titration assays (EC_{50} of 2×10^{-11} compared to 1.6×10^{-7}). 4C6 T-cell recognition of HLA-A24-LWMRLLPLL and HLA-A24-QLPRLFPLL pMHC molecules was confirmed by pMHC tetramer staining using HLA-A24 monomers I produced. Comparison of the tetramer staining data suggested that the 4C6 T-cell had a higher avidity for HLA-A24-QLPRLFPLL than the index HLA-A24-LWMRLLPLL, with mean fluorescent intensities of 27890 and 2718 respectively (**Figure 4.2B**). Data provided by Dr Garry Dolton.

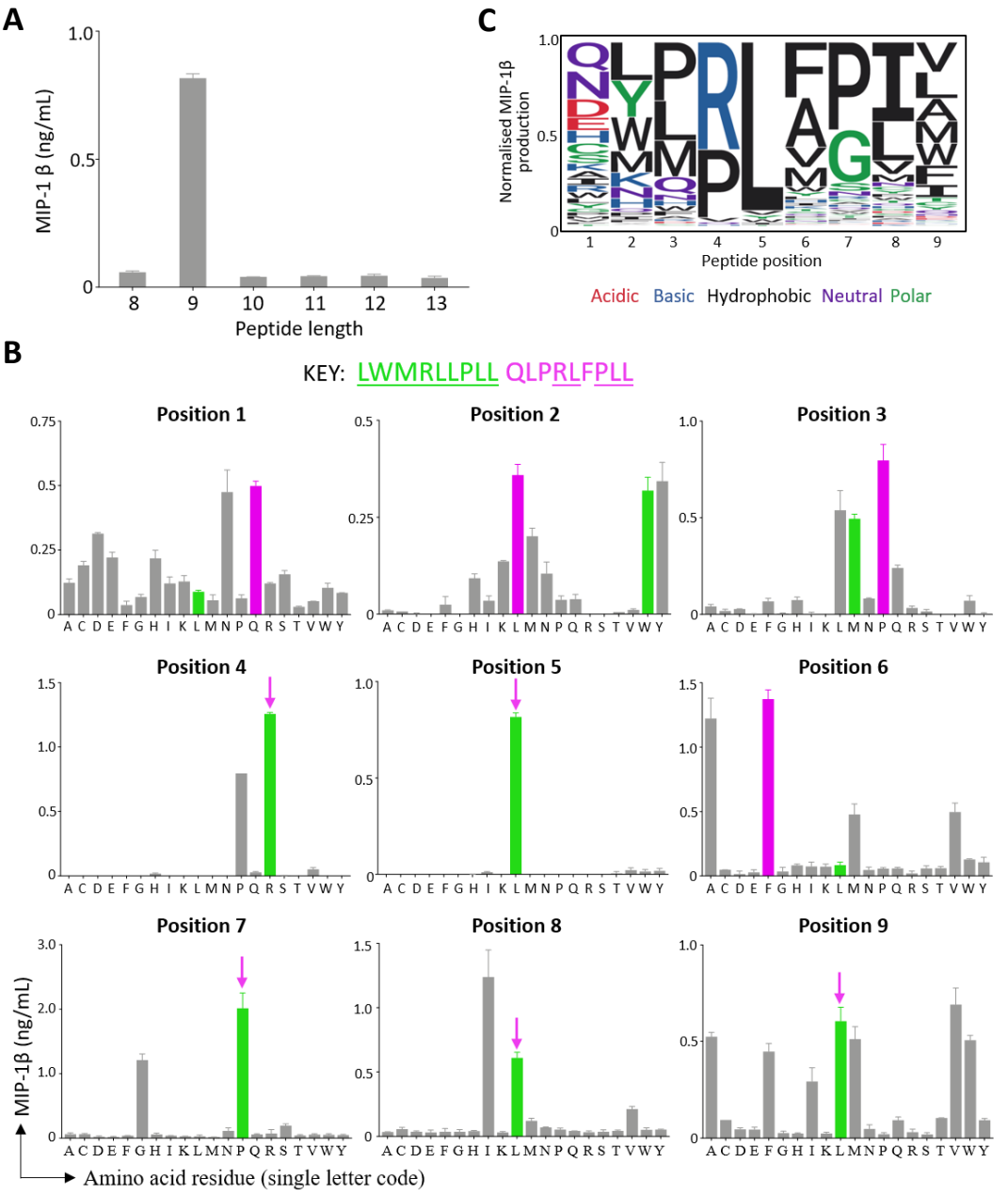

Figure 4.1. Combinatorial peptide library screening of 4C6 T-cell clone.
(**A**) 4C6 was incubated overnight with sizing scan mixtures of defined amino acid length (x-axis) using C1R-HLA-A*2402^{+} cells as antigen presenting cells. Assay supernatants used for MIP-1β ELISA. Error bars depict SD from the mean of two replicates. (**B**) Based on the results of the sizing scan, a 9mer positional scanning combinatorial peptide library (PS-CPL) screen was performed, using 4C6, T-cells and antigen presenting cells and ELISA as in A. Green bars indicate amino acid present in the natural preproinsulin epitope and magenta bars or arrows show amino acid present in the super-agonist peptide according to the key. Errors bars depict SD from the mean of two replicates. (**C**) Motif log plot summarizing the amino acid preference of 4C6 at each position of the PS-CPL. CPL scan performed by Dr Garry Dolton.

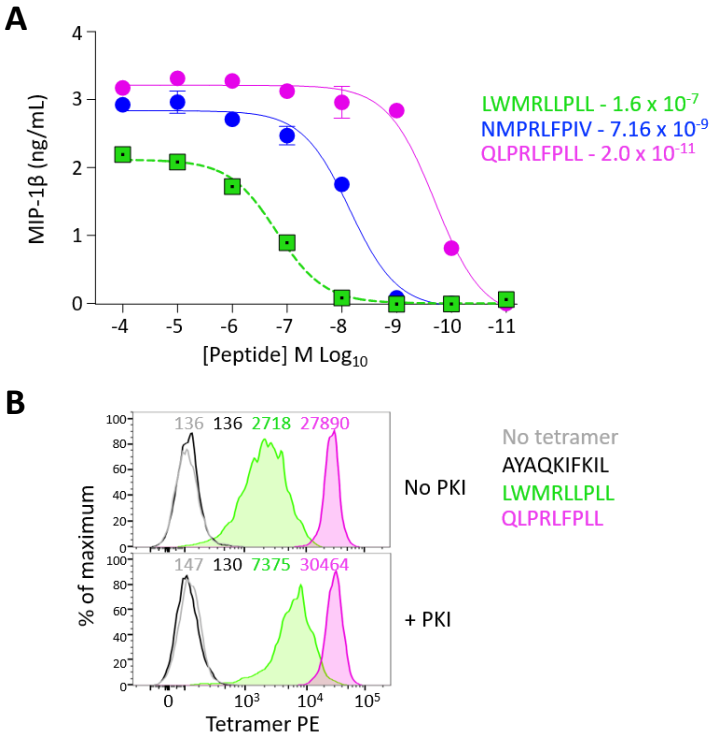

Figure 4.2. The 4C6 T-cell clone recognises the preproinsulin epitope.
(**A**) Sensitivity of 4C6 T-cell clone to preproinsulin (LWMRLLPLL) and super-agonists (NMPRLFPIV and QLPRLFPLL) peptides in a titration assay. Incubation overnight with C1R-HLA-A*24:02^{+} cells as antigen presenting cells. Assay supernatants used for MIP-1β ELISA. Error bars depict SD from the mean of two replicates. EC_{50} values are displayed in the key. Superior super-agonist QLPRLFPLL was used for downstream experiments. (**B**) Staining of 4C6 T-cell clone with irrelevant (AYAQKIFKIL from CMV), preproinsulin and super-agonist PE-conjugated tetramers. Tetramer used alone or following pretreatment with protein kinase inhibitor (PKI) Dasatinib pre-treatment. Mean fluorescence intensity of staining is displayed. Stained for CD8 APC-Vio770 and the viability stain VIVID. Data provided by Dr Garry Dolton.

4.3.3. The 4C6 TCR binds super-agonist peptide with a far higher affinity than the T1D peptide

With the 4C6 TCR binding of LWMRLLPLL and QLPRLFPLL confirmed by tetramer staining, the affinity of the 4C6 TCR for both peptides was assessed. SPR experiments confirmed the interaction of soluble 4C6 TCR with both soluble HLA-A24-LWMRLLPLL and HLA-A24-QLPRLFPLL (**Figure 4.3**). The 4C6 TCR has a 20-fold greater affinity for QLPRLFPLL than LWMRLLPLL, with measured K_Ds of 5.4 µM and 129.2 µM respectively. Furthermore, SPR data also showed the 4C6:A24-QLPRLFPLL interaction had a far slower dissociation rate than the 4C6:A24-LWMRLLPLL interaction (0.1 s^{-1} and 1.4 s^{-1} respectively). These data confirm QLPRLFPLL is indeed a high-affinity agonist of the 4C6 T-cell and demonstrates how the 4C6 T-cell has the potential to recognise peptides with a sensitivity of several orders of magnitude greater than the PPI_{3-11} epitope.

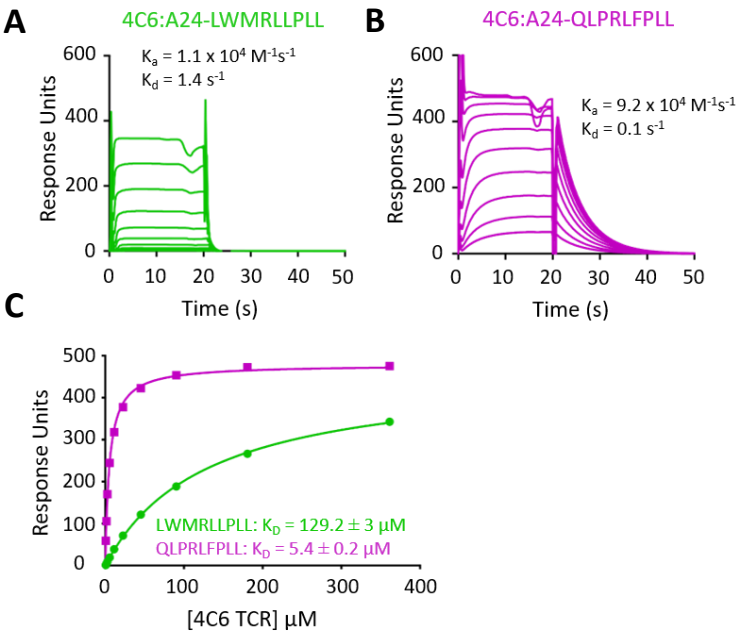

Figure 4.3. The 4C6 TCR binds the artificial super-agonist with a higher affinity than the preproinsulin epitope.
Surface Plasmon resonance (SPR) analysis of 4C6 TCR recognition of (**A**) LWMRLLPLL (green) and (**B**) QLPRLFPLL (magenta). SPR response to ten serial dilutions of 4C6 was measured, with a starting concentration of 361.5 µM. H2-Kd-SIINFEKL was used as an irrelevant. K_D values were calculated using non-linear fit curve (y= [P1 x]/[P2 + X]) (**C**).

4.3.4. The 4C6 TCR binds to its ligands with a 'peg in hole' binding conformation

4.3.4.1. Failure to crystallise the 4C6 TCR with cognate insulin ligand

To achieve greater understanding of how the 4C6 TCR binds to HLA-A24-LWMRLLPLL I attempted to generate a 3D structure of this co-complex. Multiple attempts to produce 4C6:A24-LWMRLLPLL crystals for use in x-ray diffraction were unsuccessful, despite the use of multiple proven crystallography screens including PACT screen and our own T-cell optimised screen (Bulek et al., 2012; Newman et al., 2005). To circumvent this problem, I attempted to use crystal seeding.

As the peptide in a TCR:pMHC complex is buried between the TCR and HLA and is therefore not solvent exposed, I reasoned that this might allow me to use 4C6:A24-QLPRLFPLL-containing crystals as seeds for growing crystals of the much weaker 4C6:A24-LWMRLLPLL interaction. Seeds expedite the formation of a crystal lattice from a supersaturated solution by providing a preformed lattice to precipitate upon, removing reliance on random diffusion for nucleation. This technique is known as seeding (D'arcy et al., 2007). Seeding has been used by my laboratory to aid crystallisation of pMHC monomers (Galloway et al., 2019). To

allow me to conduct seeding I generated crystals of the HLA-A24-QLPRLFPLL super-agonist ligand with and without the 4C6 TCR that successfully diffracted as described below.

4.3.4.2. Key residues in QLPRLFPLL peptide protrude towards the 4C6 TCR during binding

The 3D structure of the HLA-A24-QLPRLFPLL monomer was solved to a resolution of 2.25 Å (**Table 4.1**, **Figure 4.4, Appendix Table 2**). Analysis of this structure showed that the peptide bulges at its centre, supported by a Van der Waals interaction between the side chains of its Pro3 and Phe6 residues (**Figure 4.4A**). Central peptide residues Arg4 and Leu5 protrude upwards away from the MHC in a disordered manner making them likely TCR contact residues.

The 3D structure of the 4C6:A24-QLPRLFPLL complex was solved to a resolution of 2.2 Å. Comparison between the QLPRLFPLL peptide in its bound and unbound states showed that peptide residues Arg4 and Leu5 protruded directly upward when bound to the 4C6 TCR, confirming their importance to the interaction. Furthermore, there were four van der Waals interactions between Pro3 and Phe6 when QLPRLFPLL was bound to the TCR, compared to one Van der Waals interaction when it was unbound, suggesting greater QLPRLFPLL peptide stability when bound to the 4C6 TCR (**Figure 4.4B**).

4.3.4.3. LWMRLLPLL residues Arg4 and Leu5 are interaction hotspots

Using successfully diffracted 4C6:A24-QLPRLFPLL crystals I was able to conduct crystal seeding. 4C6:A24-QLPRLFPLL crystals were crushed into micro-seeds and added to the crystallisation condition of the 4C6:A24-LWMRLLPLL crystals (25% PEG 1500, 0.1 M PCB). The nucleation points provided by the 4C6:A24-QLPRLFPLL micro-seeds successfully resulted in 4C6:A24-LWMRLLPLL crystal growth allowing generation of a 3D structure solved at a resolution of 2.48 Å (**Appendix table 2**).

Analysis of the 4C6:A24-LWMRLLPLL structure showed that the LWMRLLPLL peptide bulged upwards in a similar manner to the HLA-A24-QLPRLFPLL structure, with the Arg4 and leu5 residues protruding upwards towards the TCR. The Van der Waal interaction between P3 and P6 was also present (**Figure 4.4C**). Analysis of the 4C6 TCR CDR loops showed how CDR1α, CDR3α, CDR1β, and CDR3β surround the peptide, while the CDR2α and CDR2β loops largely interact with the HLA-A24 molecule itself (**Figure 4.4D**).

Closer inspection of the 4C6:A24-LWMRLLPLL binding interface showed how the CDR1α, CDR3α, CDR1β, and CDR3β loops form a pocket (**Figure 4.4E**). The Arg4 and Leu5 resides of the peptide protrude into this pocket, adopting a 'peg in hole' motif. Analysis of the contacts between the peptide and 4C6 TCR CDR loops (**Table 4.1**) supports the importance of the Arg4 and Leu5 peptide residues, for example peptide residue Arg4 makes 34 contacts across the following residues: Asp27α, Ser29α, and Ser30α from CDR1α; and Pro93α, Ser94α, Gly95α, Asn96α, and Thr97α from CDR3α. These contacts contained all 8 hydrogen bonds between the 4C6 CDR loops and the LWMRLLPLL peptide. Peptide residue Leu5 made 14 contacts (all Van der Waals interactions) across the following residues: Tyr32α from CDR1α; Thr97α and Gly98α from CDR3α; Arg32 from CDR1β; and His98 and His99 from CDR3β. Between them, peptide residues Arg4 and Leu5 made up 72% of contacts (51% and 21% respectively) between the LWMRLLPLL peptide and 4C6 TCR, all of which were interactions between the residues and the pocket formed by the CDR1α, CDR3α, CDR1β, and CDR3β loops (**Figure 4.4F-H**). The 'peg and hole' binding motif was therefore critical for the interaction between the 4C6 TCR and HLA-A24-LWMRLLPLL.

CDR loop	TCR residue	Peptide residue	MHC residue	VdWs (≤4 Å)	H-bonds (≤3.4 Å)	Salt bridges
CDR1α	Asp27	Arg4		1	1	
	Ser29	Arg4		3	1	
	Ser29		Thr163	3		
	Ser30	Arg4		4	2	
	Thr31		Gln155	4	1	
	Thr31		Ala158	3		
	Thr31		Tyr159	3		
	Tyr32	Leu5		1		
	Tyr32		Gln155	1		
CDR2α	Phe51		Glu154	3		
	Phe51		Gln155	5		
	Ser52		Ala158	1		
	Asn53		Arg157	2		
	Asn53		Ala158	1		
	Asn53		Glu161	3	1	
FWα	Lys68		Gly162	2		
	Lys68		Asp166	1		
CDR3α	Pro93	Arg4		2	1	
	Ser94	Arg4		3		
	Gly95	Arg4		5	3	
	Asn96	Arg4		6	1	
	Asn96		Gly65	3		
	Asn96		Lys66	6	1	
	Asn96		Ala69	2		
	Thr97	Arg4		1		
	Thr97	Leu5		3		
	Gly98	Leu5		1		
CDR1β	Asn31	Leu8		3		
	Asn31		Lys146	1	1	
	Arg32	Leu5		1		
	Arg32	Leu6		3	1	
CDR2β	Gln51	Leu8		5		
	Gln51		Gln72	1		
	Gln51		Thr73	4	2	
	Asn52		Glu76	4	1	
	Glu53		Arg79	1	1	
	Leu56		Gln72	2		
CDR3β	Leu97		Lys146	1		
	Leu97		Ala150	1		
	His98	Leu5		7		
	His98	Leu6		2		
	His98	Pro7		5		
	His98		Val152	3		
	His98		Gln155	2	1	
	His99	Leu5		1		
	His99		Ala150	1	1	
	His99		His151		1	
	His99		Gln155	2		
	Glu100		His151	2		

Table 4.1. Contacts between the 4C6 TCR and HLA-A24-LWMRLLPLL.

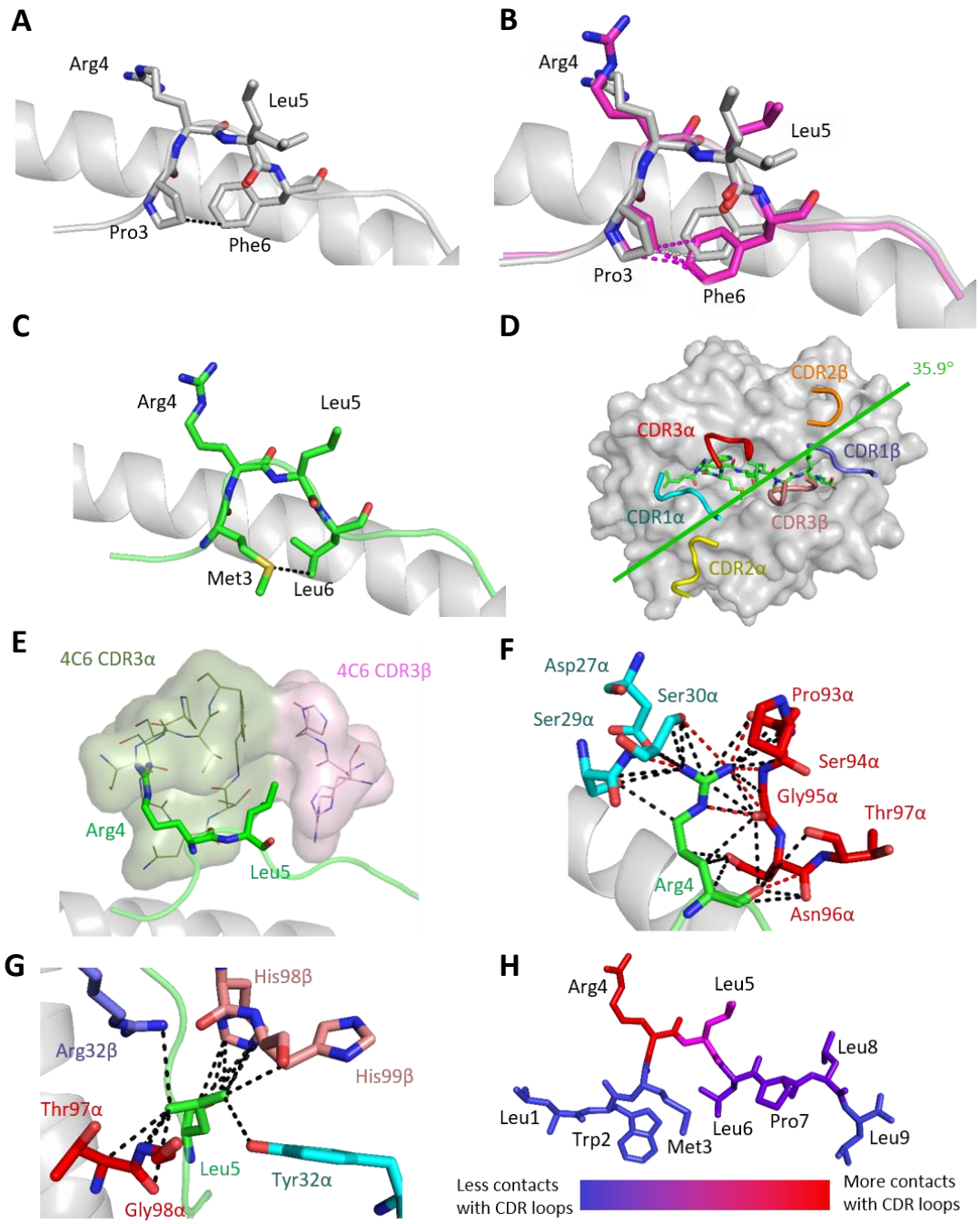

Figure 4.4. The 4C6 TCR recognises the preproinsulin peptide via hotspot recognition.
(**A**) Structure of HLA-A24-QLPRLFPLL. Peptide shown as grey sticks with MHC alpha-helix (gray) shown for orientation. Dotted lines represent Van der Waals interactions. (**B**) A comparison of HLA-A24-QLPRLFPLL (gray) and 4C6:A24-QLPRLFPLL (magenta) peptide presentation. Peptides shown as sticks with MHC alpha-helix (gray) shown for orientation. Dotted lines represent Van der Waals interactions. (**C**) Structure of 4C6:A24-LWMRLLPLL. Peptide shown as green sticks with MHC alpha-helix (gray) shown for orientation. Dotted lines represent Van der Waals interactions. (**D**) Top down view of 4C6 TCR 'footprint' on HLA-A24-LWMRLLPLL. 4C6 CDR loops shown as coloured cartoon, with the peptide shown as green sticks. Green line and number indicate crossing angle. (**E**) Close up of 4C6:HLA-A24-LWMRLLPLL structure focusing on residues Arg4 and Leu5 (green sticks) which form a 'peg in hole' formation inside the 4C6 TCR (lines and surface). (**E-F**) LWMRLLPLL peptide residues Arg4 (**F**) and Leu5 (**G**) shown as green sticks. Important 4C6 TCR residues are labeled. Black dotted lines indicate Van der Waals interactions. Red dotted lines indicate hydrogen bonds. (**H**) Heat map of 4C6 TCR contacts with the LWMRLLPLL peptide.

4.3.5. The 4C6 TCR binds the high affinity peptide in the same manner as the diabetes peptide

To assess the similarity of the binding mechanisms used by the 4C6 TCR to bind HLA-A24-LWMRLLPLL and HLA-A24-QLPRLFPLL, the complex structures were overlaid and compared (**Figure 4.5**). Analysis of peptide presentation confirmed both LWMRLLPLL and QLPRLFPLL shared the central bulge which resulted in peptide residues Arg4 and Leu5 protruding upwards. However, the QLPRLFPLL bulge protruded 0.5 Å more towards the TCR than LWMRLLPLL (**Figure 4.5A**). The greater protrusion of the QLPRLFPLL peptide may be due to the greater number of Van der Waals between QLPRLFPLL residues Pro3 and Phe6 than between LWMRLLPLL residues Met3 and Leu6. Analysis of the 4C6 TCR CDR loops showed near identical loop structure regardless of whether LWMRLLPLL or QLPRLFPLL were bound (**Figure 4.5B**). This extended to the pocket formed by the CDR loops, which was conserved between both structures. It is therefore unsurprising that the 4C6:A24-QLPRLFPLL complex shares many of the same TCR:peptide interactions as the 4C6:A24-LWMRLLPLL complex (**Figure 4.5C-D**).

It is worth noting that there were 15 less 4C6 TCR interactions between HLA-A24-QLPRLFPLL than HLA-A24-LWMRLLPLL, which included two less interactions with Arg4 and seven less interactions with Leu5 (**Table 4.2**). By extension, several 4C6 TCR CDR loop residues that were involved in the binding of LWMRLLPLL residues are not involved when interacting with Arg4 (Asp27α and Thr97α) (**Figure 4.5C**) and Leu5 (Try32α and Arg32β) (**Figure 4.5D**). Furthermore, the average bond length between the 4C6 TCR and the LWMRLLPLL residues Arg4 and Leu5 (3.51 Å and 3.77 Å respectively) was shorter than the bonds between the 4C6 TCR and QLPRLFPLL residues Arg4 and Leu5 (3.76 Å and 3.8 Å respectively). Despite the substantial differences in affinity of both interactions, the 4C6:A24-QLPRLFPLL binding interface was an almost complete molecular mimic of the 4C6:A24-LWMRLLPLL binding interface, where what few differences there were in the interaction landscape could not comprehensively explain the differences in affinity.

CDR loop	TCR residue	Peptide residue	MHC residue	VdWs (≤4 Å)	H-bonds (≤3.4 Å)
CDR1α	Asp26	Arg4		5	1
	Ser28	Arg4		4	1
	Ser28		Thr163	1	
	Ser29	Arg4		3	3
	Thr30		Gln155	3	1
	Thr30		Ala158	2	
	Thr30		Tyr159	2	
	Tyr31		Gln155	1	
CDR2α	Phe50		Glu154	2	
	Phe50		Gln155	4	
	Ser51		Ala158	2	
	Asn52		Ala158	3	
	Asn52		Glu161	4	1
FWα	Lys68		Glu162	1	
CDR3α	Pro92	Arg4		5	1
	Ser93	Arg4		2	
	Gly94	Arg4		5	1
	Asn95	Arg4		6	1
	Asn95		Gly65	2	
	Asn95		Lys66	5	
	Asn95		Ala69	2	
	Gly97	Leu5		1	
CDR1β	Asn30	Leu8		2	
	Asn30		Lys146	1	
	Arg31	Leu5		2	
	Arg31	Phe6		2	1
	Arg31		Thr73	1	
CDR2β	Gln50		Gln72	3	
	Gln50		Thr73	5	1
	Gln50		Glu76	1	
	Asn51		Glu76	5	1
	Leu55		Gln72	3	
CDR3β	Leu96		Ala150	2	
	His97	Leu5		8	
	His97	Phe6		1	
	His97	Pro7		4	
	His97		Gln155	3	1
	His98	Leu5		1	
	His98		Ala150	1	1
	His98		His151	1	
	Glu99		Ala150		1
	Glu99		His151		1

Table 4.2. Contacts between the 4C6 TCR and HLA-A24-QLPRLFPLL.

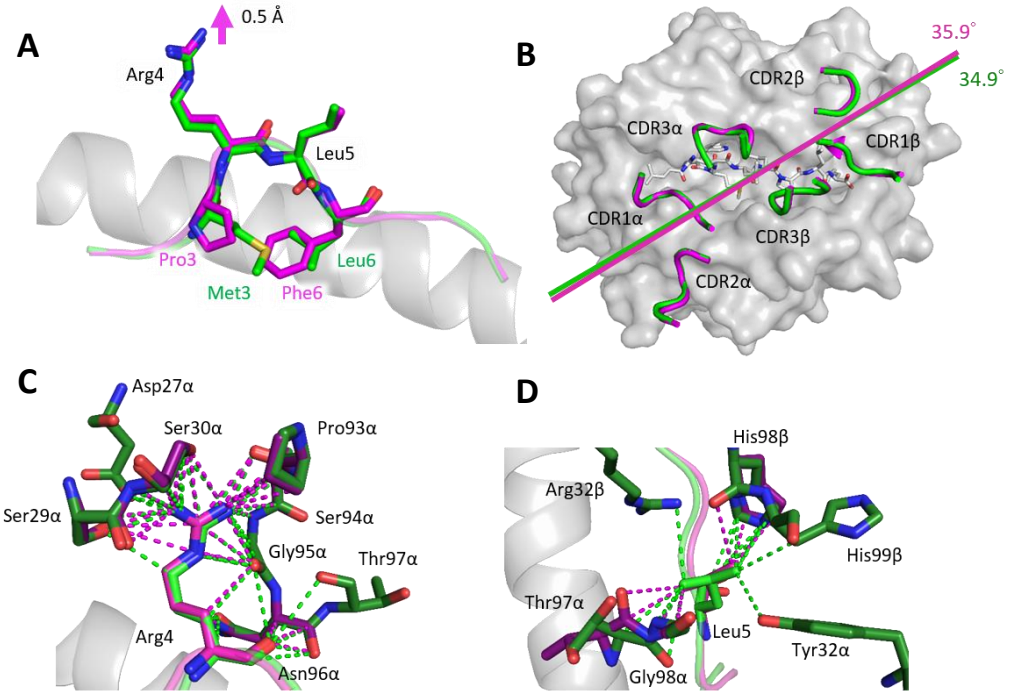

Figure 4.5. The 4C6 TCR recognises the preproinsulin and super-agonist peptides via identical molecular mechanisms.
(**A**) LWMRLLPLL (green) and QLPRLFPLL (magenta) peptides shown as sticks with MHC alpha-helix (grey) shown for orientation. (**B**) Top down view of 4C6 binding footprint on HLA-A24:02 presenting LWMRLLPLL (green) and QLPRLFPLL (magenta) peptides. Peptides shown as white sticks. Green and magenta lines and numbers indicate crossing angles of LWMRLLPLL interaction and QLPRLFPLL interaction respectively (**C-D**) LWMRLLPLL and QLPRLFPLL peptide residues Arg4 (**C**) and Leu5 (**D**) shown as green and magenta sticks respectively. Important 4C6 TCR residues bound to LWMRLLPLL and QLPRLFPLL are shown as dark green and dark purple respectively. Dotted lines indicate interactions between the 4C6 TCR and LWMRLLPLL (green) or QLPRLFPLL (magenta).

thermodynamic analysis was conducted on both TCR:pMHC complexes using SPR (**Figure 4.6**). The thermodynamic data revealed that the 4C6:A24-LWMRLLPLL interaction was entropically favourable and enthalpically unfavourable (TΔS = 14.9 kcal/mol, ΔH = 9.5 kcal/mol), whereas the 4C6:A24-QLPRLFPLL was entropically unfavourable and enthalpically favourable (TΔS = -1.9 kcal/mol, ΔH = -9.6 kcal/mol). The 4C6:A24-QLPRLFPLL interaction also exhibited a lower Gibbs free energy value than 4C6:A24-LWMRLLPLL, with ΔG = -7.7 kcal/mol and ΔG = -5.4 kcal/mol respectively. These data suggest the 4C6:A24-QLPRLFPLL interaction is more thermodynamically favourable than the 4C6:A24-LWMRLLPLL interaction, which may explain the differences in binding affinity.

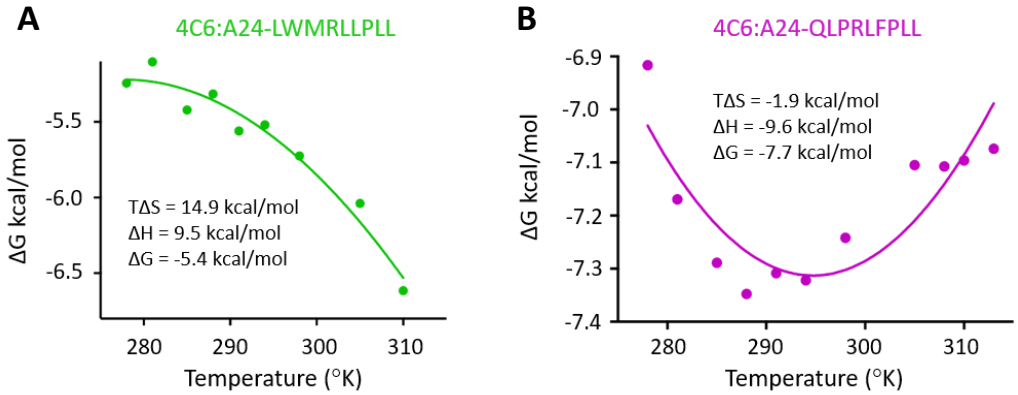

Figure 4.6. The 4C6 TCR exhibits preferable thermodynamics for the super-agonist peptide. Thermodynamic analysis of 4C6:A24-LWMRLLPLL (green) and 4C6:A24-QLPRLFPLL conducted using SPR. The binding free energies, ΔG (ΔG = RTlnKD), were plotted against temperature (K) using non-linear regression to fit the three-parameters van 't Hoff equation, (RT ln KD = ΔH° –TΔS° + ΔCp°(T-T0) – TΔCp° ln (T/T0) with T0=298 K).

4.3.7. CPL identifies potential pathogen-derived epitopes of the 4C6 T-cell

The CPL screen data in **Figure 4.1** and super-agonist peptide findings in **Figure 4.2** suggested that the 4C6 T-cell is capable of recognising a large number of different peptides, with many being much more potent agonists that the PPI-derived sequence. I hypothesised that some pathogen-derived peptides might act as strong agonists of the 4C6 T-cell. In order to confirm this hypothesis, I returned to the Szomolay webtool. In addition to searching the entire, theoretical, peptide universe, the webtool can search smaller databases consisting of the proteome of known human pathogens. The raw data from **Figure 4.1B** was used to search proteome databases of viral, fungal and bacterial human pathogens. The top 20 predicted peptides from each database were tested to see if they were recognised by the 4C6 T-cell.

The reactivity of the 4C6 T-cell clone to the chosen candidate peptides from the bacterial, viral, and fungal lists was assessed by MIP-1β ELISA using crude peptide (>40% purity). Three virus derived peptides were recognised, but none elicited a greater 4C6 T-cell response than the PPI index sequence (**Appendix Figure 2**). Conversely, multiple fungal peptides elicited a greater 4C6 T-cell response than the $PPI_{3\text{-}11}$ index peptide, with a *Cryptococcus neoformans* derived peptide (LLPRLFGLF) eliciting the greatest response (**Figure 4.7**). Multiple bacterial peptide candidates also elicited a 4C6 T-cell response, the best of which included two *Klebsiella oxytoca*-derived peptides (SLPRLFPPL, RYPRLLGIV) and a *Serratia liquefaciens*-derived peptide (RYPRLFPLL) (**Figure 4.8**). Fungal and bacterial CPL screens performed by Dr Garry Dolton.

A

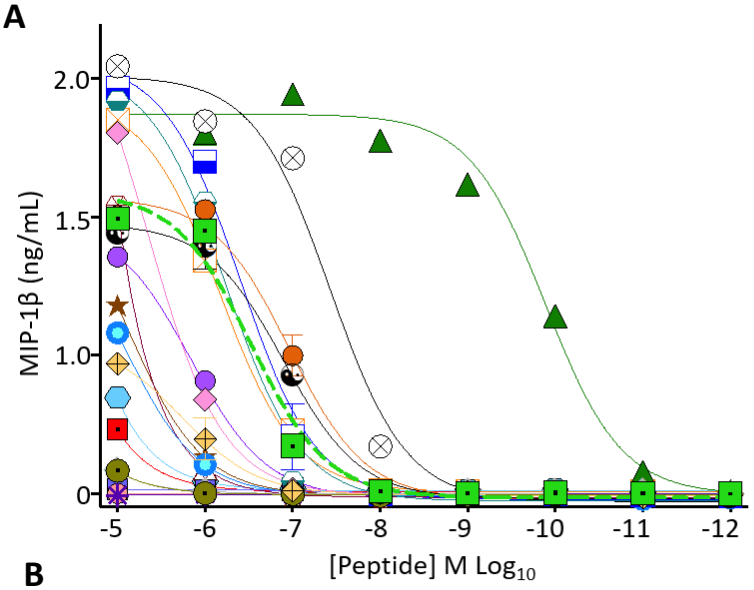

B

Score	Peptide	EC_{50}	Organism	Protein
-15.83	LWMRLLPLL	2.7 x10^{-7}	*Homo sapiens*	Preproinsulin
-9.63	QLPPLFPIV	**1.4 x10^{-7}**	*Aspergillus oryzae*	Ubiquitin-like activating enzyme
-10.23	SYPPLAPIV	3.2 x10^{-6}	*Fusarium oxysporum*	Putative protein
-10.53	NLLPLAPLA	~ 0.03	*Cryptococcus neoformans*	Nucleoside-diphosphatase putative
-10.65	QYPPLVPIM	**2.1 x10^{-8}**	*Aspergillus oryzae*	Unnamed protein product
-10.70	HLPRLAGLV	~ 0.003	*Fusarium oxysporum*	Putative protein
-10.92	EYPPLVPIL	NR	*Aspergillus niger*	Unnamed protein product
-10.92	ALPPLFPIA	**1.3 x10^{-7}**	*Aspergillus oryzae*	Putative protein
-11.05	NLPPLAPIT	4.5 x10^{-6}	*Aspergillus oryzae*	Dicer-like protein 2
-11.21	NLLRLVGLV	5.6 x10^{-7}	*Aspergillus niger*	Putative protein
-11.24	EYLPLFPLL	**5.2 x10^{-8}**	*Fusarium oxysporum*	Putative protein
-11.27	SLMRLFPLL	**3.8 x10^{-8}**	*Fusarium oxysporum*	Putative protein
-11.39	ALQRLAPIL	4.4 x10^{-7}	*Fusarium oxysporum*	Putative protein
-11.41	ILQRLAPIL	7.5 x10^{-6}	*Fusarium oxysporum*	Putative protein
-11.53	KKPRLAGIL	~ 0.08	*Sporothrix schenckii*	Putative protein
-11.75	LLLPLAGIL	1.2 x10^{-6}	*Fusarium oxysporum*	Putative protein
-12.01	DMPRLAGVL	6.4 x10^{-6}	*Sporothrix schenckii*	Putative protein
-12.04	LLPRLFGLF	**1.3 x10^{-10}**	*Cryptococcus neoformans*	Cytoplasmic protein
-12.10	RLPPLAPLI	~ 0.02	*Cryptococcus neoformans*	NAD+ diphosphatase
-12.18	LNPRLFGIL	6.8 x10^{-7}	*Fusarium oxysporum*	Delta24(24(1))-sterol reductase
-12.26	ALMRLMGIA	~ 0.06	*Saccharomyces cerevisiae*	Putative protein

Figure 4.7. 4C6 T-cells cross-react with peptides derived from fungal proteomes.
PS-CPL data for 4C6 (**Figure 1**) was used to screen a database of infectious fungi and the top 20 peptides selected for testing. (**A**) Peptide titrations using 4C6 with the top 20 bacteria peptides (listed in B). Incubation overnight with C1R-HLA-A*24:02^{+} cells as antigen presenting cells. Assay supernatants used for MIP-1β ELISA. Error bars depict SD from the mean of two replicates. (**B**) Peptide sequence and origin. Scoring indicates prediction of how likely the peptide is to be recognized by 4C6 T-cells, with the best scoring peptide at the top. EC_{50} of activation in bold indicate peptides seen more sensitively than the preproinsulin peptide in functional assays. Data provided by Dr Garry Dolton.

A

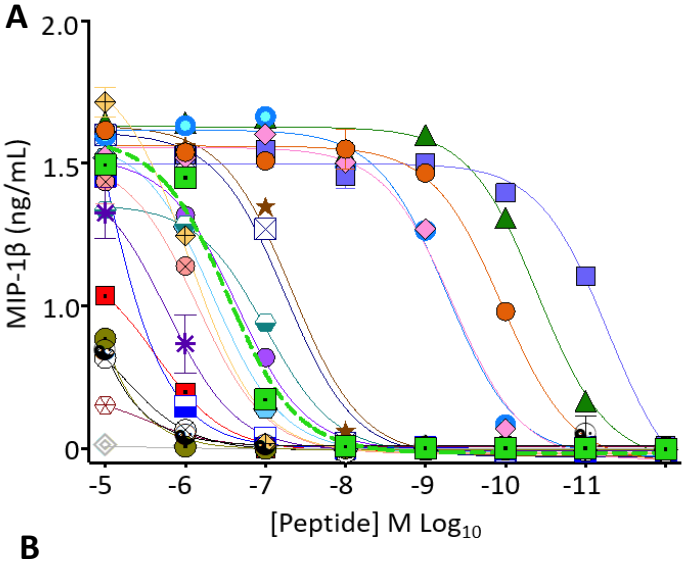

B

Score	Peptide	EC_{50}	Organism	Protein
-15.83	LWMRLLPLL	2.7 x10^{-7}	*Homo sapiens*	Preproinsulin
-9.63	QLPPLAPIL	~1.8 x10^{-4}	*Pseudomonas putida*	Putative protein
-10.18	QYLRLAGIA	8.1 x10^{-7}	*Haemophilus influenzae*	DNA transposition protein
-10.30	SLMRLAPIV	~8.1 x10^{-4}	*Pseudomonas fluorescens*	ADP-ribosylglycohydrolase
-10.35	DLLRLFPLV	1.7 x10^{-6}	*Pseudomonas stutzeri*	Putative protein
-10.36	ILPRLAPIA	NR	*Streptococcus uberis*	Sodium hydrogen antiporter
-10.63	NYLPLFPLA	7.1 x10^{-7}	*Campylobacter gracilis*	Glycosyltransferase group 1 family protein
-10.68	RYPRLFGIV	**1.1 x10^{-10}**	*Klebsiella oxytoca*	Enterochelin esterase
-10.68	DWLRLAPLF	**4.6 x10^{-10}**	*Escherichia coli*	Putative protein
-10.69	NLLPLAPLF	**9.3 x10^{-8}**	*Pseudomonas aeruginosa*	Protein nirF
-10.79	SLPRLFPLL	**5.3 x10^{-12}**	*Klebsiella oxytoca*	Glutathione ABC transporter ATP-binding protein
-10.80	ILPRLAPLV	5.4 x10^{-6}	*Escherichia coli*	Glycerate kinase
-10.80	NLLRLFPLI	1.1 x10^{-5}	*Klebsiella pneumoniae*	Membrane protein KPN78578_41360
-10.81	RYPRLFGIL	**5.2 x10^{-10}**	*Pseudomonas putida*	Cytochrome o ubiquinol oxidase subunit II
-10.90	ELPPLFPLL	2.6 x10^{-6}	*Escherichia coli*	Putative protein
-10.95	DWLRLVGIV	**2.4 x10^{-7}**	*Listeria monocytogenes*	ABC transporter ATP-binding/permease protein
-10.97	LLPRLAPLV	**4.6 x10^{-8}**	*Pseudomonas fluorescens*	ABC transporter substrate-binding protein
-11.01	RYPRLFPLL	**4.0 x10^{-11}**	*Serratia liquefaciens*	Fatty acid desaturase
-11.01	QLMRLAGLA	4.5 x10^{-7}	*Pseudomonas luteola*	Putative protein
-11.06	ILPRLAPLA	**5.7 x10^{-8}**	*Escherichia coli*	Glycerate kinase partial
-11.11	SLPPLAPLL	2.2 x10^{-6}	*Pseudomonas fluorescens*	Peptidase

Figure 4.8. 4C6 T-cells cross-react with peptides derived from bacterial proteomes.
PS-CPL data for 4C6 (**Figure 1**) was used to screen a database of infectious bacteria and the top 20 peptides selected for testing. (**A**) Peptide titrations using 4C6 with the top 20 bacteria peptides (listed in B). Incubation overnight with C1R-HLA-A*24:02^{+} cells as antigen presenting cells. Assay supernatants used for MIP-1β ELISA. Error bars depict SD from the mean of two replicates. (**B**) Peptide sequence and origin. Scoring indicates prediction of how likely the peptide is to be recognized by 4C6 T-cells, with the best scoring peptide at the top. EC_{50} of activation in bold indicate peptides seen more sensitively than the preproinsulin peptide in functional assays. Data provided by Dr Garry Dolton.

4.3.8. The 4C6 T-cell cross-reacts with pathogen-derived epitopes

The most potent pathogen-derived agonist peptide for 4C6 T-cells, SLPRLFPLL, was from the proteome of *Klebsiella oxytoca.* A second *K. oxytoca*-derived sequence RYPRLFGIV also acted as a strong agonist. A MIP-1β ELISA was conducted using >95% pure SLPRLFPLL and RYPRLFGIV peptide preparations (**Figure 4.9A**), which confirmed that these peptides elicit a greater response (EC_{50} = 5.6 x 10^{-11} and 5.6 x 10^{-10} respectively) from the 4C6 T-cell than the PPI_{3-11}-derived LWMRLLPLL epitope (EC_{50} = 1.9 x 10^{-7}). The 4C6 T-cell was stained with HLA-A24 tetramers presenting SLPRLFPLL or RYPRLFGIV, with the 4C6 T-cell showing a greater avidity to the *Klebsiella oxytoca*-derived epitopes (with mean fluorescent intensities of 26890 for SLPRLFPLL and 23999 for RYPRLFGIV) than the PPI_{3-11}-derived epitope (mean fluorescent intensity of 2699) (**Figure 4.9B**). These data confirm 4C6 T-cell cross-reactivity between a T1D-derived epitope and *Klebsiella oxytoca*-derived epitopes and suggest that cross-recognition of pathogen-derived epitopes might have acted to prime the 4C6 T-cells and trigger T1D.

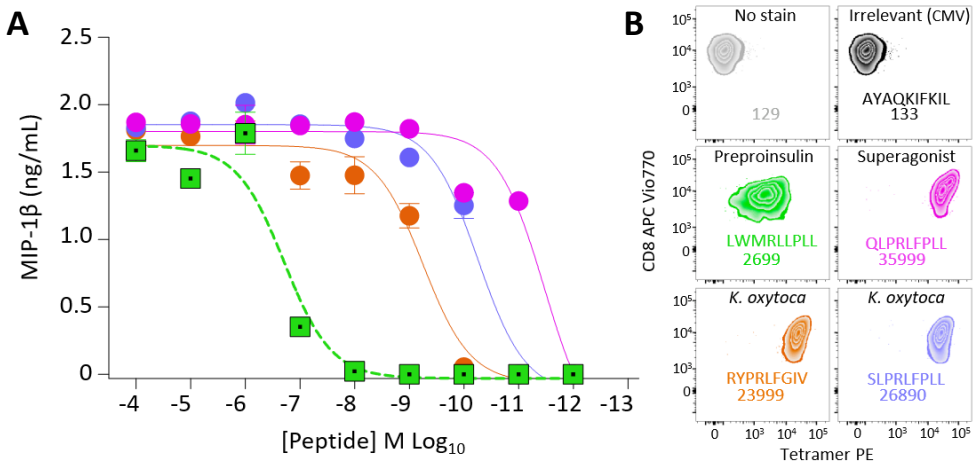

Score	Sequence	EC_{50}	Origin
-15.83	LWMRLLPLL	1.9 x10^{-7}	Preproinsulin
-9.97	QLPRLFPLL	3.4 x10^{-12}	Superagonist screen
-10.48	SLPRLFPLL	5.6 x10^{-11}	*Klebsiella oxytoca*
-10.59	RYPRLFGIV	5.6 x10^{-10}	*Klebsiella oxytoca*

Figure 4.9. The 4C6 T-cell clone exhibits greater T-cell response to pathogen epitopes then to the preproinsulin epitope.
Sensitivity of 4C6 T-cells to preproinsulin (LWMRLLPLL), super-agonist (QLPRLFPLL) and *Klebsiella oxytoca* (SLPRLFPLL and RYPRLFGIV) peptides in a titration assay. Underlined amino acid residues are the same as the preproinsulin peptide. Residues in bold are present in the super-agonist. Incubation overnight with C1R-HLA-A*24:02^{+} cells as antigen presenting cells. Assay supernatants used for MIP-1β ELISA. Error bars depict SD from the mean of two replicates. **C**) Staining of 4C6 T-cells with pMHC tetramers bearing CMV irrelevant epitope (AYAQKIFKIL), preproinsulin (LWMRLLPLL), super-agonist (QLPRLFPLL) and *Klebsiella oxytoca* (SLPRLFPLL and RYPRLFGIV) PE tetramers. Staining performed without PKI. Mean fluorescence intensity of staining is displayed. Stained for CD8 APC-Vio770 and the viability stain VIVID. Data proved by Dr Garry Dolton.

4.4. Discussion

In this chapter I expanded on the work previously published by the Peakman group showing that HLA-A24 can present residues 3-11 from preproinsulin in cells expressing the *INS* gene (Kronenberg et al, 2012). This study identified a T1D patient-derived T-cell, 4C6, that responded to the LWMRLLPLL peptide and could kill HLA-A24^{+} human β-cells harvested from deceased organ donors (Kronenberg et al, 2012). All T-cells sorted and sequenced from patient blood using an HLA-A24-LWMRLLPLL tetramer expressed the 4C6 TCR suggesting that this T-cell dominated the response *in vivo* (Kronenberg et al, 2012). I was interested in how the 4C6 TCR engaged HLA-A24-LWMRLLPLL to result in pancreatic β-cell killing.

I present what is, to my knowledge, the first 3D structure of a TCR in complex with an HLA-A24-restricted T1D diabetes epitope and only the second TCR engaging a human HLA-I-restricted autoantigen. Given the strong association of HLA-A24 and predisposition to T1D (Nejentsev et al, 2007), structural data demonstrating the mechanisms underlying this association would provide greater understanding of how HLA-A24-presented T1D epitopes can lead to autoimmune responses.

Additionally, I present data showing how the 4C6 TCR can cross-react with pathogen-derived epitopes. Autoreactive T-cells are deleted during thymic selection or suppressed in the periphery. As such, recognition of A24-LWMRLLPLL by the 4C6 T-cell must both escape central tolerance and overcome peripheral tolerance. Data concerning 4C6 T-cell cross-reactivity may provide insight into how T-cells can be primed by a pathogenic peptide and mount a subsequent autoimmune response.

4.4.1. Demonstrating 4C6 T-cell cross-reactivity

To determine what may trigger 4C6 T-cell autoreactivity, the recognition profile of the 4C6 T-cell needed to be determined (**Figure 4.1**). Firstly, a peptide sizing scan determined that the 4C6 T-cell exhibited a preference for 9-mer peptides. With this knowledge, a 9-mer CPL screen was used to determine the preferred amino acid residue at each peptide position, which suggested that Arg4 and Leu5 peptide residues are important for 4C6 T-cell recognition. CPL screens are also a proven method of identifying novel peptide ligands (Drijfhout et al, 1997; Pinilla et al, 1993; Szomolay et al, 2016), which in combination with Dr Szomolay's web tool were able to identify further ligands for the 4C6 T-cell (Szomolay et al., 2016).

The optimum peptide sequence for 4C6 T-cell recognition was thus identified as QLPRLFPLL. A MIP-1β ELISA determined that QLPRLFPLL elicits a far stronger 4C6 T-cell response than LWMRLLPLL (**Figure 4.2**). SPR data demonstrated a far higher 4C6 TCR affinity for QLPRLFPLL than LWMRLLPLL (**Figure 4.3**). SPR data also suggested that the dissociation rate of the 4C6:A24-QLPRLFPLL interaction was far slower than that of the 4C6:A24-LWMRLLPLL, however there are certain caveats to this observation which will be discussed further in **Section 6.3.1**. While the QLPRLFPLL peptide is not known to occur in nature, it was used to demonstrate that 4C6 T-cell can potentially recognise ligands with a far higher sensitivity than the autoimmune epitope.

4.4.2. Crystallisation of 4C6:A24-LWMRLLPLL complex using seeding

As discussed in **Section 4.3.4**, initial attempts to crystallise the 4C6:A24-LWMRLLPLL complex were unsuccessful. SPR data showed that the 4C6 TCR bound to HLA-A24-LWMRLLPLL with an affinity of 129.2 μM, which despite being relatively high for an autoimmune interaction, is two orders of magnitude lower than the strongest antiviral TCRs (Bridgeman et al., 2011). Anecdotally, TCR:pMHC complexes with relatively low affinities usually prove more difficult to crystallise.

Seeding was used to overcome the difficulties in crystallising the 4C6:A24-LWMRLLPLL complex. Due to the structural homology between 4C6:A24-LWMRLLPLL and 4C6:A24-QLPRLFPLL, the 4C6:A24-QLPRLFPLL micro-seeds provided a nucleation point from which 4C6:A24-LWMRLLPLL crystals could form, allowing me to conduct x-ray crystallography and acquire the 4C6:A24-LWMRLLPLL 3D structure. The use of crystals of TCRs in complex with high affinity epitopes, could potentially be used to produce crystals of other TCRs in complex with autoimmune epitopes in future, overcoming the difficulties associated with crystallising low affinity TCR:pMHC complexes.

4.4.3. Structural analysis of the 4C6 TCR interactions

4.4.3.1. Hotspot binding in autoreactive T-cells

Analysis of the 4C6:A24-LWMRLLPLL structure revealed a ‘peg in hole’ binding mode, where peptide residues Arg4 and Leu5 protruded towards the TCR due to peptide bulging (**Figure 4.4**). The peptide bulge appears to be facilitated by Van der Waals interactions between

peptide residues Met3 and Leu6. The protruding Arg4 and Leu5 peptide residues occupy a pocket made up of 4C6 CDR loops CDR1α, CDR3α, CDR1β, and CDR3β. 72% of interactions between the TCR and the peptide occur within this pocket, including all the hydrogen bonds, so it can be reasoned that this binding mechanism drives the 4C6:A24-LWMRLLPLL interaction, with the Arg4 and Leu5 residues acting as a binding hotspot. The Arg4 and Leu5 hotspot residues are conserved among the super-agonist (QLP**RL**FPLL) and the pathogenic peptides discussed in **Section 4.3.8** (LLP**RL**FGLF, SLP**RL**FPLL, RYP**RL**FGIV and RYP**RL**FPLL), further supporting the hypothesis that Arg4 and Leu5 are important for 4C6 TCR recognition.

The hotspot binding mechanism exhibited by the 4C6 TCR was also observed by the 1E6 TCR, briefly discussed in **Section 4.1,** where all 1E6 specific peptides have a xxxGPDxxxx motif (Cole, et al., 2016). This suggests that hotspot binding may be a hallmark of T1D-specific T-cell cross-reactivity. Analysis of the cross-reactive mechanism of the Hy.1B11 T-cell, a MS specific T-cell, shows that the Hy.1B11 TCR appears to utilise peptide hotspots for recognition (Sethi et al., 2013). While these data may suggest autoimmune diseases are facilitated by hotspot driven cross-reactivity, it is worth noting that very few 3D structures demonstrating autoreactive cross-reactivity are available in the literature. As such, any correlations that can be drawn at present may be subject to change as the number of available autoreactive T-cell structures expands.

4.4.3.2. Biophysical characteristics may determine 4C6 TCR binding affinity

SPR data showed how the 4C6 TCR exhibits a greater affinity for the QLPRLFPLL super-agonist than the LWMRLLPLL index peptide, with SPR confirming a >20-fold higher binding affinity for the 4C6:A24-QLPRLFPLL complex than the 4C6:A24-LWMRLLPLL complex (**Figure 4.3**). However, differences in binding interactions could not explain the differences in affinity (**Figure 4.5**). A comparison of both 3D complex structures indicated that the 4C6 TCR shared a very similar mode of binding between both epitopes despite the differences in affinity. Counterintuitively, there were 15 less interactions between the 4C6 TCR and HLA-A24-QLPRLFPLL than HLA-A24-LWMRLLPLL, which would be expected to result in a lower affinity. As such, factors beyond the number of bonds in TCR:pMHC interactions are clearly responsible for the higher affinity of the 4C6:A24-QLPRLFPLL complex.

One such factor is the presence of more Van der Waals interactions between peptide residues Pro3 and Phe6 in QLPRLFPLL than Met3 and Leu6 in LWMRLLPLL when bound to the

4C6 TCR, which may increase the stability and rigidity of the peptide bulge. The extra Van der Waals interactions may also be responsible for the extra 0.5 Å protrusion of QLPRLFPLL residues Arg4 and Leu5 when bound to the 4C6 TCR, which itself may factor into the improved binding affinity of the 4C6 TCR to the QLPRLFPLL peptide. Peptide residues Pro3 and Phe6 are also conserved in all the most strongly recognised pathogenic peptides discussed in **Section 4.3.8** (LL**P**RL**F**GLF, SL**P**RL**F**PLL, RY**P**RL**F**GIV and RY**P**RL**F**PLL), which elicit a greater 4C6 T-cell response than the $PPI_{3\text{-}11}$ index peptide which lacks Pro3 and Phe6. These data suggest that peptide residues Pro3 and Phe6 may help facilitate a higher 4C6 TCR binding affinity.

Another possible explanation for the observed differences in 4C6 binding affinity is that 4C6:A24-QLPRLFPLL has preferable thermodynamics compared to 4C6:A24-LWMRLLPLL (**Figure 4.6**). The exothermic nature and negative entropy of 4C6:A24-QLPRLFPLL indicate 4C6 TCR interaction with HLA-A24-QLPRLFPLL is driven by the net formation of bonds and a shift to a more chemically ordered state, as opposed to 4C6:A24-LWMRLLPLL which is endothermic in nature and appears to shift towards a more disordered state. The differences in thermodynamic properties may be explained by the composition of the P2 peptide anchor of each complex (**Figure 4.10**). QLPRLFPLL has a suboptimal P2 anchor in comparison to LWMRLLPLL (leucine vs tryptophan). This may allow the peptide to be pulled out of the pocket as previously reported for an HLA-A2 epitope (Madura et al., 2015). The P2 anchor has also been shown to be an allosteric modulator of the TCR:pMHC complex, which can affect binding affinity even if the binding modes among multiple epitopes are conserved (Smith et al., 2021). The pathogenic peptides in **Section 4.3.8** which elicited the greatest 4C6 T-cell response all use a leucine residue as their P2 anchor, suggesting Leu2 also facilitates a higher binding affinity.

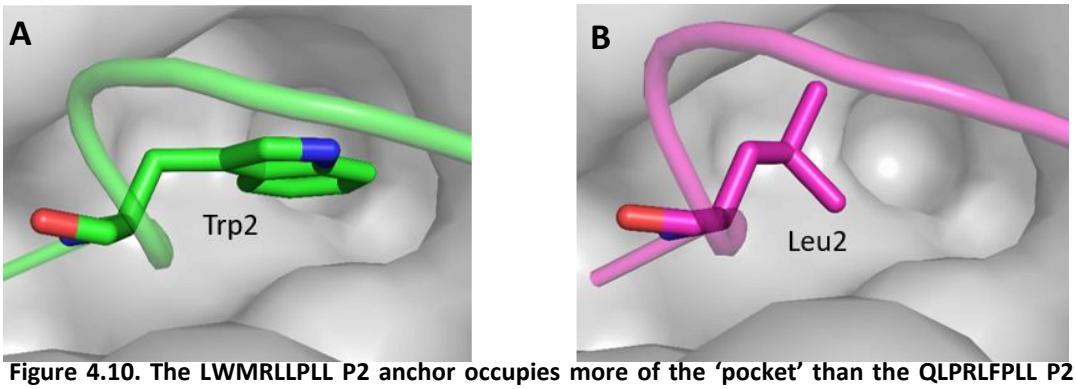

Figure 4.10. The LWMRLLPLL P2 anchor occupies more of the 'pocket' than the QLPRLFPLL P2 anchor residue.
P2 anchor residues of (**A**) LWMRLLPLL and (**B**) QLPRLFPLL shown as green and magenta sticks respectively. MHC shown as grey surface.

4.4.4. Identifying the autoimmune trigger of the 4C6 T-cell clone

CPL data, in conjunction with the webtool designed by Dr Szomolay, was used to search for pathogen-derived peptides that could be recognised by the 4C6 T-cell. Several peptides elicited greater MIP1-β responses from the 4C6 T-cell than the PPI_{3-11} epitope, with peptides derived from *Cryptococcus neoformans* (LLPRLFGLF), *Klebsiella oxytoca* (SLPRLFPLL, RYPRLFGIV), and *Serratia liquefaciens* (RYPRLFPLL) eliciting among the greatest 4C6 T-cell responses (**Figure 4.7, Figure 4.8, Figure 4.9**). While further work would need to be conducted to confirm a link between the pathogens mentioned above and the onset of T1D, this data does confirm that the 4C6 T-cell can cross-react with pathogenic peptides.

The webtool discussed above may be optimised to provide a larger list of peptides that elicit greater 4C6 T-cell response than the PPI_{3-11} peptide, by using motif restricted sampling. The importance of the xxPRLFxxx motif for 4C6 T-cell recognition has been demonstrated by the data presented in this chapter, the presence of which appears to correlate with greater 4C6 T-cell activation. As such, a search of the pathogenic peptide databases can be conducted where peptide residues 3-6 are 'fixed' so all candidate peptides contain the optimum xxPRLFxxx motif and HLA -A24 anchor residues at p2 and p9, potentially identifying further 4C6 T-cell reactive peptides and highlighting additional pathogens that may trigger T1D onset. Motif restricted sampling has been previously used by my laboratory to identify further ligands for the 1E6 T-cell (Cole, et al., 2016).

4.4.5. Conclusion

In this chapter I have expanded on the published work of the Peakman group (Kronenberg et al, 2012) to provide biochemical proof of binding between the TCR from T1D-relevant T-cell clone 4C6 and the PPI-derived peptide, LWMRLLPLL, presented on a T1D risk allele, HLA-A24 (Nejentsev et al, 2007). I solved the crystal structure of this interaction and demonstrated a peg in hole binding motif. Furthermore, I used CPL-driven database screening (Szomolay et al, 2016) to conclusively demonstrate the ability of the 4C6 T-cell to bind ligands with substantially higher affinity than that of its index T1D-associated LWMRLLPLL peptide. Finally, I showed that this well-established webtool-based methodology could identify pathogen-derived peptide antigens for the 4C6 T-cell, suggesting that, in the context of T1D, the self-tolerance of the 4C6 T-cell may be broken by cross-reactivity with a known human pathogen.

5. Crossreactivity between HLA-A*02:01-restricted herpesvirus and diabetogenic epitopes is commonplace in type 1 diabetes

5.1. Introduction

As discussed in **Chapter 4** certain HLA alleles, such as *HLA-A*24*, *HLA-B*39*, and *HLA-A*02* are linked with an increased risk of T1D (Nejentsev et al., 2007; Noble et al., 2010). Further evidence showing that *HLA-A*02* alleles can mediate T1D progression was reported using transgenic NOD mice (Marron et al., 2002). The T1D association with *HLA-A*02*, coupled with evidence discussed in **Section 1.2.3** showing that *HLA-A*02* is the most prominently expressed HLA allele in the worldwide population (**Chapter 1.2.3**), necessitates further study into the role of *HLA-A*02* in T1D.

In **Chapter 4,** I discussed studies conducted by my laboratory that showed that the 1E6 T-cell clone was able to kill pancreatic cells via a preproinsulin epitope presented by HLA-A2 (Bulek et al., 2012; Skowera et al., 2008). The 1E6 TCR was also able to cross-react with multiple peptides, some of which were derived from pathogens (Cole et al., 2016). My laboratory had another HLA-A2-restricted patient-derived T-cell clone, InsB4, that recognised the insulin B chain-derived epitope HLVEALYLV (insulin residues 10-18) (Pinkse et al., 2005). We set out to investigate the interaction between HLA-A2- HLVEALYLV and the InsB4 TCR and to see if this TCR might interact with any pathogen-derived epitopes. These studies resulted in me examining the potential role of human herpesviruses in the initiation of T1D via the most commonly expressed HLA-I allele in patients, *HLA-A*0201*.

5.2. Aims

I aimed to acquire structural/biophysical data on the interaction between the InsB4 TCR and HLA-A2-HLVEALYLV and to determine if the InsB4 T-cell clone responded to any pathogen-derived HLA-A2-restricted epitopes.

5.3. Results

5.3.1. InsB4 T-cells recognise an HLA-A2-restricted epitope from the insulin B chain

The InsB4 T-cell clone was isolated from a $CD8^+$ T-cell library that was derived from the blood of an *HLA-A*0201*$^+$ T1D patient by Dr Garry Dolton (Theaker et al., 2016). The InsB4 T-cell clone was confirmed to respond to an insulin B chain (InsB)-derived peptide, HLVEALYLV, via MIP-1β ELISA (**Figure 5.1A**). The HLVEALYLV peptide has been previously reported in the literature (Pinkse et al., 2005). Recognition of HLVEALYLV was further confirmed by successful pHLA multimer staining of InsB4 by HLA-A2-HLVEALYLV dextramers (**Figure 5.1B**). InsB4 T-cells recognised K562 cells that had been transduced with the *HLA-A*0201* and *INS* genes but did not respond to K562 cells transduced with just *HLA-A*0201* or K562 cells transduced with the *HLA-A*0201* and *GAD65* genes (**Figure 5.1C**). We concluded that the InsB4 T-cell clone recognises a genuinely processed and presented epitope from the *INS* gene which encodes the PPI protein.

We next demonstrated that the InsB4 T-cell clone and a sister clone from the same T1D patient donor that had an identical TCR called InsB6 recognised *HLA-A*0201*$^+$ pancreatic β-cells taken from a deceased organ donor. The PPI-specific T-cell clone 1E6 (Skowera et al., 2008) and a CMV-specific T-cell clone were used as positive and negative controls respectively (**Figure 5.1D**).

5.3.2. Manufacture of the InsB4 TCR and HLA-A2-HLVEALYLV

To confirm that the InsB4 TCR interacts with the HLA-A2-HLVEALYLV pMHC, I first had to produce soluble TCR and pMHC molecules. Soluble InsB4 TCR and HLA-A2-HLVEALYLV were produced as described in **Chapter 3** (**Figure 5.2A**). Once the soluble protein was produced, SPR was conducted to assess the binding affinity between the InsB4 TCR and HLA-A2-HLVEALYLV. I was unable to show a response between the InsB4 TCR and the HLVEALYLV peptide by SPR, despite *in vitro* cell-culture based data clearly demonstrating recognition (**Figure 5.2B**). I therefore hypothesised that the InsB4 T-cell recognises the InsB-derived peptide with an immeasurably low affinity. I therefore concluded that any study of InsB4 TCR-ligand interaction would require generation of more potent ligands as done for the 4C6 T-cell in **Chapter 4**. To this end, combinatorial peptide library data of the InsB4 clone from my colleague Dr Garry Dolton was used to predict peptides that may bind the InsB4 TCR with greater affinity.

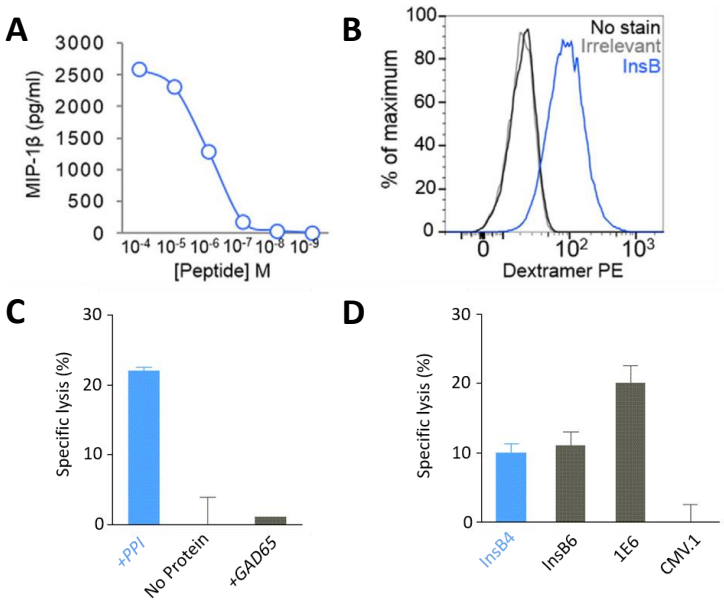

Figure 5.1. The InsB4 T-cell CD8⁺ clone kills pancreatic β-cells via an insulin B chain-derived epitope.

(**A**) Recognition of a titration of the insulin B chain-derived peptide HLVEALYLV by the InsB4 T-cell clone in a MIP-1β ELISA. (**B**) Staining of the InsB4 T-cell clone with HLA-A2-HLVEALYLV dextramers. Dextramers of HLA-A2 presenting the influenza matrix epitope GILGFVFTL were used as an irrelevant control. (**C**) InsB4 killing of surrogate pancreatic β-cells (K562 cells expressing *HLA-A*0201* and *INS* genes). K562 cells transduced with *HLA-A*0201* alone and K562 cells transduced with *HLA-A*0201 and GAD65* genes were used as controls. (**D**) InsB4 and sister clone InsB6 (expressing the same TCR) killing of pancreatic β-cells from a deceased *HLA-A*0201*⁺ organ donor. PPI-specific T-cell clone 1E6 and CMV pp65-specific T-cell clone CMV.1 were used as positive and negative controls respectively. Data shown in **A**-**B** has been published (*J Immunol Methods,* 2016, **430**, 43-50). Data shown in **C**-**D** has also been published (*Frontiers Immunology,* 2020, **11**, 1-18).

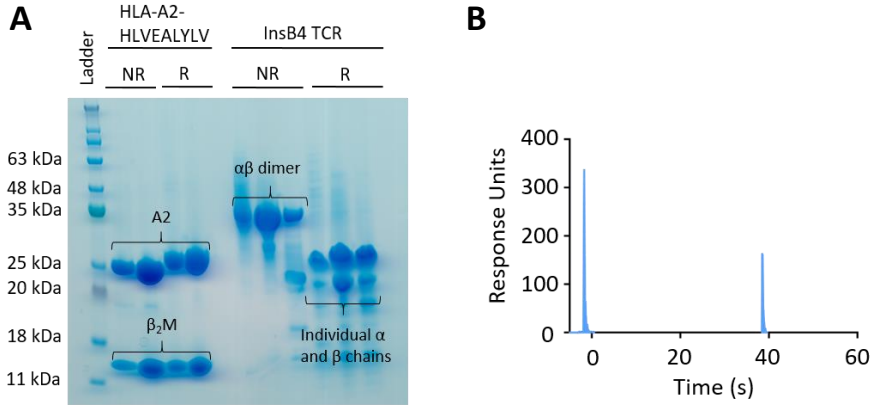

Figure 5.2. The InsB4 TCR affinity for the InsB-derived peptide is immeasurably low by SPR.

(**A**) SDS-PAGE gel of soluble InsB4 TCR and soluble HLA-A2-HLVEALYLV after size exclusion chromatography. Samples for both proteins analysed in reduced (with DTT, R) and non-reduced (without DTT, NR) conditions. Multiple lanes within each sample are indicative of different fractions. (**B**) Surface Plasmon resonance (SPR) analysis of InsB4 TCR recognition of HLVEALYLV. SPR response to ten serial dilutions of InsB4 TCR was measured, with a maximum concentration of 407 µM. HLA-A2-NLSALGIFST was used as an irrelevant control.

5.3.3. Generating a peptide recognition landscape for the InsB4 T-cell

A peptide sizing scan on InsB4 T-cells revealed that it exhibited a preference for 9-mer peptides (**Figure 5.3A**). A 9-mer CPL screen was then conducted to determine the amino acid preference of the InsB4 T-cell. The CPL data indicated that peptide recognition is relatively flexible in most peptide positions, however there was a very clear preference at position 4 for glutamic acid, suggesting that this residue, present in the HLVEALYLV InsB peptide, might be a key recognition residue for the InsB4 TCR (**Figure 5.3B-C**).

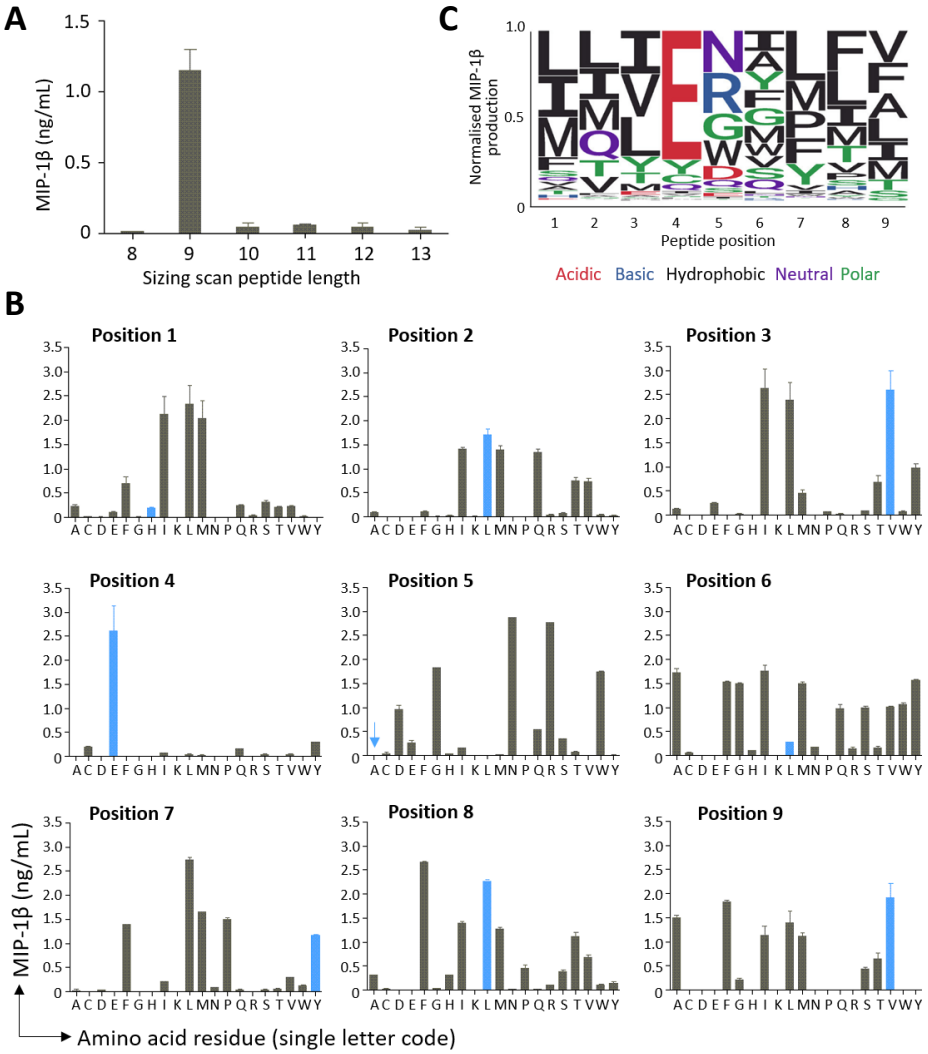

Figure 5.3. Sizing scan and positional scanning combinatorial peptide library screening of the InsB4 T-cell clone.
(**A**) 30,000 InsB4 T-cells were incubated overnight with sizing scan mixtures of defined amino acid length (x-axis) using 60,000 T2-HLA-A*02:01^{+} cells as antigen presenting cells. Assay supernatants used for MIP-1β ELISA. Error bars depict SD from the mean of two replicates. (**B**) Based on the results of the sizing scan, a 9mer positional scanning combinatorial peptide library (PS-CPL) screen was performed, using InsB4 T-cells, antigen presenting cells and ELISA as in (**A**). Blue bars indicate amino acid present in the natural insulin B-chain epitope. Errors bars depict SD from the mean of two replicates. (**C**) Motif log plot summarizing the amino acid preference of InsB4 at each position of the PS-CPL. Data has also been published (*Frontiers Immunology,* 2020, **11**, 1-18). Data provided by Dr Garry Dolton.

5.3.4. CPL data identifies potential pathogenic ligands for InsB4

The CPL data shown in **Figure 5.3B** were input into the webtool as discussed in **Chapter 3** and used to search bacterial and fungal databases for potential peptide candidates that could illicit an InsB4 T-cell response. The top 20 candidates generated from the bacterial and fungal databases respectively were tested against the InsB4 T-cell via a MIP-1β ELISA using crude (>40% purity) peptide preparations (**Figures 5.4 and 5.5**). The candidates selected from the bacterial- and fungal-derived peptides were from *Helicobacter pylori* (MLLENGLLA) and a *Candida albicans* (MIVENVPLL).

5.3.5. The InsB4 T-cell clone can cross-react with bacterial and fungal epitopes

To confirm InsB4 cross-reactivity with the bacterial and fungal epitopes, a MIP-1β ELISA was conducted using >95% pure MLLENGLLA and MIVENVPLL peptide preparations (**Figure 5.6A**). These human pathogen-derived peptides were far more potent at activating InsB4 T-cells (EC_{50} = 2.7 x 10^{-8} and 1.6 x 10^{-10} respectively) than the InsB-derived HLVEALYLV epitope (EC_{50} = 1.6 x 10^{-6}). Staining of InsB4 T-cells with HLA-A2 dextramers presenting HLVEALYLV, MLLENGLLA or MIVENVPLL peptides showed that the pathogen-derived peptides bound with greater avidity than the index InsB-derived epitope (MFIs 12,775 for MLLENGLLA, 16,385 for MIVENVPLL compared to 2910 for the index HLVEALYLV peptide) (**Figure 5.6B**).

5.3.6. The InsB4 TCR binds the bacterial and fungal peptides

I used the soluble InsB4 TCR I had successfully refolded (**Section 5.3.2** above) to examine binding of the InsB4 TCR to the *Helicobacter pylori*- and *Candida albicans*-derived peptides. SPR data showed that the InsB4 TCR bound to the MLLENGLLA and MIVENVPLL peptides with affinities of 168.5 μM and 60.7 μM respectively (**Figure 5.7**). These data confirmed InsB4 T-cell cross-reactivity between an InsB-derived epitope and pathogen-derived epitopes and were published by my laboratory as part of a study showcasing the use of graphics processing unit accelerated discovery of pathogen-derived molecular mimics of the insulin derived epitope (Whalley et al., 2020). Running of Dr Szomolay's software on an inexpensive (<£150) GPU, removed the requirement for mainframe computation and expedited running times by >50-fold (Whalley et al., 2020). I was a co-author of this study to acknowledge my contribution of having manufactured the soluble HLA-A2 ligands, InsB4 TCR and having undertaken the SPR binding analyses shown in **Figure 5.7**.

A

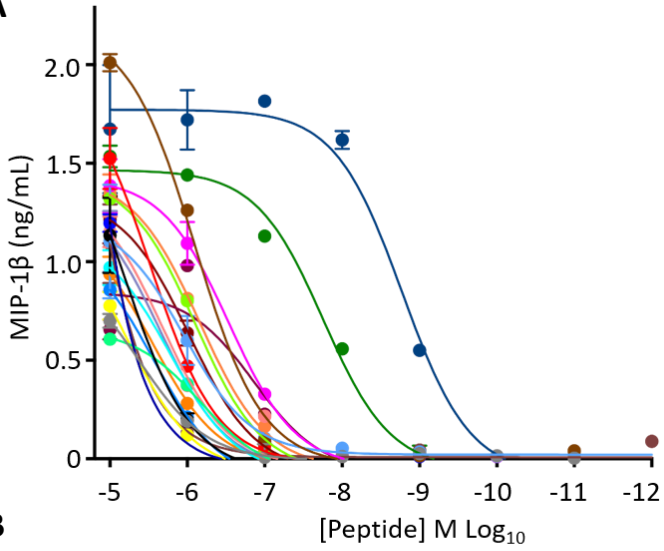

B

Score	Peptide	EC_{50}	Organism	Protein
-15.83	HLVEALYLV	9.6 x10^{-5}	*Homo sapiens*	Insulin B-chain
-12.66	LLIERYLLV	6.7 x10^{-5}	*Klebsiella pneumoniae*	Putative protein
-12.70	IMIENILFF	1.7 x10^{-6}	*Bacillus cereus*	Putative protein
-12.83	LLIERFLFL	5.7 x10^{-5}	*Helicobactor pylori*	Putative protein
-12.87	LMLERALLV	5.2 x10^{-5}	*Helicobactor pylori*	Cytochrome c biogenesis protein
-12.88	ILIERILLA	2.3 x10^{-5}	*Haemophilus influenzae*	Glycosyltransferase
-12.90	IILENFLFF	1.0 x10^{-6}	*Streptococcus mitis*	Putative protein
-12.92	LMLERALLF	7.8 x10^{-5}	*Helicobactor pylori*	Cytochrome c biogenesis protein
-12.93	IILENILLF	6.4 x10^{-5}	*Clostridium novyi*	Putative protein
-12.94	LLIERGLLA	5.4 x10^{-6}	*Pseudomonas aeruginosa*	LysR family transcriptional regulator
-12.97	LLVEGILLV	3.7 x10^{-4}	*Streptococcus oralis*	Putative protein
-13.05	MLVERYLLA	1.6 x10^{-6}	*Escherichia coli*	Putative protein
-13.07	IIIEGILFV	7.8 x10^{-8}	*Streptococcus caballi*	Putative protein
-13.08	ILIERFLLL	8.6 x10^{-6}	*Clostridium butyricum*	Putative protein
-13.13	MLLENGLLA	7.6 x10^{-7}	*Helicobactor pylori*	Putative protein
-13.14	LMIERGLLA	0.2 x10^{-6}	*Pseudomonas aeruginosa*	Putative protein
-13.16	LILERALLL	5.5 x10^{-5}	*Pseudomonas stutzeri*	FlgN family protein
-13.17	LIIENQLFF	NR	*Haemophilus aegyptius*	Putative protein
-13.24	MLVENQLLV	1.9 x10^{-5}	*Pseudomonas mendocina*	AraC family transcriptional regulator
-13.26	ILIENALMF	1.0 x10^{-6}	*Pseudomonas stutzeri*	Polysaccharide biosynthesis protein
-13.28	ILLERILIF	3.9 x10^{-5}	*Salmonella enterica*	Putative protein

Figure 5.4. InsB4 CD8$^+$ T-cell clone cross-react with peptides derived from bacterial proteomes. PS-CPL data for InsB4 (**Figure 5.3**) was used to screen a database of infectious bacteria and the top 20 peptides selected for testing. (**A**) Peptide titrations using InsB4 with the top 20 bacterial peptides (listed in **B**). 30,000 InsB4 T-cells were incubated overnight with 60,000 T2 (HLA-A*02:01$^+$) antigen presenting cells. Assay supernatants used for MIP-1β ELISA. Error bars depict SD from the mean of two replicates. EC_{50} of activation shown in **B**. (**B**) Peptide sequence and origin. Scoring indicates prediction of how likely the peptide is to be recognized by InsB4 T-cells, with the best scoring peptide at the top. Data has also been published (*Frontiers Immunology,* 2020, **11**, 1-18). Data provided by Dr Garry Dolton.

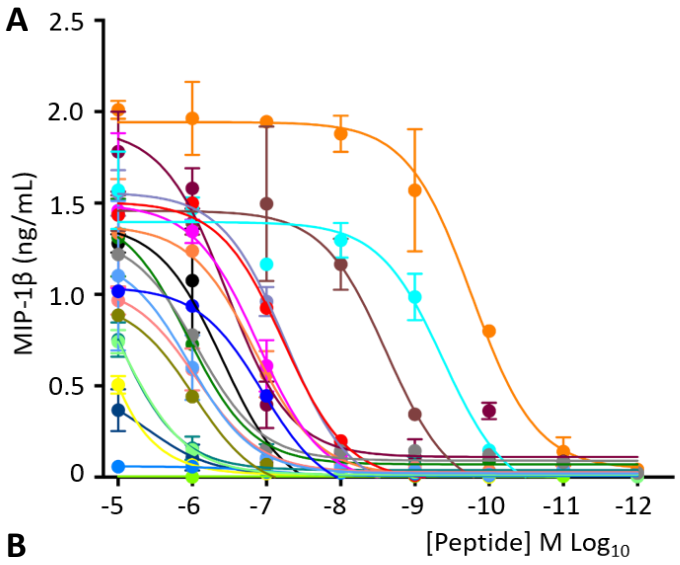

Score	Peptide	EC_{50}	Organism	Protein
-15.83	HLVEALYLV	9.6 x10^{-5}	*Homo sapiens*	Insulin B-chain
-13.48	LILENYMFA	0.5 x10^{-6}	*Candida tropicalis*	Putative protein
-13.59	IQLENSLFA	0.5 x10^{-5}	*Mucor circinelloides*	Putative protein
-13.61	ILVERALFT	0.3 x10^{-7}	*Fusarium oxysporum*	Putative protein
-13.73	MIVEGFLLL	2.3 x10^{-7}	*Sporothrix schenckii*	Putative protein
-13.81	ITIERILFI	0.7 x10^{-4}	*Crytococcus neoformans*	Putative protein
-13.82	IMLENGPFL	NR	*Aspergillus niger*	Putative protein
-13.84	LIIENAPLI	3.8 x10^{-9}	*Saccharomyces cerevisiae*	Tae2p
-13.90	MLVEGVLLA	2.6 x10^{-7}	*Mucor circinelloides*	Putative protein
-13.92	MIIEGFLLI	8.9 x10^{-6}	*Mucor circinelloides*	Putative protein
-13.94	LLVENWPLL	6.2 x10^{-8}	*Aspergillus niger*	Putative protein
-14.01	LIIEWIFFL	8.4 x10^{-6}	*Aspergillus clavatus*	Putative protein
-14.14	MQVEWILTF	9.2 x10^{-4}	*Candida albicans*	Putative protein
-14.19	LQLEGQLLL	4.1 x10^{-5}	*Fusarium oxysporum*	Putative protein
-14.22	LVVEGSLFV	4.7 x10^{-6}	*Fusarium verticilloides*	Putative protein
-14.24	LIVEGILLT	9.5 x10^{-5}	*Aspergillus oryzae*	Putative protein
-14.31	MIVENVPLL	7.7 x10^{-9}	*Candida Albicans*	Putative protein
-14.32	LLVEDMLLM	4.1 x10^{-6}	*Sporothrix schenckii*	Putative protein
-14.32	LIIEWYLIM	0.7 x10^{-6}	*Candida tropicalis*	Putative protein
-14.34	MLLEGMMIV	9.5 x10^{-6}	*Fusarium oxysporum*	Putative protein
-14.34	FLLERILIV	0.2 x10^{-6}	*Saccharomyces cerevisiae*	Swf1p

Figure 5.5. InsB4 CD8$^+$ T-cell clone cross-react with peptides derived from fungal proteomes. PS-CPL data for InsB4 (**Figure 5.3**) was used to screen a database of infectious fungi and the top 20 peptides selected for testing. (**A**) Peptide titrations using InsB4 with the top 20 fungal peptides (listed in **B**). 30,000 InsB4 T-cells were incubated overnight with 60,000 T2 (HLA-A*02:01$^+$) antigen presenting cells. Assay supernatants used for MIP-1β ELISA. Error bars depict SD from the mean of two replicates. EC_{50} of activation shown in B. (**B**) Peptide sequence and origin. Scoring indicates prediction of how likely the peptide is to be recognized by InsB4 T-cells, with the best scoring peptide at the top. Data has also been published (*Frontiers Immunology,* 2020, **11**, 1-18). Data provided by Dr Garry Dolton.

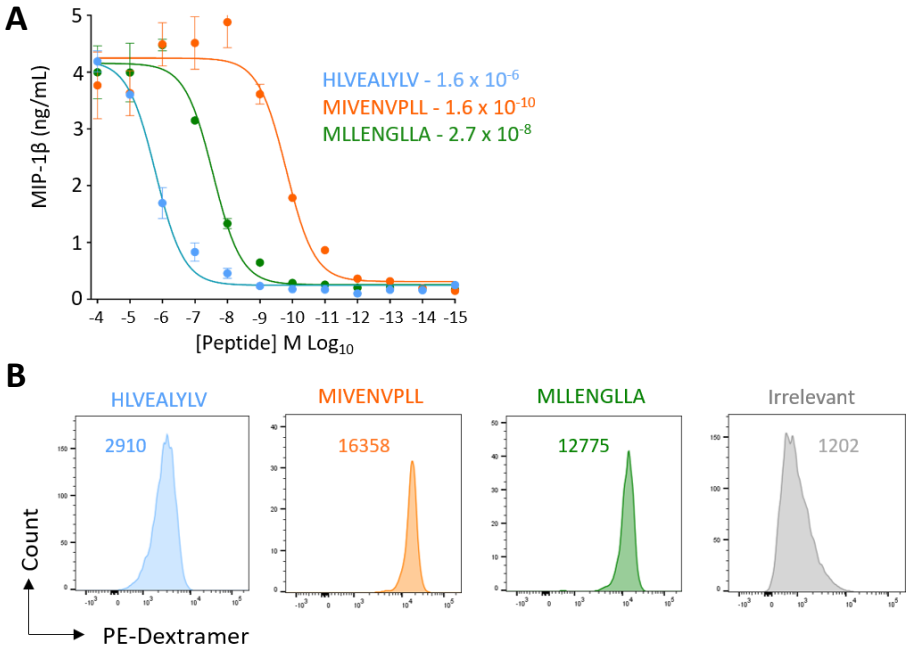

Figure 5.6. InsB4 CD8⁺ T-cell clone responds to bacterial and fungal epitopes.
(**A**) Sensitivity of InsB4 T-cell clone to insulin B-chain (HLVEALYLV), bacterial (*Helicobacter pylori*, MLLENGLLA) and fungal (*Candida albicans*, MIVENVPLL) peptides in a titration assay. 30,000 InsB4 T-cells were incubated overnight with 60,000 T2 (HLA-A*02:01⁺) antigen presenting cells. Assay supernatants used for MIP-1β ELISA. Error bars depict SD from the mean of two replicates. (**B**) 50,000 InsB4 T-cells were stained with 0.5 µg of dextramer (relative to the pMHC component), with a PE-conjugated backbone. Dextramers presenting insulin B-chain (HLVEALYLV), bacterial (*Helicobacter pylori*, MLLENGLLA) and fungal (*Candida albicans*, MIVENVPLL) peptides were used. Cells previously gated on live $CD3^+CD8^+$ single lymphocytes. The human telomerase reverse transcriptase-derived ILAKFLHEL was used as a negative control. Numbers on the histograms correspond to mean fluorescence intensity of dextramer staining.

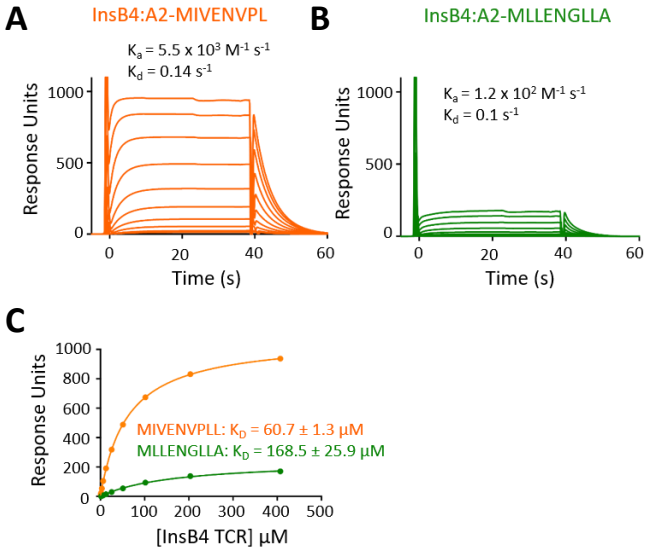

Figure 5.7. InsB4 T-cell responds to bacterial/fungal epitopes.
(**A-C**) Surface Plasmon resonance (SPR) analysis of InsB4 TCR recognition of MIVENVPLL (**A**) and MLLENGLLA (**B**). SPR response to ten serial dilutions of InsB4 TCR was measured, with a maximum concentration of 407 µM. HLA-A2-NLSALGIFST was used as an irrelevant control. K_D values were calculated using non-linear fit curve (y= [P1 x]/[P2 + X]) (**C**). Data has also been published (*Frontiers Immunology,* 2020, **11**, 1-18).

5.3.7. CPL data identifies potential viral ligands for the InsB4 T-cell clone

We next searched for viral ligands that might activate the InsB4 T-cell. As viruses have much smaller genomes than bacteria and fungi, we anticipated that there would be fewer peptides of viral origin that might activate InsB4 T-cells than observed from the much larger proteomes of pathogenic fungi and bacteria (as demonstrated with 4C6 TCR, **Appendix Figure 2**). The InsB4 T-cell CPL data were used to screen a proteomic database of human viruses. As per **Section 5.3.4**, the top 20 candidate peptides were tested by MIP-1β ELISA using crude (>40% purity) peptide (**Figure 5.8**). Multiple peptides elicited a greater response from InsB4 T-cells than the InsB-derived peptide. The top five peptides were derived from varicella-zoster virus (VZV, ILIEGIFFI), herpes simplex virus 1 (HSV-1, ILIEGIFFA), Epstein-barr virus (EBV, LLIEGIFFI), herpes simplex virus 2 (HSV-2, ILIEGVFFA), and Kaposi's sarcoma-associated herpesvirus (LIVEGIYFI), all of which are herpesviruses. A MIP-1β ELISA was conducted using >95% pure viral peptide preparations (**Figure 5.9**), which confirmed that the viral peptides elicit a response (EC_{50} = 9.0 x 10^{-9} for ILIEGIFFI, 7.7 x 10^{-10} for ILIEGIFFA, 7.6 x 10^{-9} for ILIEGVFFA, 4.9 x 10^{-9} for LIVEGIYFI and 6.9 x 10^{-9} for LLIEGIFFI respectively) from the InsB4 T-cell.

A

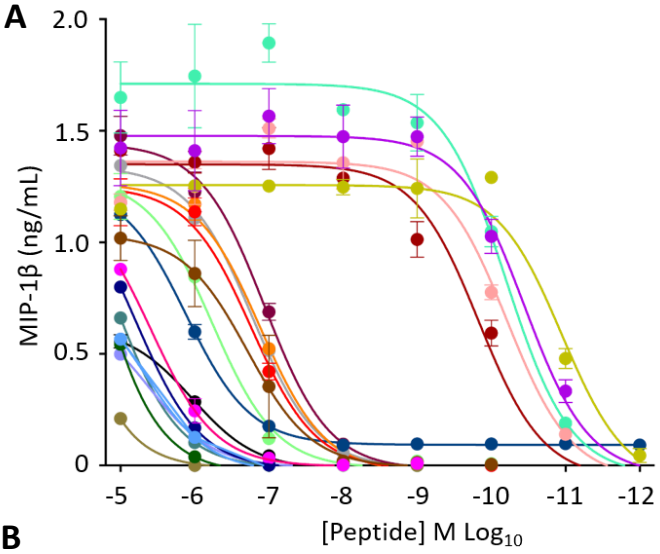

B

Score	Peptide	EC_{50}	Organism	Protein
-15.83	HLVEALYLV	4.6 x10^{-6}	*Homo sapiens*	Insulin B-chain
-13.5611	ILIEGIFFV	1.1 x10^{-11}	Varicella zoster virus	Ribonucleotide reductase subunit 2
-13.8002	ILIEGIFFA	3.6 x10^{-11}	Herpes simplex virus 1	Ribonucleotide reductase subunit 2
13.9884	LLIEGIFFI	6.2 x10^{-11}	Epstein barr virus	BARF1
-14.3542	ILIEGVFFA	1.5 x10^{-10}	Herpes simplex virus 2	Ribonucleotide reductase subunit 2
-14.368	LIVEGIYFI	6.4 x10^{-11}	Human herpes virus 8	Putative protein
-14.8688	ITIENALVA	5.8 x10^{-7}	Variola virus	Tae2p
-15.2035	ILIENFFTT	1.7 x10^{-7}	Human TMEV-like cardiovirus	Putative protein
-15.3499	LQTERALVV	1.2 x10^{-6}	Herpes simplex virus 2	Tegument protein UL37
-16.0225	LVIENSPLS	1.3 x10^{-7}	Human parainfluenza virus 1	Putative protein
-16.2609	IILQGILLF	1.3 x10^{-6}	Cytomegalo virus	Membrane protein US19
-16.6616	LQIEDWLAL	1.1 x10^{-7}	Herpes simplex virus 1	Putative protein
-16.6739	ILTEGGPVL	4.1 x10^{-6}	Human herpesvirus 6B	Putative protein
-16.7119	MQIENNLLS	1.2 x10^{-5}	Human herpesvirus 6A	DNA packaging protein UL17
-17.0081	LLIERFVSL	1.6 x10^{-7}	Human enteric coronavirus	Putative protein
-17.1685	QLIEQSLFL	1.1 x10^{-6}	Human metapneumovirus	RNA dependent RNA polymerase
-17.1836	ILLERYVSL	6.1 x10^{-6}	Human coronavirus	Replicase polyprotein 1AB
-17.3067	IVYERQPPF	3.1 x10^{-5}	Torque teno midi virus	Putative protein
-16.7415	FVIYRFLFV	1.9 x10^{-7}	Variola virus	A-type inclusion body protein
-17.2107	LMIERFVSL	3.9 x10^{-6}	SARS coronavirus	Putative protein

Figure 5.8. InsB4 CD8⁺ T-cell clone cross-react with peptides derived from viral proteomes.
PS-CPL data for InsB4 (**Figure 5.3**) was used to screen a protein database of infectious viruses and the top 20 peptides selected for testing. (**A**) Peptide titrations using InsB4 with the top 20 viral peptides (listed in **B**). 30,000 InsB4 T-cells were incubated overnight with 60,000 T2 (HLA-A*02:01⁺) antigen presenting cells. Assay supernatants used for MIP-1β ELISA. Error bars depict SD from the mean of two replicates. EC_{50} of activation shown in B. (**B**) Peptide sequence and origin. Scoring indicates prediction of how likely the peptide is to be recognized by the InsB4 clone, with the best scoring peptide at the top.

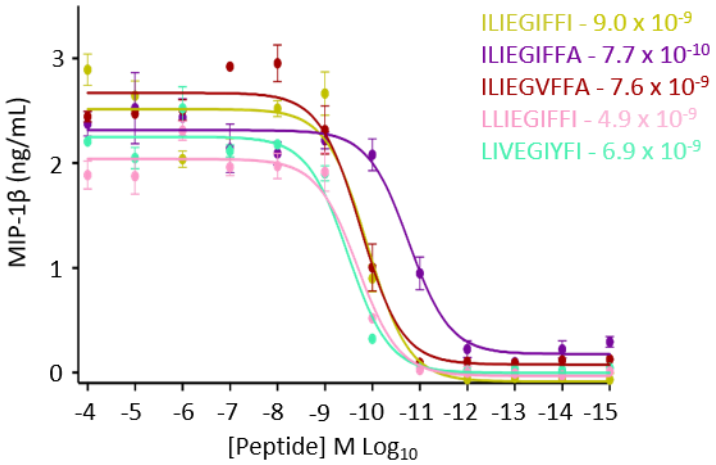

Figure 5.9. InsB4 T-cell responds to viral epitopes.
Sensitivity of InsB4 T-cells to insulin B-chain VZV (ILIEGIFFI), HSV1 (ILIEGIFFA), HSV2 (ILIEGVFFA), EBV (LLIEGIFFI) and Kaposi's sarcoma-associated herpesvirus (LIVEGIYFI) peptides in a titration assay. 30,000 InsB4 T-cells were incubated overnight with 60,000 T2 (HLA-A*02:01+) antigen presenting cells. Assay supernatants used for MIP-1β ELISA. Error bars depict SD from the mean of two replicates.

5.3.8. Herpesvirus epitopes are genuinely processed and presented

The herpesvirus epitopes described in **Section 5.3.7** are derived from ribonucleotide reductase of VSV (ILIEGIFFI) and HSV-1 (ILIEGIFFA) and the EBV BARF-1 gene (LLIEGIFFI). My colleague, Dr Jade Hopkins, transduced these genes into MOLT-3 cells with and without the *HLA-A*0201* gene. InsB4 T-cells produced both TNF and CD107a in response to HLA-A2 targets expressing all three viral proteins (**Figure 5.10**). These data indicate that all three epitopes are genuinely processed and presented in the context of HLA-A2.

Dr Hopkins was further able to demonstrate that InsB4 T-cells responded to EBV-infected *HLA-A*0201*$^+$ B-cells (often called lymphoblastoid cell lines or LCL cells) (**Figure 5.11**). Interestingly, broadly reactive T-cells that recognise these shared epitopes between VSV, HSV and EBV have previously been described (Chiu et al., 2014). This previous description of T-cells in multiple *HLA-A*0201*$^+$ individuals that cross-react with these genuine herpesvirus epitopes makes it likely that the InsB4 T-cells might have been initially primed by a herpesvirus. This finding also raised the question of whether herpesvirus-specific T-cells in healthy donors might also cross-react with the InsB-derived peptide HLVEALYLV and, if so, why such T-cells did not destroy insulin-producing cells in these donors.

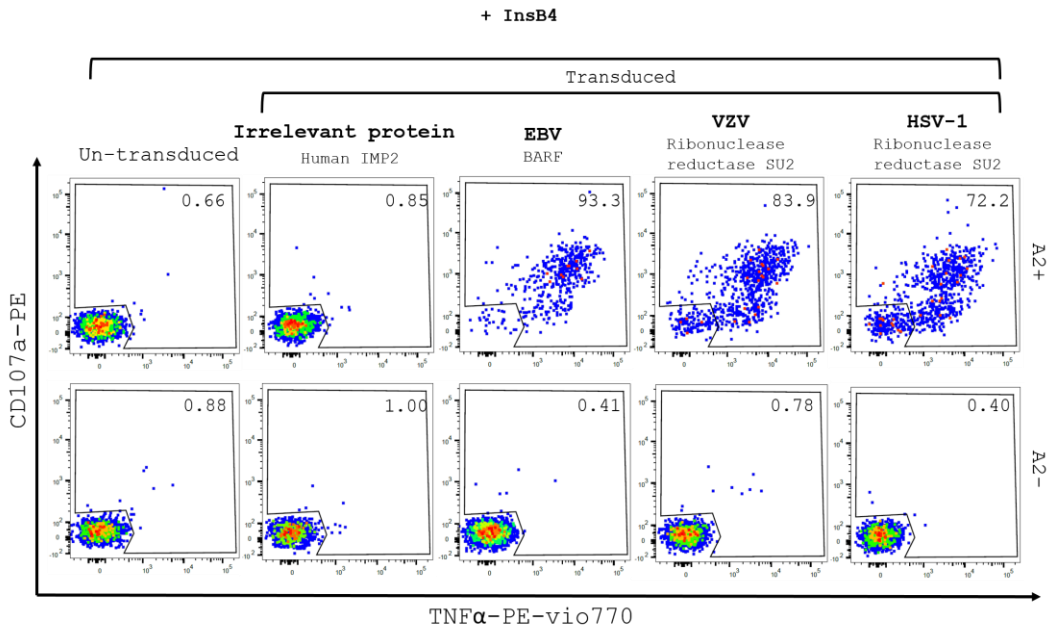

Figure 5.10. InsB4 T-cell viral epitopes are successfully processed and presented.
InsB4 cells were co-cultured with MOLT-3 cells (+/- *HLA-A*0201)* transduced with lentivirus encoding the three proteins from which the viral epitopes are derived for 4h. The cells were harvested and analyzed via a TAPI-0 assay, followed by viable sorting based on expression of CD107a and TNF. Cells previously gated on live $CD3^{+}CD8^{+}$ single lymphocytes. Numbers on dot plots correspond to the percentage of cells in the gated population. Data provided by Dr Jade Hopkins.

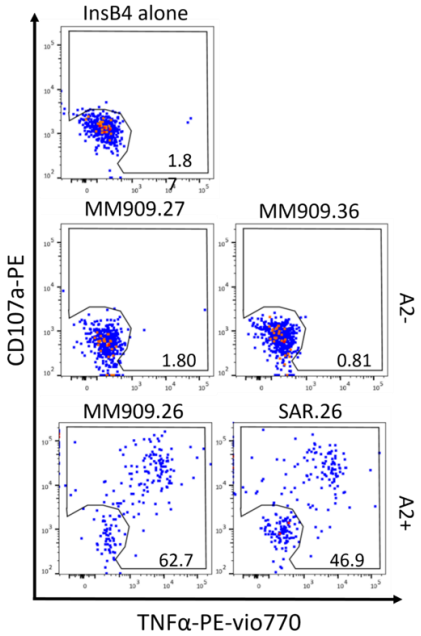

Figure 5.11. InsB4 responses to EBV-transformed lymphoblastic cell lines (LCLs) in an HLA-A*02:01 dependent manner.
InsB4 T-cell clone was cultured in the presence of LCLs (+/- *HLA-A*0201*) for 4h, before cells were harvested and analysed via TAPI-0 assay, followed by viable sorting based on expression of CD107a and TNF. Displayed cells gated on live $CD3^{+}CD8^{+}$ single lymphocytes. Numbers on dot plots correspond to the percentage of cells in the gated population. Data provided by Dr Jade Hopkins. LCLs generated and provided by Dr Garry Dolton.

5.3.9. Insulin-specific T-cells in an *HLA-A*0201*$^{+}$ T1D patient recognise EBV

We next aimed to determine whether insulin-specific T-cells from another T1D patient might also recognise EBV. These experiments were undertaken by Dr Garry Dolton and Dr Jade Hopkins and are included here to provide a complete story of insulin-herpesvirus crossreactivity. Briefly, InsB-reactive T-cells were separated from T1D patient blood via magnetic activated cell sorting (MACS) using HLA-A2-HLVEALYLV tetramers. The resulting population was then stained with HLA-A2-ILIEGIFFI, HLA-A2-ILIEGIFFA, and HLA-A2-LLIEGIFFI tetramers, resulting in 1.3%, 1.0% and 1.7% positive staining compared to 0% from the irrelevant tetramer. The T-cell population remaining from the HLA-A2-HLVEALYLV separation were then sorted again using HLA-A2-LLIEGIFFI. This resulting population sorted by HLA-A2-LLIEGIFFI was then also stained with HLA-A2-ILIEGIFFI, HLA-A2-ILIEGIFFA, and HLA-A2-LLIEGIFFI tetramers, with positive staining of 37%, 35% and 56% respectively. The population was also stained with HLA-A2-HLVEALYLV tetramers, resulting in 0.12% positive staining (**Figure 5.12**).

The final experiment conducted by Dr Jade Hopkins was to assess herpes virus cross-reactivity in healthy donors (**Figure 5.13**). Three separate healthy donor samples were separated using HLA-A2-LLIEGIFFI tetramers, and subsequently stained with HLA-A2-HLVEALYLV, HLA-A2-ILIEGIFFI, and HLA-A2-ILIEGIFFA tetramers. Interestingly, neither insulin nor herpesvirus crossreactivity was observed within the LLIEGIFFI-specific T-cell lines grown from three healthy donors. These results indicate that healthy donors and T1D patients use different TCRs for recognition of herpesviruses with only the latter also showing crossreactivity with the insulin-derived epitope. This finding suggests a possible mechanism by which T1D might be triggered in *HLA-A*02:01*$^{+}$ patients and makes TCRs like InsB4 especially interesting. I next set out to confirm that the InsB4 TCR bound to herpesvirus-derived epitopes.

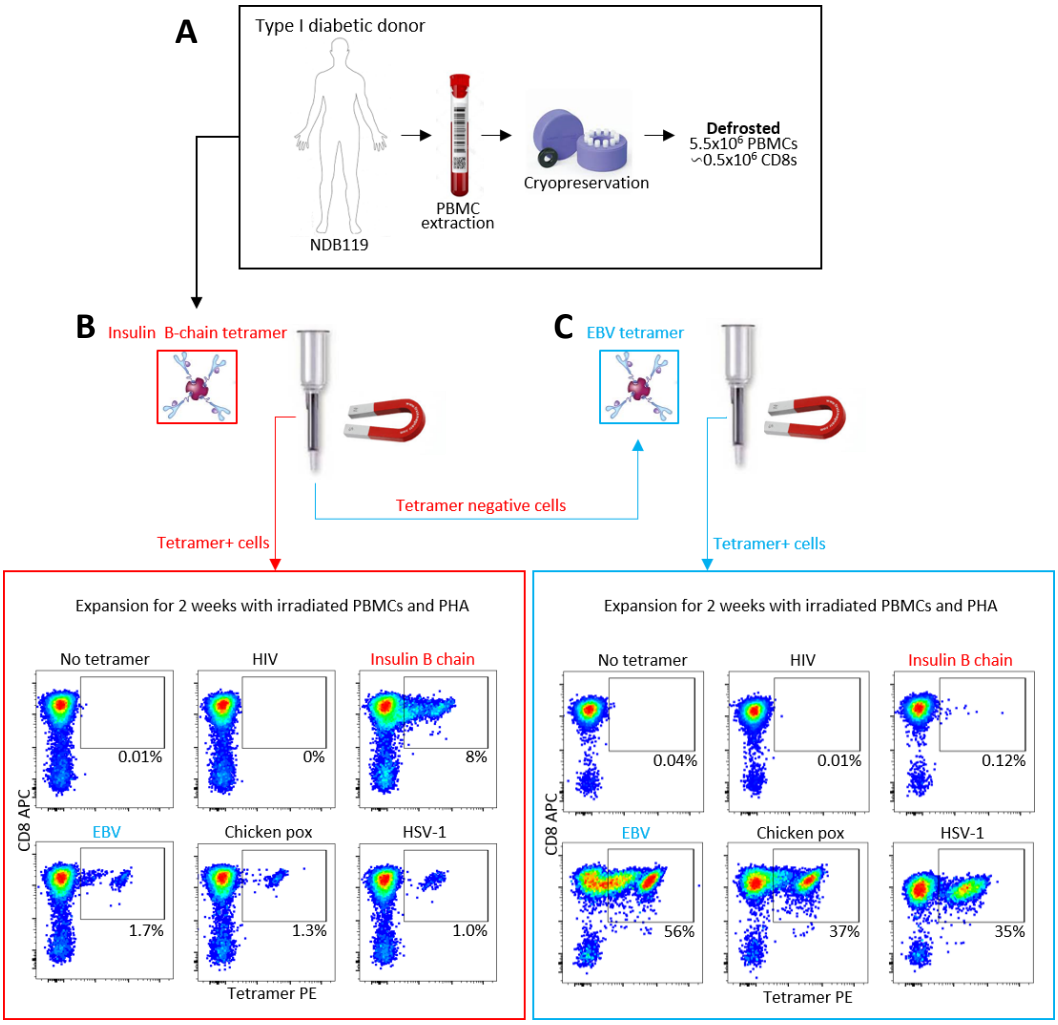

Figure 5.12. Insulin-specific cells in an *HLA-A*0201*⁺ T1D donor can recognise three viral epitopes. (**A**) A schematic detailing the experimental workflow used in this figure. (**B**) HLA-A2-HLVEALYLV⁺ (InsB) cells from the NDB119 donor were isolated using magnetic separation and expanded. 50,000 T-cells were stained with 0.5 µg of tetramer (relative to the pMHC component), with a PE-conjugated backbone. Numbers on dot plots represent percentage of tetramer-positive cells in the 10,000 events recorded. (**C**) HLA-A2-HLVEALYLV⁻ cells from the NDB119 donor were isolated via magnetic separation based on HLA-A2-LLIEGIFFI tetramer binding. HLA-A2-LLIEGIFFI⁺ (EBV) cells were then expanded. 50,000 T-cells were stained with 0.5 µg (relative to pMHC component) of tetramer, with PE-conjugated backbones. Numbers on dot plots represent percentage of tetramer-positive cells in the 10,000 events recorded. HLA-A2-SLYNTVATL tetramers used as a negative control. Data provided by Dr Garry Dolton.

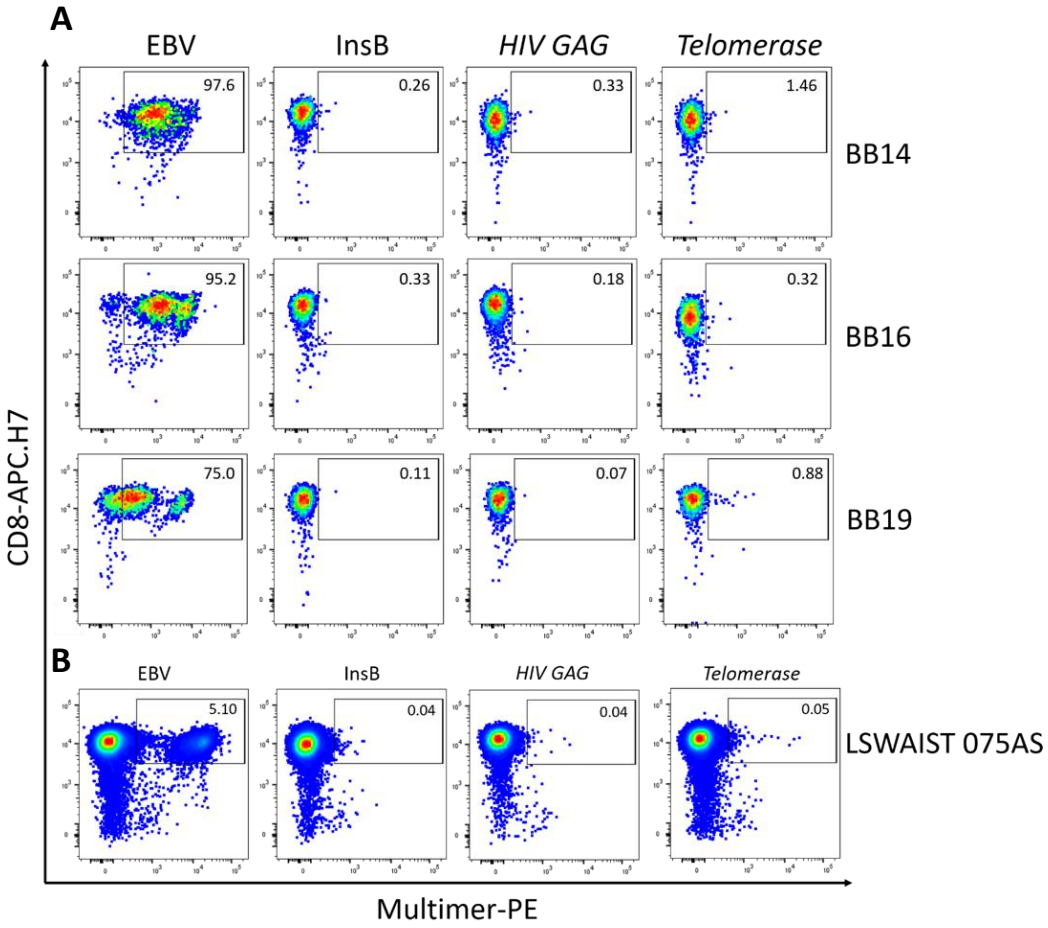

Figure 5.13. EBV/Insulin B chain crossreactivity is not present in healthy donors.
(**A**) PBMC samples from healthy donors were isolated via magnetic separation based on HLA-A2-LLIEGIFFI (EBV) tetramer specificity. 50,000 T-cells were stained with 0.5 µg of tetramer (relative to the pMHC component), with a PE-conjugated backbone. Numbers on dot plots represent percentage of tetramer-positive cells in the 10,000 events recorded. (**B**) PBMC samples from a T1D patient were isolated via magnetic separation based on HLA-A2-LLIEGIFFI (EBV) tetramer specificity. Following this 50,000 T-cells were stained with 0.5 µg of various tetramer (relative to the pMHC component), with a PE-conjugated backbone. Numbers on dot plots represent percentage of tetramer-positive cells in the 100,000 events recorded. HLA-A2-SLYNTVATL (HIV-GAG) and HLA-A2-ILAKFLHWL (human telomerase) tetramers were used as negative controls. Data provided by Dr Jade Hopkins.

5.3.10. The InsB4 T-cells bind herpesvirus epitopes with high avidity

I next manufactured biotinylated HLA-A2 monomers with ILIEGIFFI (VZV), ILIEGIFFA (HSV-1), and LLIEGIFFI (EBV) epitopes. These monomers were used to manufacture pHLA dextramers for staining of the InsB4 T-cell clone. Dextramers of ILIEGIFFI, ILIEGIFFA, and LLIEGIFFI stained InsB4 T-cells with mean fluorescence intensities (MFIs) of 5926, 6697, 8581 respectively (**Figure 5.14**). In each case staining had more than double the MFI with dextramers made with the index HLVEALYLV insulin epitope (MFI 2910) in parallel experiments. I next set out to formally characterise the binding of InsB4 TCR to these herpesvirus epitopes by SPR.

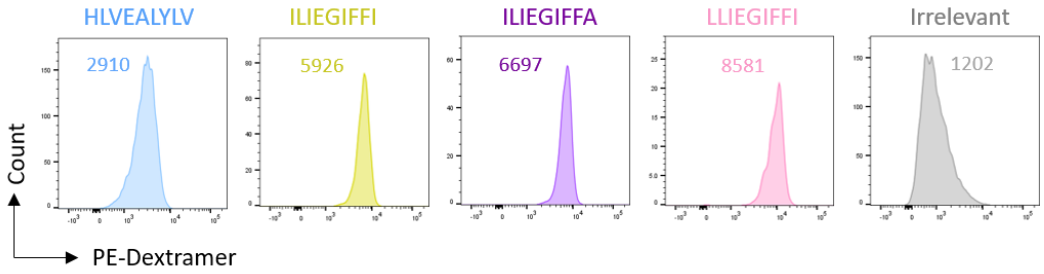

Figure 5.14. InsB4 T-cell has a higher avidity for viral epitopes than the T1D epitope.
50,000 InsB4 T-cells were stained with 0.5 µg of dextramer (relative to the pMHC component), with a PE-conjugated backbone. Dextramers presenting to insulin B-chain (HLVEALYLV), VZV (ILIEGIFFI), HSV1 (ILIEGIFFA), HSV2 (ILIEGVFFA), EBV (LLIEGIFFI) and Kaposi's sarcoma-associated herpesvirus (LIVEGIYFI) peptides were used. 30,000 InsB4 T-cells were incubated overnight with 60,000 T2 (HLA-A*02:01^{+} Cells previously gated on live CD3^{+}CD8^{+} single lymphocytes. The human telomerase reverse transcriptase-derived ILAKFLHEL was used as an irrelevant control. Numbers on the histograms correspond to mean fluorescence intensity, of 10,000 events.

5.3.11. InsB4 TCR bind herpesvirus epitopes with high affinity

As described above, the binding between InsB4 TCR and HLA-A2-HLVEALYLV is below the limits of detection by SPR. SPR data showed that the InsB4 TCR bound to the ILIEGIFFI, ILIEGIFFA, ILIEGVFFA, and LLIEGIFFI peptides with affinities of 30.8 µM, 76.6 µM, 40.1 µM, and 30.8 µM, respectively (**Figure 5.15**). I next set out to attempt to understand how the InsB4 TCR is able to engage four different herpesvirus-derived HLA-A2-restricted epitopes and a very different insulin-derived epitope.

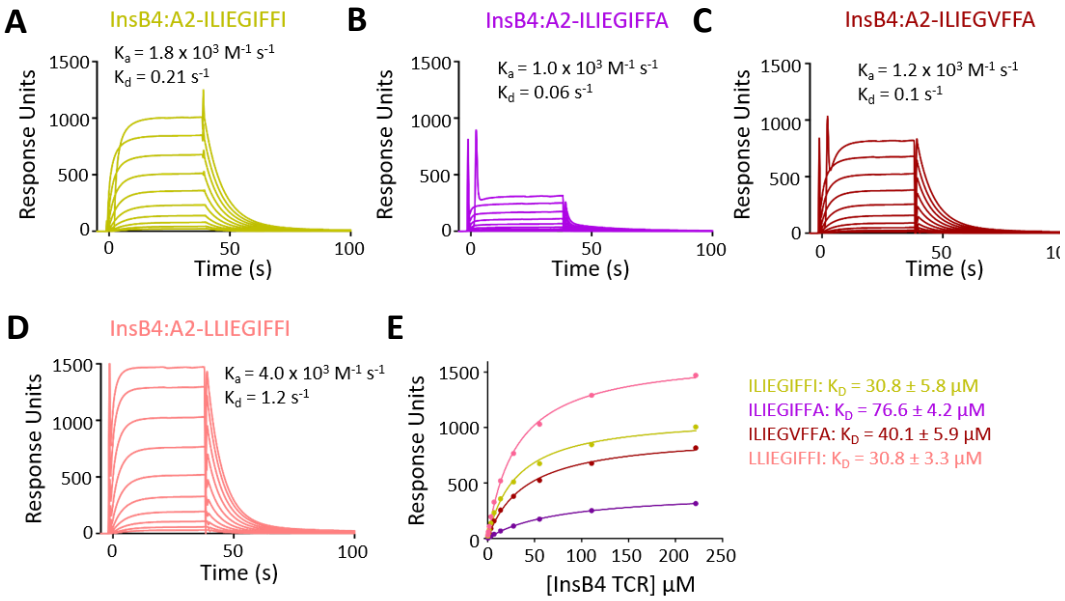

Figure 5.15. InsB4 TCR successfully binds to viral epitopes.
(**A-E**) Surface Plasmon resonance (SPR) analysis of InsB4 TCR recognition of VZV (ILIEGIFFI) (**A**), HSV-1 (ILIEGIFFA) (**B**), HSV-2 (ILIEGVFFA) (**C**) and EBV (LLIEGIFFI) (**D**). SPR response to ten serial dilutions of InsB4 TCR was measured, with a starting concentration of 221.5 µM. HLA-A2-ITSGIGILTV was used as a negative control. K_D values were calculated using non-linear fit curve (y= [P1 x]/[P2 + X]) (**E**).

5.3.12. Peptide residue Glu4 appears to drive InsB4 peptide recognition

To determine the mechanism by which the InsB4 TCR binds the various ligands discussed in this chapter, 3D structural information was required. Whilst I have attempted to crystallise the InsB4 TCR in complex with all ligands highlighted in **Section 5.3.8**, to date I have acquired 3D structures of the InsB4:A2-MIVENVPLL (**Table 5.1**), InsB4:A2-ILIEGIFFA (**Table 5.2**), and InsB4:A2-ILIEGVFFA (**Table 5.3**) complexes at resolutions of 2.31 Å, 2.24 Å, and 2.17 Å respectively (**Appendix Table 3**).

5.3.12.1. Peptide residue Glu4 is instrumental for InsB4 TCR recognition of the fungal-derived peptide

Analysis of peptide presentation within the InsB4:A2-MIVENVPLL structure showed peptide residue Glu4 protrudes further toward the TCR than any other residue, suggesting that it may be important for TCR binding (**Figure 5.16A**). The CPL data shown in **Section 5.3.5** supports the importance of Glu4 by showing minimal degeneracy at peptide position 4. Analysis of the InsB4 TCR CDR loop conformations showed the CDR1α, CDR3α and CDR3β loops sit above the N-terminus and mid-point of the peptide, while CDR1β sits above the C-terminus of the peptide and CDR2α and CDR2β sit above the MHC molecule (**Figure 5.16B**).

Closer analysis of the contacts between the InsB4 TCR and the HLA-A2-MIVENVPLL molecule revealed two points of interest (**Table 5.1**). Firstly, the TCR residue Gln31α occupies a pocket formed by peptide residues 1-4, facilitating the formation of multiple bonds (**Figure 5.16C**). As discussed in **Chapter 3**, Gln31α interactions with the N-terminus of the peptide in this way is a hallmark of TCRs exhibiting TRAV12-2 gene usage, like the InsB4 TCR, and has been linked to improved TCR:pMHC binding affinity. The second point of interest concerns peptide reside Glu4, which occupies a pocket formed by CDR1α (Gln31α, Ser32α), CDR3α (Ser92α, Ser93α, Ser94α, Tyr95α), and CDR3β (Leu100β, Thr101β) (**Figure 5.16D-E**). The contacts between peptide residue Glu4 and the InsB4 TCR make up ~45% of all TCR:peptide contacts, further highlighting the importance of Glu4 to InsB4 binding (**Figure 5.16F**).

5.3.12.2. The InsB4 TCR binding mechanism is shared across multiple pMHC molecules

Analysis of peptide presentation within the InsB4:A2-ILIEGIFFA and InsB4:A2-ILIEGVFFA complexes showed the same protrusion of peptide residue Glu4 and the same 'pocket' formed by peptide residues 1-4 present in the InsB4:A2-MIVENVPLL complex. The conformation of peptide residues 5-7 is shared by the two viral peptides, with a different conformation adopted by the equivalent residues in MIVENVPLL, however the conformation of peptide residues 8 and 9 remains conserved across all three complexes (**Figure 5.17A**). Analysis of the CDR loop conformation of the three TCR:pMHC complexes showed largely conserved conformations regards of the presented peptide (**Figure 5.17B**).

The conserved 'pocket' formed by peptide residues 1-4 is occupied by Gln31α in InsB4:A2-ILIEGIFFA and InsB4:A2-ILIEGVFFA complexes (**Figure 5.17C**). Additionally, peptide residue Glu4 of these viral peptides also occupies a pocket formed by CDR1α, CDR3α, and CDR3β, resulting in a large proportion of the TCR:peptide interactions (42% and 43% for ILIEGIFFA and ILIEGVFFA respectively) (**Figure 5.17D-F**). Owing to their increased protrusion towards the TCR, peptide residues 6 and 7 form more TCR:peptide interactions in the InsB4:A2-ILIEGIFFA and InsB4:A2-ILIEGVFFA complexes (24% and 18% respectively), several of which involve the InsB4 CDR2β loop, compared to equivalent residues in InsB4:A2-MIVENVPLL (8%). Conversely, peptide residue 5 contributes less TCR:peptide interactions in the InsB4:A2-ILIEGIFFA and InsB4:A2-ILIEGVFFA complexes (both 9% respectively) than in the InsB4:A2-MIVENVPLL (20%) complex, due to a larger amino acid being present at that position in the viral peptides (Gln compared to Gly in MIVENVPLL) (**Figure 5.17G**). As a result,

the number of TCR:peptide contacts in all three complexes remains broadly similar (99, 106 and 98 for InsB4:A2-MIVENVPLL, InsB4:A2-ILIEGIFFA and InsB4:A2-ILIEGVFFA respectively), which may contribute to the similar binding affinities for these three complexes. In all three complex structures peptide residue Glu4 contributes the largest proportion of TCR:peptide interactions, which in conjunction with the CPL data suggests that this residue is instrumental for the function of InsB4 TCR.

CDR loop	TCR residue	Peptide residue	MHC residue	VdWs (≤4 Å)	H-bonds (≤3.4 Å)
CDR1α	Arg28	Met1		1	
	Arg28		Trp167	1	
	Arg28		Arg170	4	
	Gly29	Met1		3	
	Gln31	Met1		2	
	Gln31	Ile2		1	1
	Gln31	Val3		3	
	Gln31	Glu4		4	1
	Gln31		Lys66	1	
	Gln31		Tyr159	1	
	Gln31		Thr163	1	
	Ser32	Glu4		3	1
CDR2α	Phe49		Glu154	1	
	Tyr51		Gln155	2	
	Tyr51		Ala158	2	
	Ser52		Ala158	1	
	Asn53		Glu166	2	
FWα	Lys67		Thr163	2	
	Lys67		Glu166	3	
CDR3α	Ser92	Glu4		7	2
	Ser93	Glu4		8	
	Ser93		Lys66	1	
	Ser94	Glu4		2	
	Ser94		Arg65	3	2
	Ser94		Lys66	2	
	Tyr95	Glu4		3	1
	Tyr95	Asn5		16	
	Lys96		Arg65	2	2
CDR1β	Asp30	Leu8		2	
CDR2β	Lys51	Leu8		2	
	Gln55		Gln72	8	
	Asp56		Arg65	5	
CDR3β	Gly97	Pro7		1	
	Gly98	Asn5		3	1
	Gly98	Val6		1	
	Gly98	Pro7		5	
	Gly98		Gln155	2	
	Ala99	Ile3		1	
	Ala99	Glu4		3	
	Ala99	Gly5		8	2
	Ala99	Pro7		1	
	Ala99		Gln155	4	1
	Ala99		Leu156	2	
	Leu100	Glu4		5	
	Leu100		Gln155	9	
	Thr101	Glu4		3	2

Table 5.1. Contacts between the InsB4 TCR and HLA-A2-MIVENVPLL.

CDR loop	TCR residue	Peptide residue	MHC residue	VdWs (≤4 Å)	H-bonds (≤3.4 Å)
CDR1α	Asp27		Glu58	1	
	Arg28		Trp167	1	
	Arg28		Arg170	6	
	Gly29	Ile1		1	
	Gln31	Ile1		1	
	Gln31	Leu2		2	1
	Gln31	Ile3		2	
	Gln31	Glu4		6	1
	Gln31		Lys66	1	
	Gln31		Thr163	1	
	Ser32	Glu4		3	2
CDR2α	Tyr51		Ala158	1	
	Ser52		Ala158	1	
	Asn53		Glu166	2	
FWα	Lys67		Thr163	3	1
	Lys67		Glu166	5	1
CDR3α	Ser92	Glu4		6	2
	Ser93	Glu4		6	1
	Ser93		Lys66	1	
	Ser94	Glu4		2	
	Ser94		Arg65	4	
	Tyr95	Glu4		8	1
	Tyr95	Gly5		3	
	Tyr95	Ile6		8	1
CDR1β	Asp30	Phe8		5	
CDR2β	Val50	Ile6		1	
	Lys51	Phe8		3	
	Ser53		Gln72	1	
	Gln55		Ala69	1	
	Asp56		Arg65	3	
CDR3β	Gly97	Ile6		1	
	Gly97		Ala150	1	
	Gly98	Gly5		2	
	Gly98	Ile6		5	3
	Gly98	Phe7		8	
	Gly98		Val152	1	
	Gly98		Gln155	2	
	Ala99	Ile3		3	
	Ala99	Glu4		1	
	Ala99	Gly5		4	1
	Ala99	Phe7		5	
	Ala99		Val152	1	
	Ala99		Gln155	4	1
	Ala99		Leu156	2	
	Leu100	Glu4		3	
	Leu100		Gln155	7	2
	Thr101	Glu4		2	2

Table 5.2. Contacts between the InsB4 TCR and HLA-A2-ILIEGIFFA.

CDR loop	TCR residue	Peptide residue	MHC residue	VdWs (≤4 Å)	H-bonds (≤3.4 Å)
CDR1α	Arg28		Trp167	1	
	Arg28		Arg170	7	2
	Gly29	Ile1		2	
	Gln31	Ile1		1	
	Gln31	Leu2		2	1
	Gln31	Ile3		2	
	Gln31	Glu4		3	1
	Gln31		Lys66	1	
	Gln31		Try159	2	
	Gln31		Thr163	1	
	Ser32	Glu4		3	1
CDR2α	Tyr51		Gln155	1	1
	Tyr51		Ala158	1	
	Ser52		Ala158	1	
FWα	Lys67		Thr163	3	1
	Lys67		Glu166	3	1
CDR3α	Ser92	Glu4		7	1
	Ser93	Glu4		5	
	Ser94	Glu4		2	
	Ser94		Arg65	4	
	Tyr95	Glu4		8	1
	Tyr95	Gly5		2	
	Tyr95	Val6		5	
	Lys96		Arg65	2	
CDR1β	Asp30	Phe8		2	
CDR2β	Val50	Val6		2	
	Val50	Phe8		2	
	Val50		Gln72	2	
	Lys51	Phe8		6	
	Lys51		Val76	1	
	Ser53		Gln72	2	
	Gln55		Arg65	3	2
	Gln55		Ala69	1	
	Gln55		Gln72	2	1
	Asp56		Arg65		1
CDR3β	Gly97	Val6		2	
	Gly97		Ala150	1	
	Gly98	Gly5		2	
	Gly98	Val6		3	2
	Gly98	Phe7		4	
	Gly98		Gln155		
	Ala99	Ile3		4	
	Ala99	Glu4		1	
	Ala99	Gly5		4	1
	Ala99	Phe7		5	
	Ala99		Val152	2	
	Ala99		Gln155	1	
	Ala99		Leu156	2	
	Leu100	Glu4		4	
	Leu100		Gln155	7	1
	Thr101	Glu4		4	3

Table 5.3. Contacts between the InsB4 TCR and HLA-A2-ILIEGVFFA.

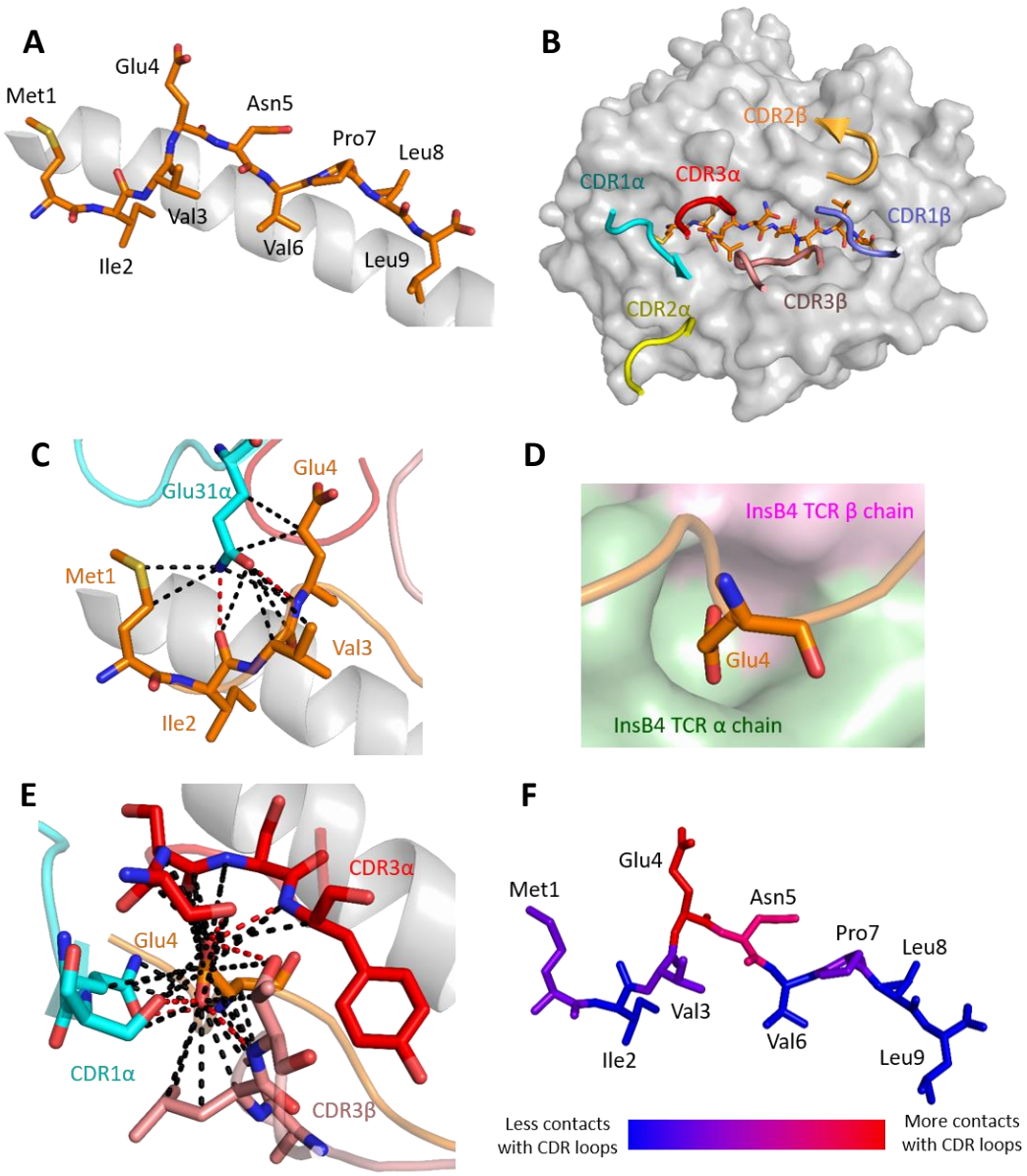

Figure 5.16. Peptide residue 4 is instrumental for InsB4 TCR recognition of HLA-A2-MIVENVPLL. (**A**) MIVENVPLL peptide (orange) shown as sticks. MHC alpha helix (grey) shown as cartoon for orientation. (**B**) Top-down view of the MIVENVPLL peptide (orange sticks) presented by HLA-A*02:01 (grey, shown as surface). InsB4 CDR loops are shown as cartoon. Crossing angle is indicated by the orange line. (**C**) Close up of Gln31α (light blue) interacting with the EAAGIGILTV peptide (orange). Van Der Waals forces (black dotted lines) and hydrogen bonds (red dotted lines) are shown. (**D**) Close up of MIVENVPLL peptide residue Glu4 (orange sticks) which occupies a pocket formed by the InsB4 TCR (surface). (**E**) Contacts between the InsB4 CDR loops and MIVENVPLL peptide Glu4 (orange sticks). Important CDR loop residues shown as sticks. (**F**) Heat map of MIVENVPLL peptide showing number of interactions each residue makes with the InsB4 CDR loops.

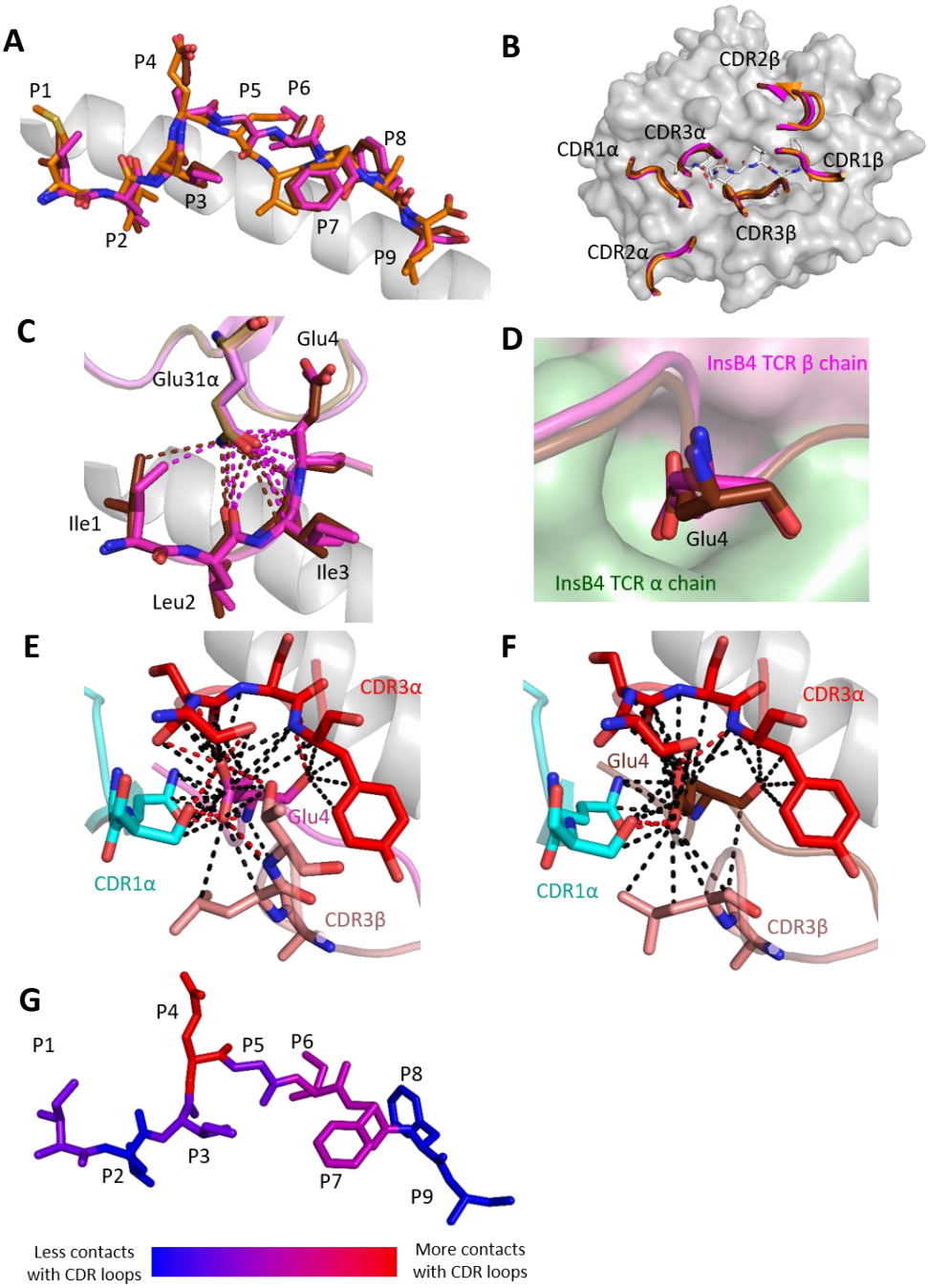

Figure 5.17. InsB4 recognises multiple peptides via hotspot recognition.
(**A**) MIVENVPLL (orange), ILIEGIFFA (magenta), and ILIEGVFFA (brown) peptides shown as sticks. MHC alpha helix (grey) shown as cartoon for orientation. (**B**) Top-down view of the ILIEGIFFA peptide (white sticks) presented by HLA-A*02:01 (grey, shown as surface). InsB4 CDR loops in complex with ILIEGIFFA (magenta) and ILIEGVFFA (brown) are shown as cartoon. Crossing angles are indicated by the orange line. (**C**) Close-up of Gln31α (light purple in complex ILIEGIFFA, light brown in complex with ILIEGVFFA) interacting with ILIEGIFFA (magenta) and ILIEGVFFA (purple) peptides. Interactions with ILIEGIFFA and ILIEGVFFA shown with magenta and brown dotted lines respectively. (**D**) Close up of ILIEGIFFA and ILIEGVFFA peptide residue Glu4 (magenta and brown sticks respectively) which occupies a pocket formed by the InsB4 TCR (surface). (**E-F**) Contacts between the InsB4 CDR loops and ILIEGIFFA (**E**) or ILIEGVFFA (**F**) peptide residue Glu4 (magenta and brown sticks respectively). Important CDR loop residues shown as sticks. (**G**) Heat map of ILIEGIFFA peptide showing number of interactions each residue makes with the InsB4 CDR loops.

5.3.13. Further cross-reactivity between herpesvirus and diabetogenic epitopes occurs in T1D patients

Human cytomegalovirus (hCMV) is known to induce very large T-cell responses that 'inflate' with time (O'Hara et al., 2012; Kim et al., 2015). This T-cell 'memory inflation' is thought to contribute to age-related senescence of the immune system (Pita-lopez et al., 2009). T-cells have been suggested to respond to a vast array of hCMV-specific proteins, with a study by Sylwester *et al.* highlighting T-cell responses to at least 70% of hCMV open reading frames. Additionally, Sylwester *et al*. highlighted three open reading frames which elicited $CD8^+$ T-cell responses in over half of the studied patient cohort (n = 33): UL48 (≈60%), pp65 (≈57%), and IE1 (≈55%) (Sylwester et al., 2005).

The role of pp65 in $CD8^+$ T-cell response against hCMV has previously been studied (McLaughlin-Taylor et al., 1994; Wills et al., 1996). The pp65-derivied HLA-A2-restricted epitope, NLVPMVATV, has been identified as an immunodominant epitope in *HLA-A*0201*$^+$ individuals (Peggs et al., 2002). Memory inflation of this HLA-A2-restricted, pp65-specific T-cell population (Komatsu et al., 2003) means that it is easy to detect NLVPMVATV-specific responses in PBMC, making these T-cells one of the easiest antigen-specific T-cell population to work with directly *ex vivo*. The T-cell response to HLA-A2-NLVPMVATV across the population includes 'public' TCRs that are frequently observed in multiple unrelated individuals (Peggs et al., 2002; Trautmann et al., 2015; Yang et al., 2015) in addition to donor-specific 'private' TCRs.

My laboratory was interested in comparing the peptide degeneracy of public and private NLVPMVATV-specific T-cell clones. In order to undertake this study, we generated multiple T-clones from healthy controls. We also included NLVPMVATV-specific T-cell clones that had previously been procured from diabetic patients to be used as comparative controls with T-cells from the same patients that recognized known diabetogenic epitopes. During a comparative study of the NLVPMVATV-specific T-cell clones, Dr Garry Dolton used the 9mer variant of a diabetogenic T-cell epitope from the GAD65 protein (VMNILLQYV) as a negative control peptide (Giuliani et al., 2009; Knight et al., 2014). One of the NLVPMVATV-specific T-cell clones being studied was Clone 29, which surprisingly responded to both the CMV-NLVPMVATV and GAD65-VMNILLQYV peptides. A follow-up peptide sensitivity assay showed that Clone 29 preferred the 10mer version of the GAD65 epitope (VMNILLQYVV), with a greater response elicited by the CMV-derived peptide (**Figure 5.18A**). The peptides differ at

every position except for the HLA-A2 C-terminal anchor (**Figure 5.18A**). Clone 29 T-cell recognition of the GAD65-derived peptides, with preferred avidity to the 10mer variant, was also confirmed by dextramer staining (**Figure 5.18B**). To assess whether the Clone 29 T-cell can recognise an endogenously processed GAD65 peptide, 'surrogate β-cells' were made by transducing *HLA-A*0201* and *GAD65* genes into K562 cells, as discussed in **Section 5.3.1**. Clone 29 reactivity to these surrogate β-cells was determined by an overnight TNF ELISA assay (**Figure 5.18C**). The fact that the Clone 29 T-cell had been isolated from a T1D patient, combined with our knowledge of the existence of crossreactivity between insulin and other herpes viruses in T1D patients, made this finding of particular interest to my laboratory.

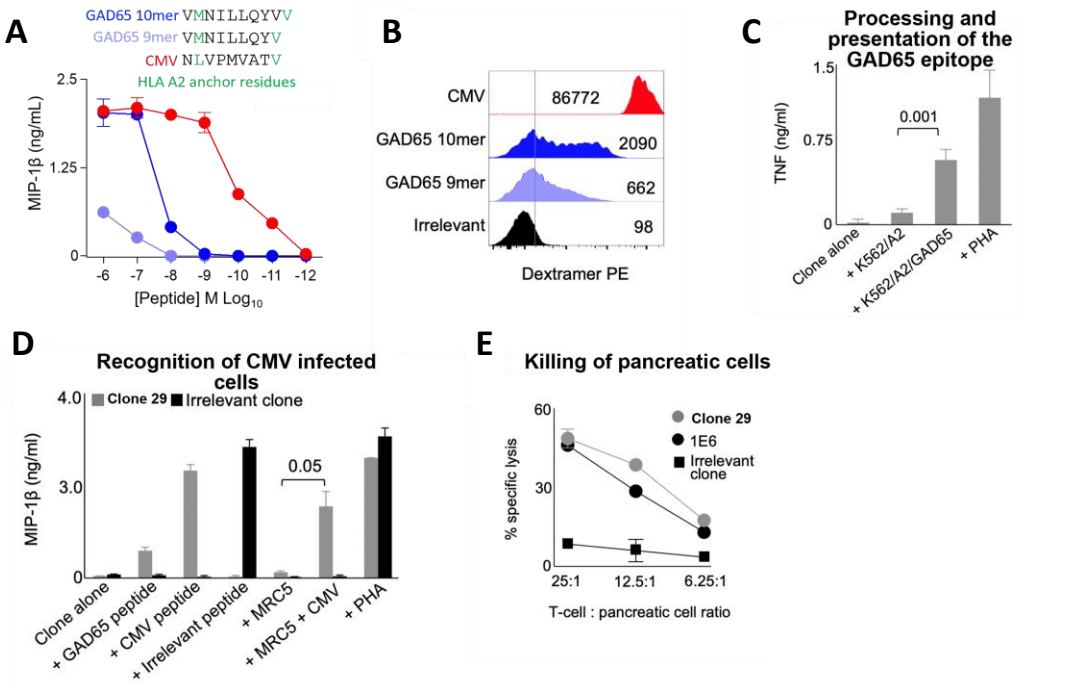

Figure 5.18. Clone 29 T-cell cross-reacts with CMV and GAD65 peptides and kills pancreatic cells. (**A**) Clone 29 T-cell sensitivity to insulin GAD65 (VMNILLQYVV), and hCMV (pp65, NLVPMVATV) peptides in a titration assay. 30,000 Clone 29 T-cells were incubated overnight with 60,000 T2 (HLA-A*02:01+) antigen presenting cells. Assay supernatants used for MIP-1β ELISA. Error bars depict SD from the mean of two replicates. (**B**) Clone 29 T-cells stained with HLA-A2-GAD65 and CMV peptide dextramers. Irrelevant dextramer: HLA-A2-ALAAAAAAL. The mean fluorescence intensity of staining is displayed. (**C**) Clone 29 recognized endogenously processed GAD65 protein (p=0.001, unpaired 2-tailed t-test). Overnight activation assay with surrogate pancreatic β-cells; K562 + HLA-A2 + GAD65 protein, with K562 + HLA-A2 used as a negative control. TNF ELISA with error bars depicting SEM of duplicates. (**D**) Clone 29 recognized HCMV 1172 infected fibroblasts (MRC5 cells) (p=0.05, unpaired 2-tailed t-test). An irrelevant clone (MEL13), which does not recognise CMV derived peptides, and its cognate peptide (HLA-A2-ELAGIGILTV), were also included. Overnight assay performed in duplicate and MIP-1β ELISA with errors bars depicting SEM. (**E**) Clone 29 killed pancreatic cells. 4h incubation with labelled target cells using a nonradioactive europium TDA cytotoxicity assay. Preproinsulin reactive clone 1E6 (peptide ALWGPDPAAA) was included as a positive control. The irrelevant clone, NLV7, recognizes the NLVPMVATV peptide from pp65 of CMV. Data provided by Dr Garry Dolton. Experiment in **D** also performed by Dr Ceri Fielding. **C** & **E** performed by Dr Garry Dolton with members of Mark Peakman's group at King's College London.

5.3.14. The Clone 29 T-cell recognises CMV infected cells and kills islet cells

To further probe the diabetic properties of the Clone 29 T-cell we wanted to determine whether it could potentially cause onset of T1Ds. First, we confirmed that the Clone 29 T-cell could recognise cells (fibroblasts) infected with hCMV (**Figure 5.18D**). Secondly, the ability of the Clone 29 T-cell to kill real pancreatic islet cells harvested from a deceased organ donor was also confirmed by a cytotoxicity assay (**Figure 5.18E**). These data demonstrate that the Clone 29 T-cell cross-reacts with hCMV and T1D and derived epitopes and kills pancreatic β-cells. This finding implicates hCMV as a possible trigger of T1D in *HLA-A*0201*$^{+}$ individuals. A peptide sizing scan was conducted on the Clone 29 T-cell, showing a preference for 9mer peptides despite exhibiting stronger reactivity to the 10mer GAD65-derived epitope (**Figure 5.19A**). A subsequent 9mer CPL screen of the Clone 29 T-cell suggests that peptide recognition is very degenerate in all 9 positions, implying the Clone 29 may be highly cross-reactive (**Figure 5.19B**). To date, this CPL data has not yet been used to generate further peptide candidates for the Clone 29 T-cell.

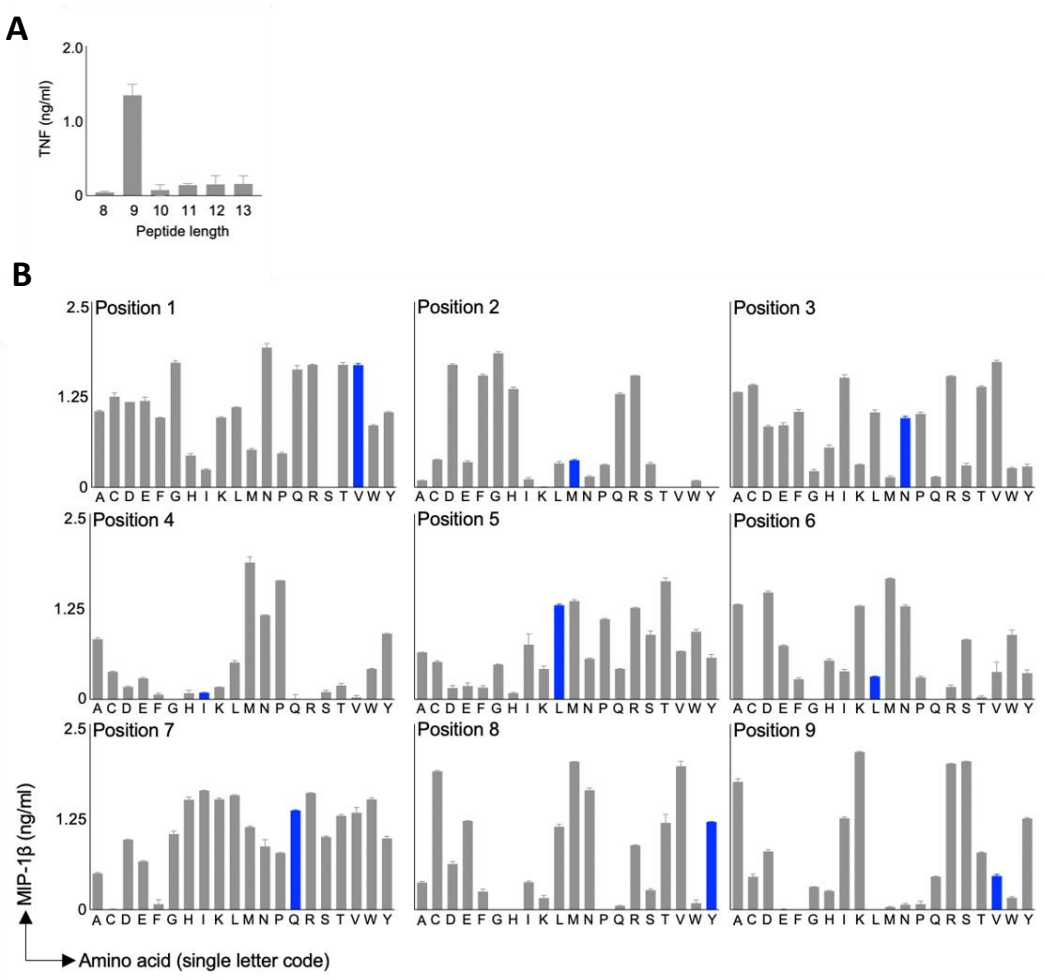

Figure 5.19. Clone 29 exhibits extensive peptide degeneracy.
(**A**) Clone 29 T-cell prefers nonamer peptides. Overnight sizing scan assay with peptide mixtures of defined length. MIP-1β ELISA with error bars depicting SEM of duplicates. (**B**) Nonamer CPL screen of Clone 29 revealing amino acid residue preference at each position of a peptide. Performed overnight in duplicate with T2s as antigen presenting cells. MIP-1β ELISA with error bars depicting SEM. Data in this figure provided by Dr Garry Dolton.

5.3.15. CMV-specific T-cells are present in pancreatic lesions

To further establish the link between CMV and T1D, pancreatic tissue from a T1D-donor was stained *in vivo* with PE-conjugated HLA-A2-NLVPMVATV multimers. Histology data shows positive staining within the exocrine portion and islets of the patient, suggesting the presence of CMV-specific T-cells within the pancreas (**Figure 5.20A-D**). Positive staining was not observed in healthy pancreatic tissue (**Figure 5.20E**). *In situ* multimer staining was conducted by Drs Garry Dolton and Guido Sebastini.

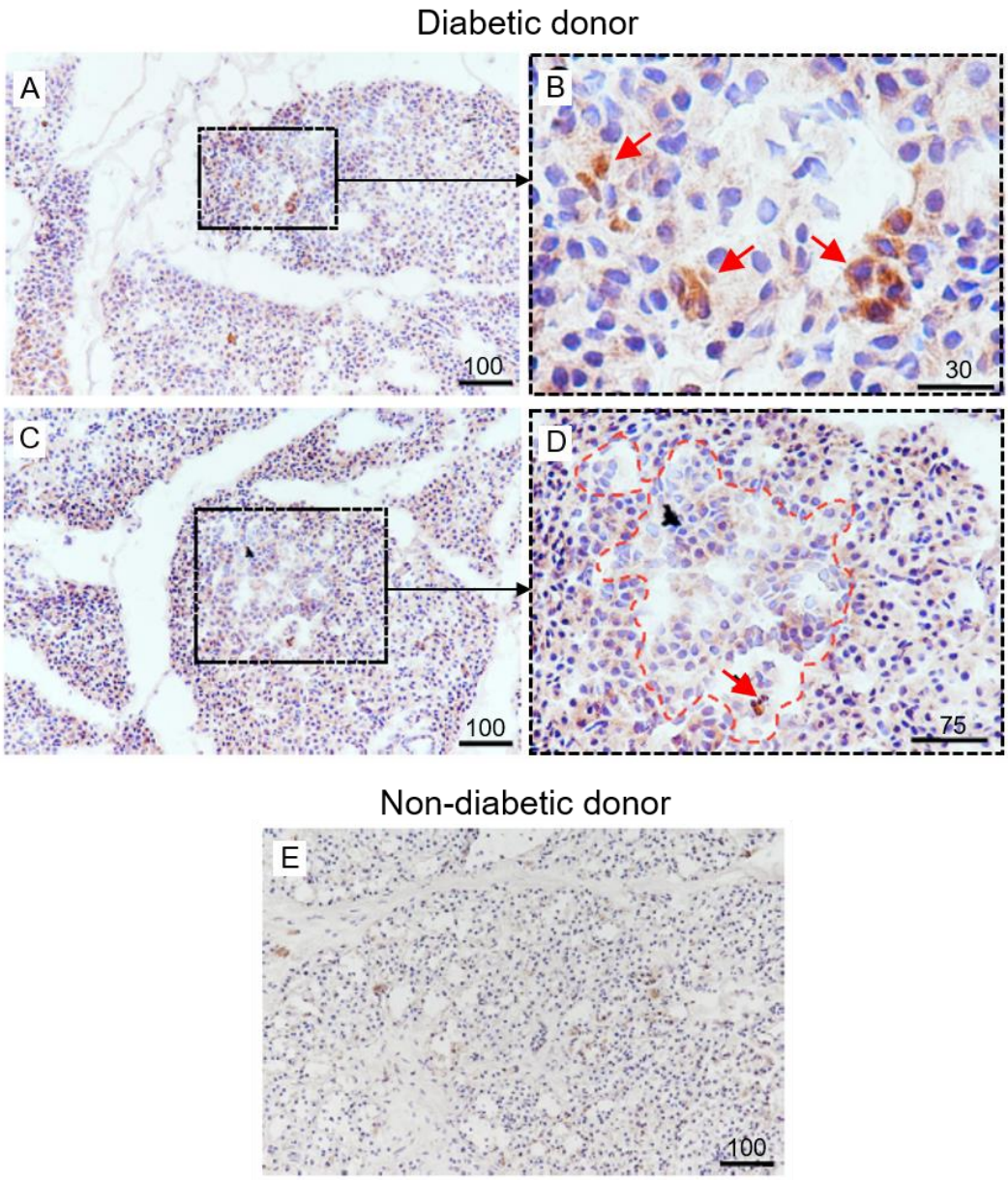

Figure 5.20. CMV specific T-cells infiltrate the islet of a diabetic pancreas.
(**A**) T1Ds donor 6052 (sourced from the network for pancreatic organ donors with diabetes: nPOD) frozen tissue and formalin-fixed paraffin-embedded (FFPE) pancreatic section stained with PE-conjugated HLA-A2-NLVPMVATV tetramers showed positive cells scattered in the exocrine. Scale bar 100 µM. (**B**) Zoom-in on a region of interest in panel (**A**). Scale bar 30 µM. (**C**) Using the same donor as in (**A**), FFPE pancreatic section stained with PE-conjugated HLA-A2-NLVPMVATV tetramers showed positive cells within one islet. Scale bar 100 µM. (**D**) Zoom in on a region of interest of panel (**C**). Islet contour is indicated in red arrow indicates positive cells. Scale bar 75 µM. (**E**) Non-diabetic donor FFPE pancreatic section stained with PE-conjugated HLA-A2-NLVPMVATV tetramers showed no sign of positivity. Scale bar 100 µM. Data in this figure provided by Dr Garry Dolton, Dr Guido Sebastini and Prof. Francesco Dotta.

5.4 Discussion

This chapter highlights two T1D patient-derived T-cell clones, InsB4 and Clone 29, that cross-react with T1D-derived peptides (from InsB and GAD65 respectively) and herpesvirus-derived epitopes (VZV/HSV-1/HSV-2/EBV and hCMV respectively). Both T-cell clones kill *HLA-A*0201*$^{+}$ pancreatic β-cells, as well as cells transduced with T1D-associated genes. The affinity of the InsB4 TCR for the InsB-derived peptide was too low to measure accurately by SPR, perhaps explaining how such autoreactive T-cells can escape negative selection. I hypothesise that herpesvirus infections can help these T-cells break self-tolerance. This hypothesis was supported by data acquired by my colleagues, Dr Garry Dolton and Dr Jade Hopkins, who showed how the InsB4 and Clone 29 T-cell clones responded to EBV-infected LCLs and CMV-infected fibroblasts, respectively.

My own studies involved examining how the InsB4 and Clone 29 TCRs were able to bind to herpesvirus and diabetogenic epitopes in the context of T1D disease-risk molecule *HLA-A*0201*. I present 3D crystallographic structures of the InsB4 TCR in complex with a fungal-derived peptide and two herpesvirus-derived peptides. To my knowledge, this is the first example of structural data showing TCR cross-reactivity between epitopes derived from two different herpesvirus species. These InsB4 complex structures demonstrated how InsB4 TCR promiscuity is underpinned by hotspot binding centred on the glutamic acid residue at peptide position 4. Whilst there are currently no structural data concerning InsB4 in complex with the T1D-derived peptide, the presence of the Glu4 hotspot residue implies a similar mode of binding may occur with the insulin peptide. I also present SPR data highlighting the binding affinities and kinetics of the interactions between the InsB4 TCR and the pathogenic epitopes described in this chapter; however, as mentioned in **Chapter 4** the kinetic observations are subject to caveats discussed in **Section 6.3.1**.

5.4.1. Autoreactive T-cells may have preferential 'triggers' to promote T1D onset in vivo.

As discussed, both the InsB4 and Clone 29 T-cells kill pancreatic β-cells (**Figure 5.1, Figure 5.17**). However, the affinity of the InsB4 TCR to the InsB derived peptide is so low that SPR cannot provide an accurate measurement (**Figure 5.2**). This contrasts with the 1E6 and 4C6 T-cell clones (discussed in **Chapter 4**), as while they have relatively low affinities for their cognate T1D peptides, their affinity is still measurable.

The viral-derived ligands of InsB4 were identified using a CPL scan in conjunction with Dr Szomolay's webtool (**Figure 5.3**). This approach identified several viral-derived peptides, primarily from herpesvirus species, which can elicit a response from the InsB4 T-cell, as well as bind to the InsB4 TCR (**Figure 5.8**, **Figure 5.9**, **Figure 5.14**, **Figure 5.15**). While further potential pathogen-peptide candidates for the Clone 29 T-cell have not been identified, functional data also shows cross-reactivity between T1D and hCMV epitopes (**Figure 5.18**, **Figure 5.19, Figure 5.20**). By contrast, no viral-derived peptide identified from the CPL involving the 4C6 T-cell elicited a greater response than the T1D-derived peptide (**Appendix Figure 4.2**). The 1E6 T-cell also exhibits a preference for bacterial derived peptides as opposed to viral derived-peptides. This suggests that autoimmune T-cells may possess a preference for epitopes derived from certain pathogenic contexts, with this preference differing across different T-cells, different donors and different disease-risk HLA.

5.4.2. InsB4 TCR complex structure analysis

I successfully solved the 3D structures of the InsB4 TCR in complex with HLA-A2-MIVENVPLL, HLA-A2-ILIEGIFFA, and HLA-A2-ILIEGVFFA, analysis of which highlighted two areas of interest that are conserved across all three structures. The first is the pocket formed by peptide residues P1-P5 which is occupied by InsB4 TCR residue Gln31α. The P1-P5 pocket is present in all three peptides irrespective of amino acid composition. As discussed in **Chapter 3**, the P1-P5 pocket and its subsequent occupation by Gln31α is a feature present in TCRs exhibiting *TRAV12-2* gene usage, which includes InsB4. A study by Johnson *et al.* highlighted the potential improvement to binding affinity afforded by *TRAV12-2* gene expression (Johnson et al., 2006), which may facilitate the binding of the InsB4 TCR to pathogenic peptides.

The second structural feature of note is the Glu4 binding hotspot. As discussed, the CPL data implied the importance of Glu4 for InsB4 binding when very little degeneracy was observed at the P4 position. The role of Glu4 during InsB4 binding was confirmed structurally, as this peptide residue makes the greatest number of contacts with the InsB4 TCR compared to the other peptide residues. This is true in all three InsB4:pMHC complex structures. The importance of the other peptide residues varies depending on which epitope is bound to the InsB4 TCR, which the CPL data showing degeneracy in all positions apart from P4. Not only is Glu4 present in all InsB4 T-cell ligands discussed in this chapter (HLV**E**ALYLV, MIV**E**NVPLL, MLL**E**NGLLA, ILI**E**GIFFI, ILI**E**GIFFA, ILI**E**GVFFA, LLI**E**GIFFI, LIV**E**GIYFI), but it is also present in all but one of the 60 pathogenic candidate peptides identified via the CPL data. This binding

hotspot mechanism of InsB4 T-cell cross-reactivity is consistent with the 1E6 and 4C6 TCRs, which both cross-react with pathogen and diabetogenic epitopes via hotspot binding. In conclusion, the presence of Glu4 appears to be essential for InsB4 binding.

I discussed hotspot driven cross-reactivity in **Section 1.3.1.2**, where I highlighted studies by our laboratory as well as Adams *et al*. which discussed TCRs that had been found to utilise hotspot binding (Adams et al., 2016; Cole, Rizkallah, et al., 2016). There have been further examples of hotspot recognition. One such example by Archbold *et al* demonstrated how hotspot recognition may facilitate alloreactivity, thus implicating it in GvHD (Archbold et al., 2006). The data in this chapter, in conjunction with the 1E6 T-cell study (Cole, et al., 2016) and the data presented in **Chapter 4** indicate that hotspot recognition may play an important role in the progression of T1D and GvHD.

Despite multiple attempts, I was unable to crystallise the InsB4 TCR in complex with HLA-A2-HLVEALYLV, so I cannot confirm that the observations highlighted in this section would apply to the InsB4-A2-HLVEALYLV complex. However, the CPL data, the ubiquity of the Glu4 residue across known InsB4 ligands, and the number of Glu4:InsB4 contacts present in known InsB4 complex structures suggest that Glu4 would also be important for the InsB4-A2-HLVEALYLV complex. However, the low affinity of the InsB4-A2-HLVEALYLV interaction, immeasurable by SPR, suggests the P1-P5 pocket may not be present for occupation by Gln31α, perhaps due to the bulky His1 residue in comparison to Met1 and Ile1 present in the InsB4 complexes shown during this chapter. In the absence of an atomic resolution InsB4-A2-HLVEALYLV structure any discussion is purely speculative. The InsB4 TCR could be stained with multimers of HLA-A2-HLVEALYLV. I predict that it would not be possible to stain cells using pHLA multimers where Glu4 were substituted with another amino acid.

I also attempted to acquire 3D structures of the Clone 29 TCR in complex with either the HLA-A2-VMNILLQYVV or HLA-A2-NLVPMVATV pMHCs, though this was unsuccessful. However, the differences in peptide length between the GAD65 and hCMV derived peptides, as well as their dissimilar amino acid compositions, suggests larger conformation shifts would be required for Clone 29 T-cell cross-reactivity, as opposed to the hotspot binding mechanism exhibited by the 4C6 (**Chapter 4**) and InsB4 T-cells discussed in this thesis. The hypothesis that Clone 29 cross-reactivity will require more dramatic conformational shifts is supported by the CPL data which highlights degeneracy at each peptide position, making the presence

of a rigid binding hotspot less likely. Again, without 3D structures, the mechanism of Clone 29 cross-reactivity remains speculative.

5.4.3. Conclusion

In this chapter I present functional data demonstrating cross-reactivity between diabetogenic and herpesvirus-derived peptides by two separate T1D patient-derived T-cell clones, in the context of the disease-risk allele *HLA-A*0201*. I also present structural data showing cross-reactivity between two different herpesvirus species via hotspot binding. These data support the findings present in **Chapter 4** by highlighting potential pathogenic triggers of T1D, while suggesting that cross-recognition of pancreatic self-peptides by T-cells specific to pathogenic peptides may contribute to the onset of T1D. Future work will involve confirming the binding mechanism of the InsB4 and Clone 29 TCRs to their cognate T1D antigens, as well as further investigating the ability for the pathogens discussed in this chapter to induce T1D onset.

6. General Discussion

6.1. Understanding the biological consequences of T-cell cross-reactivity

The aim of this thesis was to gain a greater understanding of the structural and biophysical mechanisms that govern T-cell cross-reactivity in the context of clinically relevant T-cell responses. I discussed many structural mechanisms of T-cell cross-reactivity in my introduction (**Section 1.3.1**), however many of those examples involved mouse models (such as the 2C T-cell (Colf et al., 2007)) or synthetic peptides (such as the YAe62 T-cell (Yin et al., 2011)). While these studies have provided fascinating insight into the potential mechanisms that govern the TCR:pMHC interaction, they are not human or clinically relevant.

To address my aims, each of my results chapters investigated the cross-reactive mechanisms of potentially clinically relevant T-cells. **Chapter 3** discussed the MEL8 T-cell, which was isolated from the TIL infusion product used to successfully treat a stage 4 melanoma patient and shown to persist in the patient's blood long after complete durable remission. The MEL8 T-cell was shown to interact with multiple TAAs in an additive manner. I have subsequently used structural data to demonstrate that MEL8 cross-reactivity was mediated by molecular mimicry among the target TAAs. **Chapters 4** and **5** concerned T-cells which recognised T1D-specific antigens in the context of HLA-A24 (the 4C6 T-cell **Chapter 4**) and HLA-A2 (the InsB4 and Clone 29 T-cells, **Chapter 5**). All three T1D-specific T-cells discussed were shown to cross-react with pathogenic peptides, highlighting potential pathogenic triggers of T1D. Furthermore, structural data showed how the 4C6 and InsB4 T-cells cross-react with their pathogenic ligands via molecular mimicry, facilitated by hotspot binding. While structural data was not obtained for the Clone 29 TCR, CPL data suggests that its binding interaction may not involve molecular mimicry.

6.1.1. Multipronged T-cell responses

In **Chapter 1**, I discussed the benefits of cross-reactive T-cells in the context of immune coverage with emphasis placed on heterologous immunity, where T-cells can recognise multiple pathogenic epitopes via cross-reactivity. This topic is particularly pertinent at the time of writing as T-cell cross-reactivity between human coronaviruses is thought to play a prominent role in dictating how individuals cope with the SARS-CoV-2 infection and in providing herd immunity (Lipsitch et al., 2020). In **Chapter 3**, I discussed multipronged T-cell

recognition, where a T-cell can recognise multiple epitopes presented by the same target cell (**Figure 6.1**), resulting in an additive effect on the overall T-cell response. Multipronged T-cell recognition has been discussed by my colleague Dr Rius Rafael (Rius Rafael, 2019) and to my knowledge has not been reported elsewhere in the literature. In contrast to heterologous immunity, which provides broad immune coverage across multiple pathogens, the additive effect conferred by multipronged recognition may provide 'deep' immune coverage, allowing an increased T-cell response against a single target. My laboratory has other examples of cancer-specific T-cells isolated from patients in complete remission that kill cancer targets via a known epitope but that also kill cancer cells that do not express this TAA suggesting that they must recognise a further TAA. It is possible that recognition of multiple different epitopes on the surface of the same cancer cell by a single T-cell might be a common feature of successful T-cells. However, as discussed in **Section 3.4.1**, the concept of multipronged recognition has not yet been proven and further data are required to support the hypothesis. It will also be important to observe multipronged recognition in additional patients, or even in additional immunological contexts such as autoimmune disease.

6.1.2.1. Advantages of multipronged T-cells

T-cells that target epitopes from multiple TAA on the surface of the same cancer cell (defined as multipronged T-cells herein; **Figure 6.1**) might offer some significant advantage over regular T-cells that target cancer cells via a single TAA. As briefly discussed above, the recognition of multiple epitopes on the same cancer cell results in an enhanced T-cell response compared to recognition of an individual epitope. This improved T-cell response is likely due to the higher T-cell epitope density present on the cancer cell, which can result in greater T-cell polyfunctionality (Tan et al., 2015). Due to the immunosuppressive tumour microenvironment, the improved T-cell response offered by multipronged recognition may be invaluable for the cancer immune response.

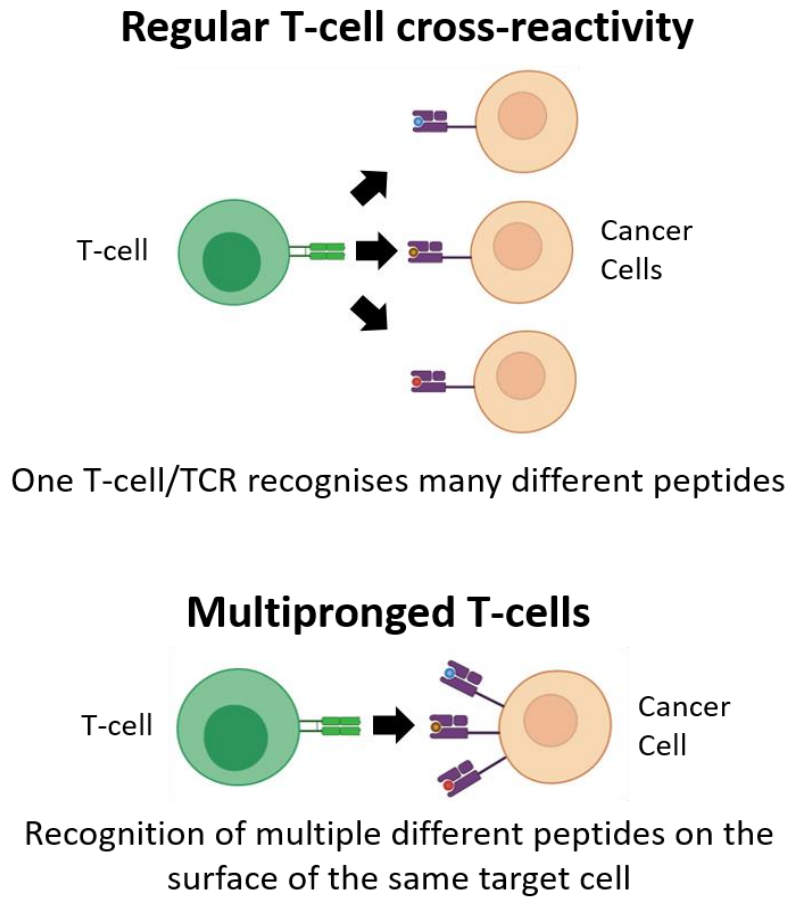

Figure 6.1. Multipronged T-cell recognition.
A schematic demonstrating multipronged T-cell recognition. Regular T-cell cross-reactivity involves the recognition of different peptides on different targets. The new phenomenon described within my thesis involves the recognition of multiple targets on the surface of the same antigen -presenting cell. We have used the term "multipronged" recognition to distinguish these two different circumstances.

A further advantage of multipronged T-cells is a reduction of tumour immune escape. While tumours could theoretically escape from $CD8^+$ T-cells by deletion of the HLA-I heavy chain or β-2-microglobulin, such escape leaves cancer cells vulnerable to natural killer (NK) cell targeting. NK cells are switched off by HLA-I and are said to recognise "missing self" (Ljunggren et al, 1990). In contrast, loss of a specific epitope of TAA can allow T-cell escape without triggering NK cell attack. Any tumour that escapes from a given host T-cell response will have a selective advantage and it will be possible for cancer cells to serially lose antigen over time to escape other host T-cell responses. As a multipronged T-cell can recognise multiple epitopes, loss of any single antigen will offer little or no selective advantage (**Figure 6.2**).

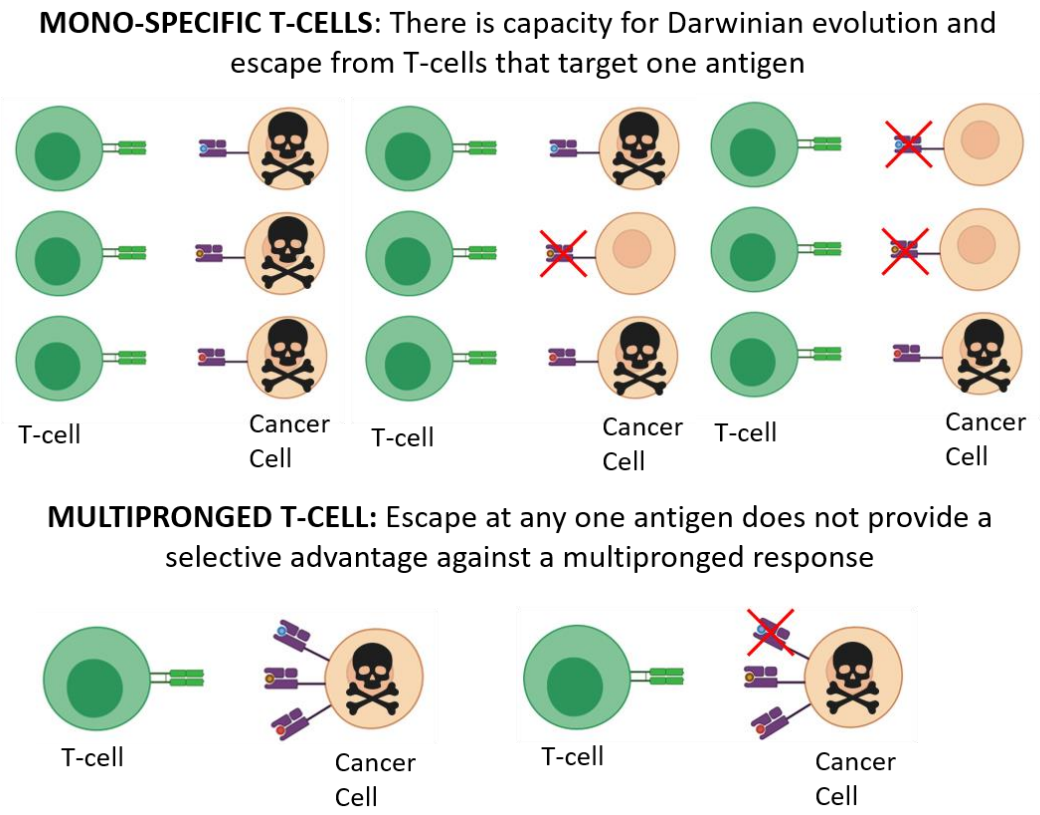

Figure 6.2. Multipronged T-cell response can overcome immune escape.
A schematic demonstrating how multipronged T-cell recognition can prevent immune escape. Red crosses indicate epitope escape, and skulls indicate cell death.

Finally, targeting of multiple self-epitopes may allow potent anti-cancer T-cells to pass through negative selection in the thymus. The process of negative selection in the thymus culls any T-cell bearing a TCR with a high affinity for self-antigen (as discussed in **Section 1.1.1.2**). This process ensures that T-cells with capacity to be autoreactive are deleted before they can cause harm. Cancer-specific T-cells are known to bear TCRs with ~5-fold lower affinity compared to those that target pathogen-derived (non-self) epitopes (Cole et al., 2007). Our discovery that potentially multipronged T-cells persist in patient blood following complete durable cancer remission suggests that these cells might play a key role in cancer clearance *in vivo*. It can be hypothesised that recognition of multiple self-antigens weakly in the thymus allows potent multipronged T-cells to escape negative selection (**Figure 6.3**). A similar process could potentially occur with autoimmune T-cells.

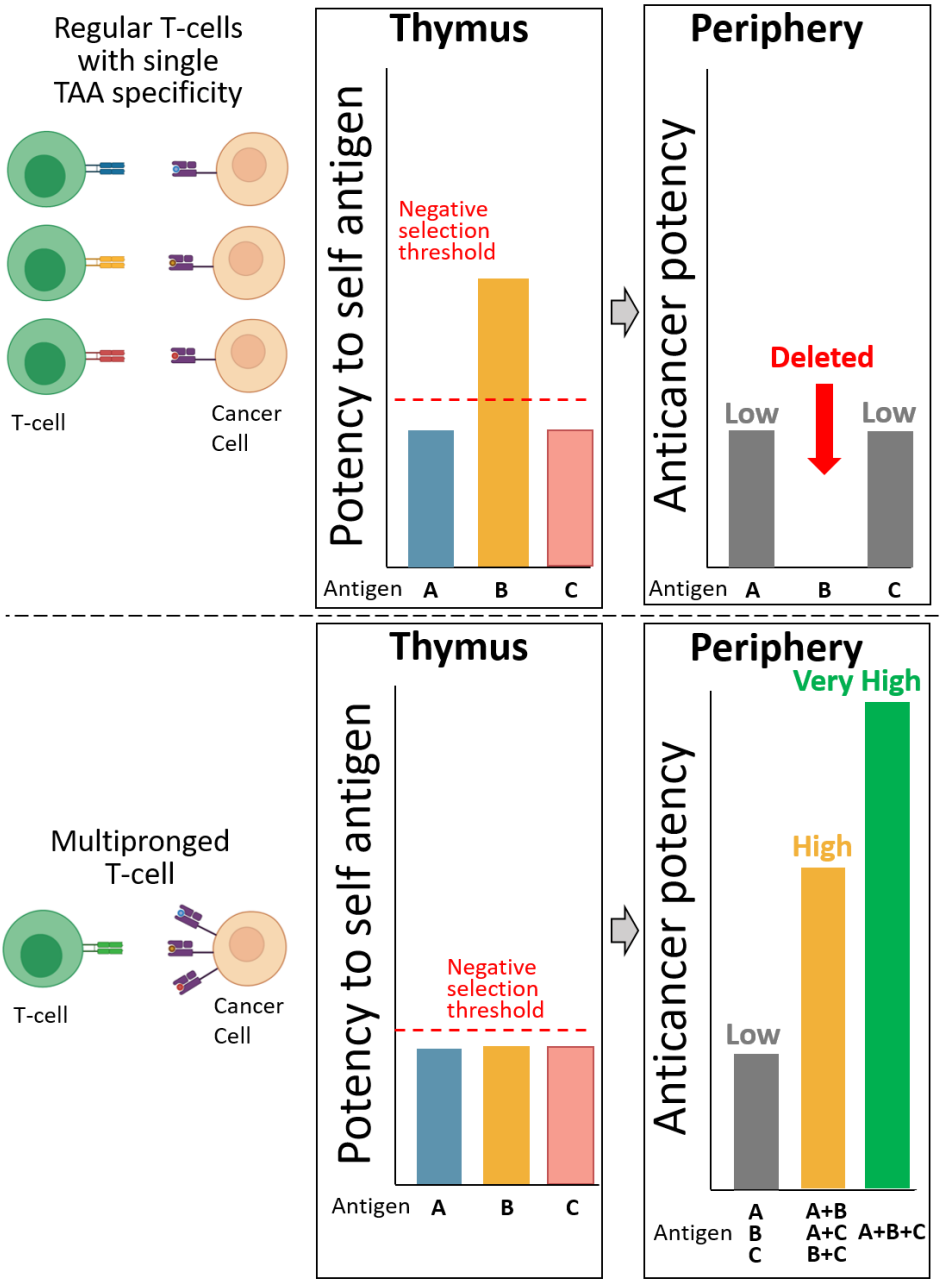

Figure 6.3. Multipronged T-cells recognition may allow potent self-reactive T-cells to escape thymic negative selection.
A schematic illustrating how multipronged T-cells may escape negative selection in the thymus but then act potently to targets expressing more than one antigen in the periphery.

6.1.2. Molecular mimicry in autoimmune disease

In **Chapter 1**, I discussed the drawbacks of T-cell cross-reactivity, particularly the aberrant recognition of self-tissue resulting in autoimmunity. Studies discussed in **Section 1.3.3.1** show how T-cell cross-reactivity, facilitated by molecular mimicry, has been implicated in the progression of autoimmune diseases such as MS and Parkinson's disease (Sethi et al., 2013; Sulzer et al., 2017). In **Chapter 4**, I specifically discussed the role of cross-reactivity in T1D, highlighting evidence suggesting that it may also be facilitated by molecular mimicry with a pathogenic trigger (Cole et al., 2016).

The data I presented in **Chapters 4 and 5** further supports the hypothesis that molecular mimicry may be a key driver for the onset of T1D. While structural data directly showing 4C6 and InsB4 T-cell cross-reactivity between a T1D epitope and a pathogenic epitope is presently absent, structural data is available showing these T-cells can indeed cross-react with multiple epitopes via molecular mimicry, with peptide sequence similarities implying the feasibility of molecular mimicry between T1D and pathogenic epitopes. While more functional data into the role of pathogens in 4C6 T-cell activation is required, data presented here regarding the InsB4 T-cell strongly suggest that the herpesvirus strains may facilitate T1D onset. The data presented in **Chapters 4 and 5** support a growing hypothesis that molecular mimicry plays a key role in the onset of autoimmune disease.

My laboratory recently added to the 4C6 cross-reactivity story by demonstrating that 7/7 *HLA-A*2402*$^{+}$ healthy donors had T-cells that could be sorted with a Klebsiella peptide tetramer which, when expanded, were capable of killing insulin-producing target cells via HLA-A24. We are currently examining whether this means that there is a 'public' TCR motif that defines this common cross-reactivity. It remains possible that a conserved peptide-TCR motif defines CD8^{+} T-cell crossreactivity between HLA-A24-restricted peptides from bacteria and insulin in T1D. If we see a motif in the *Klebsiella*-insulin dual-reactive T-cells, then the next step will be to show that this TCR resides in the naïve T-cell compartment in healthy donors and in the effector/memory compartment in patients. If we do find these 'public' TCRs, then it may be possible to use TCR motifs to predict disease in those at risk before the onset of symptoms, as has been suggested in other autoimmune diseases such as ankylosing spondylitis (Zheng et al., 2019).

An early biomarker of T1D has been widely viewed as a 'holy grail', as it has become evident that early diagnosis leads to improved prognosis due to the ability of exogenous insulin to protect the patient's remaining β-cell mass (Liu et al., 2018). The "honeymoon phase" in T1D is used to describe the period shortly following diagnosis when the pancreas is still able to produce enough insulin to maintain some control over blood glucose. Once a patient starts insulin injections the pancreas is less under pressure to produce insulin during blood sugar peaks which in turn makes it less of a target for autoimmune attack. Currently, this honeymoon period can last for several years in some patients (Abdul-Rasoul et al., 2006). It is possible that the diagnosis before the onset of symptoms that might be afforded by early TCR diagnoses could extend this honeymoon period to decades and save the UK National Health Service a fortune (it is estimated that the annual cost of T1D and its complications to the NHS exceeds £1 billion with all forms of diabetes accounting for >10% of the entire NHS budget (Hex et al., 2012)).

6.1.2.1 Alternate mechanisms for type 1 diabetes induction

In this thesis I have discussed how T1D may be triggered by T-cell cross-reactivity between a pathogenic-epitope and a self-epitope, however other mechanisms of T1D induction have been proposed. One such mechanism is viral-induced T1D triggering through the direct infection and subsequent $CD8^+$ T-cell targeting of pancreatic islet cells. A study by Yoon *et al.* isolated human enterovirus (HEV) from the pancreatic islets of a T1D patient, before demonstrating pancreatic β-cell necrosis in NOD mice infected with the same HEV (Yoon et al., 1989). Since then further studies have identified HEV in the pancreatic cells of T1D patients, as well as highlighting a correlation between HEV infection and incidences of T1D, suggesting a link between T1D and HEV infection (Krogvold et al., 2015; Stene et al., 2010).

In addition to HEV some herpesviruses, such as HSV-1 and EBV, have also been suggested to directly infect the pancreas (Chen et al., 2006). Given the data presented in **Chapter 5**, it could be hypothesised that direct viral infection of pancreatic islets and $CD8^+$ T-cell cross-reactivity via molecular mimicry may not be mutually exclusive mechanisms of T1D triggering. The lysis of virally infected β-cells via $CD8^+$ T-cells may result in viral antigen release that could result in $CD8^+$ autoreactivity, thus accelerating T1D progression via both mechanisms.

A link has also be made between T1D and the hygiene hypothesis. Strachan postulated that pathogenic infection could protect from atopy, based on data that suggested first-borns exhibit greater incidences of hay fever than subsequently born siblings do. Strachan hypothesised that first-borns are less likely to encounter pathogenic infection and are more likely to develop hay fever (Strachan, 1989). Strachan's study led to the hygiene hypothesis, which postulates that there is an inverse correlation between environmental infection burden and the incidence of allergy, which has since been supported by further epidemiological data (Ege et al., 2011). Studies have found that the hygiene hypothesis may also apply to autoimmune disease where pathogenic infections may confer protection against such diseases, including T1D. This was demonstrated by a study where NOD mice infected with lymphotropic virus did not develop T1D (Oldstone, 1988). Further epidemiological data has since supported the hypothesis that pathogenic infection may protect against T1D progression (Kondrashova et al., 2007; Patterson et al., 1996). Several biological mechanisms have been proposed to explain how pathogens may confer atopic protection, such as antigenic competition (Pross et al., 1974), direct immune regulation by pathogens (Tian et al., 2009), and signalling via Toll-like receptors (Karumuthil-Melethil et al., 2008).

In the context of T1D it is interesting to consider the relationship between the hygiene hypothesis and pathogen-induced T1D (whether through molecular mimicry or direct viral infection), as the evidence for both suggest a paradox whereby pathogens confer both protection and triggering of T1D respectively. It could be postulated that the productive and inductive effects of pathogens in respect to T1D are in balance and T1D triggering is reliant on the failure of the protective component. However, another hypothesis could be that T1D triggering requires infection of a pathogen not traditionally present in an individual's environment, thus an individual would not be tolerised to it and the pathogen would not provide a protective benefit. Based on the current evidence, it is clear the relationship between T1D and pathogenic infection is complicated and more evidence in all aspects of this relationship will be required to understand it.

6.2. The role of structural biology in T-cell immunology

Throughout this thesis I have utilised 3D structural data to determine the binding mechanisms of specific TCR:pMHC interactions. While other techniques can provide insight into the TCR:pMHC interaction such as alanine scanning mutagenesis (Bianchi et al., 2016)

and the aforementioned CPL-screens, a 3D structure offers the most comprehensive understanding of the biochemical mechanisms involved in TCR-antigen recognition. Using 3D structural data, the relative conformations of TCR and pMHC components can be determined and compared to the current literature. 3D structural data can also highlight the relative importance of certain amino acid residues to TCR:pMHC interactions by assessing how many contacts are formed with other amino acid residues within the structure.

3D structural data have been instrumental to our understanding of various core components of the TCR:pMHC interaction. Whilst the existence of the heavy chain and β_2M components of the pMHC were already hypothesised (Peterson et al., 1974), the orientation of these components, as well as the role of the peptide binding groove in antigen presentation, were only elucidated by structural evidence (Bjorkman et al., 1987). The structure of HLA-A2 showed that the membrane-distal part of the molecule formed a platform of eight β-strands topped by two α-helices to form a "groove", allowing researchers to determine where the binding site must be for an unknown antigen. Likewise, TCR gene usage and presence of the CDR loops had been described prior to the first 3D structure, along with hypothesises of their roles (Davis et al, 1988). However, the first 3D structure of a TCR:pMHC co-complex, published by Garboczi *et al.*, established the core mechanism by which the CDR loops interact with the pMHC molecule (Garboczi et al., 1996), with the structural studies highlighted in **Section 1.2.5.1** serving to further refine and expand upon the observations made by Garboczi *et al*. Our understanding of the biochemical mechanisms governing T-cell cross-reactivity have also been improved by 3D structural data, with specific mechanisms such as molecular mimicry, hotspot binding, and conformational changes highlighted by the structural studies discussed in **Section 1.3.1.1**. I believe the structural data presented throughout this thesis contributes to the growing body of 3D structural data which informs our understanding of T-cell cross-reactivity.

Beyond providing an understanding of the TCR:pMHC interaction, 3D structural data can also allow for artificial modifications of both TCR and pMHC components via rational design. T-cell-based immunotherapies, discussed in **Section 1.4** and **Section 3.1**, could benefit greatly through the application of rational design. This has been demonstrated with antibody design in the context of T-cell leukaemia. T-cell leukaemias are especially aggressive and there are no current successful treatments for these rare conditions. The human TRBC locus includes a gene duplication which means that T-cells express a TCR using either TRBC1 or TRBC2 (~45%

and 55% of T-cells use each respectively). TRBC1 and TRBC2 differ by two cell surface-exposed amino acids (Maciocia et al., 2017). My laboratory was recently involved in the structure-based rational design of an antibody that specifically bound to the *TRBC2* gene product (submitted for publication). The rational design of antibodies that distinguish between TRBC1 and TRBC2-containing TCRs allows targeting of tumour while sparing the healthy T-cells that express the other C-domain (Maciocia et al., 2017).

In an example of the rational design of a TCR, Bennett *et al* used previously described HIV-specific TCRs (TCR 1.9 and TCR 1803) to design a HIV-specific TCR with greater affinity than the wild type TCRs, with improved recognition for escape mutants (Bennett et al., 2010). Additionally, the potential off-target effects that can be exhibited by affinity enhanced TCRs produced by directed evolution can be mitigated using rational design (Raman et al., 2016). The structural data presented in **Chapter 3** could form the basis of rationally designed TCR-based anti-cancer therapeutics.

6.3. Future perspectives

6.3.1. Optimising Surface Plasmon Resonance experiments

Chapters 3, 4, and 5 of this thesis all featured the use of SPR to highlight the interaction between a TCR and a pMHC. In addition, **Chapters 4 and 5** utilised SPR to quantify the binding affinity and binding kinetics associated with various TCR:pMHC interactions. While in certain examples the theoretical K_D value (calculated from the measured binding kinetics using $K_D = K_d/K_a$) agreed with the experimental K_D value, such as with 4C6:A24-LWMRLLPLL, in some examples this was not the case (4C6:A24-QLPRLFPLL theoretical K_D was 1.1 µM compared to the experimentally measured 5.4 µM). This suggests that in some cases the measured binding kinetics were underestimated and may not be correct.

A potential explanation for the underestimation of binding kinetics is protein re-binding. Protein re-binding occurs when previously associated TCR molecules re-associate with the pMHC on the chip during the dissociation phase of the SPR experiment, resulting in lower measured dissociation rates (Felder et al., 1993). A key factor in protein re-binding is the influence of mass-transport limitation, which is characterised by non-homogenous concentration of TCR near the pMHC caused by low TCR transport rates. This results in both TCR re-binding during the dissociation phase, as well as uneven ligand replenishment during

the association phase, resulting in lower measured dissociation and association rates (Schuck, 1997).

To measure binding kinetics more accurately, the SPR protocol used in this thesis will need to be optimised appropriately. One adjustment could be to increase the flow rate of the TCR from 10 µl/min to 50 µl/min. Additionally, the amount of pMHC bound to the SPR chip could be lowered from 500RU to 300RU. Both of these optimisations would allow a single TCR molecule less opportunity to bind the pMHC molecules multiple times and ensure a consistent TCR concentration, thus circumventing the mass-transport limitation and providing a more accurate measurement of binding kinetics (Willcox et al., 1999). Future work will involve repeating the SPR experiments highlighted in **Chapers 4 and 5**, using the optimisations discussed above, to ensure accurate binding kinetics are measured.

6.3.2. Alternatives for epitope discovery

During my project, I have made considerable use of CPL-screens and Dr Szomolay's webtool to identify potential, clinically relevant epitopes for the T-cells under investigation. The use of CPLs to determine the specificity of T-cells has long been established (Davenport et al., 1997; Pinilla et al., 1999; Stevens et al., 1998), with subsequent studies demonstrating the effectiveness of combining CPLs with biometric analysis (Nino-vasquez et al., 2004). Our laboratory has optimised the use of CPLs in epitope discovery through use of the original webtool (Szomolay et al., 2016) and by running this webtool via a graphics processing unit to vastly improve the efficiency of database searches (Whalley et al., 2020). These optimisations have resulted in an efficient and proven workflow for discovering novel T-cell epitopes.

Despite the success my laboratory has had using CPL screens for epitope discovery, there are drawbacks to this approach. While the raw CPL data are derived from a functional assay, this data is used to identify theoretical T-cell epitopes. The use of pathogenic-peptide databases restricts the theoretical peptide list to biologically relevant peptides but there is no guarantee that the generated peptides will be successfully processed by APCs, or that the T-cell will recognise them. As a result, some epitopes predicted by the CPL data have proven to be less effective T-cell antigens than expected (**Section 4.3.2**), however the number of highly effective epitopes discovered via the CPL-screen far exceeds the number of epitope candidates that are less effective.

An alternative to using CPL screens for epitope discovery is to use yeast-displayed peptide libraries, which have been shown to identify novel T-cell epitopes with no prior knowledge of likely ligands required (Adams et al., 2016; Birnbaum et al., 2014). In brief, a library of approximately 10^8 peptides is presented by yeast cells, with each individual yeast cell encoding a single, unique peptide. The yeast cells are selected for by a multimerised variant of the TCR under investigation. Successfully selected yeast cells are deep sequenced to determine their presented peptide and a new yeast-display library is produced encoding sequence-similar peptides to those selected for. This process is repeated multiple times and the peptide sequences identified by the 'final' library is used to predict the recognition landscape of the T-cell under investigation (Gee et al., 2018). However, the use of multimerised TCR molecules means that peptides are selected via T-cell avidity, rather than by T-cell activation. Furthermore, the process of repeatedly optimising the yeast-display library would arguably be more time and cost prohibitive than a CPL screen and can only be applied to TCRs that refold well as soluble molecules. In addition, the size of the peptide library that can be screened by yeast display is over 100,000 times smaller than allowed by CPL screen. These approaches also use a fixed MHC anchor and would have failed to find that the very best agonists of TCRs like MEL5 and 1E6 use a sub-optimal HLA-A2 anchor at P2 (alanine and glutamine respectively) (Bulek et al., 2012; Madura et al., 2015).

Two recently developed platforms for T-cell epitope discovery are 'T-scan' and 'SABR'. T-scan involves transducing an oligonucleotide library into HEK293T target cells encoding the relevant *HLA* and a fluorescent marker sensitive to granzyme B cleavage, with each cell containing a small oligonucleotide sequence. Target cells that are successfully selected by the T-cell under investigation will fluoresce due to secretion of granzyme B by the activated T-cell. Positive target cells are then sequenced to determine their expressed peptides (Kula et al., 2019). By contrast, SABR involves transducing an oligonucleotide library into modified Jurkat cells encoding HLA molecules associated with CD3ζ and CD28. Positive selection by a T-cell causes CD3ζ dimerisation, resulting in the expression of GFP under the influence of the NFAT transcription factor, allowing positive target cells to be identified. As with T-scan, positive cells are sequenced to determine the presented peptides (Joglekar et al., 2019). Like yeast-display libraries, T-scan and SABR both account for peptide presentation and cover the full breadth of amino acids, while T-scan additionally uses functional T-cell outputs for positive selection. However, a CPL screen is arguably more cost and time effective than both

T-scan and SABR and their date of publication meant they could not be considered for my studies.

6.3.3. Optimising structural determination

X-ray crystallography is the de-facto standard for 3D structural determination within my laboratory, featuring in all results chapters presented in this thesis. However, the requirement to acquire protein crystals to subject to x-ray diffraction has, to date, proven an insurmountable task for several TCR:pMHC complexes that I have studied, despite the promising results shown using crystal seeding (**Chapter 4**). The need to produce protein crystals has been compounded in several cases by difficulties in producing soluble TCR molecules in the high yields required for crystallisation trials. Additional methods to optimise crystallisation of proteins have been developed, including additive screens which can supplement crystallography conditions (Gorrec, 2016), as well as nucleants which promote crystallisation by forming concentrated pockets of protein within porous beads (Chayen et al., 2005). Despite these optimisations, protein crystallisation remains a major bottleneck for our structural studies.

Perhaps the most promising alternative to x-ray crystallography is cryogenic election microscopy (cryo-EM). Cryo-EM involves cryogenically freezing the soluble protein of interest onto conductive transmission-electron microscope support grids. Images are then taken of the protein, which are subsequently used to reconstruct its 3D structure (Bhella, 2019). As cryo-EM directly images soluble proteins, this not only allows for structure determination of the protein in its 'native' state, but also removes the obstacles associated with crystallising the protein sample, while requiring less protein to conduct. Previously, the drawbacks with cryo-EM were the low resolution of the 3D structures, as well as a lower limit on the molecular weight of protein samples required to discriminate between protein and background. However, advances in cryo-EM technology are beginning to lessen these drawbacks. According to the electron microscopy data bank (EMDB), the average resolution of cryo-EM structures has fallen rapidly, measuring at approximately 6 Å in 2019 compared with approximately 12 Å in 2015 (**Figure 6.3**). A recent study by Yip *et al* has presented a 3D structure determined by cryo-EM with a resolution of just 1.25 Å, demonstrating the potential resolution for this technique (Yip et al., 2020). Furthermore, cryo-EM has successfully determined the 3D structure of haemoglobin (a 64 kDa protein) to a resolution of 3.2 Å (Khoshouei et al., 2017). As TCR and pMHC molecules have a molecular weight of

approximately 50 kDa, it may be possible to use cryo-EM for structure determination in the near future, thus removing the bottlenecks associated with x-ray crystallography and allowing us to acquire the 3D structures that are 'missing' from the studies presented in this thesis.

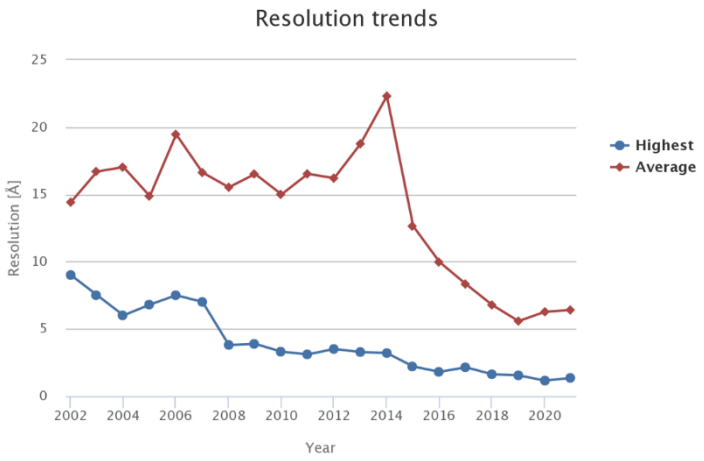

Figure 6.4. Improvements to cryo-EM structure resolutions over time.
The average and highest resolutions achieved by cryo-EM over time. Data taken from the Electron Microscopy Data Bank (https://www.ebi.ac.uk/pdbe/emdb/statistics_main.html/).

6.4. Closing remarks

By combining functional cellular data with biophysical data and 3D structural data, I have demonstrated the important role that T-cell cross-reactivity plays in both cancer immunology and autoimmunity. The data presented in this thesis contributes to the growing body of literature regarding T-cell cross-reactivity and its consequences for health and disease. As this field expands and our collective understanding of T-cell cross-reactivity grows, so does the potential to harness this understanding for therapeutic benefit. Recent curated databases of TCR sequences with known antigen-specificity (such VDJdb: https://vdjdb.cdr3.net) (Bagaev et al., 2019; Shugay et al., 2017) are currently being combined with advanced computation to begin allowing the prediction of what peptides a given TCR might recognise. My laboratory plans to add CPL "training" data to these attempts so that within as little as 5 years it might be possible to predict TCR cross-reactivities *in silico*.

7. Appendix

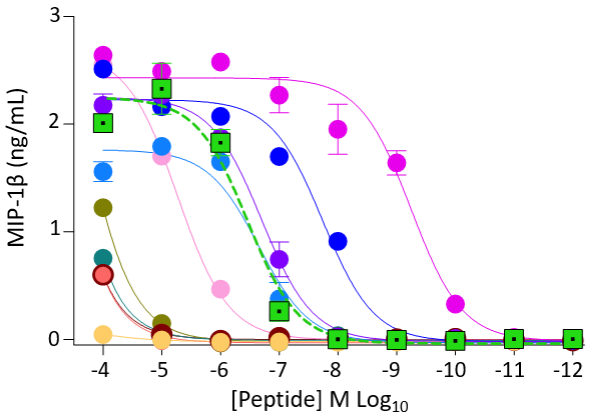

Score	Sequence	EC_{50}
-15.83	LWMRLLPLL	3.49×10^{-7}
-9.97	QWPRLFPIV	**2.00×10^{-7}**
-10.48	NMPRLFPIV	**1.82×10^{-8}**
-10.59	NYLRLAPIL	**2.23×10^{-7}**
-10.67	NLPPLFPIW	NC
-10.70	QLPRLFPLL	**5.66×10^{-10}**
-10.87	QLLRLAGIV	~ 0.74
-10.96	DLLRLAPIL	~ 0.52
-11.03	NYPPLAGIV	5.41×10^{-6}
-11.22	DLMRLAPIW	2.55×10^{-4}
-11.37	HMPRLAPIV	~ 0.2173

Appendix Figure 1. Identification of a super-agonist peptide for 4C6 T-cells.
Top ten scoring peptides from 500 'randomly' selected peptides based on the PS-CPL of 4C6, tested in comparison to the preproinsulin peptide LWMRLLPLL. Incubation overnight with C1Rs expressing HLA-A*24:02 as antigen presenting cells. Crude (>40%) purity peptides used for screening. Assay supernatants harvested for MIP-1β ELISA. Error bars depict SD from the mean of two replicates. EC_{50} values in bold indicated peptides seen more sensitively than the preproinsulin peptide. NC = EC_{50} not calculated.

A

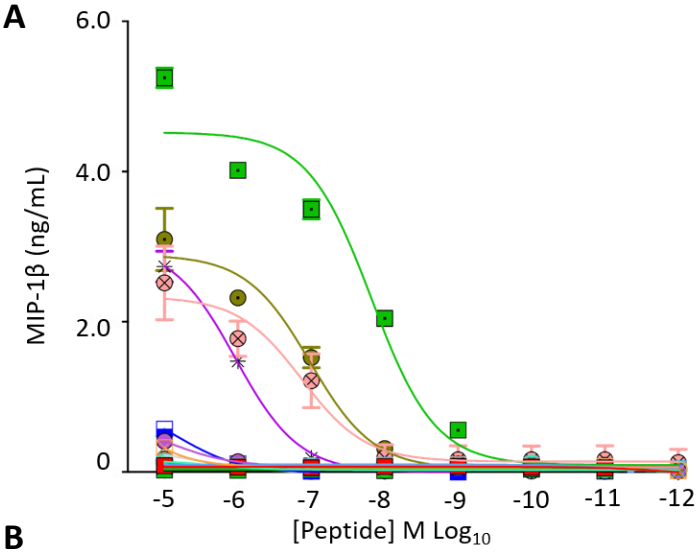

B

Score	Peptide	EC_{50}	Organism	Protein
-15.83	LWMRLLPLL	8.2 x10^{-7}	*Homo sapiens*	Preproinsulin
-16.06	NMYPPVRML	NR	STL Polyomavirus	Middle T antigen
-17.04	QRNLPLRRL	9.8 x10^{-6}	Torque teno virus 1	VP2
-17.04	AVLLLQRVL	9.6 x10^{-5}	Human herpesvirus 3	Tegument protein VP13/14
-17.2	PMLPPQPDL	NR	Human herpesvirus 4	EBNA3A nuclear protein
-17.25	SSLRLARCL	8.6 x10^{-6}	Human herpesvirus 1	Tegument protein VP11/12
-17.37	LKLLPNRVL	NR	Human herpesvirus 7	Deoxyuridine triphosphatase
-17.61	EGLLLIPDL	NR	Human coronavirus OC43	N2 protein
-17.65	IMKQLQPAL	NR	Human rhinovirus B4	Genome polyprotein
-17.89	ISLLPGPSL	NR	Human parainfluenza virus 1	HN glycoprotein
-18.03	QQLQQQRLL	NR	Torque teno virus 3	Putative protein
-18.11	ALWPPRRVL	1.6 x10^{-5}	Human herpesvirus 2	Envelope glycoprotein
-18.33	CSLSQQRKL	NR	Human herpesvirus 2	Tegument protein UL37
-18.40	AGLVLQRLL	NR	Human herpesvirus 1	Tegument protein VP13/14
-18.49	SNYLQPPRL	5.3 x10^{-5}	Human herpesvirus 3	Tegument protein UL16
-18.53	YYLLQAPRL	NR	Human herpesvirus 2	Helicase-primase primase subunit
-18.6	QPPLPQPPL	NR	Human herpesvirus 2	Cytoplasmic Large tegument protein
-18.66	SSLTLAPHL	NR	Human herpesvirus 4	BFRF2
-18.75	LQMLMARDL	NR	Human adenovirus 1	POL
-18.82	RSLPLPPLL	~ 0.02	Human T-lymphotropic virus 2	REX 26 KD protein
-18.85	CGNLHQREL	NR	Human coronavirus OC43	Replicase polyprotein

Appendix Figure 2. 4C6 shows poor reactivity with viral derived peptides.
Positional-scanning combinatorial peptide library data for 4C6 was used to screen a database of disease viral species and the top 20 peptides selected for testing. (**A**) Peptide titrations using 4C6 and the top 20 viral peptides (listed in B). Incubation overnight with C1Rs expressing HLA-A*24:02 as antigen presenting cells. Assay supernatants used for MIP-1β ELISA. Error bars depict SD from the mean of two replicates. (**B**) Peptide sequence and origin. Scoring indicates prediction of how likely the peptide is to be recognized by 4C6 T-cells, with the best scoring peptide at the top. EC_{50} of activation in bold indicate peptides seen more sensitively than the preproinsulin peptide in functional assays.

Complex	MEL5:A2-LLLGIGILVL	MEL5:A2-NLSALGIFST	MEL8:A2-EAAGIGILTV
Data Collection			
Diamond Beamline	I04	I04	I03
Wavelength	0.97951	0.97951	0.97625
Crystallisation Conditions	0.1M TRIS, 15% PEG 8000, 15% Glycerol	0.1M HEPES, 25% PEG 4000, 15% Glycerol	0.1M HEPES, 25% PEG 4000, 0.2 M $(NH_4)_2SO_4$
pH	7.5	7.5	7.5
Crystal Data			
a,b,c (Å)	122.02, 122.02, 82.418	121.28, 121.28, 81.314	99.984, 53.669, 203.571
α, β, γ (°)	90.0, 90.0, 90.0	90.0, 90.0, 90.0	90.0, 94.307, 90.0
Space group	$P4_3$	$P4_3$	P 1 2_1 1
Resolution (Å)	2.1 – 61.02	2.55 – 60.65	2.80 – 99.70
Outer shell	2.10 – 2.14	2.55 – 2.59	2.80 – 3.121
R-merge (%)	10.5 (260.3)	19.7 (386.4)	27.7 (86.0)
R-pim	4.0 (98.9)	7.5 (152.1)	16.3 (50.8)
R-meas (%)	11.3 (278.6)	21.1 (415.7)	32.5 (97.7)
CC1/2	0.998 (0.312)	0.995 (0.221)	0.970 (0.542)
I / σ(I)	10.6 (0.3)	7.2 (0.4)	4.5 (1.5)
Completeness (%)	100 (100)	100 (100)	50.9 (9.2)
Multiplicity	7.7 (7.8)	7.8 (7.4)	3.7 (3.8)
Total Measurements	541,775 (27,332)	303,254 (14,105)	102,222 (52,36)
Unique Reflections	70,731 (3,512)	38,671(7.84)	27,508 (1,375)
Wilson B-factor(Å^2)	44.0	53.5	65.1
Refinement Statistics			
Non-H Atoms	6,888	6,666	13,298
R-work reflections	67,098	36,363	26,063
R-free reflections	3,633	1,905	1,446
R-work/R-free (%)	20.6 / 24.7	21.5 / 27.6	22.9 / 30.4
Mean B value (Å^2)	62.1	69.8	31.1
[1]rms deviations			
Bond lengths (Å)	0.011	0.010	0.007
Bond Angles (°)	1.743	1.827	1.619
[2]Coordinate error	0.202	0.370	0.532
Ramachandran Statistics			
Favoured/allowed/Outliers	771 / 34 / 4	755 / 56 / 7	1,465 / 155 / 3
%	95.3 / 4.2 / 0.5	92.3 / 6.8 / 0.9	90.3 / 9.6 / 0.2

* One crystal was used for determining each structure.
* Figures in brackets refer to outer resolution shell, where applicable.

[1]Figures in brackets are rms targets

[2]Coordinate Estimated Standard Uncertainty in (Å), calculated based on maximum likelihood statistics.

Appendix Table 1. Statistics for 3D structures presented in Chapter 3.

Protein	HLA-A24-QLPRLFPLL	4C6:A24-QLPRLFPLL	4C6:A24-LWMRLLPLL
Data Collection			
Diamond Beamline	DLS-I03	DLS-I03	DLS-I04
Wavelength	0.97625	0.97623	0.97949
Crystallisation Conditions	20% PEG 4000, 0.1 M TRIS,, 15% glycerol	20% PEG 3350, 0.2M NaBr, 0.1 M Bis-Tris Propane	25% PEG 1500, 0.1M PCTP Buffer
pH	7.5	7.5	9
Crystal Data			
a,b,c (Å)	79.54, 48.68, 123.07	63.38, 72.25, 114.84	54.32, 72.13, 230.65
α, β, γ (°)	90.0, 105.43, 90.0	90.0, 102.98, 90.0	90.0, 90.0, 90.0
Space group	P 1 2_1 1	P 1 2_1 1	P 2_1 2_1 2_1
Resolution (Å)	2.25 – 73.99	2.98 – 60.08	2.48 – 52.87
Outer shell	2.25 – 2.31	2.98 – 3.06	2.48 – 2.58
R-merge (%)	14.9 (121.7)	17.0 (97.7)	8.4 (117.5)
R-pim	8.9 (74.1)	10.2 (57.7)	5.0 (69.0)
R-meas (%)	11.9 (93.8)	19.9 (113.9)	10.8 (148.6)
CC1/2	0.984 (0.400)	0.985 (0.582)	0.997 (0.513)
I / σ(I)	5.4 (1.0)	8.4 (1.5)	11.6 (1.3)
Completeness (%)	99.0 (98.3)	99.3 (99.8)	99.8 (99.9)
Multiplicity	3.7 (3.6)	3.6 (3.8)	4.4 (4.4)
Total Measurements	160,482 (11,406)	75,554 (5,809)	144,009 (16,321)
Unique Reflections	43,149 (3,179)	20,758 (1,514)	33,057 (3,692)
Wilson B-factor(Å^2)	37.2	28.5	42.3
Refinement Statistics			
Resolution Range Used	2.25 – 74.01	2.98 – 60.08	2.48 – 52.93
Non-H Atoms	6,588	6,675	6,758
R-work reflections	41,059	19,688	31,375
R-free reflections	2,050	1,433	1,616
R-work/R-free (%)	21.4 / 26.9	18.5 / 28.8	19.9 / 27.7
rms deviations (target)			
Bond lengths (Å)	0.012 (0.013)	0.012 (0.013)	0.011 (0.013)
Bond Angles (°)	1.318 (1.660)	1.414 (1.652)	1.571 (1.652)
[1]Coordinate error	0.248	0.451	0.294
Mean B value (Å^2)	47.5	61.6	51.5
Ramachandran Statistics			
Favoured/allowed/Outliers	718 / 48 / 2	680 / 70 / 48	754 / 44 / 8
%	93.5 / 6.3 / 0.3	83.1 / 11.0 / 5.9	89.6 / 7.5 / 2.9

* One crystal was used for determining each structure.
* Figures in brackets refer to outer resolution shell, where applicable.

[1] Figures in brackets are rms targets

[2] Coordinate Estimated Standard Uncertainty in (Å), calculated based on maximum likelihood statistics.

Appendix Table 2. Statistics for 3D structures presented in Chapter 4.

Complex	InsB4:A2-MIVENVPLL	InsB4:A2-ILIEGIFFA	InsB4:A2-ILIEGVFFA
Data Collection			
Diamond Beamline	DLS-I04	DLS-I03	DLS-I03
Wavelength	0.97950	0.97625	0.97623
Crystallisation conditions	0.2 M lithium sulphate, 0.1 M MES, 20% v/v PEG 4000	0.1 M potassium chloride, 0.1 M sodium HEPES, 15% PEG 5000 MME	0.1 M potassium chloride, 0.1 M sodium HEPES, 15% PEG 5000 MME
pH	6.0	7.0	7.0
Crystal Data			
a,b,c (Å)	225.76, 48.87, 93.4	226.3, 49.26, 93.64	226.44, 49.12, 93.83
α, β, γ (°)	90.0, 92.95, 90.0	90.0, 94.15, 90.0	90.0, 94.85, 90.0
Space group	C 1 2 1	C 1 2 1	C 1 2 1
Resolution (Å)	2.31 – 93.28	2.24 – 56.44	2.17 – 56.41
Outer shell	2.31 – 2.35	2.24 – 2.28	2.17 – 2.21
R-merge (%)	15.7 (216.7)	5.2 (278.6)	2.7 (80)
R-pim	9.1 (121.9)	2.2 (116.9)	3.3 (331)
R-meas (%)	18.2 (249.3)	5.7 (302.6)	8.5 (867)
CC1/2	0.984 (0.383)	0.998 (0.356)	0.999 (0.283)
I / σ(I)	5.3 (0.8)	14.1 (0.3)	11 (0.1)
Completeness (%)	99.8 (96)	99.9 (99.5)	99.9 (99.1)
Multiplicity	3.8 (3.9)	6.6 (6.6)	3.6 (3.8)
Total Measurements	171,581 (8,476)	333,168 (16,176)	363,599 (18,240)
Unique Reflections	45,287 (2,162)	50,123 (2,450)	55,074 (2,715)
Wilson B-factor(Å^2)	41.2	60.3	47
Refinement Statistics			
Resolution Range Used	2.31 – 93.3	2.24 – 56.4	2.17 – 56.4
Non-H Atoms	6779	6,668	6,661
R-work reflections	42,949	43,773	46,243
R-free reflections	2,160	2,140	2,358
R-work/R-free (%)	25.7 / 30.1	28.5 / 34	28.6 / 35.5
rms deviations (target)			
Bond lengths (Å)	0.013 (0.013)	0.021 (0.013)	0.007 (0.013)
Bond Angles (°)	1.939 (1.648)	1.996(1.649)	1.568 (1.648)
[1]Coordinate error	0.40	0.4178	0.383
Mean B value (Å^2)	15.7	56.8	91.4
Ramachandran Statistics			
Favoured/allowed/Outliers	728 / 62 / 26	733 / 65 / 17	693 / 81 / 42
%	89.2 / 7.6 / 3.2	89.8 / 8 / 2.1	84.9 / 9.9 / 5.2

* One crystal was used for determining each structure.
* Figures in brackets refer to outer resolution shell, where applicable.

[1] Figures in brackets are rms targets

[2] Coordinate Estimated Standard Uncertainty in (Å), calculated based on maximum likelihood statistics.

Appendix Table 3. Statistics for 3D structures presented in Chapter 5.

References

Abdul-Rasoul, M., Habib, H., & Al-khouly, M. (2006). The honeymoon phase' in children with type 1 diabetes mellitus: frequency, duration, and influential factors. *Pediatric Diabetes*, *7*, 101–107.

Acierno, P. M., Newton, D. A., Brown, E. A., Maes, L. A., Baatz, J. E., & Gattoni-celli, S. (2003). Cross-reactivity between HLA-A2-restricted FLU-M1:58–66 and HIV p17 GAG:77–85 epitopes in HIV-infected and uninfected individuals. *Journal of Translational Medicine*, *11*, 58–66.

Acosta-Rodriguez, E. V, Rivino, L., Geginat, J., Jarrossay, D., Gattorno, M., Lanzavecchia, A., Sallusto, F., & Napolitani, G. (2007). Surface phenotype and antigenic specificity of human interleukin 17 – producing T helper memory cells. *Nature Immunology*, *8*(6), 639–646. https://doi.org/10.1038/ni1467

Acuto, O., & Michel, F. (2003). CD28-Mediated co-stimilation: A quantitative support for TCR signalling. *Nature Reviews Immunology*, *3*, 939–951. https://doi.org/10.1038/nri1248

Adams, J. J., Narayanan, S., Birnbaum, M. E., Sidhu, S. S., Blevins, S. J., Gee, M. H., Sibener, L. V, Baker, B. M., Kranz, D. M., & Garcia, K. C. (2016). Structural interplay between germline interactions and adaptive recognition determines the bandwidth of TCR-peptide-MHC cross-reactivity. *Nature Immunology*, *17*(1), 1–10. https://doi.org/10.1038/ni.3310

Adrain, C., Murphy, B. M., & Martin, S. J. (2005). Molecular Ordering of the Caspase Activation Cascade Initiated by the Cytotoxic T Lymphocyte/Natural Killer (CTL/NK) Protease Granzyme B. *The Journal of Biological Chemistry*, *280*(6), 4663–4673. https://doi.org/10.1074/jbc.M410915200

Afonina, I. S., Cullen, S. P., & Martin, S. J. (2010). Cytotoxic and non-cytotoxic roles of the CTL ⁄ NK protease granzyme B. *Immunological Reviews*, *235*, 105–116.

Afzali, B., & Lechler, R. I. (2007). Allorecognition and the alloresponse: clinical implications. *Tissue Antigens*, *69*, 545–556. https://doi.org/10.1111/j.1399-0039.2007.00834.x

Alberti, K. G. M. M., & Zimmet, P. Z. (1998). Definition, diagnosis and classification of diabetes mellitus and its complications. Part 1: Diagnosis and classification of diabetes mellitus. Provisional report of a WHO consultation. *Diabetic Medicine*, *15*(7), 539–553. https://doi.org/10.1002/(SICI)1096-9136(199807)15:7<539::AID-DIA668>3.0.CO;2-S

Aleksic, M., Liddy, N., Molloy, P. E., Pumphrey, N., Vuidepot, A., Chang, K., & Jakobsen, B. K. (2012). Different affinity windows for virus and cancer-specific T-cell receptors: Implications for therapeutic strategies. *European Journal of Immunology*, *42*, 3174–

3179. https://doi.org/10.1002/eji.201242606

Alexandra, L., Bonneville, M., Oliver, L., Vallette, M., Vie, H., Jarry, U., Chauvin, C., Jaolland, N., Minault, S., Robard, M., Pecqeur, C., & Scotet, E. (2016). Stereotaxic administrations of allogeneic human Vg9Vd2 T cells efficiently control the development of human glioblastoma brain tumors. *OncoImmunology*, *5*(6). https://doi.org/10.1080/2162402X.2016.1168554

Alimonti, J. B., Shi, L., Baijal, P. K., & Greenberg, A. H. (2001). Granzyme B Induces BID-mediated Cytochrome c Release and Mitochondrial Permeability Transition. *The Journal of Biological Chemistry*, *276*(10), 6974–6982. https://doi.org/10.1074/jbc.M008444200

Anderson, M. S., Venanzi, E. S., Klein, L., Chen, Z., Berzins, S. P., Turley, S. J., Boehmer, H. Von, Bronson, R., Dierich, A., Benoist, C., & Mathis, D. (2002). Projection of an Immunological Self Shadow Within the Thymus by the Aire Protein. *Science*, *298*(November), 1395–1402.

Anton van der Merwe, P., & Davis, S. J. (2003). Molecular Interactions Mediating T Cell Antigen Recognition. *Annual Review of Immunology*, *21*, 659–684. https://doi.org/10.1146/annurev.immunol.21.120601.141036

Archbold, J. K., Macdonald, W. A., Miles, J. J., Brennan, R. M., Kjer-nielsen, L., Mccluskey, J., Burrows, S. R., & Rossjohn, J. (2006). Alloreactivity between Disparate Cognate and Allogeneic pMHC-I Complexes Is the Result of Highly Focused, Peptide-dependent Structural Mimicry. *Journal of Biological Chemistry*, *281*(45), 34324–34332. https://doi.org/10.1074/jbc.M606755200

Ardakani, M. S., Pak, F., Kokhaei, P., & Fazeli, M. S. (2019). In Vitro Evaluation of CMV Specific CD8 T Cells Function in CMV+ Colorectal Cancer Patients Compared to Healthy Controls. *Iran Journal of Allergy, Asthma and Immunology*, *18*(August), 379–392.

Arstila, T. P., Casrouge, A., Baron, V., Even, J., Kanellopoulos, J., & Kourilsky, P. (1999). A direct estimate of the human αβ T cell receptor diversity. *Science*, *286*(5441), 958–961. https://doi.org/10.1126/science.286.5441.958

Artyomov, M. N., Lis, M., Devadas, S., Davis, M. M., & Chakraborty, A. K. (2010). CD4 and CD8 binding to MHC molecules primarily acts to enhance Lck delivery. *PNAS*, *107*(39), 16916–16921. https://doi.org/10.1073/pnas.1010568107/-/DCSupplemental.www.pnas.org/cgi/doi/10.1073/pnas.1010568107

Attaf, M., Holland, S. J., Bartok, I., & Dyson, J. (2016). αβ T cell receptor germline CDR regions moderate contact with MHC ligands and regulate peptide cross-reactivity. *Scientific*

Reports, *6*(February), 1–11. https://doi.org/10.1038/srep35006

Auphan-anezin, N., Mazza, C., Guimezanes, A., Barrett-wilt, G. A., Montero-julian, F., Roussel, A., Hunt, D. F., Malissen, B., & Partial, Á. E. R. K. Á. (2006). Distinct orientation of the alloreactive monoclonal CD8 T cell activation program by three different peptide/ MHC complexes. *European Journal of Immunology*, *36*, 1856–1866. https://doi.org/10.1002/eji.200635895

Bäckström, B. T., Milia, E., Peter, A., Jaureguiberry, B., Baldari, C. T., & Palmer, E. (1996). A motif within the T cell receptor α chain constant region connecting peptide domain controls antigen responsiveness. *Immunity*, *5*(5), 437–447. https://doi.org/10.1016/S1074-7613(00)80500-2

Baeuerle, P. A., Ding, J., Patel, E., Thorausch, N., Horton, H., Gierut, J., Scarfo, I., Choudhary, R., Kiner, O., Krishnamurthy, J., Le, B., Morath, A., Baldeviano, G. C., Quinn, J., Tavares, P., Wei, Q., Weiler, S., Maus, M. V, Getts, D., … Hofmeister, R. (2019). Synthetic TRuC receptors engaging the complete T cell receptor for potent anti-tumor response. *Nature Communications*, *10*, 1–12. https://doi.org/10.1038/s41467-019-10097-0

Bagaev, D. V, Vroomans, R. M. A., Samir, J., Stervbo, U., Dolton, G., Greenshields-watson, A., Attaf, M., Egorov, E. S., Zvyagin, I. V, Babel, N., Cole, D. K., Godkin, A. J., Sewell, A. K., Kesmir, C., Chudakov, D. M., Luciani, F., & Shugay, M. (2019). VDJdb in 2019: database extension , new analysis infrastructure and a T-cell receptor motif compendium. *Nucleic Acids Research*, *48*, 1057–1062. https://doi.org/10.1093/nar/gkz874

Barba-spaeth, G., Dejnirattisai, W., Rouvinski, A., Vaney, M., Medits, I., Sharma, A., Simon-lorière, E., Sakuntabhai, A., & Haouz, A. (2016). Structural basis of potent Zika – dengue virus antibody cross-neutralization. *Nature*, *536*, 48–53. https://doi.org/10.1038/nature18938

Bassing, C. H., Alt, F. W., Hughes, M. M., Auteuil, M. D., Wehrly, T. D., Woodman, B. B., White, J. M., Davidson, L., & Sleckman, B. P. (2000). Recombination signal sequences restrict chromosomal V(D)J recombination beyond the 12/23 rule. *Letters to Nature*, *405*, 3–6.

Bassing, C. H., Swat, W., & Alt, F. W. (2002). The mechanism and regulation of chromosomal V(D)J recombination. *Cell*, *109*(2 SUPPL. 1), 45–55. https://doi.org/10.1016/S0092-8674(02)00675-X

Beach, D., Gonen, R., Bogin, Y., Reischl, I. G., & Yablonski, D. (2007). Dual Role of SLP-76 in Mediating T Cell Receptor-induced Activation of Phospholipase C-γ1. *The Journal of Biological Chemistry*, *282*(5), 2937–2946. https://doi.org/10.1074/jbc.M606697200

Belkhir, R., Burel, S. Le, Dunogeant, L., Marabelle, A., Hollebecque, A., Besse, B., Leary, A.,

Voisin, A., Pontoizeau, C., Coutte, L., Pertuiset, E., Mouterde, G., Fain, O., Lambotte, O., & Mariette, X. (2017). Rheumatoid arthritis and polymyalgia rheumatica occurring after immune checkpoint inhibitor treatment. *Ann Rheum Dis*, *76*, 1747–1750. https://doi.org/10.1136/annrheumdis-2017-211216

Bennett, M. S., Joseph, A., Ng, H. L., Goldstein, H., & Yang, O. O. (2010). Fine-tuning of T-cell receptor avidity to increase HIV epitope variant recognition by cytotoxic T lymphocytes. *AIDS*, *24*, 2619–2628. https://doi.org/10.1097/QAD.0b013e32833f7b22

Beringer, D. X., Kleijwegt, F. S., Wiede, F., Slik, A. R. Van Der, Loh, K. L., Petersen, J., Dudek, N. L., Duinkerken, G., Laban, S., Joosten, A., Vivian, J. P., Chen, Z., Uldrich, A. P., Godfrey, D. I., Mccluskey, J., Price, D. A., Radford, K. J., Purcell, A. W., Nikolic, T., … Rossjohn, J. (2015). T cell receptor reversed polarity recognition of a self-antigen major histocompatibility complex. *Nature Immunology*, *16*(11), 1153–1161. https://doi.org/10.1038/ni.3271

Betts, M. R., Brenchley, J. M., Price, D. A., Rosa, S. C. De, Douek, D. C., Roederer, M., & Koup, R. A. (2003). Sensitive and viable identification of antigen-specific CD8 + T cells by a flow cytometric assay for degranulation. *Journal of Immunological Methods*, *281*, 65–78. https://doi.org/10.1016/S0022-1759(03)00265-5

Bhardwaj, V., Kumar, V., Geysen, H. M., & Sercarz, E. E. (1993). Degenerate recognition of a dissimilar antigenic peptide by myelin basic protein-reactive T cells: Implications for thymic education and autoimmunity. *Journal of Immunology*, *151*(9), 5000–5010.

Bhella, D. (2019). Cryo-electron microscopy: an introduction to the technique, and considerations when working to establish a national facility. *Biophysical Reviews*, *11*, 515–519.

Bianchi, V., Bulek, A., Fuller, A., Lloyd, A., Attaf, M., Rizkallah, P. J., Dolton, G., Sewell, A. K., & Cole, D. K. (2016). A Molecular Switch Abrogates Glycoprotein 100 (gp100) T-cell Receptor (TCR) Targeting of a Human Melanoma Antigen. *Journal of Biological Chemistry*, *291*(17), 8951–8959. https://doi.org/10.1074/jbc.M115.707414

Birnbaum, M. E., Mendoza, J. L., Sethi, D. K., Dong, S., Glanville, J., Dobbins, J., Davis, M. M., Wucherpfennig, K. W., & Garcia, K. C. (2014). Deconstructing the Peptide-MHC Specificity of T Cell Recognition. *Cell*, *157*, 1073–1087. https://doi.org/10.1016/j.cell.2014.03.047

Bjorkman, P. J., Saper, M. A., Samraoui, B., Bennett, W. S., Strominger, J. L., & Wiley, D. C. (1987). Structure of the human class I histocompatibility antigen, HLA-A2. *Nature*, *329*, 506–512.

Blair, M. (2016). Diabetes Mellitus Review. *Urologic Nursing*, *36*(1), 27–36. https://doi.org/10.7257/1053-816x.2016.36.1.27

Blum, J. S., & Cresswell, P. (1988). Role for intracellular proteases in the processing and transport of class II HLA antigens. *Proc Natl Acad Sci USA*, *85*, 3975–3979.

Boehmer, H. Von, & Hans, J. (1997). Structure and function of thepre-T cell receptor. *Annual Review of Immunology*, *15*, 433–452.

Bonilla, F. a, & Oettgen, H. C. (2010). Adaptive immunity. *The Journal of Allergy and Clinical Immunology*, *125*, 33–40. https://doi.org/10.1016/j.jaci.2009.09.017

Borbulevych, O. Y., Piepenbrink, K. H., Gloor, B. E., Scott, D. R., Sommese, R. F., Cole, D. K., Sewell, A. K., & Baker, B. M. (2009). T Cell Receptor Cross-reactivity Directed by Antigen-Dependent Tuning of Peptide-MHC Molecular Flexibility. *Immunity*, *31*(6), 885–896. https://doi.org/10.1016/j.immuni.2009.11.003

Borbulevych, O. Y., Santhanagopolan, S. M., Hossain, M., & Baker, B. M. (2011). TCRs Used in Cancer Gene Therapy Cross-React with MART-1/Melan-A Tumor Antigens via Distinct Mechanisms. *The Journal of Immunology*, *187*(5), 2453–2463. https://doi.org/10.4049/jimmunol.1101268

Borch, T. H., Andersen, R., Ellebaek, E., Met, Ö., Donia, M., & Svane, I. M. (2020). Future role for adoptive T-cell therapy in checkpoint inhibitor-resistant metastatic melanoma. *Journal for ImmunoTherapy of Cancer*, *8*, 1–7. https://doi.org/10.1136/jitc-2020-000668

Boulter, J. M., Glick, M., Todorov, P. T., Baston, E., Sami, M., Rizkallah, P., & Jakobsen, B. K. (2003). Stable, soluble T-cell receptor molecules for crystallization and therapeutics. *Protein Engineering Design and Selection*, *16*(9), 707–711. https://doi.org/10.1093/protein/gzg087

Boulter, J. M., Schmitz, N., Sewell, A. K., Godkin, A. J., Bachmann, M. F., & Gallimore, A. M. (2007). Potent T cell agonism mediated by a very rapid TCR / pMHC interaction. *European Journal of Immunology*, *37*, 798–806. https://doi.org/10.1002/eji.200636743

Bovay, A., Zoete, V., Dolton, G., Bulek, A. M., Cole, D. K., Rizkallah, P. J., Fuller, A., Beck, K., Michielin, O., Speiser, D. E., Sewell, A. K., & Marraco, S. A. F. (2018). T cell receptor alpha variable 12-2 bias in the immunodominant response to Yellow fever virus. *European Journal of Immunology*, *48*, 258–272. https://doi.org/10.1002/eji.201747082

Bowlus, C. L., Ahn, J., Chu, T., & Gruen, J. R. (1999). Cloning of a Novel MHC-Encoded Serine Peptidase Highly Expressed by Cortical Epithelial Cells of the Thymus. *Cellular Immunology*, *86*, 80–86.

Brady, B. L., Steinel, N. C., & Bassing, C. H. (2010). Antigen Receptor Allelic Exclusion: An Update and Reappraisal. *The Journal of Immunology*, *185*(7), 3801–3808. https://doi.org/10.4049/jimmunol.1001158

Brentjens, R. J., Latouche, J., Santos, E., Marti, F., Gong, M. C., Lddane, C., King, P. D., Larson, S., Weiss, M., Riviere, I., & Sadelain, M. (2003). Eradication of systemic B-cell tumors by genetically targeted human T lymphocytes co-stimulated by. *Nature Medicine*, *9*(3), 279–286. https://doi.org/10.1038/nm

Bridgeman, J. S., Sewell, K., Miles, J. J., Price, D. A., & Cole, D. K. (2011). Structural and biophysical determinants of ab T-cell antigen recognition. *Immunology*, *135*, 9–18. https://doi.org/10.1111/j.1365-2567.2011.03515.x

Brown, C. E., Ph, D., Alizadeh, D., Ph, D., Starr, R., Ostberg, J. R., Ph, D., Blanchard, M. S., Ph, D., Kilpatrick, J., Simpson, J., Kurien, A., Priceman, S. J., Ph, D., Wang, X., Ph, D., Harshbarger, T. L., Apuzzo, M. D., Ressler, J. A., … Badie, B. (2016). Regression of Glioblastoma after Chimeric Antigen Receptor T-Cell Therapy. *The New England Journal of Medicine*, *375*(26), 2561–2569. https://doi.org/10.1056/NEJMoa1610497

Brown, J. H., Jardetzky, T. S., Gorga, J. C., Stern, L. J., Urban, R. G., Strominger, J. L., & Wiley, D. C. (1993). Three-dimensional structure of the human class II histocompatibility antigen HLA-DR1. *Nature*, *364*(6432), 33–39. https://doi.org/10.1038/364033a0

Brown, S. D., Warren, R. L., Gibb, E. A., Martin, S. D., Spinelli, J. J., Nelson, B. H., & Holt, R. A. (2014). Neo-antigens predicted by tumor genome meta-analysis correlate with increased patient survival. *Genome Research*, *24*, 743–750. https://doi.org/10.1101/gr.165985.113.Freely

Bulek, A. M., Cole, D. K., Skowera, A., Dolton, G., Gras, S., Madura, F., Fuller, A., Miles, J. J., Gostick, E., Price, D. A., Jan, W., Knight, R. R., Huang, G. C., Lissin, N., Molloy, P. E., Jakobsen, B. K., Rossjohn, J., Peakman, M., & Pierre, J. (2012). Structural basis of human β-cell killing by CD8+ T cells in Type 1 diabetes. *Nature Immunology*, *13*(3), 283–289. https://doi.org/10.1038/ni.2206.Structural

Bulek, A. M., Madura, F., Fuller, A., Holland, C. J., Schauenburg, A. J. a, Sewell, A. K., Rizkallah, P. J., & Cole, D. K. (2012). TCR/pMHC Optimized Protein crystallization Screen. *Journal of Immunological Methods*, *382*(1–2), 203–210. https://doi.org/10.1016/j.jim.2012.06.007

Burnet, F. M. (1957). A Modification of Jerne's Theory of Antibody Production using the Concept of Clonal Selection. *Australian Journal of Science*, *20*(3), 67–69. https://doi.org/10.3322/canjclin.26.2.119

Burrows, S. R., Chen, Z., Archbold, J. K., Tynan, F. E., Beddoe, T., Kjer-Nielsen, L., Miles, J. J., Khanna, R., Moss, D. J., Liu, Y. C., Gras, S., Kostenko, L., Brennan, R. M., Clements, C. S., Brooks, A. G., Purcell, A. W., McCluskey, J., & Rossjohn, J. (2010). Hard wiring of T cell receptor specificity for the major histocompatibility complex is underpinned by TCR adaptability. *Proceedings of the National Academy of Sciences of the United States of America*, *107*(23), 10608–10613. https://doi.org/10.1073/pnas.1004926107

Canavan, J. B., Scottà, C., Vossenkämper, A., Goldberg, R., Elder, M. J., Shoval, I., Marks, E., Stolarczyk, E., Lo, J. W., Powell, N., Fazekasova, H., Irving, P. M., Sanderson, J. D., Howard, J. K., Yagel, S., Afzali, B., Macdonald, T. T., Hernandez-fuentes, M. P., Shpigel, N. Y., … Lord, G. M. (2016). Developing in vitro expanded CD45RA+ regulatory T cells as an adoptive cell therapy for Crohn's disease. *Gut*, *65*, 584–594. https://doi.org/10.1136/gutjnl-2014-306919

Candia, M., & Pickl, W. F. (2016). On Peptides and Altered Peptide Ligands: From Origin, Mode of Action and Design to Clinical Application. *Int Arch Allergy Immunol*, *170*, 211–233. https://doi.org/10.1159/000448756

Cantoni, N., Hirsch, H. H., Khanna, N., Gerull, S., Buser, A., Bucher, C., Heim, D., Gratwohl, A., & Stern, M. (2010). Evidence for a Bidirectional Relationship between Cytomegalovirus Replication and acute Graft-versus-Host Disease. *American Society for Blood and Marrow Transplantation*, *16*, 1309–1314. https://doi.org/10.1016/j.bbmt.2010.03.020

Carreno, L. J., Bueno, S., Bull, P., Nathenson, S., & Kalergis, A. (2007). The half-life of the T-cell receptor / peptide – major histocompatibility complex interaction can modulate T-cell activation in response to bacterial challenge. *Immunolgy*, *121*, 227–237. https://doi.org/10.1111/j.1365-2567.2007.02561.x

Carrington, P. E., Sandu, C., Wei, Y., Hill, J. M., Morisawa, G., Huang, T., Gavathiotis, E., Wei, Y., & Werner, M. H. (2006). The Structure of FADD and Its Mode of Interaction with Procaspase-8. *Molecular and Cellular Biology*, *22*, 599–610. https://doi.org/10.1016/j.molcel.2006.04.018

Chapuis, A. G., Egan, D. N., Bar, M., Schmitt, T. M., Mcafee, M. S., Paulson, K. G., Voillet, V., Gottardo, R., Ragnarsson, G. B., Bleakley, M., Yeung, C. C., Muhlhauser, P., Nguyen, H. N., Kropp, L. A., Castelli, L., Wagener, F., Hunter, D., Lindberg, M., Cohen, K., … Greenberg, P. D. (2019). T cell receptor gene therapy targeting WT1 prevents acute myeloid leukemia relapse post-transplant. *Nature Medicine*, *25*(July), 1064–1072. https://doi.org/10.1038/s41591-019-0472-9

Chayen, N. E., Saridakis, E., & Sear, R. P. (2005). Experiment and theory for heterogeneous

nucleation of protein crystals in a porous medium. *PNAS*, *103*(3), 597–601.

Chen, T., & Hudnall, S. D. (2006). Anatomical mapping of human herpesvirus reservoirs of infection. *Modern Pathology*, *19*, 726–737. https://doi.org/10.1038/modpathol.3800584

Cheroutre, H., & Lambolez, F. (2008). Doubting the TCR Coreceptor Function of CD8 aa. *Immunity*, *February*, 149–159. https://doi.org/10.1016/j.immuni.2008.01.005

Chiu, C., Mccausland, M., Sidney, J., Duh, F., Rouphael, N., Mehta, A., Mulligan, M., Carrington, M., Wieland, A., Sullivan, N. L., Weinberg, A., Levin, M. J., Pulendran, B., Peters, B., Sette, A., & Ahmed, R. (2014). Broadly Reactive Human CD8 T Cells that Recognize an Epitope Conserved between VZV , HSV and EBV. *Plos Pathogens*, *10*(3), 1–12. https://doi.org/10.1371/journal.ppat.1004008

Choudhuri, K., Parker, M., Milicic, A., Cole, D. K., Shaw, M. K., Sewell, A. K., Stewart-jones, G., Dong, T., Gould, K. G., & Anton van der Merwe, P. (2009). Peptide-Major Histocompatibility Complex Dimensions Control Proximal Kinase-Phosphatase Balance during. *Journal of Biological Chemistry*, *284*(38), 26096–26105. https://doi.org/10.1074/jbc.M109.039966

Choudhuri, K., Wiseman, D., Brown, M. H., Gould, K., & Van Der Merwe, P. (2005). T-cell receptor triggering is critically dependent on the dimensions of its peptide-MHC ligand. *Letters to Nature*, *436*(July), 578–582. https://doi.org/10.1038/nature03843

Cole, D. K., Bulek, A. M., Dolton, G., Schauenberg, A. J., Szomolay, B., Rittase, W., Trimby, A., Jothikumar, P., Fuller, A., Skowera, A., Rossjohn, J., Zhu, C., Miles, J. J., Peakman, M., Wooldridge, L., Rizkallah, P. J., & Sewell, A. K. (2016). Hotspot autoimmune T cell receptor binding underlies pathogen and insulin peptide cross-reactivity. *Journal of Clinical Investigation*, *126*(6), 2191–2204. https://doi.org/10.1172/JCI85679

Cole, D. K., Edwards, E. S. J., Wynn, K. K., Clement, M., Miles, J. J., Ladell, K., Ekeruche, J., Gostick, E., Adams, K. J., Skowera, A., Peakman, M., Wooldridge, L., Price, D. A., & Sewell, A. K. (2010). Modification of MHC Anchor Residues Generates Heteroclitic Peptides That Alter TCR Binding and T Cell Recognition. *The Journal of Immunology*, *185*(4), 2600–2610. https://doi.org/10.4049/jimmunol.1000629

Cole, D. K., Pumphrey, N. J., Boulter, J. M., Sami, M., Bell, J. I., Gostick, E., Price, D. A., Gao, G. F., Sewell, A. K., Jakobsen, B. K., Cole, D. K., Pumphrey, N. J., Boulter, J. M., Sami, M., Bell, J. I., Gostick, E., Price, D. A., Gao, G. F., Sewell, A. K., & Jakobsen, B. K. (2007). Human TCR-Binding Affinity is Governed by MHC Class Restriction. *The Journal of Immunology*, *178*, 5727–5734. https://doi.org/10.4049/jimmunol.178.9.5727

Cole, D. K., Rizkallah, P. J., Sewell, A. K., Cole, D. K., Bulek, A. M., Dolton, G., Schauenberg, A. J., Szomolay, B., Rittase, W., Trimby, A., Jothikumar, P., Fuller, A., Skowera, A., Rossjohn, J., Zhu, C., Miles, J. J., Peakman, M., Wooldridge, L., Rizkallah, P. J., & Sewell, A. K. (2016). Hotspot autoimmune T cell receptor binding underlies pathogen and insulin peptide cross- reactivity. *Journal of Clinical Investigation*, *126*(September), 2191–2204. https://doi.org/10.1172/JCI85679.Several

Cole, D. K., Sami, M., Scott, D. R., Rizkallah, P. J., Borbulevych, O. Y., Todorov, P. T., Moysey, R. K., Jakobsen, B. K., Boulter, J. M., & Baker, B. M. (2013). Increased peptide contacts govern high affinity binding of a modifiedTCR whilst maintaining a native pMHC docking mode. *Frontiers in Immunology*, *4*(June), 1–8. https://doi.org/10.3389/fimmu.2013.00168

Cole, D. K., van den Berg, H. A., Lloyd, A., Crowther, M. D., Beck, K., Ekeruche-Makinde, J., Miles, J. J., Bulek, A. M., Dolton, G., Schauenburg, A. J., Wall, A., Fuller, A., Clement, M., Laugel, B., Rizkallah, P. J., Wooldridge, L., & Sewell, A. K. (2017). Structural mechanism underpinning cross-reactivity of a CD8+ T-cell clone that recognises a peptide derived from human telomerase reverse transcriptase. *Journal of Biological Chemistry*, *292*, 802–813. https://doi.org/10.1074/jbc.M116.741603

Cole, D. K., Yuan, F., Rizkallah, P. J., Miles, J. J., Gostick, E., Price, D. a., Gao, G. F., Jakobsen, B. K., & Sewell, A. K. (2009). Germ line-governed recognition of a cancer epitope by an immunodominant human T-cell receptor. *Journal of Biological Chemistry*, *284*(40), 27281–27289. https://doi.org/10.1074/jbc.M109.022509

Colf, L. A., Bankovich, A. J., Hanick, N. A., Bowerman, N. A., Jones, L. L., Kranz, D. M., & Garcia, K. C. (2007). How a Single T Cell Receptor Recognizes Both Self and Foreign MHC. *Cell*, *1*, 135–146. https://doi.org/10.1016/j.cell.2007.01.048

Cosmi, L., Cimaz, R., Maggi, L., Santarlasci, V., Capone, M., Borriello, F., Frosali, F., Querci, V., Simonini, G., Barra, G., Piccinni, M. P., Liotta, F., Palma, R. De, Maggi, E., Romagnani, S., & Annunziato, F. (2011). Evidence of the Transient Nature of the Th17 Phenotype of CD4 ᵋ CD161 ᵋ T Cells in the Synovial Fluid of Patients With Juvenile Idiopathic Arthritis. *Arthritis and Rheumatology*, *63*(8), 2504–2515. https://doi.org/10.1002/art.30332

Coulie, P. G., Brichard, V., Van Pel, A., Wolfel, T., Schneider, J., Traverari, C., Mattei, S., Plaen, E., Lurquin, C., Szikora, J. P., Renauld, J. C., & Boon, T. (1996). A new gene coding for an antigen recognized by autologous cytolytic T lymphocytes on a human renal carcinoma. *Immunogenetics*, *44*(5), 323–330. https://doi.org/10.1007/BF02602776

Crean, R. M., Maclachlan, B. J., Madura, F., Whalley, T., Rizkallah, P. J., Holland, C. J.,

Mcmurran, C., Harper, S., Godkin, A., Sewell, A. K., Pudney, C. R., Kamp, M. W. Van Der, & Cole, D. K. (2020). Molecular Rules Underpinning Enhanced Affinity Binding of Human T Cell Receptors Engineered for Immunotherapy. *Molecular Therapy: Oncolytics*, *18*(September), 443–456. https://doi.org/10.1016/j.omto.2020.07.008

Critchfield, J. M., Racke, M. K., Zúñiga-pflücker, J. C., Raine, C. S., Goverman, J., Lenardo, M. J., Critchfield, J. M., Racke, M. K., Zunriga-pflucker, J. C., Cannella, B., Raine, C. S., Goverman, J., & Lenardot, M. J. (1994). T Cell Deletion in High Antigen Dose Therapy of Autoimmune Encephalomyelitis. *American Association for the Advancement of Science*, *263*(5150), 1139–1143.

D'arcy, A. D., Villard, F., & Marsh, M. (2007). An automated microseed matrix-screening method for protein crystallization. *Biological Crystallography*, *D63*, 550–554. https://doi.org/10.1107/S0907444907007652

Dai, S., Huseby, E. S., Rubtsova, K., Scott-Browne, J., Crawford, F., Macdonald, W. a., Marrack, P., & Kappler, J. W. (2008). Crossreactive T Cells Spotlight the Germline Rules for ab T Cell-Receptor Interactions with MHC Molecules. *Immunity*, *28*(3), 324–334. https://doi.org/10.1016/j.immuni.2008.01.008

Daniels, M. A., Devine, L., Miller, J. D., Moser, J. M., Lukacher, A. E., Altman, J. D., Kavathas, P., Hogquist, K. A., Jameson, S. C., & Haven, N. (2001). CD8 Binding to MHC Class I Molecules Is Influenced by T Cell Maturation and Glycosylation. *Immunity*, *15*, 1051–1061.

Davenport, B. M. P., Smith, K. J., Barouch, D., Reid, S. W., Bodnar, W. M., Willis, A. C., Hunt, D. F., & Hill, A. V. S. (1997). HLA Class I Binding Motifs Derived from Random Peptide Libraries Differ at the COOH Terminus from Those of Elute Peptides. *Journal of Experimental Medicine*, *185*(2).

Davis, M. M., & Bjorkmant, P. J. (1988). T-cell antigen receptor genes and T-cell recognition. *Nature*, *334*, 395–402.

Davis, S. J., Ikemizu, S., Evans, E. J., Fugger, L., Bakker, T. R., & Merwe, P. A. Van Der. (2003). The nature of molecular recognition by T cells. *Nat Rev Immunol*, *4*(3), 217–224.

Davis, S. J., & Merwe, P. A. Van Der. (2006). The kinetic-segregation model : TCR triggering and beyond. *Nature Immunology*, *7*(8), 803–809. https://doi.org/10.1038/ni1369

Deng, L., Langley, R. J., Wang, Q., Topalian, S. L., & Mariuzza, R. A. (2012). Structural insights into the editing of germ-line-encoded interactions between T-cell receptor and MHC class II by Vα CDR3. *Proceedings of the National Academy of Sciences of the United States of America*, *109*(37), 14960–14965. https://doi.org/10.1073/pnas.1207186109

Desiderio, S. V, Yancopoulost, G. D., Paskind, M., Thomas, E., Boss, M. A., Landau, N., Altt, F. W., & Baltimore, D. (1984). Insertion of N regions into heavy-chain genes is correlated with expression of terminal deoxytransferase in B cells. *Letters to Nature*, *311*, 16–19.

Dolton, G., Tungatt, K., Lloyd, A., Bianchi, V., Theaker, S. M., Trimby, A., Holland, C. J., Donia, M., Godkin, A. J., Cole, D. K., Thor Straten, P., Peakman, M., Svane, I. M., & Sewell, A. K. (2015). More tricks with tetramers: A practical guide to staining T cells with peptide-MHC multimers. *Immunology*, *146*(1), 11–22. https://doi.org/10.1111/imm.12499

Dolton, G., Zervoudi, E., Rius, C., Wall, A., Thomas, H. L., Fuller, A., Yeo, L., Legut, M., Wheeler, S., Attaf, M., Chudakov, D. M., Choy, E., Peakman, M., & Sewell, A. K. (2018). Optimized peptide-MHC multimer protocols for detection and isolation of autoimmune T-cells. *Frontiers in Immunology*, *9*(JUN), 1–18. https://doi.org/10.3389/fimmu.2018.01378

Dominguez-Romero, A. N., Martinez-Cortes, F., Munguia, M. E., Odales, J., Gevorkian, G., & Manoutcharian, K. (2020). Generation of multiepitope cancer vaccines based on large combinatorial libraries of survivin-derived mutant epitopes. *Immunolgy*, 123–138. https://doi.org/10.1111/imm.13233

Dong, D., Zheng, L., Lin, J., Zhang, B., Zhu, Y., Li, N., Xie, S., Wang, Y., Gao, N., & Huang, Z. (2019). Structural basis of assembly of the human T cell receptor–CD3 complex. *Nature*, *573*(7775), 546–552. https://doi.org/10.1038/s41586-019-1537-0

Donia, M., Junker, N., Ellebaek, E., Andersen, M. H., Straten, P. T., & Svane, I. M. (2012). Characterization and comparison of “standard” and “young” tumour-infiltrating lymphocytes for adoptive cell therapy at a danish translational research institution. *Scandinavian Journal of Immunology*, *75*(2), 157–167. https://doi.org/10.1111/j.1365-3083.2011.02640.x

Dudley, M. E., Wunderlich, J. R., Robbins, P. F., Yang, J. C., Hwu, P., Schwartzentruber, D. J., Topalian, S. L., Sherry, R., Restifo, N. P., Hubicki, A. M., Robinson, M. R., Raffeld, M., Duray, P., Seipp, C. A., Rogers-freezer, L., Morton, K. E., Mavroukakis, S. A., White, D. E., & Rosenberg, S. A. (2002). Cancer Regression and Autoimmunity in Patients After Clonal Repopulation with Antitumor Lymphocytes. *Science Reports*, *298*(October), 850–855.

Dudley, M. E., Yang, J. C., Sherry, R., Hughes, M. S., Royal, R., Kammula, U., Robbins, P. F., Huang, J., Citrin, D. E., Leitman, S. F., Wunderlich, J., Restifo, N. P., Thomasian, A., Downey, S. G., Smith, F. O., Klapper, J., Morton, K., Laurencot, C., White, D. E., & Rosenberg, S. A. (2008). Adoptive Cell Therapy for Patients With Metastatic Melanoma: Evaluation of Intensive Myeloablative Chemoradiation Preparative Regimens. *Journal*

of Clinical Oncology, *26*(32), 5233–5239. https://doi.org/10.1200/JCO.2008.16.5449

Dupont-rouzeyrol, M., Connor, O. O., Calvez, E., Daures, M., John, M., Grangeon, J., & Gourinat, A. (2015). Co-infection with Zika and Dengue Viruses in 2 Patients , New Caledonia , 2014 Fatal Meningoencephalitis in Child and Isolation of Naegleria fowleri from Hot Springs in Costa Rica. *Emerging Infectious Diseases*, *21*(2), 381–382.

Early, P., Huang, H., Davis, M., Calame, K., & Hood, L. (1980). An lmmunoglobulin Heavy Chain Variable Region Gene Is Generated from Three Segments of DNA: VH , D and JH. *Cell*, *19*, 981–992.

Ege, M. J., Mayer, M., Normand, A. C., Genuneit, J., Cookson, W. O. C. M., Braun-Fahrlander, C., Heederik, D., Piarroux, R., & von Mutis, E. (2011). Exposure to Environmental Microorganisms and Childhood Asthma. *New England Journal of Medicine*, *364*(8), 701–709.

Egerton, M., Shortman, K., & Scollay, R. (1990). The kinetics of immature murine thymocyte development in vivo. *International Immunology*, *2*(6), 501–506.

Eibel, H., Kraus, H., Sic, H., Kienzler, A. K., & Rizzi, M. (2014). B cell biology: An overview topical collection on basic and applied science. *Current Allergy and Asthma Reports*, *14*(5). https://doi.org/10.1007/s11882-014-0434-8

Ekeruche-makinde, J., Clement, M., Cole, D. K., Edwards, E. S. J., Ladell, K., Miles, J. J., Matthews, K. K., Fuller, A., Lloyd, K. A., Madura, F., Dolton, G. M., Pentier, J., Lissina, A., Gostick, E., Baxter, T. K., Baker, B. M., Rizkallah, P. J., Price, D. A., Wooldridge, L., & Sewell, A. K. (2012). T-cell Receptor-optimized Peptide Skewing of the T-cell Repertoire Can Enhance Antigen Targeting. *Journal of Biological Chemistry*, *287*(44), 37269–37281. https://doi.org/10.1074/jbc.M112.386409

Ekeruche-Makinde, J., Miles, J. J., Van Den Berg, H. A., Skowera, A., Cole, D. K., Dolton, G., Schauenburg, A. J. A., Tan, M. P., Pentier, J. M., Llewellyn-Lacey, S., Miles, K. M., Bulek, A. M., Clement, M., Williams, T., Trimby, A., Bailey, M., Rizkallah, P., Rossjohn, J., Peakman, M., … Wooldridge, L. (2013). Peptide length determines the outcome of TCR/peptide-MHCI engagement. *Blood*, *121*(7), 1112–1123. https://doi.org/10.1182/blood-2012-06-437202

Ellebaek, E., Iversen, T., Junker, N., Donia, M., Engell-Noerregaard, L., Met, Ö., Hölmich, L., Andersen, R., Hadrup, S., Andersen, M., thor Straten, P., & Svane, I. (2012). Adoptive cell therapy with autologous tumor infiltrating lymphocytes and low-dose Interleukin-2 in metastatic melanoma patients. *Journal of Translational Medicine*, *10*(169). https://doi.org/10.1186/1479-5876-10-169

Elliott, S. L., Suhrbier, A., Miles, J. J., Lawrence, G., Pye, S. J., Le, T. T., Rosenstengel, A., Nguyen, T., Allworth, A., Burrows, S. R., Cox, J., Pye, D., Moss, D. J., & Bharadwaj, M. (2008). Phase I Trial of a CD8+ T-Cell Peptide Epitope-Based Vaccine for Infectious Mononucleosis. *Journal of Virology*, *82*(3), 1448–1457. https://doi.org/10.1128/JVI.01409-07

Elliott, T., Townsend, A., & Cerundolo, V. (1990). Naturally processed peptides. *Nature News and Views*, *348*, 195–197.

Emsley, P., & Cowtan, K. (2004). Coot: model-building tools for molecular graphics research. *Acta Crystallographica Section D Biological Crystallography*, *D60*, 2126–2132. https://doi.org/10.1107/S0907444904019158

European Bioinformatics Institute. (2020). https://www.ebi.ac.uk/ipd/imgt/hla/stats.html

Evnouchidou, I., Weimershaus, M., Saveanu, L., & van Endert, P. (2014). ERAP1–ERAP2 Dimerization Increases Peptide-Trimming Efficiency. *The Journal of Immunology*, *193*(2), 901–908. https://doi.org/10.4049/jimmunol.1302855

Fahl, S. P., Coffey, F., & Wiest, D. L. (2014). Origins of γδ T Cell Effector Subsets: A Riddle Wrapped in an Enigma. *The Journal of Immunology*, *193*(9), 4289–4294. https://doi.org/10.4049/jimmunol.1401813

Farhood, B. (2019). CD8 + cytotoxic T lymphocytes in cancer immunotherapy : A review. *Journal of Cellular Physiology*, *234*, 8509–8521. https://doi.org/10.1002/jcp.27782

Felder, S., Zhou, M., Hu, P., Ureña, J., Ullrich, A., Chaudhuri, M., White, M., Shoelson, S. E., & Schlessinger, J. (1993). SH2 domains exhibit high-affinity binding to tyrosine-phosphorylated peptides yet also exhibit rapid dissociation and exchange. *Molecular and Cellular Biology*, *13*(3), 1449–1455. https://doi.org/10.1128/mcb.13.3.1449-1455.1993

Feng, D., Bond, C. J., Ely, L. K., Maynard, J., & Garcia, K. C. (2007). Structural evidence for a germline-encoded T cell receptor-major histocompatibility complex interaction "codon". *Nature Immunology*, *8*(9), 975–983. https://doi.org/10.1038/ni1502

Fontenot, J. D., Gavin, M. A., & Rudensky, A. Y. (2003). Foxp3 programs the development and function of CD4+ CD25+ regulatory T cells. *Nature Immunology*, *4*, 330–336. https://doi.org/10.1038/ni904

Fouchier, R. A. M., Ph, D., Berger, A., Ph, D., Burguière, A., Ph, D., Cinatl, J., Ph, D., Eickmann, M., Ph, D., Escriou, N., Ph, D., Grywna, K., Sc, M., Kramme, S., Manuguerra, J., Ph, D., Müller, S., Sc, M., … Doerr, H. W. (2003). Identification of a Novel Coronavirus in Patients with Severe Acute Respiratory Syndrome. *The New England Journal of*

Medicine, *348*, 1967–1976.

Freeman, G. J., Long, A. J., Iwai, Y., Bourque, K., Chernova, T., Nishimura, H., Fitz, L. J., Malenkovich, N., Okazaki, T., Byrne, M. C., Horton, H. F., Fouser, L., Carter, L., Ling, V., Bowman, M. R., Carreno, B. M., Collins, M., Wood, C. R., & Honjo, T. (2000). Engagement of the PD-1 Immunoinhibitory Receptor by a Novel B7 Family Member Leads to Negative Regulation of Lymphocyte Activation. *Journal of Experimental Medicine*, *192*(7), 1027–1034.

Frey, A. B. (2015). Suppression of T cell responses in the tumor microenvironment. *Vaccine*, *33*(51), 7393–7400. https://doi.org/10.1016/j.vaccine.2015.08.096

Fry, T. J., Shah, N. N., Orentas, R. J., Stetler-stevenson, M., Yuan, C. M., Ramakrishna, S., Wolters, P., Martin, S., Delbrook, C., Yates, B., Shalabi, H., Fountaine, T. J., Shern, J. F., Majzner, R. G., Stroncek, D. F., Sabatino, M., Feng, Y., Dimitrov, D. S., Zhang, L., … Mackall, C. L. (2018). CD22-targeted CAR T cells induce remission in B-ALL that is naive or resistant to CD19-targeted CAR immunotherapy. *Nature Medicine*, *24*(1), 20–28. https://doi.org/10.1038/nm.4441

Fuller, A., Wall, A., Crowther, M., Lloyd, A., Zhurov, A., Sewell, A., Cole, D., & Beck, K. (2017). Thermal Stability of Heterotrimeric pMHC Proteins as Determined by Circular Dichroism Spectroscopy. *Bio-Protocol*, *7*(13). https://doi.org/10.21769/bioprotoc.2366

Galloway, S. A. E., Dolton, G., Attaf, M., Wall, A., Fuller, A., Rius, C., Bianchi, V., Theaker, S., Lloyd, A., Caillaud, M. E., Svane, I. M., Donia, M., Cole, D. K., Szomolay, B., Rizkallah, P., & Sewell, A. K. (2019). Peptide super-agonist enhances T-cell responses to melanoma. *Frontiers in Immunology*, *10*(MAR), 1–18. https://doi.org/10.3389/fimmu.2019.00319

Gao, G. F., Tormo, J., Gerth, U. C., Wyer, J. R., Mcmichael, A. J., Stuart, D. I., Bell, J. I., Jones, E. Y., & Jakobsen, B. K. (1997). Crystal structure of the complex between human CD8aa and HLA-A2. *Letters to Nature*, *387*, 630–634.

Garboczi, D. N., Ghosh, P., Utz, U., Fan, Q. R., Biddison, W. E., & Wiley, D. C. (1996). Structure of the complex between human T-cell receptor, viral peptide and HLA-A2. *Nature*, *384*(6605), 134–141. https://doi.org/10.1038/384134a0

Garcia, K. C., Adams, J. J., Feng, D., & Ely, L. K. (2009). The molecular basis of TCR germline bias for MHC is surprisingly simple. *Nature Immunology*, *10*(2), 143–147. https://doi.org/10.1038/ni.f.219

Garcia, K. C., Degano, M., Pease, L. R., Huang, M., Peterson, P. A., Teyton, L., & Wilson, I. A. (1998). Structural Basis of Plasticity in T Cell Receptor Recognition of a Self Peptide – MHC Antigen. *Science*, *279*(February), 1166–1172.

Gee, M. H., Han, A., Lofgren, S. M., Quake, S. R., Davis, M. M., Garcia, K. C., Gee, M. H., Han, A., Lofgren, S. M., Beausang, J. F., Mendoza, J. L., Birnbaum, M. E., Fernandes, R. A., Velasco, A., Baltimore, D., Schumacher, T. N., Khatri, P., & Quake, S. R. (2018). Antigen Identification for Orphan T Cell Receptors Expressed on Tumor-Infiltrating Lymphocytes Antigen Identification for Orphan T Cell Receptors Expressed on Tumor-Infiltrating Lymphocytes. *Cell*, *172*(3), 549-556.e16. https://doi.org/10.1016/j.cell.2017.11.043

Geginat, J., Paroni, M., Facciotti, F., Gruarin, P., Kastirr, I., Caprioli, F., Pagani, M., & Abrignani, S. (2013). The CD4-centered universe of human T cell subsets. *Seminars in Immunology*, *25*(4), 252–262. https://doi.org/10.1016/j.smim.2013.10.012

Genot, E., & Cantrell, D. A. (2000). Ras regulation and function in lymphocytes. *Current Opinion in Immunology*, *12*, 289–294.

Gepts, W. (1965). Pathologic anatomy of the pancreas in juvenile diabetes mellitus. *Diabetes*, *14*(10), 619–633. https://doi.org/10.2337/diab.14.10.619

Germain, R. N. (2002). T-cell development and the cd4–cd8 lineage decision. *Nature Reviews Immunology*, *2*(May), 309–322. https://doi.org/10.1038/nri798

Giuliani, L., Mele, R., Giovine, M. Di, Altieri, L., Crin, A., Rav, L., & Fierabracci, A. (2009). Detection of GAD65 Autoreactive T-Cells by HLA Class I Tetramers in Type 1 Diabetic Patients. *Journal of Biomedicine and Biotechnology*, *2009*, 1–7. https://doi.org/10.1155/2009/576219

Gorrec, F. (2016). Protein crystallization screens developed at the MRC Laboratory of Molecular Biology. *Drug Discovery Today*, *21*(5), 819–825. https://doi.org/10.1016/j.drudis.2016.03.008

Grant, E. J., Josephs, T. M., Loh, L., Clemens, E. B., Sant, S., Bharadwaj, M., Chen, W., Rossjohn, J., Gras, S., & Kedzierska, K. (2018). Broad CD8+ T cell cross-recognition of distinct influenza A strains in humans. *Nature Communications*, *9*, 1–16. https://doi.org/10.1038/s41467-018-07815-5

Gras, S., Chadderton, J., Campo, C. M. Del, Quinn, K. M., Rossjohn, J., Gruta, N. L. La, Gras, S., Chadderton, J., Campo, C. M. Del, Farenc, C., & Wiede, F. (2016). Reversed T Cell Receptor Docking on a Major Histocompatibility Class I Complex Limits Involvement in the Immune Response Reversed T Cell Receptor Docking on a Major Histocompatibility Class I Complex Limits Involvement in the Immune Response. *Immunity*, *45*(4), 749–760. https://doi.org/10.1016/j.immuni.2016.09.007

Gras, S., Kedzierski, L., Valkenburg, S. A., Laurie, K., Chih, Y., & Denholm, J. T. (2010). Cross-reactive CD8+ T-cell immunity between the pandemic H1N1-2009 and H1N1-1918 in fl

uenza A viruses. *PNAS*, *107*(28), 12599–12604. https://doi.org/10.1073/pnas.1007270107

Greenbaum, J. A., Kotturi, M. F., Kim, Y., Oseroff, C., Vaughan, K., Salimi, N., Vita, R., Ponomarenko, J., Scheuermann, R. H., Sette, A., & Peters, B. (2009). Pre-existing immunity against swine-origin H1N1 influenza viruses in the general human population. *PNAS*, *106*(48), 20365–20370.

Greenshields-Watson, A., Attaf, M., Maclachlan, B. J., Sewell, A. K., Godkin, A. J., Cole, D. K., Greenshields-watson, A., Attaf, M., Maclachlan, B. J., Whalley, T., & Rius, C. (2020). CD4 + T Cells Recognize Conserved Influenza A Epitopes through Shared Patterns of V-Gene Usage and Complementary Biochemical Features. *Cell Reports*, *32*(2), 107885. https://doi.org/10.1016/j.celrep.2020.107885

Guo, L., Zhang, H., & Chen, B. (2017). Nivolumab as Programmed Death-1 (PD-1) Inhibitor for Targeted Immunotherapy in Tumor. *Journal of Cancer*, *8*(3), 410–416. https://doi.org/10.7150/jca.17144

Hall, C. E., Koparde, V. N., Jameson-lee, M., Elnasseh, G., Scalora, A. F., Kobulnicky, D. J., Serrano, M. G., Roberts, H., Buck, G. A., Neale, M. C., Nixon, D. E., & Toor, A. A. (2017). Sequence homology between HLA-bound cytomegalovirus and human peptides : A potential trigger for alloreactivity. *PLoS ONE*, *12*(8), 1–23.

Haney, D., Quigley, M. F., Asher, T. E., Ambrozak, D. R., Gostick, E., Price, D. A., Douek, D. C., & Betts, M. R. (2011). Isolation of viable antigen-specific CD8+ T cells based on membrane-bound tumor necrosis factor (TNF)-α expression. *Journal of Immunological Methods*, *369*(1–2), 33–41. https://doi.org/10.1016/j.jim.2011.04.003.Isolation

Hanninen, A; Jalkanen, S; Salmi, M; Toikkanen, S; Nikolakaros, G; Simeli, O. (1992). Macrophages , T Cell Receptor Usage , and Endothelial Cell Activation in the Pancreas at the Onset of Insulin-dependent Diabetes Mellitus. *Journal of Clinical Investigation*, *90*(November), 1901–1910.

Harkiolaki, M., Holmes, S. L., Svendsen, P., Gregersen, J. W., Jensen, L. T., Mcmahon, R., Friese, M. A., Boxel, G. Van, Etzensperger, R., Tzartos, J. S., Kranc, K., Sainsbury, S., Harlos, K., Mellins, E. D., Palace, J., Esiri, M. M., Merwe, P. A. Van Der, & Jones, E. Y. (2006). T Cell-Mediated Autoimmune Disease Due to Low-Affinity Crossreactivity to Common Microbial Peptides. *Immunity*, *30*(3), 348–357. https://doi.org/10.1016/j.immuni.2009.01.009

Hartmann, J., Schüßler-lenz, M., Bondanza, A., & Buchholz, C. J. (2017). Clinical development of CAR T cells — challenges and opportunities in translating innovative treatment

concepts. *EMBO Molecular Medicine*, *9*(9), 1183–1197. https://doi.org/10.15252/emmm.201607485

Hawse, W. F., De, S., Greenwood, A. I., Nicholson, L. K., Zajicek, J., Kovrigin, E. L., Kranz, D. M., Garcia, K. C., & Baker, B. M. (2014). TCR Scanning of Peptide/MHC through Complementary Matching of Receptor and Ligand Molecular Flexibility. *The Journal of Immunology*, *192*(6), 2885–2891. https://doi.org/10.4049/jimmunol.1302953

Hawse, W. F., Gloor, B. E., Ayres, C. M., Kho, K., Nuter, E., & Baker, B. M. (2013). Peptide Modulation of Class I Major Histocompatibility Complex Protein Molecular Flexibility and the Implications for Immune Recognition. *Journal of Biological Chemistry*, *288*(34), 24372–24381. https://doi.org/10.1074/jbc.M113.490664

Heald, A., Stedman, M., Davies, M., Livingston, M., Alshames, R., Lunt, M., Rayman, G., & Gadsby, R. (2020). Estimating life years lost to diabetes : outcomes from analysis of National Diabetes Audit and Office of National Statistics data. *Cardiovascular Endocrinology and Metabolism*, *June*. https://doi.org/10.1097/XCE.0000000000000210

Hellmann, M. D., Ares, L. P., Caro, R. B., Zurawski, B., Kim, S., Costa, E. C., Park, K., Alexandru, A., Lupinacci, L., Jimenez, E. D. M., Sakai, H., Albert, I., Vergnenegre, A., Peters, S., Syrigos, K., Barlesi, F., Reck, M., Borghaei, H., Brahmer, J. R., … Bhagavatheeswaran, P. (2019). Nivolumab plus Ipilimumab in Advanced Non–Small-Cell Lung Cancer. *The New England Journal of Medicine*, *381*, 2020–2031. https://doi.org/10.1056/NEJMoa1910231

Hernandez, J. B., Newton, R. H., & Walsh, C. M. (2010). Life and death in the thymus — cell death signaling during T cell development. *Current Opinion in Cell Biology*, *22*(6), 865–871. https://doi.org/10.1016/j.ceb.2010.08.003

Heusel, J. W., Wesselschmidt, R. L., Russell, J. H., & Ley, T. J. (1994). Cytotoxic Lymphocytes Require Granzyme B for the Rapid Induction of DNA Fragmentation and Apoptosis in Allogeneic Target Cells. *Cell*, *76*, 977–987.

Hex, N., Bartlett, C., Wright, D., Taylor, M., & Varley, D. (2012). Estimating the current and future costs of Type 1 and Type 2 diabetes in the UK , including direct health costs and indirect societal and productivity costs. *Diabetic Medicine*, *29*, 855–862. https://doi.org/10.1111/j.1464-5491.2012.03698.x

Hiemstra, H. S., Duinkerken, G., Benckhuijsen, W. E., Amons, R., Vries, R. R. P., Roep, B. A., & Drijfhout, J. W. (1997). The identification of CD4+ T cell epitopes with dedicated synthetic peptide libraries. *Proc Natl Acad Sci U S A*, *94*(September), 10313–10318.

Hodi, F. S., Chiarion-sileni, V., Gonzalez, R., Grob, J., Rutkowski, P., Cowey, C. L., Lao, C. D., Schadendorf, D., Wagstaff, J., Dummer, R., Ferrucci, P. F., Smylie, M., Hill, A., Hogg, D., Marquez-rodas, I., Jiang, J., Rizzo, J., Larkin, J., & Wolchok, J. D. (2018). Nivolumab plus ipilimumab or nivolumab alone versus ipilimumab alone in advanced melanoma (CheckMate 067): 4-year outcomes of a multicentre , randomised , phase 3 trial. *Lancet Oncology*, *19*(11), 1480–1492. https://doi.org/10.1016/S1470-2045(18)30700-9

Holland, C. J., Dolton, G., Scurr, M., Schauenburg, A. J., Miners, K., Sewell, A. K., Price, D. A., Cole, D. K., Godkin, A. J., Schauenburg, A. J., Miners, K., Madura, F., & Sewell, A. K. (2020). Enhanced Detection of Antigen-Specific CD4 + T Cells Using Altered Peptide Flanking Residue Peptide − MHC Class II Multimers. *The Journal of Immunology*, *195*, 5827–5836. https://doi.org/10.4049/jimmunol.1402787

Holland, C. J., Vuidepot, A., Cole, D. K., Holland, C. J., Crean, R. M., Pentier, J. M., Wet, B. De, Lloyd, A., Srikannathasan, V., Lissin, N., Lloyd, K. A., Blicher, T. H., Conroy, P. J., Hock, M., Pengelly, R. J., Spinner, T. E., Cameron, B., Potter, E. A., Jeyanthan, A., … Cole, D. K. (2020). Specificity of bispecific T cell receptors and antibodies targeting peptide-HLA. *Journal of Clinical Investigation*, *130*(5), 2673–2688.

Hopkins, J. R., Crean, R. M., Catici, D. A. M., Sewell, A. K., Arcus, V. L., Kamp, M. W. Van Der, & Cole, D. K. (2020). Peptide cargo tunes a network of correlated motions in human leucocyte antigens. *FEBS Journal*, *287*, 3777–3793. https://doi.org/10.1111/febs.15278

Howarth, M., Williams, A., Tolstrup, A. B., & Elliott, T. (2004). Tapasin enhances MHC class I peptide presentation according to peptide half-life. *Proceedings of the National Academy of Sciences of the United States of America*, *101*(32), 11737–11742. https://doi.org/10.1073/pnas.0306294101

Hozumi, N., & Tonegawa, S. (1976). Evidence for somatic rearrangement of immunoglobulin genes coding for variable and constant regions. *Proceedings of the National Academy of Sciences of the United States of America*, *73*(10), 3628–3632. https://doi.org/10.1073/pnas.73.10.3628

Huang, H. S., Su, H. Y. L., Li, P. H., Chiang, P. H., Huang, C. H., Chen, C. H., & Hsieh, M. C. (2018). Prognostic impact of tumor infiltrating lymphocytes on patients with metastatic urothelial carcinoma receiving platinum based chemotherapy. *Scientific Reports*, *8*(1), 1–7. https://doi.org/10.1038/s41598-018-25944-1

Hughes, M. M., Yassai, M., Sedy, J. R., Wehrly, T. D., Kanagawa, O., Gorski, J., & Sleckman, B. P. (2003). T cell receptor CDR3 loop length repertoire is determined primarily by features of the V(D)J recombination reaction. *European Journal of Immunology*, 1568–

1575. https://doi.org/10.1002/eji.200323961

Huseby, E. S., Crawford, F., White, J., Marrack, P., & Kappler, J. W. (2006). Interface-disrupting amino acids establish specificity between T cell receptors and complexes of major histocompatibility complex and peptide. *Nature Immunology*, *7*(11), 1191–1199. https://doi.org/10.1038/ni1401

Huseby, E. S., White, J., Crawford, F., Vass, T., Becker, D., Pinilla, C., Marrack, P., Kappler, J. W., & Diego, S. (2005). How the T Cell Repertoire Becomes Peptide and MHC Specific. *Cell*, *122*, 247–260. https://doi.org/10.1016/j.cell.2005.05.013

Izumi Negishi, Noboru Motoyama, Kel-lchl Nakayama, K. N., Senju, S., Hatakeyama, S., Zhang, Q., Chant, A. C., & Loh, D. Y. (1995). Essential role for ZAP-70 in both positive and negative selection of thymocytes. *Letters to Nature*, *376*(August), 435–438.

Jakest, R., Hasegawat, M., Spillantini, M. G., & Crowthert, R. A. (1998). α -Synuclein in Filamentous Inclusions of Lewy Bodies from Parkinson ' s Disease and Dementia with Lewy Bodies. *PNAS*, *95*(11), 6469–6473.

Jarchum, I., Nichol, L., Trucco, M., Santamaria, P., & Dilorenzo, T. P. (2008). *Identification of novel IGRP epitopes targeted in type 1 diabetes patients*. 359–365. https://doi.org/10.1016/j.clim.2008.01.015

Jiang, S., Herrera, O., & Ã, R. I. L. (2004). New spectrum of allorecognition pathways: implications for graft rejection and transplantation tolerance. *Current Opinion in Immunology*, *16*, 550–557. https://doi.org/10.1016/j.coi.2004.07.011

Joglekar, A. V, Leonard, M. T., Jeppson, J. D., Swift, M., Li, G., Wong, S., Peng, S., Zaretsky, J. M., Heath, J. R., Ribas, A., Bethune, M. T., & Baltimore, D. (2019). T cell antigen discovery via signaling and antigen-presenting bifunctional receptors. *Nature Methods*, *16*(February), 191–198. https://doi.org/10.1038/s41592-018-0304-8

Johnson, L. A., Heemskerk, B., Powell, D. J., Cohen, C. J., Morgan, R. A., Dudley, M. E., Robbins, F., Rosenberg, S. A., Cells, M., Lymphocytes, T., Johnson, L. A., Heemskerk, B., Powell, D. J., Cohen, C. J., Morgan, R. A., Dudley, M. E., Robbins, P. F., & Rosenberg, S. A. (2006). Gene Transfer of Tumor-Reactive TCR Confers Both High Avidity and Tumor Reactivity to Nonreactive Peripheral Blood Mononuclear Cells and Tumor-Infiltrating Lymphocytes. *The Journal of Immunology*, *177*, 6548–6559. https://doi.org/10.4049/jimmunol.177.9.6548

Kageyama, S., Ikeda, H., Miyahara, Y., Imai, N., Ishihara, M., Saito, K., Sugino, S., Ueda, S., Ishikawa, T., Kokura, S., Naota, H., Ohishi, K., Shiraishi, T., Inoue, N., Tanabe, M., Kidokoro, T., Yoshioka, H., Tomura, D., & Nukaya, I. (2015). Adoptive Transfer of MAGE-

A4 T-cell Receptor Gene-Transduced Lymphocytes in Patients with Recurrent Esophageal Cancer. *Clinical Cancer Research*, *21*(10), 2268–2277. https://doi.org/10.1158/1078-0432.CCR-14-1559

Kalergis, A. M., Boucheron, N., Doucey, M., Palmieri, E., Goyarts, E. C., Vegh, Z., Luescher, I. F., & Nathenson, S. G. (2001). Efficient T cell activation requires an optimal dwell-time of interaction between the TCR and the pMHC complex. *Nature Immunology*, *2*(3), 229–234.

Karumuthil-Melethil, S., Perez, N., Li, R., & Vasu, C. (2008). Induction of Innate Immune Response through TLR2 and Dectin 1 Prevents Type 1 Diabetes. *The Journal of Immunology*, *181*, 8323–8334. https://doi.org/10.4049/jimmunol.181.12.8323

Kawakami, Y., Eliyahu, S., Delgado, C. H., Robbins, P. F., Rivoltini, L., Topalian, S. L., Miki, T., & Rosenberg, S. A. (1994). Cloning of the gene coding for a shared human melanoma antigen recognized by autologous T cells infiltrating into tumor. *Proceedings of the National Academy of Sciences*, *91*(9), 3515–3519. https://doi.org/10.1073/pnas.91.9.3515

Kersh, B. G. J., & Allen, P. M. (1996). Structural Basis for T Cell Recognition of Altered Peptide Ligands: A Single T Cell Receptor Can Productively Recognize a Large Continuum of Related Ligands. *Journal of Experimental Medicine*, *184*(October), 1259–1268.

Kersh, G. J., Kersh, E. N., Fremont, D. H., Allen, P. M., & Louis, S. (1998). High- and Low-Potency Ligands with Similar Affinities for the TCR : The Importance of Kinetics in TCR Signaling. *Immunity*, *9*, 817–826.

Khoja, L., Butler, M. O., Kang, S. P., Ebbinghaus, S., & Joshua, A. M. (2015). Pembrolizumab. *Journal for ImmunoTherapy of Cancer*, *3*(36), 1–13. https://doi.org/10.1186/s40425-015-0078-9

Khoshouei, M., Radjainia, M., Baumeister, W., & Danev, R. (2017). Cryo-EM structure of haemoglobin at 3.2 Å determined with the Volta phase plate. *Nature Communications*, *8*(May), 1–6. https://doi.org/10.1038/ncomms16099

Kim, J., Kim, A., & Shin, E. (2015). Cytomegalovirus Infection and Memory T Cell Inflation. *Immune Network*, *15*(4), 186–190.

Kjer-Nielsen, L., Clements, C. S., Purcell, A. W., Brooks, A. G., Whisstock, J. C., Burrows, S. R., Mccluskey, J., & Rossjohn, J. (2003). A Structural Basis for the Selection of Dominant ab T Cell Receptors in Antiviral Immunity. *Immunity*, *18*, 53–64.

Klenerman, P., Wu, Y., & Phillips, R. (2002). HIV: Current opinion in escapology. *Current Opinion in Microbiology*, *5*(4), 408–413. https://doi.org/10.1016/S1369-

5274(02)00339-9

Klug, D., Carter, C., Crouch, E., Roop, D., Conti, C. J., & Richie, E. R. (1998). *Interdependence of cortical thymic epithelial cell differentiation and T-lineage commitment*. *95*(September), 11822–11827.

Knight, R. R., Dolton, G., Kronenberg-Versteeg, D., Eichmann, M., Zhao, M., Huang, G. C., Beck, K., Cole, D. K., Sewell, A. K., Skowera, A., & Peakman, M. (2014). A distinct immunogenic region of glutamic acid decarboxylase 65 is naturally processed and presented by human islet cells to cytotoxic CD8 T cells. *Clinical & Experimental Immunology*, *179*, 100–107. https://doi.org/10.1111/cei.12436

Koch, J., & Tampé, R. (2006). The macromolecular peptide-loading complex in MHC class I-dependent antigen presentation. *Cellular and Molecular Life Sciences*, *63*(6), 653–662. https://doi.org/10.1007/s00018-005-5462-z

Koelle, D. M., Chen, H. B., Mcclurkan, C. M., & Petersdorf, E. W. (2002). Brief report Herpes simplex virus type 2 – specific CD8 cytotoxic T lymphocyte cross-reactivity against prevalent HLA class I alleles. *The American Society of Hematology*, *99*(10), 3844–3847.

Komatsu, H., Sierro, S., Cuero, A. V, & Klenerman, P. (2003). Population analysis of antiviral T cell responses using MHC class I-peptide tetramers. *Clinical & Experimental Immunology*, *134*, 9–12. https://doi.org/10.1046/j.1365-2249.2003.02266.x

Kondrashova, A., Viskari, H., Kulmala, P., Romanov, A., Ilonen, J., Hyöty, H., & Knip, M. (2007). Signs of β-cell autoimmunity in nondiabetic schoolchildren: A comparison between Russian Karelia with a low incidence of type 1 diabetes and Finland with a high incidence rate. *Diabetes Care*, *30*, 95–100. https://doi.org/10.2337/dc06-0711

Kostine, M., Chiche, L., Lazaro, E., Halfon, P., Charpin, C., Arniaud, D., Retornaz, F., Blanco, P., Jourde-chiche, N., Richez, C., & Stavris, C. (2017). Opportunistic autoimmunity secondary to cancer immunotherapy (OASI): An emerging challenge. *Societe Nationale Francaise de Medecine Interne*, *38*(8), 513–525. https://doi.org/10.1016/j.revmed.2017.01.004

Koutsakos, M., Illing, P. T., Nguyen, T. H. O., Mifsud, N. A., Crawford, J. C., Rizzetto, S., Eltahla, A. A., Clemens, E. B., Sant, S., Chua, B. Y., Wong, C. Y., Allen, E. K., Teng, D., Dash, P., Boyd, D. F., Grzelak, L., Zeng, W., Hurt, A. C., Barr, I., … Kedzierska, K. (2019). Human CD8 + T cell cross-reactivity across influenza A, B and C viruses. *Nature Immunology*, *20*(5), 613–625. https://doi.org/10.1038/s41590-019-0320-6

Krogvold, L., Edwin, B., Buanes, T., Frisk, G., Skog, O., Anagandula, M., Korsgren, O., Undlien, D., Eike, M. C., Richardson, S. J., Leete, P., Morgan, N. G., Oikarinen, S., Oikarinen, M.,

Laiho, J. E., Hyöty, H., Ludvigsson, J., Hanssen, K. F., & Dahl-Jørgensen, K. (2015). Detection of a low-grade enteroviral infection in the islets of langerhans of living patients newly diagnosed with type 1 diabetes. *Diabetes*, *64*, 1682–1687. https://doi.org/10.2337/db14-1370

Kronenberg, D., Knight, R. R., Estorninho, M., Ellis, R. J., Kester, M. G., Ru, A. De, Eichmann, M., Huang, G. C., Powrie, J., Dayan, C. M., Skowera, A., Veelen, P. A. Van, & Peakman, M. (2012). Circulating, Preproinsulin Signal Peptide – Specific CD8 T Cells Restricted by the Susceptibility Molecule HLA-A24 Are Expanded at Onset of Type 1 Diabetes and Kill b-cells. *Diabetes*, 1–8. https://doi.org/10.2337/db11-1520

Kula, T., Wang, C. I., Wucherpfennig, K. W., Lyerly, H. K., Dezfulian, M. H., Wang, C. I., Abdelfattah, N. S., Hartman, Z. C., & Elledge, S. J. (2019). T-Scan : A Genome-wide Method for the Systematic Discovery of T Cell Epitopes Resource T-Scan : A Genome-wide Method for the Systematic Discovery of T Cell Epitopes. *Cell*, *178*(4), 1016-1028.e13. https://doi.org/10.1016/j.cell.2019.07.009

Kurobe, H., Liu, C., Ueno, T., Saito, F., Ohigashi, I., Seach, N., Arakaki, R., Hayashi, Y., Kitagawa, T., Lipp, M., & Boyd, R. L. (2006). CCR7-Dependent Cortex-to-Medulla Migration of Positively Selected Thymocytes Is Essential for Establishing Central Tolerance. *Immunity*, *24*, 165–177. https://doi.org/10.1016/j.immuni.2005.12.011

Ladell, K., Hashimoto, M., Iglesias, M. C., Wilmann, P. G., Mclaren, J. E., Chikata, T., Kuse, N., Gostick, E., Bridgeman, J. S., Venturi, V., Agut, H., Bockel, D. J. Van, Almeida, J. R., Douek, D. C., Meyer, L., Venet, A., Takiguchi, M., Rossjohn, J., & Price, D. A. (2013). A Molecular Basis for the Control of Preimmune Escape Variants. *Immunity*, *38*, 425–436. https://doi.org/10.1016/j.immuni.2012.11.021

Laethem, V., Sarafova, S. D., Park, J., Tai, X., Pobezinsky, L., Guinter, T. I., Adoro, S., Adams, A., Sharrow, S. O., Feigenbaum, L., & Singer, A. (2007). Deletion of CD4 and CD8 Coreceptors Permits Generation of ab T Cells that Recognize Antigens Independently of the MHC Franc. *Immunity*, *November*, 735–750. https://doi.org/10.1016/j.immuni.2007.10.007

Laethem, V., Tikhonova, A. N., & Singer, A. (2012). MHC restriction is imposed on a diverse T cell receptor repertoire by CD4 and CD8 co-receptors during thymic selection. *Trends in Immunology*, *33*(9), 437–441. https://doi.org/10.1016/j.it.2012.05.006

Landgraf, K. E., Williams, S. R., Steiger, D., Gebhart, D., Lok, S., Martin, D. W., Roybal, K. T., & Kim, K. C. (2020). convertible CARs : A chimeric antigen receptor system for fl exible control of activity and. *Communications Biology*, *3*, 1–13.

https://doi.org/10.1038/s42003-020-1021-2

Laugel, B., Berg, H. A. Van Den, Gostick, E., Cole, D. K., Wooldridge, L., Boulter, J., Milicic, A., Price, D. A., & Sewell, A. K. (2007). Different T Cell Receptor Affinity Thresholds and CD8 Coreceptor Dependence Govern Cytotoxic T Lymphocyte Activation and Tetramer Binding Properties. *Journal of Biological Chemistry*, *282*(33), 23799–23810. https://doi.org/10.1074/jbc.M700976200

Lechler, R. I., & Batchelor, J. R. (1982). Immunogenicity of retransplanted rat kidney allografts. Effect of Inducing Chimerism in the First Recipient and Quantitative Studies on Immunosuppression of the Second Recipient. *Journal of Experimental Medicine*, *156*(December), 1835–1841.

Legut, M., Dolton, G., Mian, A. A., Ottmann, O. G., & Sewell, A. K. (2018). CRISPR-mediated TCR replacement generates superior anticancer transgenic T cells. *Blood*, *131*(3), 311–322. https://doi.org/10.1182/blood-2017-05-787598

Lehner, P. J., Wang, E. C. Y., Moss, P. A. H., Williams, S., Platt, K., Friedman, S. M., Bell, J. I., & Borysiewicz, L. K. (1995). Human HLA-A0201-restricted Cytotoxic T Lymphocyte Recognition of Influenza A Is Dominated by T Cells Bearing the VB17 Gene Segment. *Journal of Experimental Medicine*, *181*, 79–91.

Levet, S., Charvet, B., Bertin, A., Deschaumes, A., Perron, H., & Hober, D. (2019). Human Endogenous Retroviruses and Type 1 Diabetes. *Current Diabetes Reports*, *19*(41).

Li, D., Li, X., Zhou, W., Huang, Y., Liang, X., Jiang, L., Yang, X., Sun, J., Li, Z., & Han, W. (2019). Genetically engineered T cells for cancer immunotherapy. *Signal Transduction and Targeted Therapy*, *28*, 1–17. https://doi.org/10.1038/s41392-019-0070-9

Li, Y., Huang, Y., Lue, J., Quandt, J. A., Martin, R., & Mariuzza, R. A. (2005). Structure of a human autoimmune TCR bound to a myelin basic protein self-peptide and a multiple sclerosis-associated MHC class II molecule. *The EMBO Journal*, *24*(17), 2968–2979. https://doi.org/10.1038/sj.emboj.7600771

Li, Y., Yin, Y., & Mariuzza, R. A. (2013). Structural and biophysical insights into the role of CD4 and CD8 inT cell activation. *Frontiers in Immunology*, *4*(July), 1–11. https://doi.org/10.3389/fimmu.2013.00206

Limozin, L., Bridge, M., Bongrand, P., Dushek, O., Anton, P., & Merwe, V. Der. (2019). TCR – pMHC kinetics under force in a cell-free system show no intrinsic catch bond , but a minimal encounter duration before binding. *PNAS*, *116*(34), 16943–16948. https://doi.org/10.1073/pnas.1902141116

Linette, G. P., Stadtmauer, E. A., Maus, M. V, Rapoport, A. P., Levine, B. L., Emery, L., Litzky,

L., Bagg, A., Carreno, B. M., Cimino, P. J., Binder-scholl, G. K., Smethurst, D. P., Gerry, A. B., Pumphrey, N. J., Bennett, A. D., Brewer, J. E., Dukes, J., Harper, J., Tayton-martin, H. K., … June, C. H. (2013). Cardiovascular toxicity and titin cross-reactivity of af fi nity-enhanced T cells in myeloma and melanoma. *Blood*, *122*(6), 863–871. https://doi.org/10.1182/blood-2013-03-490565.G.P.L.

Lipsitch, M., Grad, Y. H., Sette, A., & Crotty, S. (2020). Cross-reactive memory T cells and herd immunity to SARS-CoV-2. *Nature Reviews Immunology*, *20*, 709–713. https://doi.org/10.1038/s41577-020-00460-4

Liu, L., Yan, J., Xu, H., Zhu, Y., Liang, H., Pan, W., Yao, B., Han, X., Ye, J., & Weng, J. (2018). Two Novel MicroRNA Biomarkers Related to b -Cell Damage and Their Potential Values for Early Diagnosis of Type 1 Diabetes. *J Clin Endocrinol Metab*, *103*(June 2017), 1320–1329. https://doi.org/10.1210/jc.2017-01417

Ljunggren, H., & Kirre, K. (1990). search of the ’ missing self ’: MHC molecules NK cell recognition. *Immunology Today*, *11*(7), 237–244.

Locke, F. L., Ghobadi, A., Jacobson, C. A., Miklos, D. B., Lekakis, L. J., Oluwole, O. O., Lin, Y., Braunschweig, I., Hill, B. T., Timmerman, J. M., Deol, A., Reagan, P. M., Stiff, P., Flinn, I. W., Farooq, U., Goy, A., Mcsweeney, P. A., Munoz, J., Siddiqi, T., … Neelapu, S. S. (2019). Long-term safety and activity of axicabtagene ciloleucel in refractory large B-cell lymphoma (ZUMA-1): a single-arm, multicentre, phase 1 – 2 trial. *Lancet Oncology*, *20*(1), 31–42. https://doi.org/10.1016/S1470-2045(18)30864-7

Loenen, M. M. Van, Boer, R. De, Amir, A. L., Hagedoorn, R. S., & Volbeda, G. L. (2010). Mixed T cell receptor dimers harbor potentially harmful neoreactivity. *PNAS*, *107*(24), 10972–10977. https://doi.org/10.1073/pnas.1005802107

Lowance, D., Neumayer, H. H., Legendre, C. M., Squifflet, J. P., Kovarik, J., Brennan, P. J., Norman, D., Mendez, R., Keating, M. R., Coggon, G. L., Crisp, A., & Lee, I. C. (1999). Valacyclovir for the prevention of cytomegalovirus disease after renal transplantation. International Valacyclovir Cytomegalovirus Prophylaxis Transplantation Study Group. *The New England Journal of Medicine*, *340*(19), 1462.

Maciocia, P. M., Wawrzyniecka, P. A., Philip, B., Ricciardelli, I., Akarca, A. U., Onuoha, S. C., Legut, M., Cole, D. K., Sewell, A. K., Gritti, G., Somja, J., Piris, M. A., Peggs, K. S., Linch, D. C., Marafioti, T., & Pule, M. A. (2017). Targeting the T cell receptor β -chain constant region for immunotherapy of T cell malignancies. *Nature Publishing Group*, *23*(12), 1416–1423. https://doi.org/10.1038/nm.4444

Maclachlan, B. J., Dolton, G., Papakyriakou, A., Greenshields-watson, A., Mason, G. H.,

Schauenburg, A., Besneux, M., Szomolay, B., Elliott, T., Sewell, A. K., Gallimore, A., Rizkallah, P., Cole, D. K., & Godkin, A. (2019). Human leukocyte antigen (HLA) class II peptide flanking residues tune the immunogenicity of a human tumor-derived epitope. *Journal of Biological Chemistry*, *294*(52), 20246–20258. https://doi.org/10.1074/jbc.RA119.009437

Madura, F., Rizkallah, P. J., Holland, C. J., Fuller, A., Bulek, A., Godkin, A. J., Schauenburg, A. J., Cole, D. K., & Sewell, A. K. (2015). Structural basis for ineffective T-cell responses to MHC anchor residue-improved "heteroclitic" peptides. *European Journal of Immunology*, *45*(2), 584–591. https://doi.org/10.1002/eji.201445114

Marek-Trzonkowska, Natalia ; Mysliwiec, Malgorzata ; Dobyszuk, Anita ; Grabowska, Marcelina ; Techmanska, Ilona ; Juscinska, Jolanta ; Wujtewicz, Magdalena A ; Witkowski, Piotr ; Mlynarski, Wojciech ; Balcerska, Anna ; Mysliwska, Jolanta ; Trzonkowski, P. (2012). Regulatory T Cells Preserves b -Cell Function in Type 1 Diabetes in Children. *Diabetes Care*, *35*, 1817–1820. https://doi.org/10.2337/dc12-0038.

Marjorie A. Oettinger; Ben Stanger; David G. Schatz; Tom Glaser; Kathy Call; David Housman; Baltimore, D. (1992). The recombination activating genes, RAG 1 and RAG 2, are on chromosome 11p in humans and chromosome 2p in mice. *Immuno-Genetics*, *35*, 97–101.

Marron, M. P., Graser, R. T., Chapman, H. D., Serreze, D. V, & Hla-a, A. (2002). Functional evidence for the mediation of diabetogenic T cell responses by HLA-A2 .1 MHC class I molecules through transgenic expression in NOD mice. *PNAS*, *99*(21), 13753–13758.

Mason, D. (1998). A very high level of crossreactivity is an essential feature of the T- cell receptor. *Immunology Today*, *19*(9), 395–404. https://doi.org/10.1016/S0167-5699(98)01299-7

Maugh, T. H. (1981). FDA Approves Hepatitis B Vaccine. *Science*, *214*(4525), 1113.

Mazza, C., Auphan-Anezin, N., Gregoire, C., Guimezanes, A., Kellenberger, C., Roussel, A., Kearney, A., van der Merwe, P. A., Schmitt-Verhulst, A.-M., & Malissen, B. (2007). How much can a T-cell antigen receptor adapt to structurally distinct antigenic peptides? *The EMBO Journal*, *26*(7), 1972–1983. https://doi.org/10.1038/sj.emboj.7601605

Mccoy, A. J., Grosse-kunstleve, R. W., Adams, P. D., Winn, M. D., Storoni, L. C., & Read, R. J. (2007). Phaser crystallographic software. *Journal of Applied Crystallography*, *40*, 658–674. https://doi.org/10.1107/S0021889807021206

McKeithan, T. W. (1995). Kinetic proofreading in T-cell receptor signal transduction. *Proc Natl Acad Sci U S A*, *92*(May), 5042–5046.

McLaughlin-Taylor, E., Pande, H., Forman, S. J., Tanamachi, B., Li, C. -R, Zaia, J. A., Greenberg, P. D., & Riddell, S. R. (1994). Identification of the major late human cytomegalovirus matrix protein pp65 as a target antigen for CD8+ virus-specific cytotoxic T lymphocytes. *Journal of Medical Virology*, *43*(1), 103–110. https://doi.org/10.1002/jmv.1890430119

McMichael, A. J., Gotch, F. M., Noble, G. R., & Beare, P. A. S. (1983). Cytotoxic T-cell immunity to influenza. *The New England Journal of Medicine*, *306*, 13–17.

Medawar, P. B. (1944). The behaviour and fatr of skin autografts and skin homografts in rabbits. *Journal of Anatomy*, *76*(5), 176–199.

Mellins, E. D., & Stern, L. J. (2014). HLA-DM and HLA-DO , key regulators of MHC-II processing and presentation. *Current Opinion in Immunology*, *26*, 115–122. https://doi.org/10.1016/j.coi.2013.11.005

Meng, Q., Valentini, D., Rao, M., Moro, C. F., Paraschoudi, G., Jäger, E., Dodoo, E., Rangelova, E., del Chiaro, M., & Maeurer, M. (2019). Neoepitope targets of tumour-infiltrating lymphocytes from patients with pancreatic cancer. *British Journal of Cancer*, *120*(1), 97–108. https://doi.org/10.1038/s41416-018-0262-z

Middleton, D., Williams, F., Meenagh, A., Daar, A. S., Gorodezky, C., Hammond, M., Nascimento, E., Briceno, I., & Perez, M. P. (2000). Analysis of the Distribution of HLA-A Alleles in Populations from Five Continents. *Human Immunology*, *8859*(00).

Mkaddem, S. Ben, Murua, A., Flament, H., Titeca-beauport, D., Bounaix, C., Danelli, L., Launay, P., Benhamou, M., Blank, U., Daugas, E., Charles, N., & Monteiro, R. C. (2017). Lyn and Fyn function as molecular switches that control immunoreceptors to direct homeostasis or inflammatio. *Nature Communications*. https://doi.org/10.1038/s41467-017-00294-0

Moebius, U., Kober, G., Griscelw, A. L., & Meuer, S. C. (1991). Expression of different 0 8 isoforms on distinct human lymphocyte subpopulations. *European Journal of Immunology*, *21*, 1793–1800.

Moine, A. L. M., Oldman, M., & Abramowicz, D. (2002). Multiple pathways to allograft rejection. *Transplantation*, *73*(9), 1373–1381.

Morgan, R. A., Dudley, M. E., Wunderlich, J. R., Hughes, M. S., Yang, J. C., Sherry, R. M., Royal, R. E., Topalian, S. L., Kammula, U. S., Restifo, N. P., Zheng, Z., Nahvi, A., de Vries, C. R., Rogers-Freezer, L. J., Mavroukakis, S. A., & Rosenberg, S. A. (2006). Cancer Regression in Patients After Transfer of Genetically Engineered Lymphocytes. *Science*, *314*(5796), 126–129. https://doi.org/10.1126/science.1129003

Morgan, Richard A, Chinnasamy, N., Abate-daga, D. D., Gros, A., Robbins, F., Zheng, Z.,

Feldman, S. A., Yang, J. C., Sherry, R. M., Phan, Q., Hughes, M. S., Kammula, U. S., Miller, A. D., Hessman, C. J., Stewart, A. A., Restifo, N. P., Quezado, M. M., Alimchandani, M., Rosenberg, Z., … Rosenberg, S. A. (2013). Cancer regression and neurologic toxicity following anti-MAGE- A3 TCR gene therapy. *Journal of Immunotherapy*, *36*(2), 133–151. https://doi.org/10.1097/CJI.0b013e3182829903.Cancer

Morgan, Richard A, Dudley, M. E., Wunderlich, J. R., Hughes, M. S., Yang, J. C., Sherry, R. M., Royal, R. E., Topalian, S. L., Kammula, U. S., Restifo, N. P., Zheng, Z., Nahvi, A., Vries, C. R. De, Rogers-freezer, L. J., Mavroukakis, S. A., & Rosenberg, S. A. (2006). Cancer Regression in Patients Engineered Lymphocytes. *Science*, *314*(October), 126–130.

Morrice, N. A., & Powis, S. J. (1998). A role for the thiol-dependent reductase ERp57 in the assembly of MHC class I molecules. *Current Biology*, *8*(12), 713–716. https://doi.org/10.1016/S0960-9822(98)70279-9

Moss, A. D. J., Suhrbier, A., & Elliott, S. L. (1998). Candidate Vaccines for Epstein-Barr Virus : Several Promising Approaches for Vaccines against Primary Infection Candidate vaccines for Epstein-Barr virus. *British Medical Journal*, *317*(7156), 423–424.

Murata, S., Sasaki, K., Kishimoto, T., Niwa, S., Hayashi, H., Takahama, Y., & Tanaka, K. (2007). Regulation of CD8+ T cell development by thymus-specific proteasomes. *Science*, *316*(June), 1349–1354.

Murshudov, G. N., & Nicholls, R. A. (2011). REFMAC5 for the refinement of macromolecular crystal structures. *Biological Crystallography*, *67*, 355–367. https://doi.org/10.1107/S0907444911001314

Nagata, S., & Golstein, P. (1995). The Fas Death Factor. *Science*, *267*(March), 1449–1456.

Naito, Y., Saito, K., Shiiba, K., Ohuchi, A., Saigenji, K., Nagura, H., & Ontani, H. (1998). CD8 + T Cells Infiltrated within Cancer Cell Nests as a Prognostic Factor in Human Colorectal Cancer. *Cancer Research*, *58*, 3491–3495.

Nakagawa, T., Roth, W., Wong, P., Nelson, A., Farr, A., Deussing, J., Villadangos, J. A., Ploegh, H., Peters, C., & Rudensky, A. Y. (1998). Cathepsin L: Critical Role in Ii Degradation and CD4 T Cell Selection in the Thymus. *Science*, *280*(April), 450–453.

Neefjes, J. J., Momburg, F., & Hämmerling, G. J. (1993). Selective and ATP-dependent translocation of peptides by the MHC-encoded transporter. *Science*, *261*(5122), 769–771. https://doi.org/10.1126/science.8342042

Neelapu, S. S., Locke, N. L., Bartlett, L. J., Lekakis, D. B., Miklos, C. A., Jacobson, I., Go, W. Y., & Al., E. (2017). Axicabtagene Ciloleucel CAR T-Cell Therapy in Refractory Large B-Cell Lymphoma. *New England Journal of Medicine*, *377*(26), 2531–2544.

https://doi.org/10.1056/NEJMoa1707447.Axicabtagene

Nejentsev, S., Howson, J. M. M., Walker, N. M., Szeszko, J., Sarah, F., Stevens, H. E., Reynolds, P., Hardy, M., King, E., Hulme, J., Maier, L. M., Smyth, D., Bailey, R., Jason, D., Ribas, G., Campbell, R. D., Wellcome, T., Case, T., Clayton, D. G., & Todd, J. A. (2007). Localization of type 1 diabetes susceptibility to the MHC class I genes HLA-B and HLA-A. *Nature*, *450*(7171), 887–892. https://doi.org/10.1038/nature06406.Localization

Newman, J., Egan, D., Walter, T. S., Meged, R., Berry, I., Jelloul, B. M., Sussman, J. L., Stuart, D. I., & Perrakis, A. (2005). Towards rationalization of crystallization screening for small-to medium-sized academic laboratories : the PACT / JCSG + strategy. *Biological Crystallography*, *D61*, 1426–1431. https://doi.org/10.1107/S0907444905024984

Nino-vasquez, J. J., Allicotti, G., Borras, E., Wilson, D. B., Valmori, D., Simon, R., Martin, R., & Pinilla, C. (2004). A powerful combination : the use of positional scanning libraries and biometrical analysis to identify cross-reactive T cell epitopes. *Molecular Immunology*, *40*, 1063–1074. https://doi.org/10.1016/j.molimm.2003.11.005

Nishimura, H., Okazaki, T., & Tanaka, Y. (2001). Autoimmune dilated cariomyopathy in PD-1 receptor-deficient mice. *Science*, *291*(January), 319–323.

Noble, J. A., Valdes, A. M., Varney, M. D., Carlson, J. A., Moonsamy, P., Fear, A. L., Lane, J. A., Lavant, E., Rappner, R., Louey, A., Concannon, P., Mychaleckyj, J. C., Erlich, H. A., & Diabetes, T. (2010). HLA Class I and Genetic Susceptibility to Type 1. *Diabetes*, *59*(November), 2972–2979. https://doi.org/10.2337/db10-0699.

Norton, D. L., & Haque, A. (2009). Insights into the Role of GILT in HLA Class II Antigen Processing and Presentation by Melanoma. *Journal of Oncology*, *2009*, 1–8. https://doi.org/10.1155/2009/142959

O'Hara, G. A., Welten, S. P. M., Klenerman, P., & Arens, R. (2012). Memory T cell inflation : understanding cause and effect. *Trends in Immunology*, *33*(2), 84–90. https://doi.org/10.1016/j.it.2011.11.005

Oers, N. S. C., Boehmer, H., & Weiss, A. (1995). The Pre-T Cell Receptor (TCR) Complex is Functionally Coupled to the TCR-z subunit. *Journal of Experimental Medicine*, *182*, 1585–1590.

Oldstone, M. B. A. (1988). Prevention of type I diabetes in nonobese diabetic mice by virus infection. *Science*, *239*, 500–502. https://doi.org/10.1126/science.3277269

Oldstone, M. B. A. (1998). Molecular mimicry and immune-mediated diseases. *The FASEB Journal*, *12*(13), 1255–1265.

Oliver, J. D., Roderick, H. L., Llewellyn, D. H., & High, S. (1999). ERp57 functions as a subunit

of specific complexes formed with the ER lectins calreticulin and calnexin. *Molecular Biology of the Cell*, *10*(8), 2573–2582. https://doi.org/10.1091/mbc.10.8.2573

Ortiz-navarrete, V., Seeligt, A., Gernoldt, M., & Hammerling, J. (1991). *Subunit of the "20S" proteasome (multicatalytic protease) encoded by the major histocompatibility complex*. *3*(October), 662–664.

Ott, P. A., Hu, Z., Keskin, D. B., Shukla, S. A., Sun, J., Bozym, D. J., Zhang, W., Luoma, A., Giobbie-hurder, A., Peter, L., Chen, C., Olive, O., Carter, T. A., Li, S., Lieb, D. J., Eisenhaure, T., Gjini, E., Stevens, J., Lane, W. J., … Wu, C. J. (2017). An immunogenic personal neoantigen vaccine for patients patients with melanoma. *Letters to Nature*, *547*, 217–221. https://doi.org/10.1038/nature22991

Pageon, S. V, Tabarin, T., Yamamoto, Y., Ma, Y., Nicovich, P. R., Bridgeman, J. S., Cohenen, A., Benzing, C., Gao, Y., Crowther, M. D., Tungatt, K., Dolton, G., Sewell, A. K., Price, D. A., Acuto, O., Parton, R. G., Gooding, J. J., Rossy, J., Rossjohn, J., & Gaus, K. (2016). Functional role of T-cell receptor nanoclusters in signal initiation and antigen discrimination. *PNAS*, 454–463. https://doi.org/10.1073/pnas.1607436113

Pak, C. Y., Mcarthur, R. G., Eun, H., & Yoo, J.-W. (1988). Association of cutomegalovirus infection with autoimmune type 1 diabetes. *The Lancet*, 1–4.

Panina-Bordignon, B. P., Lang, R., Endert, P. M. Van, Benazzi, E., Felix, A. M., Pastore, I. I. R. M., Spinas, G. A., & Sinigaglia, F. (1995). Cytotoxic T cells specific for glutamic acid decarboxylase in autoimmune diabetes. *The Journal of Experimental Medicine*, *181*(May).

Parente-pereira, A. C., Shmeeda, H., Lynsey, M., Zambirinis, C. P., Foster, J., Stegen, J. C. Van Der, Beatson, R., Zabinski, T., Brewig, N., Sosabowski, J. K., Mather, S., Gabizon, A., & Maher, J. (2014). Adoptive Immunotherapy of Epithelial Ovarian Cancer with V γ 9V δ 2 T Cells, Potentiated by Liposomal Alendronic Acid. *Journal of Immunology*, *193*, 5557–5566. https://doi.org/10.4049/jimmunol.1402200

Patterson, C. C., Carson, D. J., & Hadden, D. R. (1996). Epidemiology of childhood IDBM in Northern Ireland 1989-1994: Low incidence in areas with highest population density and most household crowding. *Diabetologia*, *39*, 1063–1069. https://doi.org/10.1007/BF00400655

Peggs, K., Verfuerth, S., Pizzey, A., Ainsworth, J., Moss, P., & Mackinnon, S. (2002). Characterization of human cytomegalovirus peptide – specific CD8 ƨ T-cell repertoire diversity following in vitro restimulation by antigen-pulsed dendritic cells. *Immunobiology*, *99*(1), 213–223.

Pernis, B. Y. B., Chiappino, G., Kelus, A. S., & Gell, P. G. H. (1965). Cellular localisation of immunoglobulins with different allotypic specificities in rabbit lymphoid tissues. *Cellular Localization of Immunoglobulins*, *6*.

Peterson, P. A., Rask, L., & Lindblom, J. B. (1974). Highly Purified Papain-Solubilized HL-A Antigens Contain β 2-microglobulin. *Proc Natl Acad Sci U S A*, *71*(1), 35–39.

Petry, N. M., Cengiz, E., Wagner, J. A., Weyman, K., Tichy, E., & Tamborlane, W. V. (2015). Testing for Rewards: A Pilot Study to Improve Type 1 Diabetes Management in Adolescents. *Diabetes Care*, *38*, 1952–1954. https://doi.org/10.2337/dc15-0765

Phillips, R. E., Rowland-Jones, S., Nixon, D. F., Gotch, F. M., Edwards, J. P., Ogunlesi, A. O., Elvin, J. G., Rothbard, J. A., Bangham, C. R. M., Rizza, C. R., & McMichael, A. J. (1991). Human immunodeficiency virus genetic variation that can escape cytotoxic T cell recognition. *Nature*, *354*, 453–459. https://doi.org/10.1038/354453a0

Pinilla, C., & Houghten, R. A. (1993). Rapid identification of high affinity peptide ligands using positional scanning synthetic peptide combinatorial libraries. *Biotechniques*, *13*(6), 901–905.

Pinilla, C., Martin, R., Grant, B., Appel, J. R., Boggiano, C., Wilson, D. B., & Houghteng, R. A. (1999). Exploring immunological combinatorial libraries specificity using synthetic peptide. *Current Opinion in Immunology*, *11*, 193–202.

Pinkse, G. G. M., Tysma, O. H. M., Bergen, C. A. M., Kester, M. G. D., Ossendorp, F., Veelen, P. A. Van, Keymeulen, B., Pipeleers, D., Drijfhout, J. W., & Roep, B. O. (2005). Autoreactive CD8 T cells associated with b-cell destruction in type 1 diabetes. *PNAS*, *102*(51), 18425–18430.

Pita-lopez, M. L., Gayoso, I., Delarosa, O., Casado, J. G., Alonso, C., Muñoz-gomariz, E., Tarazona, R., & Solana, R. (2009). Immunity & Ageing Effect of ageing on CMV-specific CD8 T cells from CMV seropositive healthy donors. *Immunity & Ageng*, *6*(11), 1–10. https://doi.org/10.1186/1742-4933-6-11

Pozzilli, P., Maddaloni, E., & Buzzetti, R. (2015). Combination immunotherapies for type 1 diabetes mellitus. *Nature Publishing Group*, *11*(May), 289–297. https://doi.org/10.1038/nrendo.2015.8

Pross, H. F., & Eidinger, D. (1974). Antigenic Competition : A Review of Nonspecific Antigen-Induced Suppression. *Advances in Immunology*, *18*, 133–168.

Pui, J. C., Allman, D., Xu, L., Derocco, S., Karnell, F. G., Bakkour, S., Lee, J. Y., Kadesch, T., Hardy, R. R., Aster, J. C., & Pear, W. S. (1999). Notch1 Expression in Early Lymphopoiesis Influences B versus T Lineage Determination. *Immunity*, *11*, 299–308.

Purwar, R., Schlapbach, C., Xiao, S., Kang, H. S., Elyaman, W., Jiang, X., Jetten, A. M., Khoury, S. J., Fuhlbrigge, R. C., Kuchroo, V. K., Clark, R. A., & Kupper, T. S. (2012). Robust tumor immunity to melanoma mediated by interleukin-9 – producing T cells. *Nature Medicine*, *18*(8), 1248–1254. https://doi.org/10.1038/nm.2856

Raman, M. C. C., Rizkallah, P. J., Simmons, R., Donnellan, Z., Dukes, J., Bossi, G., Le Provost, G. S., Todorov, P., Baston, E., Hickman, E., Mahon, T., Hassan, N., Vuidepot, A., Sami, M., Cole, D. K., & Jakobsen, B. K. (2016). Direct molecular mimicry enables off-target cardiovascular toxicity by an enhanced affinity TCR designed for cancer immunotherapy. *Scientific Reports*, *6*(November 2015), 18851. https://doi.org/10.1038/srep18851

Ramsden, D. A., & Gellert, M. (1995). Formation and resolution of double-strand break intermediates in V(D)J rearrangement. *Genes and Development*, *9*, 2409–2420.

Reay, P. A., Kantor, R. M., & Davis, M. M. (1994). Use of global amino acid replacements to define the requirements for MHC binding and T cell recognition of moth cytochrome c (93-103). *Journal of Immunology*, *152*(8), 3946–3957. http://www.ncbi.nlm.nih.gov/pubmed/7511662

Reimann, J., & Kaufmannt, S. H. E. (1997). Alternative antigen processing pathways in anti-infective immunity. *Current Opinion in Immunology*, *9*, 462–469.

Reiser, J., Darnault, C., Grégoire, C., Mosser, T., Mazza, G., Kearney, A., Merwe, P. A. Van Der, Fontecilla-camps, J. C., Housset, D., & Malissen, B. (2003). CDR3 loop flexibility contributes to the degeneracy of TCR recognition. *Nature Immunology*, *4*(3), 241–247. https://doi.org/10.1038/ni891

Reiser, J., Darnault, C., Guimezanes, A., Grégoire, C., Fontecilla-camps, J. C., Malissen, B., Housset, D., & Mazza, G. (2000). Crystal structure of a T cell receptor bound to an allogeneic MHC molecule. *Nature Immunology*, *1*(4), 291–297.

Reynolds, S. R. R., Oratz, R. O., Shapiro, R. L. S., Hao, P. H., Yun, Z. Y., Fotino, M. F., Vukmanovic, S., & Bystryn, J. (1997). Stimulation of CD8+ T cell responses to MAGE-3 and MELAN A/MART-1 by immunization to a polyvalent melanoma vaccine. *International Journal of Cancer*, *72*, 972–976.

Ribeiro, T. C., & Latronico, A. C. (2012). Insulin-like growth factor system on adrenocortical tumorigenesis. *Molecular and Cellular Endocrinology*, *351*(1), 96–100. https://doi.org/10.1016/j.mce.2011.09.042

Richardson, A. K., Walker, L. C., Cox, B., Rollag, H., Robinson, B. A., Morrin, H., Pearson, J. F., Potter, J. D., Paterson, M., Surcel, H. M., Pukkala, E., & Currie, M. J. (2020). Breast cancer

and cytomegalovirus. *Clinical and Translational Oncology*, *22*(4), 585–602. https://doi.org/10.1007/s12094-019-02164-1

Riera Romo, M., Pérez-Martínez, D., & Castillo Ferrer, C. (2016). Innate immunity in vertebrates: An overview. *Immunology*, *148*(2), 125–139. https://doi.org/10.1111/imm.12597

Riley, T. P., Hellman, L. M., Gee, M. H., Mendoza, J. L., Alonso, J. A., Foley, K. C., Nishimura, M. I., Vander Kooi, C. W., Garcia, K. C., & Baker, B. M. (2018). T cell receptor cross-reactivity expanded by dramatic peptide–MHC adaptability. *Nature Chemical Biology*, *14*(10), 934–942. https://doi.org/10.1038/s41589-018-0130-4

Rius Rafael, C. (2019). Identification of novel cancer-specific T cell targets by dissection of successful tumour- infiltrating lymphocyte therapy. *Cardiff University*.

Rock, K. L., Farfán-arribas, D. J., Shen, L., Shen, L., Rock, K. L., & Farfa, D. J. (2010). Proteases in MHC Class I Presentation and Cross-Presentation. *The Journal of Immunology*, *184*, 9–15. https://doi.org/10.4049/jimmunol.0903399

Rock, K. L., York, I. A., Saric, T., & Goldberg, A. L. (2002). Protein degradation and the generation of MHC class I-presented peptides. *Advances in Immunology*, *80*, 1–70. https://doi.org/10.1016/S0065-2776(02)80012-8

Roger, A. J., Svard, S. G., Tovar, J., Clark, C. G., Smith, M. W., Gillin, F. D., & Sogin, M. L. (1998). A mitochondrial-like chaperonin 60 gene in Giardia lamblia : Evidence that diplomonads once harbored an endosymbiont related to the progenitor of mitochondria. *Proc Natl Acad Sci U S A*, *5*, 229–234.

Rosenberg, S. A., Yang, J. C., Sherry, R. M., Kammula, U. S., Hughes, M. S., Phan, G. Q., Citrin, D. E., Restifo, N. P., Robbins, P. F., Wunderlich, J. R., Morton, K. E., Laurencot, C. M., Steinberg, S. M., White, D. E., & Dudley, M. E. (2011). Durable Complete Responses in Heavily Pretreated Patients with Metastatic Melanoma Using T-Cell Transfer Immunotherapy. *Clinical Cancer Research*, *17*(13), 4550–4558. https://doi.org/10.1158/1078-0432.CCR-11-0116

Roth, D. B., Zhu, C., & Gellert, M. (1993). Characterization of broken DNA molecules associated with V(D)J recombination. *Proceedings of the National Academy of Sciences of the United States of America*, *90*(22), 10788–10792. https://doi.org/10.1073/pnas.90.22.10788

Rudolph, M. G., Luz, J. G., & Wilson, I. A. (2002). Structural and Thermodynamic Correlates of T Cell Signalling. *Annu. Rev. Biophys. Biomol. Struct*, *31*, 121–149. https://doi.org/10.1146/annurev.biophys.31.082901.134423

Sakaguchi, S., Miyara, M., Costantino, C. M., & Hafler, D. A. (2010). FOXP3 + regulatory T cells in the human immune system. *Nature Reviews Immunology*, *10*(7), 490–500. https://doi.org/10.1038/nri2785

Salgaller, M., Marincola, M., Cormier, N., & Rosenberg, A. (1996). Immunization against Epitopes in the Human Melanoma Antigen gp1OO following Patient Immunization with Synthetic Peptides. *Journal of Cancer Research*, *56*, 4749–4758.

Sandt, C. E. Van De, Dou, Y., Vogelzang-van, S. E., Westgeest, K. B., Pronk, M. R., Albert, D. M., Osterhaus, E., Fouchier, R. A. M., Rimmelzwaan, G. F., & Hillaire, M. L. B. (2015). Influenza B virus-specific CD8 + T-lymphocytes strongly cross-react with viruses of the opposing influenza B lineage. *Journal of General Virology*, *96*, 2061–2073. https://doi.org/10.1099/vir.0.000156

Saric, T., Chang, S. C., Hattori, A., York, I. A., Markant, S., Rock, K. L., Tsujimoto, M., & Goldberg, A. L. (2002). An IFN-γ-induced aminopeptidase in the ER, ERAP I, trims precursors to MHC class I-presented peptides. *Nature Immunology*, *3*(12), 1169–1176. https://doi.org/10.1038/ni859

Savignac, M., Mellström, B., & Naranjo, J. R. (2007). Calcium-dependent transcription of cytokine genes in T lymphocytes. *Pflugers Archiv European Journal of Physiology*, *454*(4), 523–533. https://doi.org/10.1007/s00424-007-0238-y

Sayeed, A., Luciani-Torres, G., Meng, Z., Bennington, J. L., Moore, D. H., & Dairkee, S. H. (2013). Aberrant Regulation of the BST2 (Tetherin) Promoter Enhances Cell Proliferation and Apoptosis Evasion in High Grade Breast Cancer Cells. *PLoS ONE*, *8*(6), 1–10. https://doi.org/10.1371/journal.pone.0067191

Schlissel, M., Constantinescu, A., Morrow, T., Baxter, M., & Peng, A. (1993). Double-strand signal sequence breaks in V(D)J recombination are blunt, 5'-phosphorylated, RAG-dependent, and cell cycle regulated. *Genes and Development*, *7*, 2520–2532.

Schloss, J., Ali, R., Racine, J. J., Chapman, H. D., Serreze, D. V., & DiLorenzo, T. P. (2018). HLA-B*39:06 Efficiently Mediates Type 1 Diabetes in a Mouse Model Incorporating Reduced Thymic Insulin Expression. *The Journal of Immunology*, *200*(10), 3353–3363. https://doi.org/10.4049/jimmunol.1701652

Schneider-brachert, W., Tchikov, V., Neumeyer, J., Jakob, M., Winoto-morbach, S., Held-feindt, J., Heinrich, M., Merkel, O., Ehrenschwender, M., Adam, D., Mentlein, R., Kabelitz, D., Schu, S., Kiel, D.-, Kiel, D.-, & Kiel, D.-. (2004). Compartmentalization of TNF Receptor 1 Signaling : Internalized TNF Receptosomes as Death Signaling Vesicles. *Immunity*, *21*, 415–428.

Schuck, P. (1997). Use of surface plasmon resonance to probe the equilibrium and dynamic aspects of interactions between biological macromolecules. *Annual Review of Biophysics and Biomolecular Structure*, *26*, 541–566. https://doi.org/10.1146/annurev.biophys.26.1.541

Schwarz, K., de Giuli, R., Schmidtke, G., Kostka, S., van den Broek, M., Kim, K. B., Crews, C. M., Kraft, R., & Groettrup, M. (2000). The Selective Proteasome Inhibitors Lactacystin and Epoxomicin Can Be Used to Either Up- or Down-Regulate Antigen Presentation at Nontoxic Doses. *The Journal of Immunology*, *164*(12), 6147–6157. https://doi.org/10.4049/jimmunol.164.12.6147

Sethi, D. K., Gordo, S., Schubert, D. A., & Wucherpfennig, K. W. (2013). Crossreactivity of a human autoimmune TCR is dominated by a single TCR loop. *Nature Communications*, *29*(6), 997–1003. https://doi.org/10.1016/j.biotechadv.2011.08.021.Secreted

Setia, M. S., Steinmaus, C., Ho, C. S., & Rutherford, G. W. (2006). The role of BCG in prevention of leprosy : a meta-analysis. *The Journal of Infection*, *6*(March), 162–170.

Sewell, A. K. (2012). Why must T cells be cross-reactive? *Nature Reviews. Immunology*, *12*(9), 669–677. https://doi.org/10.1038/nri3279

Shapiro, James; Lakey, R. T. Jonathan; Ryan, E. A; Korbutt, G. S; Toth, E; Warnock, G. L; Kneteman, N. M; Rajotte, R. V. (2000). Islet Transplantation in sevenpatients with type-1 diabetes mellitus using a glucocorticoid-free immunosuppressive regimen. *New England Medical Journal*, *343*(4).

Sharma, P., & Allison, J. P. (2015). The future of immune checkpoint therapy. *Cancer Immunology, Immunotherapy*, *348*(6230), 56–61.

Shugay, M., Bagaev, D. V, Zvyagin, I. V, Vroomans, R. M., Crawford, J. C., Dolton, G., Komech, E. A., Sycheva, A. L., Koneva, A. E., Egorov, E. S., Eliseev, A. V, Dyk, E. Van, Dash, P., Attaf, M., Rius, C., Ladell, K., Mclaren, J. E., Matthews, K., Clemens, E. B., … Chudakov, D. M. (2017). VDJdb : a curated database of T-cell receptor sequences with known antigen specificity. *Nucleic Acids Research*, *46*, 419–427. https://doi.org/10.1093/nar/gkx760

Siddiqui, M. A. A., & Perry, C. M. (2006). Human Papillomavirus Quadrivalent (types 6, 11, 16, 18) Recombinant Vaccine (Gardasil®). *Drugs*, *66*(9), 1263–1271.

Skowera, A., Ellis, R. J., Varela-calviño, R., Arif, S., Huang, G. C., Van-krinks, C., Zaremba, A., Rackham, C., Allen, J. S., Tree, T. I. M., Zhao, M., Dayan, C. M., Sewell, A. K., Unger, W., Drijfhout, J. W., Ossendorp, F., Roep, B. O., & Peakman, M. (2008). CTLs are targeted to kill β cells in patients with type 1 diabetes through recognition of a glucose-regulated preproinsulin epitope. *The Journal of Clinical Investigation*, *118*(10), 3390–3402.

https://doi.org/10.1172/JCI35449DS1

Smith, A. R., Alonso, J. A., Ayres, C. M., Singh, N. K., & Hellman, L. M. (2021). Structurally silent peptide anchor modifications allosterically modulate T cell recognition in a receptor-dependent manner. *PNAS*, *118*, 1–10. https://doi.org/10.1073/pnas.2018125118/-/DCSupplemental.Published

Sommers, C. L., Lee, J., Steiner, K. L., Gurson, J. M., Depersis, C. L., El-khoury, D., Fuller, C. L., Shores, E. W., Love, P. E., & Samelson, L. E. (2005). Mutation of the phospholipase C- 1 – binding site of LAT affects both positive and negative thymocyte selection. *Journal of Experimental Medicine*, *201*(7), 1125–1134. https://doi.org/10.1084/jem.20041869

Somoza, N., Vargas, F., Roura-mir, C., Vives-pi, M., Fermindez-figueras, M. T., Ariza, A., Comis, R., Bragado, R., Marti, M., Jaraquemada, D., & Pujol-borrel, R. (1994). Pancreas in Recent Onset Insulin-Dependent Diabetes Mellitus. *The American Association of Immunologists*, *153*, 1360–1377.

Sondak, V. K., Smalley, K. S. M., Kudchadkar, R., Grippon, S., & Kirkpatrick, P. (2011). Ipilimumab. *Nature Reviews Drug Discovery*, *10*(JUNE), 411–412. https://doi.org/10.1038/nrd3463

Spear, T. T., Wang, Y., Foley, K. C., Murray, D. C., Scurti, G. M., Simms, P. E., Garrett, E., Hellman, L. M., Baker, B. M., & Nishimura, M. I. (2017). Critical biological parameters modulate affinity as a determinant of function in T - cell receptor gene - modified T - cells. *Cancer Immunology, Immunotherapy*, *66*(11), 1411–1424. https://doi.org/10.1007/s00262-017-2032-9

Speir, J. A., Stevens, J., Joly, E., Butcher, G. W., & Wilson, I. A. (2001). Two different, highly exposed, bulged structures for an unusually long peptide bound to rat MHC class I RT1-Aa. *Immunity*, *14*(1), 81–92. https://doi.org/10.1016/S1074-7613(01)00091-7

Stärck, L., Popp, K., Pircher, H., Popp, K., Pircher, H., & Uckert, W. (2014). Immunotherapy with TCR-Redirected T Cells: Comparison of TCR-Transduced and TCR-Engineered Hematopoietic Stem Cell − Derived T Cells. *Journal of Immunology*, *192*, 206–213. https://doi.org/10.4049/jimmunol.1202591

Stedman, M., Lunt, M., Davies, M., Livingston, M., Duff, C., Fryer, A., Anderson, S. G., Gadsby, R., & Gibson, M. (2020). Cost of hospital treatment of type 1 diabetes (T1DM) and type 2 diabetes diabetes (T2DM) compared to the non-diabetes -population: a detailed economic evaluation. *BMJ Open*, *10*, 1–10. https://doi.org/10.1136/bmjopen-2019-033231

Stene, L. C., Oikarinen, S., Hyöty, H., Barriga, K. J., Norris, J. M., Klingensmith, G., Hutton, J.

C., Erlich, H. A., Eisenbarth, G. S., & Rewers, M. (2010). Enterovirus infection and progression from islet autoimmunity to type 1 diabetes: The Diabetes and Autoimmunity Study in the Young (DAISY). *Diabetes*, *59*, 3174–3180. https://doi.org/10.2337/db10-0866

Stevens, J., Wiesmu, K., Barker, P. J., Walden, P., Butcher, G. W., & Joly, E. (1998). Efficient Generation of Major Histocompatibility Complex Class I-Peptide Complexes Using Synthetic Peptide Libraries. *Journal of Biological Chemistry*, *273*(5), 2874–2884. https://doi.org/10.1074/jbc.273.5.2874

Stewart-jones, G. B. E., Mcmichael, A. J., Bell, J. I., Stuart, D. I., & Jones, E. Y. (2003). A structural basis for immunodominant human T cell receptor recognition. *Nature Immunology*, *4*(7), 657–663.

Stewart-jones, G. B., Simpson, P., Merwe, P. A. Van Der, & Easterbrook, P. (2012). Structural features underlying T-cell receptor sensitivity to concealed MHC class I micropolymorphisms. *PNAS*, 3483–3492. https://doi.org/10.1073/pnas.1207896109

Stewart, A. J., & Devlin, P. M. (2006). The history of the smallpox vaccine. *The Journal of Infection*, *52*, 329–334. https://doi.org/10.1016/j.jinf.2005.07.021

Stone, J. D., Adam, S., & Kranz, D. M. (2009). T-cell receptor binding affinities and kinetics : impact on T-cell activity and specificity. *Immunolgy*, *126*, 165–176. https://doi.org/10.1111/j.1365-2567.2008.03015.x

Stone, J. D., & Stern, L. J. (2006). CD8 T Cells, Like CD4 T Cells, Are Triggered by Multivalent Engagement of TCRs by MHC-Peptide Ligands but Not by Monovalent Engagement. *The Journal of Immunology*, *176*, 1498–1505. https://doi.org/10.4049/jimmunol.176.3.1498

Strachan, D. P. (1989). Hay fever, hygiene, and household size. *BMJ*, *299*, 1259–1260. https://doi.org/10.1177/036319909502000302

Streeter, H. B., Rigden, R., Martin, K. F., & Scolding, N. J. (2015). Preclinical development and first-in-human study of ATX-MS-1467 for immunotherapy of MS. *American Academy of Neurology*, 1–10. https://doi.org/10.1212/NXI.0000000000000093

Stumpf, M., Hasenburg, A., Riener, M. O., Jütting, U., Wang, C., Shen, Y., Orlowska-Volk, M., Fisch, P., Wang, Z., Gitsch, G., Werner, M., & Lassmann, S. (2009). Intraepithelial CD8-positive T lymphocytes predict survival for patients with serous stage III ovarian carcinomas: Relevance of clonal selection of T lymphocytes. *British Journal of Cancer*, *101*(9), 1513–1521. https://doi.org/10.1038/sj.bjc.6605274

Sulzer, D., Alcalay, R. N., Garretti, F., Cote, L., Kanter, E., Agin-Liebes, J., Liong, C., McMurtrey,

C., Hildebrand, W. H., Mao, X., Dawson, V. L., Dawson, T. M., Oseroff, C., Pham, J., Sidney, J., Dillon, M. B., Carpenter, C., Weiskopf, D., Phillips, E., … Sette, A. (2017). T cells from patients with Parkinson's disease recognize α-synuclein peptides. *Nature*, *546*(7660), 656–661. https://doi.org/10.1038/nature22815

Sylwester, A. W., Mitchell, B. L., Edgar, J. B., Taormina, C., Pelte, C., Ruchti, F., Sleath, P. R., Grabstein, K. H., Hosken, N. A., Kern, F., Nelson, J. A., & Picker, L. J. (2005). Broadly targeted human cytomegalovirus-specific CD4+ and CD8+ T cells dominate the memory compartments of exposed subjects. *Journal of Experimental Medicine*, *202*(5), 673–685. https://doi.org/10.1084/jem.20050882

Szabo, S. J., Kim, S. T., Costa, G. L., Zhang, X., Fathman, C. G., Glimcher, L. H., & Carolina, S. (2000). A Novel Transcription Factor , T-bet , Directs Th1 Lineage Commitment. *Cell*, *100*, 655–669.

Szomolay, B., Liu, J., Brown, P. E., Miles, J. J., Clement, M., Llewellyn-lacey, S., Dolton, G., Ekeruche-makinde, J., Lissina, A., Schauenburg, A. J., Sewell, A. K., Burrows, S. R., Roederer, M., Price, D. A., Wooldridge, L., & Berg, H. A. Van Den. (2016). Identification of human viral protein-derived ligands recognized by individual MHCI-restricted T-cell receptors. *Immunology and Cell Biology*, *January*, 573–582. https://doi.org/10.1038/icb.2016.12

Tan, M. P., Gerry, A. B., Brewer, J. E., Melchiori, L., Bridgeman, J. S., Bennett, A. D., Pumphrey, N. J., Jakobsen, B. K., Price, D. A., Ladell, K., & Sewell, A. K. (2015). T cell receptor binding affinity governs the functional profile of cancer-specific CD8 $^{+}$ T cells. *Clinical & Experimental Immunology*, *180*(2), 255–270. https://doi.org/10.1111/cei.12570

Tang, Q., Henriksen, K. J., Bi, M., Finger, E. B., Szot, G., Ye, J., Masteller, E. L., Mcdevitt, H., Bonyhadi, M., & Bluestone, J. A. (2004). In Vitro – expanded Antigen-specific Regulatory T Cells Suppress Autoimmune Diabetes. *Journal of Experimental Medicine*, *199*(11), 1455–1465. https://doi.org/10.1084/jem.20040139

Theaker, S. M., Rius, C., Greenshields-watson, A., Lloyd, A., Trimby, A., Fuller, A., Miles, J. J., Cole, D. K., Peakman, M., Sewell, A. K., & Dolton, G. (2016). T-cell libraries allow simple parallel generation of multiple peptide-speci fi c human T-cell clones. *Journal of Immunological Methods*, *430*, 43–50. https://doi.org/10.1016/j.jim.2016.01.014

Tian, B., Hao, J., Zhang, Y., Tian, L., Yi, H., O'Brien, T. D., Sutherland, D. E. R., Hering, B. J., & Guo, Z. (2009). Upregulating CD4+CD25+FOXP3+ regulatory T cells in pancreatic lymph nodes in diabetic NOD mice by adjuvant immunotherapy. *Transplantation*, *87*, 198–206. https://doi.org/10.1097/TP.0b013e3181933261

Tison, A., Quéré, G., Misery, L., Funck-Brentano, E., Danlos, F. X., Routier, E., Robert, C., Loriot, Y., Lambotte, O., Bonniaud, B., Scalbert, C., Maanaoui, S., Lesimple, T., Martinez, S., Marcq, M., Chouaid, C., Dubos, C., Brunet-Possenti, F., Stavris, C., … Kostine, M. (2019). Safety and Efficacy of Immune Checkpoint Inhibitors in Patients With Cancer and Preexisting Autoimmune Disease: A Nationwide, Multicenter Cohort Study. *Arthritis and Rheumatology*, *71*(12), 2100–2111. https://doi.org/10.1002/art.41068

Todd, J. A., Beir, J. I., & Mcdevitt, H. (1987). HLA-DQp gene contributes to susceptibility and resistance to insulin-dependent diabetes mellitus. *Nature*, *2*, 5–10.

Tracy, S., Drescher, K. M., & Chapman, N. M. (2011). Enteroviruses and type 1 diabetes. *Diabetes/Metabolism Research and Reviews*, *27*, 820–823. https://doi.org/10.1002/dmrr

Trautmann, L., Rimbert, M., Echasserieau, K., Saulquin, X., Neveu, B., Dechanet, J., Trautmann, L., Rimbert, M., Echasserieau, K., Saulquin, X., & Bonneville, M. (2015). Selection of T Cell Clones Expressing High-Affinity Public. *The Journal of Immunology*, *175*, 6123–6132. https://doi.org/10.4049/jimmunol.175.9.6123

Trifari, S., Kaplan, C. D., Tran, E. ., Crellin, N. K., & Spits, H. (2009). Identification of a human helper T cell population that has abundant production of interleukin 22 and is distinct from TH-17, TH1 and TH2 cells. *Nature Publishing Group*, *10*(8), 864–871. https://doi.org/10.1038/ni.1770

Trzonkowski, P., Bieniaszewska, M., Ju, J., Dobyszuk, A., Krzystyniak, A., & Marek, N. (2009). First-in-man clinical results of the treatment of patients with graft versus host disease with human ex vivo expanded CD4 + CD25 + CD127 − Tregulatory cells. *Clinical Immunology*, *133*, 22–26. https://doi.org/10.1016/j.clim.2009.06.001

Tsuchiya, Y., Wako, H., & Tsurui, H. (2017). A study of CDR3 loop dynamics reveals distinct mechanisms of peptide recognition by T-cell receptors exhibiting different levels of cross-reactivity. *Immunolgy*, *153*, 466–478. https://doi.org/10.1111/imm.12849

Tungatt, K., Bianchi, V., Crowther, M. D., Powell, W. E., Schauenburg, A. J., Trimby, A., Donia, M., Miles, J. J., Holland, C. J., Cole, K., Godkin, A. J., Peakman, M., Thor, P., Svane, I. M., Sewell, A. K., Tungatt, K., Bianchi, V., Crowther, M. D., Powell, W. E., … Dolton, G. (2015). Antibody Stabilization of Peptide − MHC Multimers Reveals Functional T Cells Bearing Extremely Low-Affinity TCRs. *The Journal of Immunology*, *194*, 463–474. https://doi.org/10.4049/jimmunol.1401785

Turner, S. J., Doherty, P. C., Mccluskey, J., & Rossjohn, J. (2006). Structural determinants of T-cell receptor bias in immunity. *Nat Rev Immunol*, *6*(December), 883–894.

https://doi.org/10.1038/nri1977

Tynan, F. E., Burrows, S. R., Buckle, A. M., Clements, C. S., Borg, N. A., Miles, J. J., Beddoe, T., Whisstock, J. C., Wilce, M. C., Silins, S. L., Burrows, J. M., Kjer-nielsen, L., Kostenko, L., Purcell, A. W., Mccluskey, J., & Rossjohn, J. (2005). T cell receptor recognition of a ' super-bulged ' major histocompatibility complex class I – bound peptide. *Nature Immunology*, *6*(11), 1114–1122. https://doi.org/10.1038/ni1257

Uhlig, H. H., Coombes, J., Mottet, C., Izcue, A., Thompson, C., Fanger, A., Tannapfel, A., Fontenot, J. D., Ramsdell, F., & Powrie, F. (2006). Characterization of Foxp3 + CD4 + CD25 + and IL-10-Secreting CD4 + CD25 + T Cells during Cure of Colitis . *The Journal of Immunology*, *177*(9), 5852–5860. https://doi.org/10.4049/jimmunol.177.9.5852

Vallabhapurapu, S., & Karin, M. (2009). Regulation and Function of NF-κB Transcription Factors in the Immune System. *Annual Review of Immunology*, *27*(1), 693–733. https://doi.org/10.1146/annurev.immunol.021908.132641

Varela-rohena, A., Molloy, P. E., Dunn, S. M., Li, Y., Suhoski, M. M., Carroll, R. G., Milicic, A., Mahon, T., Sutton, D. H., Laugel, B., Moysey, R., Cameron, B. J., Vuidepot, A., Purbhoo, M. A., Cole, D. K., Phillips, R. E., June, C. H., Jakobsen, B. K., Sewell, A. K., & Riley, J. L. (2008). Control of HIV-1 immune escape by CD8 T cells expressing enhanced T-cell receptor. *Nature Medicine*, *14*(12), 1390–1395. https://doi.org/10.1038/nm.1779

Venturi, V., Price, D. A., Douek, D. C., & Davenport, M. P. (2008). The molecular basis for public T-cell responses? *Nature Reviews Immunology*, *8*, 231–238.

Walunas, T. L., Lenschow, D. J., Bakker, C. Y., Linsley, P. S., Freeman, G. J., Green, J. M., Thompson, C. B., & Bluestone, J. A. (1994). CTLA-4 Can Function as a Negative Regulator of T Cell Activation. *Immunity*, *1*, 405–413.

Wang, D., Forman, S. J., Brown, C. E., Wang, D., Aguilar, B., Starr, R., Alizadeh, D., Brito, A., Sarkissian, A., Ostberg, J. R., Forman, S. J., & Brown, C. E. (2018). Glioblastoma-targeted CD4 + CAR T cells mediate superior antitumor activity Find the latest version : Glioblastoma-targeted CD4 + CAR T cells mediate superior antitumor activity. *JCI Insight*, *3*(10).

Wang, R., Natarajan, K., & Margulies, D. H. (2009). Structural Basis of the CD8ab/MHC Class I Interaction: Focused Recognition Orients CD8ab to a T Cell Proximal Position. *The Journal of Immunology*, *183*, 2554–2564. https://doi.org/10.4049/jimmunol.0901276

Wang, Z., Cd, T., Zhu, Z., Loh, L., Tian, D., Wan, Y., Qiu, C., Quin, S., Ren, Y., Hu, Y., Zhang, X., Thomas, P. G., Inouye, M., & Doherty, P. C. (2015). Recovery from severe H7N9 disease is associated with diverse response mechanisms dominated by. *Nature*

Communications, *May*, 1–12. https://doi.org/10.1038/ncomms7833

Watanabe, K., Kuramitsu, S., Jr, A. D. P., June, C. H., & June, C. H. (2018). Expanding the Therapeutic Window for CAR T Cell Therapy in Solid Tumors: The Knowns and Unknowns of CAR T Cell Biology. *Frontiers in Immunology*, *9*(October), 1–12. https://doi.org/10.3389/fimmu.2018.02486

Watanabe, N., Arase, H., & Onodera, M. (2000). The Quantity of TCR Signal Determines Positive Selection and Lineage Commitment of T Cells. *The Journal of Immunology*, *165*, 6252–6261. https://doi.org/10.4049/jimmunol.165.11.6252

Waterhouse, P., Penninger, J. M., Timms, E., Wakeham, A., Shahinian, A., Lee, K. P., Thompson, C. B., Griesser, H., & Mak, T. W. (1995). Lymphoproliferative Disorders with Early Lethality in Mice Deficient in Ctla-4 B C-. *Science*, *270*, 985–988.

Webb, B., & Sali, A. (2014). Protein Structure Modeling with MODELLER. *Methods in Molecular Biology*, *3*, 1–17.

Weber, K. S., Donermeyer, D. L., Allen, P. M., & Kranz, D. M. (2005). Class II-restricted T cell receptor engineered in vitro for higher affinity retains peptide specificity and function. *PNAS*, *102*(52), 19033–19038.

Wedemeyer, H., Mizukoshi, E., Davis, A. R., Bennink, J. R., & Rehermann, B. (2001). Cross-reactivity between hepatitis C virus and Influenza A virus determinant-specific cytotoxic T cells. *Journal of Virology*, *75*(23), 11392–11400. https://doi.org/10.1128/JVI.75.23.11392

Weiss, B. Y. A., & Stobo, J. D. (1984). Requirement for the coexpression of T3 and the T-cell antigen receptor on a malignant human T cell line. *Journal of Experimental & Clinical Cancer Research*, *160*, 1284–1299.

Welsh, R. M., & Selin, L. K. (2002). No one is naive: the significance of heterologous T-cell immunity. *Nature Reviews Immunology*, *2*, 417–426. https://doi.org/10.1038/nri820

Wen, J., Elong Ngono, A., Angel Regla-Nava, J., Kim, K., Gorman, M. J., Diamond, M. S., & Shresta, S. (2017). Dengue virus-reactive CD8+ T cells mediate cross-protection against subsequent Zika virus challenge. *Nature Communications*, *8*(1), 1459. https://doi.org/10.1038/s41467-017-01669-z

Wen, J., Tang, W. W., Sheets, N., Ellison, J., Sette, A., Kim, K., & Shresta, S. (2017). Identification of Zika virus epitopes reveals immunodominant and protective roles for dengue virus cross-reactive CD8+T cells. *Nature Microbiology*, *2*(March). https://doi.org/10.1038/nmicrobiol.2017.36

Whalley, T., Dolton, G., Brown, P. E., Wall, A., Wooldridge, L., Berg, H. Van Den, Fuller, A.,

Hopkins, J. R., Crowther, M. D., Szomolay, B., & Sewell, A. K. (2020). GPU-Accelerated Discovery of Pathogen-Derived Molecular Mimics of a T-Cell Insulin Epitope. *Frontiers in Immunology*, *11*(February), 1–18. https://doi.org/10.3389/fimmu.2020.00296

Willcox, B. E., Gao, G. F., Wyer, J. R., Ladbury, J. E., Bell, J. I., Jakobsen, B. K., & Van der Merwe, P. a. (1999). TCR binding to peptide-MHC stabilizes a flexible recognition interface. *Immunity*, *10*, 357–365.

Wills, M. R., Carmichael, A. J., Mynard, K. I. M., Jin, X. I. A., Weekes, M. P., Plachter, B., & Sissons, J. G. P. (1996). The Human Cytotoxic T-Lymphocyte (CTL) Response to Cytomegalovirus Is Dominated by Structural Protein pp65 : Frequency , Specificity , and T-Cell Receptor Usage of pp65-Specific CTL. *Journal of Virology*, *70*(11), 7569–7579.

Wilson, D. B., Wilson, D. H., Schroder, K., Pinilla, C., Blondelle, S., Houghten, R. A., & Garcia, K. C. (2004). Specificity and degeneracy of T cells. *Molecular Immunology*, *40*(14–15), 1047–1055. https://doi.org/10.1016/j.molimm.2003.11.022

Winn, M. D., Charles, C., Cowtan, K. D., Dodson, E. J., Leslie, A. G. W., Mccoy, A., Stuart, J., Garib, N., Powell, H. R., & Randy, J. (2011). Overview of the CCP 4 suite and current developments. *Biological Crystallography*, *67*, 235–242. https://doi.org/10.1107/S0907444910045749

Wissemann, W. T., Hill-burns, E. M., Zabetian, C. P., Factor, S. A., Patsopoulos, N., Hoglund, B., Holcomb, C., Donahue, R. J., Thomson, G., Erlich, H., & Payami, H. (2013). Association of Parkinson Disease with Structural and Regulatory Variants in the HLA Region. *The American Journal of Human Genetics*, *93*(5), 984–993. https://doi.org/10.1016/j.ajhg.2013.10.009

Wolf, E., Spencer, K. M., Cudworth, A. G., Unit, M., & Bartholomew, S. (1983). The Genetic Susceptibility to Type 1 (Insulin-Dependent) Diabetes Analysis of the HLA-DR Association. *Diabetologia*, *1*, 224–230.

Wooldridge, L., Clement, M., Lissina, A., Edwards, S. J., Ladell, K., Ekeruche, J., Rachel, E., Laugel, B., Gostick, E., Cole, D. K., Berrevoets, C., Miles, J. J., Burrows, S. R., Price, D. A., Sewell, A. K., Wooldridge, L., Clement, M., Lissina, A., Edwards, E. S. J., … Burrows, S. R. (2010). MHC Class I Molecules with Superenhanced CD8 Binding Properties Bypass the Requirement for Cognate TCR Recognition and Nonspecifically Activate CTLs. *The Journal of Immunology*, *184*, 3357–3366. https://doi.org/10.4049/jimmunol.0902398

Wooldridge, L., Ekeruche-Makinde, J., Van Den Berg, H. A., Skowera, A., Miles, J. J., Tan, M. P., Dolton, G., Clement, M., Llewellyn-Lacey, S., Price, D. A., Peakman, M., & Sewell, A. K. (2012). A single autoimmune T cell receptor recognizes more than a million different

peptides. *Journal of Biological Chemistry*, *287*(2), 1168–1177. https://doi.org/10.1074/jbc.M111.289488

Wu, A., Peng, Y., Huang, B., Ding, X., Wang, X., Niu, P., Meng, J., Zhu, Z., Zhang, Z., Wang, J., Sheng, J., Quan, L., Xia, Z., & Tan, W. (2020). Genome Composition and Divergence of the Novel Coronavirus (2019-nCoV) Originating in China. *Cell Host and Microbe*, *27*(3), 325–328. https://doi.org/10.1016/j.chom.2020.02.001

Wucherpfennig, K. W., & Strominger, J. L. (1995). Molecular mimicry in T cell-mediated autoimmunity: Viral peptides activate human T cell clones specific for myelin basic protein. *Cell*, *80*(5), 695–705. https://doi.org/10.1016/0092-8674(95)90348-8

Wyer, J. R., Willcox, B. E., Gao, G. F., Gerth, U. C., Davis, S. J., Bell, J. I., van der Merwe, P. a, & Jakobsen, B. K. (1999). T cell receptor and coreceptor CD8 aa bind peptide-MHC independently and with distinct kinetics. *Immunity*, *10*(2), 219–225. https://doi.org/10.1016/S1074-7613(00)80022-9

Xhangolli, I., Dura, B., Lee, G., Kim, D., Xiao, Y., & Fan, R. (2019). Single-cell Analysis of CAR-T Cell Activation Reveals A Mixed T H 1 / T H 2 Response Independent of Differentiation. *Genomics, Proteomics & Bioinformatics*, *17*(2), 129–139. https://doi.org/10.1016/j.gpb.2019.03.002

Xiang, X., Li, Y., Yin, Y., Mo, M., Wang, Q., Gao, W., Wang, L., & Mariuzza, R. A. (2011). Affinity maturation of human CD4 by yeast surface display and crystal structure of a CD4-HLA-DR1 complex. *PNAS*, *108*(38), 1–6. https://doi.org/10.1073/pnas.1109438108

Yadav, M., Jhunjhunwala, S., Phung, Q. T., Lupardus, P., Tanguay, J., Bumbaca, S., Franci, C., Cheung, T. K., Fritsche, J., Weinschenk, T., Modrusan, Z., Mellman, I., & Lill, J. R. (2014). Predicting immunogenic tumour mutations by combining mass spectrometry and exome sequencing. *Letters to Nature*, *515*, 572–576. https://doi.org/10.1038/nature14001

Yang, X., Gao, M., Chen, G., Pierce, B. G., Lu, J., Weng, N., & Mariuzza, R. A. (2015). Structural Basis for Clonal Diversity of the Public T Cell Response to a Dominant Human Cytomegalovirus Epitope * □. *Journal of Biological Chemistry*, *290*(48), 29106–29119. https://doi.org/10.1074/jbc.M115.691311

Yaqinuddin, A. (2020). Cross-immunity between respiratory coronaviruses may limit COVID-19 fatalities. *Medical Hypotheses*, *144*(June), 110049. https://doi.org/10.1016/j.mehy.2020.110049

Yeo, L., Pujol-Autonell, I., Baptista, R., Eichmann, M., Kronenberg-Versteeg, D., Heck, S., Dolton, G., Sewell, A. K., Härkönen, T., Mikk, M. L., Toppari, J., Veijola, R., Knip, M.,

Ilonen, J., & Peakman, M. (2020). Circulating β cell-specific CD8+ T cells restricted by high-risk HLA class I molecules show antigen experience in children with and at risk of type 1 diabetes. *Clinical and Experimental Immunology*, *199*(3), 263–277. https://doi.org/10.1111/cei.13391

Yin, L., Huseby, E., Scott-browne, J., Rubtsova, K., Pinilla, C., Crawford, F., Marrack, P., Dai, S., & Kappler, J. W. (2011). A Single T Cell Receptor Bound to Major Histocompatibility Complex Class I and Class II Glycoproteins Reveals Switchable TCR Conformers. *Immunity*, *35*(1), 23–33. https://doi.org/10.1016/j.immuni.2011.04.017

Yip, K. M., Fischer, N., Paknia, E., Chari, A., & Stark, H. (2020). Atomic-resolution protein structure determination by cryo-EM. *Nature*, *587*, 157–161. https://doi.org/10.1038/s41586-020-2833-4

Yoon, J., Austin, M., Onodera, T., & Notkins, A. L. (1989). Isolation of a virus from the pancreas of a child with diabetic ketoacidosis. *N Engl J Med*, *300*(21), 1173–1179.

Young, J. D., Cohn, Z. A., & Podack, E. R. (n.d.). *The Ninth Component of Complement and the Similarities*. *Perforin 1*.

Zheng, M., Zhang, X., Zhou, Y., Tang, J., Han, Q., Zhang, Y., Ni, Q., Chen, G., Jia, Q., Yu, H., Liu, S., Robins, E., Jenny, N., Wan, Y., Li, Q., Chen, Z., & Zhu, P. (2019). TCR repertoire and CDR3 motif analyses depict the role of αβ T cells in Ankylosing spondylitis. *EBioMedicine*, *47*, 414–426. https://doi.org/10.1016/j.ebiom.2019.07.032

Zheng, W., Flavell, R. A., & Alerts, E. (1997). The Transcription Factor GATA-3 Is Necessary and Sufficient for Th2 Cytokine Gene Expression in CD4 T Cells. *The Journal of Immunology*, *196*, 4426–4435.

Zhou, X., Tu, S., Wang, C., Huang, R., Deng, L., Song, C., Yue, C., He, Y., Yang, J., Liang, Z., Wu, A., Li, M., Zhou, W., Du, J., Guo, Z., Li, Y., Jiao, C., Liu, Y., Chang, L., & Li, Y. (2020). Phase I Trial of Fourth-Generation Anti-CD19 Chimeric Antigen Receptor T Cells Against Relapsed or Refractory B Cell Non-Hodgkin Lymphomas. *Frontiers in Immunology*, *11*(November), 1–12. https://doi.org/10.3389/fimmu.2020.564099

Zinkernagel, R. F., & Doherty, P. C. (1974). Immunological surveillance against altered self components by sensitised T lymphocytes in lymphocytes choriomeningitis. *Nature*, *251*, 547–548. https://doi.org/10.1038/251547a0

Zinkernagel, R. M., & Doherty, P. C. (1974). Restriction of in vitro T cell-mediated cytotoxicity in lymphocytic chorio-meningitis within a syngeneic or semiallogenioc system. *Nature*, *248*, 701–702.

Zucca, F. A., Mauri, P., Steinbeck, J. A., Studer, L., Scherzer, C. R., Kanter, E., Budhu, S.,

Mandelbaum, J., Vonsattel, J. P., Zecca, L., & Loike, J. D. (2014). MHC-I expression renders catecholaminergic neurons susceptible to T-cell-mediated degeneration. *Nature Communications*. https://doi.org/10.1038/ncomms4633

Zweerink, H. J., Biddison, W. E., Coligan, J. E., & Parker, K. C. (1992). Sequence motifs important for peptide binding to the human MHC class I molecule. *The Journal of Immunology*, *149*, 3580–3587.